University of Cape Town

Faculty of Medicine

INACTIVATION SYNERGY BETWEEN HIGH ENERGY NEUTRONS AND ^{60}Co GAMMA RAYS

Jacobus P. Slabbert

Thesis submitted to the
University of Cape Town
for the degree of
Doctor of Philosophy

February 1993

Inactivation Synergy between High Energy Neutrons and ^{60}Co γ–rays

Abstract: The interaction between sublesions produced by neutrons [p(66)/Be and d(16)/Be] and ^{60}Co γ–rays was investigated using mammalian cells, meristematic cells and human lymphocytes. The quality of each radiation source was quantified in terms of molecular yield per unit dose absorbed in a ferrous sulphate xylenol orange solution and was found to vary inversely with the mean LET of the radiation field.

Inactivation parameters determined for mammalian and meristematic cells were not significantly different following simultaneous or sequential exposures to d(16)/Be neutrons and ^{60}Co γ–rays. Synergistic interaction was observed to be most pronounced in a radiation mixture consisting of about one part neutrons and three parts photons and appeared to be optimal at approximately 5 Gy. This phenomenon led to dose enhancement ratios that increase with radioresistance.

Multi–target parameters indicated that on a per gray basis, priming doses of p(66)/Be neutrons and ^{60}Co γ–rays induce comparative levels of sublethal damage. However, non–parametric analysis of the survival data showed that mammalian cells regard a priming dose of neutrons as somewhat less effective than an iso–effective photon dose.

A greater measure of synergy was observed between photons and priming doses of neutrons with less build–up. This is however mainly due to higher levels of biological damage induced with a more potent configuration of secondary charged particles. Interaction factors compared at levels of iso–effect tend to be smaller when the LET of the priming dose was increased. Split–doses of neutrons in the absence of build–up resulted in "negative" repair.

The validity of proposed biophysical models was tested using meristematic cells, as the response of these cells show an apparent absence of intertrack damage. Contrary to expectations, synergistic interaction was observed for both growth delay measurements and micronuclear formations.

Chromosome aberrations showed synergy between neutron and photon damage in human lymphocytes, as predicted by interaction functions. However, the synergistic interaction noted with micronuclear formation in binucleate cells was at variance with predictions based on biophysical models.

J.P. Slabbert
National Accelerator Centre
Foundation for Research Development
P.O. Box 72
Faure 7131
South Africa

Acknowledgements

The work reported here was supported in its entirety by the Foundation for Research Development, Republic of South Africa. The author is indebted to the director of the National Accelerator Centre, Dr. D. Reitmann and the group head of Research Dr. S.J. Mills for their continuous support.

The author would like to express his gratitude to Dr. J.H. Hough (Head, Radiation Biophysics Division, NAC) for his unselfish help and many fruitful discussions throughout the course of these investigations. The advice and encouragement of Prof. G. Blekkenhorst (Promoter) in preparing the manuscript is much appreciated, and also the help rendered by Dr. A.S. Hendrikse (University of Cape Town) in the final reading.

Central to the outcome of this study are the excellent radiation and laboratory facilities available for experimental work at the NAC. To this end the author is grateful to Dr. A.H. Botha and the accelerator group for providing stable charged particle beams, to Dr. D.T.L. Jones, Mr. A.N. Schreuder and Mr. J.E. Symons for physical dosimetry measurements and to Ms. H.L. Jones for technical assistance in the laboratory.

The pleasant cooperation of Mrs. H.J.P. Heyns and Mrs. A. van As in preparing the final manuscripts is gratefully acknowledged.

TABLE OF CONTENTS

CHAPTER 1

RELEVANCE OF MIXED RADIATION MODALITIES

Introduction

This study is concerned with an investigation of the interaction between the biological effects caused by different radiation modalities, in particular the interplay between high energy neutrons [d(16)/Be and p(66)/Be] and photons (^{60}Co γ-rays). Throughout this work, except where otherwise stated, references made to radiation will mean ionizing radiation. Central to the study are two concepts, namely "interaction" and "synergism". Two radiation types interact when either of the modalities alters the extent to which the other produces an effect. Synergism occurs when the combined effect of two irradiation modalities is greater than what might be expected if the radiation types acted independently. In this chapter some of the reasons as to the relevance of mixed modality irradiations are examined.

Understanding the Mechanism(s) of Radiation Damage

Experiments involving mixtures of different modalities have largely been designed to answer the question as to how radiation damages subcellular structures, cells and whole organisms (Tyrrell, 1978). From a high linear energy transfer (LET) point of view, the most important of these are protocols or schedules aimed at following the induction, interaction and repair of what is operationally defined as sublethal damage. Such studies can contribute to our understanding of the role of sublethal and lethal lesions in cell killing (Joiner *et al.*, 1984).

In certain instances the true mechanisms involved in radiation damage can only be ascertained after exposing the biological system to mixed radiation fields. Some of the mechanisms involved may be obscured if only the biological response to a single modality is observed. For example Ngo *et al.* (1981) demonstrated that the single-hit inactivation process, as demonstrated by a simple exponential survival curve, does not exclude repair processes. In spite of their observation that neon ions exhibit an exponential dose-survival relationship and showed no or even "negative" repair between fractionated neon exposures, the combined effects of X-rays and neon ions proved to be

synergistic. Furthermore, mixed field exposures allow the investigator to compare inactivation mechanisms for different radiation modalities at a level of iso-dose, instead of at the conventional level of iso-effect. For example McNally *et al.* (1984) demonstrated that on a per gray basis neutrons are as effective as X-rays in causing sublethal damage.

For the theorist the study of mixed radiation effects is of interest because it provides important insights into inactivation mechanisms through observation of the interaction between radiations of different quality (Lam, 1987a). In order to explain the enhanced killing in mixed field irradiations, several biophysical models have been advanced. Inactivation models concerned with the physical and statistical nature of the initial energy deposition events can be extended to correlate the shape of the dose-effect curves directly with these events (Katz and Sharma, 1974; Zaider and Rossi, 1980; Zaider and Brenner, 1984). Some of the methods introduced to predict the combined effect of radiation mixtures have led to the development of new expressions that are incompatible with the physical ideas put forward by these authors. An example is the Lesion Additivity Model of Lam (1988a).

Radiation Protection

Investigations into the effect of mixed field exposures are of interest to radiation protection legislators for the purpose of risk estimation. Of particular importance are the radiobiological implications of mixed field radiation incidents. Understanding the physical basis for the biological response of mammalian cell systems to varying mixtures of neutrons and photons is of major importance, especially in relation to the peaceful uses of atomic energy where the potential radiation hazard is in the form of mixtures of gamma rays and neutrons (McNally *et al.*, 1985). Biological risk may increase in simultaneous neutron-gamma exposures over that expected from separate exposures (Higgins *et al.*, 1983). On the other hand, it has been suggested that the use of the conventional RBE approach to predict the combined effect of simultaneous exposures may lead to an overestimation of the risk estimate (Scott, 1983). It is therefore evident that obtaining realistic estimates of risks can lead to significant financial savings since the uncertainty in the estimates is translated into either more shielding or more stringent time constraints (Shimmerling and Curtis, 1989).

Consequence for Dose Estimation Using Biological Dosimetry

In cytogenetic dosimetry the dose absorbed by a worker in a radiation accident is most reliably estimated from calibration curves relating the chromosomal aberration frequency in lymphocytes to the physical dose. Such calibration curves do not exist for mixtures of different radiation modalities. Should synergistic interaction play a role in the total aberration frequency observed in lymphocytes then the dose will be overestimated.

Potential for Radiation Therapy

Clinical interest in different radiation modalities stems from a number of observations which have bearing on the physical aspects of dose delivery. For example, when megavoltage (42 MV) photons were used in conjunction with a charged particle beam, significant skin sparing was achieved (Curtis, 1976). Furthermore, it is known that the dose from a proton beam increases with depth and reaches a sharp maximum in the region of the Bragg peak. A mixture of photons and protons has been used to take advantage of the depth-dose profile provided by the charged particle beam as well as the skin sparing provided by the megavoltage photons (Suit *et al.*, 1975).

Pertinant to the present radiobiological study are variations in beam quality arising from changes in the γ-component with depth when a patient/phantom is irradiated with d(16)/Be neutrons. Higgens *et al.*, 1983 has addressed this problem in order to predict the effective doses to deep seated tumours.

Most normal tissues appear to be particularly sensitive to high-LET radiation (Cohen, 1986). "Diluting" a flux of neutrons with low-LET photons might well be beneficial to the normal tissue, especially the central nervous system. To minimize the risk to normal tissue, a model for determining the quality of a mixed radiation beam would be valuable. A reliable model for this purpose would need to include the interaction effects of different radiation types.

The efficacy of low-LET radiation may be limited in tumours by the radioresistance of clonogenic hypoxic cells and possibly cells in the G1 and S-phases. Conversely the efficacy of high-LET radiation is limited by the recovery of normal tissue (Raju and Jett, 1974). Also, since preferential sparing for late effects is not obtained by

fractionation of neutron dose (Gahbauer *et al.*, 1985) a mixture of high- and low-LET radiation might serve as a compromise. Moreover, mixed beam treatments will allow more patients to benefit from neutron therapy (Urano and Koike, 1980).

Mixed Modality Radiation as a General Phenomenon

Any single radiation modality ultimately becomes a mixture of low- and high-LET radiation (see below). Thus the mean physical dose absorbed by cells will consist of dose contributions from a spectrum of low- and high-LET radiations.

If we consider cyclotron-produced neutrons, then the secondary charged particles produced during tissue interaction include fast protons, slow protons and nuclear reaction products such as alpha particles and heavy recoil ions (Hall, 1988). The ionization densities along the tracks of each of these particles in the medium is different. Thus distinct dose effect relationships may be expected from each particle type. Essentially then, the energy deposited is that from a mixture of radiation types. Based upon statistical consideration alone, there is a high probability that after a dose of neutron radiation, a portion of the cells are inactivated as a result of interaction between different radiation types (Ngo *et al.*, 1988).

A similar argument holds true for X-rays or gamma rays. Following compton scattering, energetic electrons are likely to eject a substantial number of bound electrons from atoms along its path (Goodhead and Brenner, 1983), thereby essentially yielding a mixed modality beam.

Exposure of biological systems to mixed modality radiation should not only be seen as a special case to follow the action of radiation damage. It is a natural extension of split dose measurements employing only one type of radiation, and as Zaider and Rossi (1980) has pointed out the purpose is similar, namely to investigate the induction of sublethal damage and repair in cellular systems.

CHAPTER 2

PERSPECTIVES ON MIXED MODALITY RADIATION

Introduction

The current concept of the combined effect of mixed radiations is based upon the interaction of reparable damage. The literature is thus reviewed in terms of those factors that influence the induction and repair of sublethal radiation damage. These factors can be diverse in origin and include both the environment of the experimental cell system (*in vitro* or *in vivo*) and the physical character of the radiation. Examples of the latter relate to the types of radiation involved, their respective macrodose contributions and uniformity of energy depositions in the target cell population, i.e. the spectrum of microscopic ionization events involved (LET distribution). Temporal effects, i.e. dose rate and the time interval between sequential exposures, are also significant.

To understand the factors that can influence the outcome of mixed radiation exposures it is convenient to think in terms of an interaction function. That is, an expression that accounts for the additional damage, over and above that caused by the individual radiation types.

The method of calculation for the latter is shown in detail in the Appendix (Part 1) and is based on a linear-quadratic fit to the dose-response data. Biophysical considerations by Kellerer and Rossi (1972, 1978) and Chadwick and Leenhouts (1981) suggests that the linear term is proportional to radiation damage initiated by the interaction of sublesions in a single track (intratrack damage) whilst the quadratic term represents the effectiveness for induction of lethality through the accumulation of damage. The α and β parameters obtained from a polynomial fit is also included in other models that relate biological damage to the dose absorbed. Notably the lethal, potential lethal (LPL) unified repair model described by Curtis (1986) and the repair-misrepair (RMR) model of Tobias *et al.,* (1980). An example of an interaction function is that given by Zaider and Rossi (1980).

$$2\sqrt{\beta_n\ \beta_\gamma}\ D_n\ D_\gamma \qquad [1]$$

where β_n and β_γ are the respective quadratic coefficients that describe in part the effect of the neutron only and photon only radiation and D_n and D_γ are the neutron and photon doses in the mixture. A schematic representation of a mode of synergistic interaction is given by Leenhouts *et al.* (1986).

Expression [1] is an interference term that reflects the interaction between sublesions produced by the two radiation types and in geometrical terms represents a saddle-shaped quadratic surface called a paraboloid (Ager and Haynes, 1987). It is clear from expression [1] that the intertrack or β-component of radiation damage is central to the outcome of a combined modality exposure. The β-component of radiation injury has been associated with reparable damage and is related to the recovery ratio as follows,

$$RR = e^{2\beta D^2} \qquad [2]$$

where RR is the recovery ratio between split dose exposures (Stephens *et al.*, 1987, Steel and Peacock, 1989). RR is the ratio of damage observed following acute exposure to that measured from fractionated exposures seperated by time. Volkmer and Virsik-Peuchert (1990) further demonstrated the relationship between β-damage and repair. They compared the effects of single and split doses on dicentric frequencies in CHO cells. The response observed following split dose exposures was adequately predicted by using the same α-value estimated from the acute response but reducing the corresponding β-parameter by half. Therefore all factors influencing the latter will also be of consequence for the combined effect of different radiation modalities.

Particle Type and LET

The nature of radiation damage is determined by the radiation type and its LET. The latter does not necessarily define the former. For example, if the LET of a proton and α-particle beam is chosen to be the same, the two radiation types can still have different qualities that result in different biological effects (Belli *et al.*, 1992). Goodhead *et al.* (1992) demonstrated this further in a direct comparison between 1.2 MeV protons (23 keV/μm) and a 30 MeV α-particle beam (23 keV/μm). The protons were found to be more effective as regards cell inactivation by a factor of up to 1.6 compared with the α-particles. It is of interest to note on closer examination of these authors results that

the majority of experiments with different cell types showed a greater β-component for α-particle irradiations compared with the β-component determined from proton irradiations. Consequently on the basis of equation [1] it is likely that a higher level of interaction will occur when these α-particles are mixed with low-LET radiation than that expected from a proton-photon mixture.

Chapman *et al.* (1977) characterized the inactivation events produced in mammalian cells by helium and heavy ions. Here an increase in β-values is noted with an increase in LET. Unlike the α-component which diminishes beyond 100 - 150 keV/μm due to saturation effects, the β-component continues to increase. The increased β-values observed in the investigations performed by both Goodhead *et al.* (1992) and Chapman *et al.* (1977) have been explained on the basis of low-LET δ-rays which are found in the penumbra surrounding the primary particle track. δ-rays are formed when the primary particle interacts with a single atomic electron and the electron is ejected with a large amount of kinetic energy. Damage caused by this low-LET radiation is more likely to be repaired, hence the greater β-component.

This is understood in terms of the basic assumption that is made in the Theory of Dual Radiation Action (TDRA) which states that radiation produces sublesions that are proportional to the specific energy (Kellerer and Rossi 1972, 1978). Therefore one should find in principle more interaction with higher LET. The work of Bird *et al.* (1983) demonstrated this when they exposed synchronized mammalian cells to X-rays, deutrons (50 keV/μm) and helium ions (160 keV/μm). An enhanced interaction effect was observed when the LET of the priming dose was increased or the magnitude of the dose increased.

Dose Magnitude

The dose window in which biological effects for high-LET radiation can be quantified is relatively small because of the high RBE. Therefore in those situations where very high-LET radiation types form part of a mixture, the dose from the high-LET component will need to be comparatively small for an observable effect. For example Barendsen *et al.* (1960) combined the α-particles from ^{210}Po and X-rays when irradiating T1 kidney cells and found that the two radiation types acted independently. This is not surprising since the highest dose of α-particles (LET ~ 170 keV/μm) used in these experiments was only 1 Gy. Zaider and Rossi (1980) argued that under such conditions it will be difficult to detect interaction because the αD term dominates the

biological response and the βD^2 term becomes insignificant. Based on the interference term [1] no interaction can be expected.

Raju and Jett (1974) irradiated human kidney cells with a mixture of α-particles and X-rays and obtained results consistant with that of Barendsen (1960). In a later investigation with α-particles and X-rays, McNally *et al.* (1988) applied doses of up to 2.5 Gy to V-79 cells and found that α-particles were in fact capable of inducing damage that interacts with X-rays. Murthy *et al.* (1975) also observed interaction between ^{210}Po α-particles and ^{60}Co γ-rays in diploid yeast cells.

The linear nature of a dose-effect curve can also be ascribed to an increased radio-sensitivity of the biological system, even where the radiation involved is not classified as high LET. For example Marshall and Bianchi (1983) found no dose-rate effect for micronuclei induction in *Vicia faba* roots at low doses (7 - 20 cGy) of low-LET. Fractionation effects are however present at higher doses where the biological effects are dominated by the quadratic (β) term.

Irradiation Protocols

A principal factor in the above interaction processes is the time lapse between sequential doses of different radiation types. Zaider and Rossi (1980) and Zaider and Brenner (1984) described the recovery process as a function of time between dose increments. They define a reduction factor q(t), the magnitude of which is a function of time (t). This reduction factor only affects the quadratic component and is consistent with the interpretation of the yield of intertrack interaction. The Incomplete Repair Model of Thames (1985) makes use of a G-function to treat residual damage during fractionation or low dose-rate irradiations. The model leads to the following relationships

$$s = e^{-\alpha D - \beta G D^2} \qquad [3]$$

$$G = \frac{2}{(\mu t)^2}(\mu t - 1 + e^{-\mu t}) \qquad [4]$$

where α and β are parameters that correspond to those in the linear quadratic equation and μ is the time-constant for repair ($\mu = \ell n\, 2/T_{1/2}$).

In as much that the extent of interaction is directly dependent on the amount of sublethal damage, sublesion repair would decrease the observed effect. This could happen when there is a time lapse between sequential exposures and implies that simultaneous exposures should be more effective than sequential exposures. To this end Higgens *et al.* (1983) demonstrated that simultaneous exposures were more potent than sequential ones in V-79 cells bombarded with 14.7 MeV neutrons and ^{60}Co γ-rays. Brooks *et al.* (1990) exposed lung epithelial cells to simultaneous doses of α-particles and X-rays and measured both the surviving fraction and the frequency of micronuclei in these cells. Their observations suggested that combined exposures produced a larger radiation insult than the sum of the individual insults. Furthermore, they compared their results with those of McNally *et al.* (1984) who used sequential exposures of high- and low-LET radiation and found that the level of interaction was more pronounced. They attributed this to the use of simultaneous exposures. In contrast McNally *et al.* (1985) found no difference in the response of V-79 fibroblasts, whether the radiations (3.2 MeV neutrons and 140 kVp X-rays) were given simultaneously or sequentially.

Inherent Radiosensitivity of Cells

As the intrinsic radiosensitivity of cells increases, the dose response curve becomes more linear, i.e. the β-component appears to be less important. Cellular radiosensitivity can affect the interaction between two types of radiation. Gray and Read (1944) measured the growth rate of bean roots following the combined exposure to X-rays plus α-particles as well as γ-rays plus neutrons. They concluded that these high- and low-LET mixtures were strictly additive. Cells at the tips of bean roots are known to be highly sensitive to radiation. Also, Wolff *et al.* (1958) used 250 kVp X-rays and monoenergetic neutrons (14.1 MeV) to investigate the interaction of two-hit (exchange) chromosome aberrations in the sensitive meristematic cells of *Vicia faba.* Although they observed that the radiation-induced breaks from two X-ray doses could rejoin to form exchanges in proportion to the square of the total dose, no quantitatively determinable interaction occurred between the breaks induced by the neutrons and the X-rays. The aberration yield (dicentrics and rings) was simply the sum of that induced by each radiation type. Heddle (1965) also failed to determine interaction between neutrons and X-rays for chromosome aberrations in primary roots of Barley seeds. This was true, irrespective of whether neutrons or X-rays were given first.

In a series of split dose exposures to determine the recovery ratios of radiosensitive and radioresistant cell lines, Peacock *et al.* (1988) found that the recovery ratio is greatest in the most radiosensitive cell line. Thus on the basis of equation [2] a higher cellular radiosensitivity implies a greater β-component and consequently more interaction might be expected.

However, experimental observations by Ngo *et al.* (1988) showed just the opposite. They measured the syngergistic effects of Ne- or Ar-ions irradiation in combination with X-rays using V-79 cells at different stages of the cell cycle. The effectiveness of interaction damage was greatest in late-S phase cells which were most resistant to both of the radiation types.

Interaction and Exponential Survival Curves

Radiation damage in cells that exhibit an exponential dose response curve can adequately be described without a β-parameter. This would imply that no reparable damage is induced that can subsequently interact with other radiation induced damage. This does not necessarily mean that the survivors in these cases were unaffected by the radiation. Ngo *et al.* (1978) reported that the single-hit mechanism inferred from the exponential dose response curves for mammalian cells exposed to Ne-ions could mean that at least some of the surviving cells were hit. When Chinese hamster cells were irradiated with two doses of Bragg-peak Ne-ions 2.5 hours apart, a significant expression of "negative" repair is observed (Ngo *et al.* 1981). "Negative" repair occur when the combined affect of a radiation dose delivered in two fractions is larger compared to when the same dose is administered in a single exposure. However, the survival curve for cells irradiated with graded doses of X-rays shortly after a priming dose of Ne-ions showed a reduced shoulder. This was interpreted as indicating that the charged particles and X-rays each produced damage which interacted with one another. When the fractionation interval between Ne and X-ray exposure was increased, the interaction effect diminished, implying that even the high-LET induced damage could be repaired.

Tobias *et al.* (1982) observed a similar potentiation effect for a priming dose of Bragg peak Ne-ions that produce sublethal lesions which could interact with subsequent X-ray damage. "Negative" repair is not limited to Ne-ions. Magnien *et al.* (1981) reported an increased biological effectiveness for split dose neutrons (~16 MeV) delivered to protoplasts from a diploid *Nicotiana* species.

Influence of Oxygen

The oxygen content of an irradiated cell can influence the degree of interaction between different radiation types. The level of oxygenation and its effect on repair have been studied by various investigators using one type of radiation only. For example Taylor and Brown (1987) did not show repair in C3H 10T1/2 cells irradiated under hypoxic conditions. In contrast, Ling *et al.* (1984) observed a dose rate effect under conditions of extreme hypoxia, implying repair of sublethal damage.

The importance of oxygen is further highlighted by the study of McNally *et al.* (1985). They observed that interaction between neutron and X-ray damage in V-79 cells was particularly marked under hypoxic conditions.

Effect of *In Vivo* Mixed Radiation Schedules

Although most of the studies cited in the previous sections of this chapter contain strong evidence for interaction between high and low-LET radiation, the cell types used in these investigations were irradiated *in vitro*. This section summarizes studies relating the effects of mixed modality exposures to normal tissues and tumours.

Hendry *et al.* (1976) irradiated mouse intestine using a fractionation schedule of 14 MeV neutrons and X-rays on alternate days and found that the combined effect of the two radiation types was additive. Irradiating gut tissue with d(16)/Be neutrons and 250 kV X-rays, but delivering the radiation within minutes or after a 3-4 hour interval, Hornsey *et al.* (1977) reported interaction between these radiation types. However, if the X-ray and neutron doses were separated long enough in time to allow full repair of sublethal injury, then the combined effect was additive. Their results further showed that stem cells surviving the first dose of radiation had accumulated the same amount of recoverable sublethal damage, regardless of whether the first dose was neutrons or X-rays. Also, the rate at which the sublethal damage was repaired was found to be the same, regardless of the initial radiation modality.

In the study of Nelson *et al.* (1975) where mouse skin and C3HBA tumours were irradiated with d(21)/Be neutrons on each of 2 days and followed by 3 daily fractions of 200 kVp X-rays, a small amount of interaction was observed. A similar finding was made by Rasey *et al.* (1977) for EMT-6 murine tumours. Both investigations suggest that some long lived lesions were unrepaired after one day. Joiner *et al.* (1984)

corroborated these findings when he measured skin reactions of the mouse foot. Using simultaneous exposures of 140 kVp X-rays and d(4)/Be neutrons full interaction was seen. Again, when the irradiations were separated by 24 hours the level of interaction decreased, but did not disappear completely.

On the other hand Ando *et al.* (1984) was not able to show interaction between d(30)/Be neutrons and ^{60}Co γ-rays in mouse fibrosarcomas when daily fractions were given as n-γ-γ-γ-n. Also, relatively little interaction was observed from growth delay measurements following split doses of neon ions and X-rays in rat rhabdomyosarcomas (Tenforde *et al.* 1989). Their data indicated that the combined effect of these modalities approached simple additivity, even if the time interval between split dose irradiations was as short as 30 minutes.

Mixed Modality Radiations and Therapeutic Gain

A number of investigators have studied the response of mixed radiation modalities *in vivo*, the aim being to determine if mixed modalities can result in therapeutic gain. The rationale was that if the therapeutic benefit of neutrons was to be gained through greater killing of hypoxic tumour cells, mixed-fractionation schemes might be beneficial, provided the neutron doses were administered at the beginning of the fractionated course. Subsequent reoxygenation would then make the tumour more amenable to conventional radiation treatment.

Rasey *et al.* (1977) reported that two daily fractions of d(21.5)/Be neutrons followed by three daily fractions of 250 kVp X-rays resulted in a therapeutic gain factor of 1.2 for EMT-6 tumours in mice, compared to five fractions of neutrons only. In contrast, Urano and Koike (1980) showed no therapeutic gain using mixed-beam treatments for spontaneous squamous cell carcinoma in mice. In this situation one daily fraction of neutrons [d(30)Be] was followed by three daily fractions of X-rays (200 kVp) and then a fraction of neutrons on day five.

Carl *et al.* (1987 a) followed the effect of mixed fractionation schedules of 240 kVp X-rays and d(4)/Be neutrons on growth delay of SaF tumours and skin reactions in mice. Five daily fractions of X-rays, neutrons and mixtures (n-n-X-X-X, X-X-X-n-n or n-X-X-X-n) were given to clamped and unclamped tumours and also to skin. The clamping ensured uniform oxygenation of both tumour and normal tissue. Under clamped conditions the same effect was observed for all three mixed-schedules. When

the tissue was unclamped the n-n-X-X-X protocol proved to be more efficient than the other two in delaying tumour growth.

The sequence of neutron and photon irradiations appears to be less important for rapidly reoxygenating tumours. This is illustrated in the findings of Nelson *et al.* (1975) where the responses of C3HBA mouse tumours and skin to mixtures of neutrons ($\bar{E}_n \sim 8$ MeV) and X-rays were followed. Both n-n-X-X-X and n-X-X-X-n fractionation schemes resulted in a therapeutic gain factor of 1.1.

Even when the neutron-photon mixtures were given as single doses a therapeutic gain could still be demonstrated. Carl *et al.* (1987b) irradiated SaF tumours in mice with different proportions of 240 kVp X-rays in a neutron beam ($\bar{E}_n \sim 6$ MeV). An improvement in the therapeutic gain was noted when the photon component in the mixture was kept below 32%.

Mixed Neutron-Photon Irradiation In Clinical Practice

Part of the reason for using neutrons in clinical practice is because they induce more extensive irreparable damage in cells compared with conventional radiotherapy. This principle holds promise for tumour types that recover during fractionated photon irradiations to the same extent as late responding normal tissue, eg. melanomas and soft tissue sarcomas (Thames *et al.* 1990). The irreparable damage caused by neutrons is unfortunately also induced in normal cells and the RBE changes faster with dose per fraction for late than acutely-reacting tissue. This results in more severe late effects in some normal tissue compared to photons (Halpern *et al.*, 1990).

By including photons in a therapeutic course with neutrons, the late effects associated with neutron only therapy can be minimized. This was demonstrated in a study by Maor *et al.* (1983) who showed that mixed-schedule irradiations were superior mainly because of a significantly lower complication rate. Furthermore, the complication rate in patients receiving neutrons only and ^{60}Co only treatments were significantly higher compared to that in patients treated with a mixture of neutrons and photons. Engenhart *et al.* (1987) employed 14 MeV neutrons in conjunction with conventional photon therapy. In spite of using relatively high neutron doses they observed no side effects. Also, following a photon-neutron schedule Franke and Schmidt (1985) observed no necrosis in normal tissues.

Although some tumours re-oxygenate during X-ray treatment and thus may not benefit from high LET radiation (Bewley and Fowler 1972), bulky tumours such as pancreatic tumours re-oxygenate to a lesser extent and remain resistant to photon therapy (Bukowski *et al.* 1982). Therefore neutrons in combination with photon treatments may theoretically produce a therapeutic gain. To this end Maruyama *et al.* (1988) reported that ^{252}Cf neutron brachytherapy combined with X-rays was the best schedule for the control of bulky human cervical cancers. They also reported that ^{252}Cf treatment before X-rays was more effective than after.

In contrast, Duncan *et al.* (1986) using d(15)/Be neutrons in combination with photons found no advantage in a randomized trial of mixed fractionation schedules over conventional therapy for astrocytomas. Results from patients treated with mixed beams for advanced head and neck cancers were inconclusive (Griffin *et al.* 1989). Mixed beam treatments proved to be more effective than photons only in controlling tumours located in nodal sites. The reverse was true in the case of patients who had no lymph node involvement.

One rationale for high-LET therapy is that there is less variation of cell sensitivity with phases of the mitotic cycle. Battermann (1981) indicated an increased RBE with tumours that take longer to double their volume. This principle has clinical support. A protocol comparing mixed neutron-photon treatments at different facilities in the USA clearly demonstrated an advantage for adenocarcinoma of the prostate (Laramore *et al.* 1985). The overall five year survival rate for patients with this slow growing tumour was 62% following neutron-photon treatment, whereas only 35% survived in the photon arm of the trial. After seven years the local failure rate was 20% in the mixed beam arm compared to 70% for photons only.

The trouble with neutrons is summarized by Scalliet (1991) who concluded that enhanced tissue sensitivity to neutrons and physical factors such as geometry and dose distribution have hindered an unambigious demonstration of the clinical advantage of fast neutrons. In an overview of the applications of fast neutrons in cancer therapy Wambersie *et al.* (1984) concluded that the advantage of combining neutrons and photons is consistant with the radiobiological principle of a reduced differential effect with increasing LET.

CHAPTER 3

THE INTERPRETATION OF MIXED FIELD DATA FUNDAMENTAL CONSIDERATIONS

Once the dose-effect or dose-response relationship for a mixture of neutrons and photons has been established, it is important to view the combined effects against predictions based on the response of the individual radiation types. This enables one to establish if the radiation damage from the constituents in the mixture act independently, or if some kind of interaction is involved. Also, it is the first step in predicting the combined effect of different radiation mixtures. By comparing the combined effect with such predictions, insights into the mechanism of radiation damage is obtained. This in turn could have implications for therapeutic gain. In this Chapter the criteria for analyzing combined-effect data are discussed.

Introduction

From the literature it is apparent that investigations of combined effects of different agents are subject to confused terminology. Many terms are used when describing combined exposures, like 'synergism', 'supra-additivity', 'potentiation', 'interference' etc. Sometimes the same term is used in an entirely different sense by different authors. Sub-classification and redefinitions of criteria that vary from one author to another further complicates the interpretation of combined effect data (Valeriote and Lin, 1975). Fortunately excellent reviews on the subject are available (Tyrrell, 1978; Berenbaum, 1981). Although consistent terminology and criteria would be highly desirable, the discord is so great that it is unlikely that this will be achieved. The aim of this chapter is to define the criteria used in the present work and to point out some of the shortcomings of these concepts.

Interaction of Radiation Damage

When different radiation types act independently of one another, neither of the radiation types in the mixture influences the effect produced by the other radiation. It is understood that both modalities cause a particular effect, e.g. cell death, induction of micronuclei, etc. Interaction occurs when either of the radiation types modifies the extent to which the other produces an effect (Rothman, 1974; Zaider, 1990). In

elementary form the combined effect of a neutron-photon mixture is the sum of three parts, namely (a) the independent damage from the neutrons, (b) the independent damage from the photons and (c) additional damage as a result of an interaction process between them. The latter is sometimes expressed in terms of an interaction function which is based on the parameters of the particular model that describes the response to the individual radiations in the mixture.

For example, in terms of the Molecular Theory of Radiation Biology (Chadwick and Leenhouts, 1981) the effect (E) on cells after a series of exposures to neutrons only and photons only is respectively given by:

$$E(D_n) = \alpha_n D_n + \beta_n D_n^2 \qquad [1]$$

and

$$E(D_\gamma) = \alpha_\gamma D_\gamma + \beta_\gamma D_\gamma^2 \qquad [2]$$

The independent action of a combined exposure to a fractional dose of neutrons (d_n) and a fractional dose of photons (d_γ) in the mixture is given by:

$$E(d_n + d_\gamma) = \alpha_n d_n + \beta_n d_n^2 + \alpha_\gamma d_\gamma + \beta_\gamma d_\gamma^2 \qquad [3]$$

When the observed effects from a combined exposure exceeds this independent prediction, an interaction function must be added to account for the extra damage resulting from the interaction. The following models and procedures have been proposed to deduce or predict the level of interaction.

The Zaider-Rossi Model

Zaider and Rossi (1980) used microdosimetric arguments to formulate an interaction function

$$2\sqrt{\beta_n \beta_\gamma}\, d_n d_\gamma \qquad [4]$$

that will explain and predict the shape of a dose-effect curve for cells exposed sequentially or similtaneously to different types of radiation.

The β-parameters in this function represent the interaction of sublethal events as formulated in the TDRA (Kellerer and Rossi, 1978) and reflect the accumulation of sublethal damage produced by each of the radiation types (Freeman *et al.*, 1983). The interference term [4] implies that the order in which different radiation types are applied is irrelevant. However, any time interval between exposures long enough to allow significant repair of the sublethal damage induced by the first radiation modality, will affect the magnitude of interaction with the second. The Zaider-Rossi model accounts for this by incorporating a reduction factor (q) as follows,

$$E = \alpha_n D_n + \alpha_\gamma D_\gamma + q(t_n)\beta_n D_n^2 + q(t_\gamma)\beta_\gamma D_\gamma^2 + 2q_{n\gamma}(t_n, t_\gamma, T)\sqrt{\beta_n \beta_\gamma}\, D_n D_\gamma \quad [5]$$

where $$q(t_i) = \frac{2t_0}{t_i} - \frac{2t_0^2}{t_i^2}\left\{1 - \exp\left[-\frac{t_i}{t_0}\right]\right\} \quad i = n, \gamma$$

and $$q_{n\gamma}(t_n, t_\gamma, T) = \frac{t_0^2}{t_n t_\gamma}\left[\exp\left[-\frac{T}{t_0}\right]\left\{1 - \exp\left[-\frac{t_n}{t_0}\right]\right\}\left\{1 - \exp\left[-\frac{t_\gamma}{t_0}\right]\right\}\right]$$

and $$t_0 = \left[\frac{\ell n 2}{T_{1/2}}\right]^{-1}.$$

T is the time between irradiations, t_i is the irradiation time of radiation i and t_0 is the time constant for recovery of the cell type in question. This model has recently been extended to account for partially or completely simultaneous irradiations (Suzuki, 1993).

The consequence of repair becomes more important as a larger initial dose of high-LET radiation is delivered. This might lead to an overestimation of the extent of interaction. For example, Bird *et al.* (1983) found that the Zaider-Rossi model underestimates the surviving fraction of cells exposed sequentially to a priming dose of helium ions (96 keV/μm) followed by X-rays. Such a *saturation* phenomenon was however not observed by McNally *et al.* (1984) who irradiated cells sequentially with a priming dose of 3.2 MeV neutrons and subsequent doses of X-rays. The Zaider-Rossi model remained valid, even when a relatively high priming dose of neutrons was used, that is a neutron dose resulting in a surviving fraction of 10% or less. On the other hand, experimental data reported by Musada (1970) and analyzed by Scott (1983) using expression [4] indicated contrary effects for cells exposed to 14 MeV neutrons and then to X-rays. However, when the exposure sequence was reversed the Zaider-Rossi model adequately predicted the experimental observations.

The simplicity of the interaction function for sequential exposures delivered in quick succession makes the Zaider-Rossi model easy to use in such cases. It has also been reformulated for simultaneous exposures using the dose rates of the radiation modalities in the mixture (Zaider and Brenner, 1984). Again, due to damage repair, a reduction in the intertrack term was required when the dose rates were low, and the time needed to deliver a dose was large with respect to the characteristic repair time of the cell type in question. In so doing, Zaider and Brenner (1984) successfully predicted the surviving fractions obtained by Higgins *et al.* (1983) who exposed V-79 cells simultaneously to low dose rates of 14.8 MeV neutrons (5 cGy/min) and ^{60}Co γ-rays (0.08 cGy/min). At higher dose rates the reduction term can be omitted. Zaider (1990) demonstrated this when he successfully predicted the surviving fractions of cells reported by McNally *et al.* (1985). In this instance various mixtures of neutrons and photons were applied simultaneously at dose rates between 15 and 45 cGy/min.

The major disadvantage with the Zaider-Rossi model is its reliance on good estimations of β-values, calculated from survival curves obtained from the individual irradiations. The uncertainty in this parameter is generally large, especially at low levels of radiation damage (Watts *et al.*, 1986). It is also difficult to determine β-values accurately when survival curves are nearly exponential. Barendsen (1990) has estimated the uncertainty in β-values to be as large as 50%.

Evaluating Interaction

In its simplest form positive interaction or synergy occurs when the combined response is greater than "expected", and negative interaction or antagonism occurs when the response is less than "expected". Berenbaum (1985) defines interaction as that when the combination of agents (radiation modalities) produces effects that are greater or smaller than what can be expected on the basis of the dose-effect relationships for the individual radiation types. Most of the confusion in terminology arises when different authors compute different expectations from a combination of agents.

Some definitions are intuitive rather than formal. A dictionary definition of synergism is: "an effect greater than the sum of the effects of each agency acting alone" (Aberchrombie *et al.*, 1973). Berenbaum (1981) pointed out that such a definition

implies the existence of a frame of reference but does not state what that frame of reference is, or how it should be calculated.

The concept of additive action is formally defined in ICRU Report No. 30 (1979) and is a frame of reference which is frequently encountered in publications. It is used when the combined effect equals the simple addition of individual effects. Supra-additivity or synergism prevails when the combined effect exceeds this addition and antagonism or sub-additivity when it is smaller (Steel and Peckham, 1979).

Isobolograms

In order to calculate a frame of reference required for the concept of additivity the dose-response relationships for both neutrons only and photons only are needed. From the individual responses an iso-effect curve, known as an isobologram is constructed. The method of construction is described by Streffer and Müller (1987). An isobologram is a line or a curve on which each point represents a coordinate of doses (neutrons, photons) that together will produce a specific level of effect. These dose combinations are termed isoboles. It is akin to an iso-effect curve, where each point (isobole) on the line indicates the dose combination that produces a specific level of effect.

Complications with Isobolograms

An isobologram is a single straight line only when both the dose-response curves used in its construction are also straight lines, e.g. the exponential survival curves from very high-LET radiations. Instances where the cellular response to both neutrons and photons follows a simple exponential route are extremely rare. In fact it is more plausible that more than one ionizing particle is required to destroy a target, that there is more than one critical target per cell and that cell mechanisms repair the damage. Under these conditions the curve is not purely exponential but has a shoulder (Berenbaum 1981). Where either of the dose response curves deviates from linearity, two options exist for calculating an iso-effect curve (Fig. 1).

The first option is when the effects of a dose of neutrons and a dose of photons are added in a hetero–additivity fashion, i.e. it is assumed that the two radiation types cause cell killing by different mechanisms. Under this assumption the coordinate of a point on the isobologram is represented by a dose of neutrons and a dose of photons, the effects of which when added together will produce the chosen level of iso-effect (upper curve in

Fig. 1). Because the mechanisms of damage are considered to be different for the two radiation types, the level of effect induced by each radiation type is independent from the other. This approach is the same as assuming that no interaction takes place between the damage from the individual radiations.

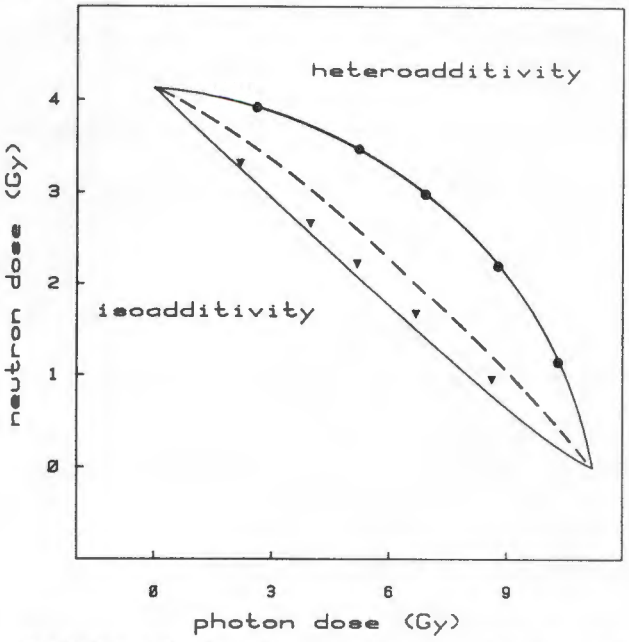

Figure 1: *Envelope of additivity calculated from dose–response curves that closely resemble that of the neutrons and ^{60}Co γ–rays used. Dashed line is an isobologram calculated for a photon followed by a neutron dose sequence and the solid line is calculated assuming that the neutron dose was given first. Solid circles represent isoboles assuming no interaction between neutron and photon damage. Triangles are isoboles calculated assuming interaction at a level predicted by the Zaider-Rossi (1980) model.*

If two radiation modalities are considered to have a similar mechanism for causing the damage, the interaction of damage between the individual radiations affects the dose combinations that will cause an iso-effect. In these calculations, known as the iso–additivity approach, the additional dose required from the second modality to reach the selected level of effect is lower (lower part in Fig. 1). This is a direct result of the curvature of the individual dose effect curves (Steel and Peckham, 1979).

The area between the hetero–additivity and iso–additivity isoboles constitutes the envelope of additivity. A combination of agents interact synergistically when the experimental dose combination required to reach the chosen level is small enough to fall below the envelope of additivity. If the dose pair falls inside the envelope, their effects combine in an additive fashion, and when they are above the envelope the interaction is considered antagonistic. Both high- and low-LET radiations produce lesions in the DNA i.e. within the same cellular target. For this reason any interaction between neutrons and photons can only be classified as synergistic if the experimental dose combination falls below the iso–additivity isobologram. On the other hand, if a source of high-LET radiation shows a true exponential surviving curve, the mechanism of cell

death can be considered as being different from that of radiations producing shouldered survival curves (Tyrrell, 1978). In this instance the synergistic interaction is anything below the hetero–additivity curve.

Because the curvature of neutron and photon dose-effect curves differ, the isobologram is dependent on the sequence of doses used in its construction (Redpath, 1980). This is also shown in Fig. 1. The dashed line is an iso–additive isobologram calculated for a photon followed by a neutron dose sequence, whilst the solid line is calculated from the same single dose effect curves but assuming that the neutron dose was given first. The dose sequence does not affect the hetero–additivity isoboles but the two iso–additive possibilities pose a dilemma. Should an experimental observation fall inside these lines, apposing conclusions can be drawn from the same data set, i.e. the combined effect is either synergistic or additive, depending on which isobologram is used as the frame of reference. Ngo *et al.* (1981), using Ne-ions and X-rays, experienced this dilemma. The combined effects are classified as additive if the neon exposure precedes X-rays and synergistic if X-rays precede the Ne radiation.

The Additive Damage Model

Scott (1983 and 1984) extended the concept of additive action to develop the Additive Damage model (AD). Scott used the equivalent dose concept, as employed in RBE calculations, to account for the combined effect of different cytotoxicants.

As with the Zaider-Rossi model, the combined effect of two radiation types is based upon the evaluation of an interaction function. Scott (1983) referred to this as the hazard function (h_s). In the Additive Damage Model the interaction function for a sequential exposure of photons followed be neutrons is given by,

$$h_s(D_\gamma,D_n) = -\alpha_n D_n + \sqrt{\alpha_n^2 D_n^2 + 4\beta_n D_n^2 \alpha_\gamma D_\gamma + 2(\beta_\gamma\beta_n)^{\frac{1}{2}} D_\gamma D_n} \quad [6]$$

When the sequence is reversed, that is neutrons followed by photons, the subscripts n and γ in expression [6] are interchanged. Unlike in the Zaider-Rossi model, the Additive Damage model predicts different composite survivals for cells exposed to different sequences of neutrons and photons. A neutron plus photon exposure is the most potent combination, followed by a simultaneous exposure, whilst photons followed by neutrons is the least effective (Scott, 1983). This is in contrast to the method of dose additivity proposed by Higgins *et al.* (1983) which does not discriminate between different sequences.

Simultaneous exposures are treated as if the additive damage is induced by a large number of very small doses of neutrons and photons given in repeated sequence. If small iso–effective dose intervals are used between a dose D and a dose D + ΔD, then the ordering of radiation types becomes unimportant. This is because a survival curve of any form is virtually linear between small dose increments.

It is important to note that apart from using the lethal component (α-parameter) of cell killing, the Additive Damage model also incorporates the entire interference term of the Zaider-Rossi model [4] in its interaction function. For a given dose and neutron-photon mixture, the level of interaction predicted by the Zaider-Rossi model lies somewhere between the simultaneous and the photon plus neutron combination predicted by the Additivity Damage model.

The Lesion Additivity Model

Because the shape of individual dose response relationships has such a profound effect on the complexity of the isobologram, definitive conclusions on synergy are sometimes prevented due to conceptual problems. For example, Tsai *et al.* (1989) reported a lack of *in vitro* synergy between a combination of anti cancer drugs that previously showed therapeutic synergy *in vivo*. They preferred to describe the combined effect of the drugs as a "spatial cooperation", thus introducing yet another term. These and other authors, when faced with the ambiguity of isobolograms, resort to the statement made by Loewe (1953), namely that synergy is only an imaginary magnitude devoid of a basis of reference.

To overcome the conceptual problems of interpretation, Berenbaum (1981) reclassified synergism and antagonism based on the concept of *zero–interaction.* By defining zero-interaction as the interaction between lesions produced by the same agent, a *linear* isobologram can be constructed such that the combined effect of different agents in a mixture can be interpreted unequivocally.

A linear isobologram is based on the observation that when an agent is mixed with itself, the isobologram at any level of effect is always a straight line. This is true for a sham "combination" of various doses of the same agent with a dose-effect curve of any geometric form. A combination of different agents with different dose-effect relationships is assumed to behave similarly. In fact, Berenbaum (1985) has shown rigorously that when an effect of a particular magnitude is produced by a combination of

n agents, the dose coordinates of individual doses representing that combination in n-dimensional space lies in the same (n-1) dimensional hyperplane as those representing other dose combinations iso-effective with it. Iso-effective amounts of the individual agents also lie in the same plane. For a combination of neutrons and photons ($n = 2$) the zero-interacting combination lies in a hyperplane with a dimension of n - 1, i.e. a straight line.

Zero-interaction does not mean that two agents do not interact with each other (non-interaction). Nor is it equivalent to the term "zero interaction" used by Tyrrell (1978), which essentially refers to independent action. In a linear isobologram zero-interaction prevails when the combination of different agents behave exactly as expected and can be calculated as follows:

$$\frac{D_n}{D_N} + \frac{D_\gamma}{D_\Gamma} = I \qquad [7]$$

where D_n and D_γ are the doses of the radiation components in a mixture required to produce a certain level of effect and D_N and D_Γ are the radiation doses that when acting by themselves, produce the same level of effect. I is an index for interaction. $I = 1$ for a level of zero-interaction, $I < 1$ for synergistic interactions and $I > 1$ when the combined effect of two agents act antagonistically.

Synergistic interactions bends the straight line presented by equation [7] so that the isoboles shows upward concavity. Antagonistic interaction result in isoboles showing downward concavity.

Lam (1987a) used this concept to develop the Lesion Additivity Model (LAM). He postulated that in the chain of radiation events the different lesions produced by different types of radiations in a mixture, although they might be functionally different at first, eventually reach a pool of common intermediate lesions. At this point and thereafter, the effects produced by each radiation type are indistinguishable and the combined effect is therefore additive. Using a mechanistic framework based on the concept of common intermediate lesions, Lam (1989a) showed that two agents that have no common intermediate lesion in their action will behave in a non-interactive (independent) manner. Because the physical interaction of different radiation types is too rapid to be recognized by the cell, the interpretation of the concept of common lesions is in a sense

similar to the cell inactivation models of Tobias *et al.* (1980) that separate the early physical stages from the biological stage of radiation action (Lam, 1988a).

Lam (1987a) showed that equation [7] can be rewritten as,

$$\frac{1}{D} = \frac{f_n}{D_N} + \frac{f_\gamma}{D_\Gamma} \qquad [8]$$

where $D = (D_n + D_\gamma)$ is the total dose in a neutron-photon mixture, $f_n = D_n/D$ and $f_\gamma = D_\gamma/D$.

Lam (1987b) used the model to predict the combined effect of different high- and low-LET radiation types and showed that the index of interaction (I) is useful to calculate multilevel linear isobolograms, i.e. at different levels of effect. Predicting the effects of a 50% mixture of Ne-ions and X-rays in V-79 cells measured by Ngo *et al.* (1981), Lam calculated I values that were close to the theoretical value of unity for a range of surviving fractions. Some deviations are however noted for surviving fractions above 0.2 and below 0.005.

The Lesion Additivity Models also satisfactorily predicted the experimental results of Railton *et al.* (1975) who used neutrons and γ-rays. Of particular interest is that the Lesion Additivity Model conforms to various mixed-field combinations where the survival curve of the the high-LET component by itself is either shouldered or exponential. The concept of zero-interaction is also consistent with that of independent action where no interaction between radiation types was observed, for example the α-particle/X-ray data of Barendsen *et al.* (1960).

Linear isobolograms were also applied to calculate and predict satisfactorily the variations in RBE and OER for mixed radiations with different high- and low-LET dose components (Lam 1987b).

From empirical results of radiobiological experiments using mixtures of radiations of different qualities, Lam (1989b, 1990a) showed that the biologically effective doses were linearly additive in a mixture. Thus in a similar way to physical doses they can be used in algorithms for treatment planning, for example pion treatment planning (Lam 1990b). Also, the lesion additivity concept provides theoretical support for the

arbitrary definitions of dose equivalent and average quality factor in radiation protection (Lam 1988b).

A principle feature of the Lesion Additivity model is that it does not rely on a knowledge of the mechanism of interaction. The concept of zero-interaction leading to a linear isobologram makes it the only method that can be used universally, irrespective of what is known or assumed about the mechanism of action by an agent (Berenbaum 1991). In fact, should the mechanism of action of different radiation types be completely understood, then the effect of a combination would eventually be shown to be precisely what was "expected". Under such idealistic conditions the combined effect of different radiation types could never become synergistic.

Interaction and Non-Stochastic Effects

The evaluation of interaction between different radiations is especially problematic when a change in the magnitude of an effect using a non-stochastic endpoint is measured as a function of dose, for example the frequency of micronuclei in a cell. Unlike a stochastic endpoint (eg. cell survival) where the probability of an effect (eg. cell death) is followed, the establishment of synergy from non-stochastic endpoints require more information than the individual dose effect relationships. Zaider (1990) demonstrated this by means of a hypothetical experiment in which the number of neoplastic transformations were observed. He showed that the frequency of foci from a mixture of agents could be classified either as the result of a synergistic or antagonistic interaction, depending on the number of cells that were available for transformation. The same dilemma arises with an analysis of the number of chromosome aberrations in a cells. Synergy can only be establish if the maximum number of aberrations possible per cell is known. It is probably impossible to obtain this information.

The level of synergy predicted by the LAM and the Zaider-Rossi interaction function proved to be very similar provided that a small but significant quadratic component was assigned to the individual radiation types.

CHAPTER 4

PHYSICAL DOSIMETRY

Introduction

In the investigations that follow a biological effect is correlated with a radiation dose that is delivered to the biological system in question, and in so doing a unique dose-effect or dose-response relationship is established. To quantify this affinity a biophysical model is adopted, mostly the linear-quadratic (L-Q) model in the present study, and it is the uncertainties surrounding the absorbed dose and the observed effect that will largely contribute to the uncertainties assigned the constants describing the L-Q relationship. The accuracy with which the desired dose is delivered to the biological sample may be optimized by using accepted dosimetric methods and recommended protocols. This is necessary not only for testing a hypothesis or model but ensures intercomparability with other published studies. A general overview for the dosimetry of an external neutron beam is given in ICRU Report 26 (1977) and ICRU Report 30 (1979). The former has recently been revised ICRU Report 45 (1989).

Dosimetric Concepts and Methods

The evaluation of neutron dose is complicated by the fact that the generated radiation field is invariably contaminated with a measurable photon component. As the RBE of the two radiation types differ considerably, individual dose assessments are needed to determine the nature of the mixed radiation field. Whilst microdosimetric techniques will yield both the neutron (D_n) and photon (D_γ) dose components from a single measurement, two observations using dosimeters with different neutron sensitivities are required when conventional macrodosimetric methods are applied.

In these investigations a tissue equivalent (TE) ionization chamber flushed with TE gas was used in conjunction with a Geiger-Müller (GM) counter, the TE chamber being equally sensitive to both neutrons and photons and the non-hydrogenous GM counter fairly transparent but not entirely insensitive to neutrons. In a mixed radiation field the approximate responses of the instruments are given by R'_T and R'_U (the quotients of the

readings of the two dosimeters in the same mixed field relative to their sensitivities to the gamma rays used for calibration):

$$R'_T = R_T \cdot \alpha_T = D_n + D_\gamma$$

$$R'_U = R_U \cdot \alpha_U = D_\gamma + k_U D_n$$

where R_T and R_U are the noted responses for the hydrogenous (T) and non-hydrogenous (U) detectors, α_T and α_U the respective response functions (expressed in Gy C^{-1} and Gy $count^{-1}$) and k_U the neutron sensitivity of the GM counter. The latter is determined experimentally in the specified radiation field.

Alternative exposures of the two dosimeters to the mixed field provides a unique solution for D_N amd D_γ;

$$D_n = \frac{R'_T - R'_U}{1 - k_U} \quad \text{and} \quad D_\gamma = \frac{R'_U - k_U R'_T}{1 - k_U}$$

Numerous corrections need be applied to accurately determine the tissue absorbed dose at a reference point in the radiation field and the compositional discrepancies between tissue and the Shonka A-150 plastic used as TE wall material must also be accounted for. These are fully discussed in a comprehensive review paper (Broerse *et al.*, 1985) and were implemented using the protocol adopted at the NAC for neutron exposures (Mijhneer *et al.*, 1987).

Radiation Facilities and Conditions for Exposure

Neutron irradiations of the biological systems used in the study were performed at two NAC centres. At the cyclotron located in Pretoria fast neutrons were generated via the $^{9}Be(d,n)^{10}B$ reaction using a thick target (Hough and Binns, 1987). For 16 MeV deuterons a mean neutron energy of 6.3 MeV was deduced from the measured energy spectrum (Binns and Hough 1987). Protons of energy 66 MeV are used to generate a more penetrating neutron beam at the Faure therapy facility where the $^{9}Be(p,n)^{9}B$ reaction is utilized (Jones *et al.*, 1988). The spectral characteristics of this beam have recently been evaluated and a mean neutron energy of 30.8 MeV determined (Jones *et al.*, 1992). The different nuclear reactions and particle energies used provided

neutron fields of differing quality that are aptly described in terms of microdose distributions measured with a Rossi-type TE proportional counter (Binns and Hough, 1988).

To ensure charged particle equilibrium a hydrogenous material (Shonka A-150 plastic or nylon type 6) was used as build-up, with the front surface positioned at SSD. Simultaneous and sequential mixed field exposures at the Pretoria cyclotron were performed with the tandem facility shown in Figure 1. Conditions at the Faure therapy centre only permitted sequential irradiations as the ^{60}Co photon unit was located in the adjacent unused therapy vault. For all neutron irradiations the integrated beam current from transmission chambers positioned downstream from the Be targets served as neutron monitor. Photon doses were delivered according to predetermined exposure times and where necessary Pb absorbers were used to realize diminished dose rates. It is assumed that Pb absorbers have no effect on the radiation quality of the ^{60}Co source measurable with chemical and biological systems.

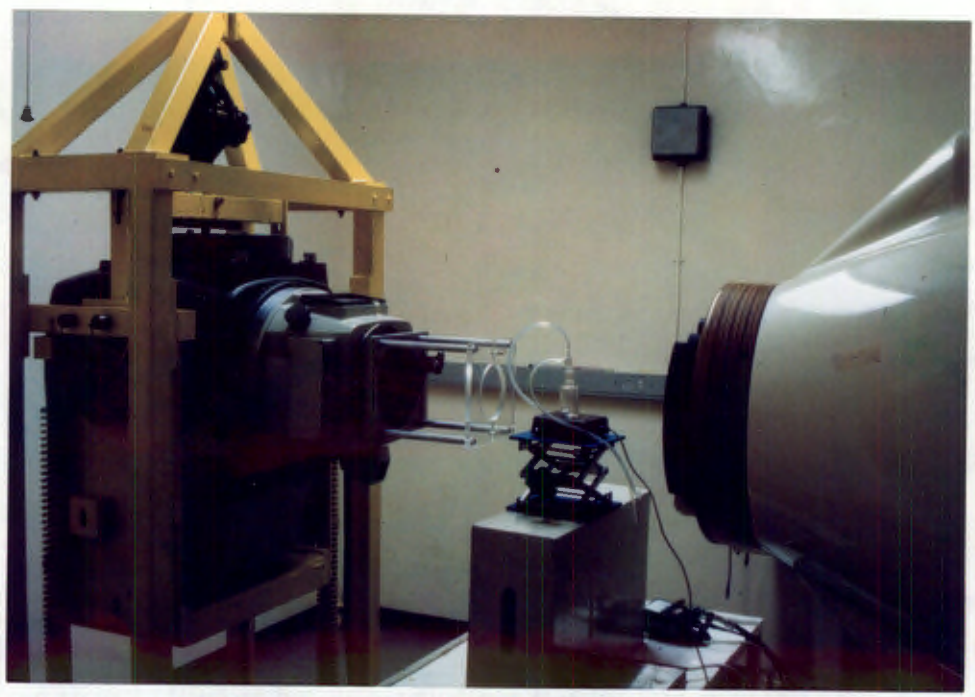

Figure 1: *Moveable trolley for supporting the experimental ^{60}Co unit. The shown source orientation is that for a tandem irradiation where the photon and neutron radiation fields have a common central axis.*

CHAPTER 5

CHEMICAL DOSIMETRY

Introduction

During the course of the investigations presented in this thesis it became clear that dosimetry performed with ionization chambers was inadequate for certain irradiation conditions. This was especially true when the irradiated object presented unusual geometry or when the absorbed dose needed to be estimated in a small volume. To accommodate these conditions, measurements were performed to determine the radiosensitivity of a suitable chemical dosimeter. A further reason for making use of a chemical dosimeter was that it provided an indirect means of assessing the radiation quality of the neutrons used in this study, namely d(16)/Be and p(66)/Be fast neutrons.

Chemical dosimeters are seldom used routinely and therefore the advantages of chemical dosimetry and the selection of a suitable chemical dosimeter are briefly outlined in this chapter.

Advantages of a Wet Chemical Dosimeter

In the appropriate mould, chemical solutions can adopt the form and volume of any object. Thus by using the sample exchange method the best correspondence between absorbed energy in the dosimeter and the mean radiation dose absorbed by the object can be achieved. The importance of the mass (m) of a dosimeter in relation to the energy/mass quotient (E/m) was considered by Rossi (1968). It was clear that an optimal mass was required to ensure that the defined quotient is indeed an expression of the absorbed dose. Since the density of wet chemical dosimeters is close to that of tissue, this requirement is fulfilled in the sample exchange method, i.e. the mass of the dosimeter approximately equals that of the irradiated object.

Furthermore, it is possible to expose either thin layers or small volumes of a liquid dosimeter in radiation conditions where the dose profile changes rapidly (Gupta *et al.*, 1982), e.g. in the build-up zone for ^{60}Co γ-rays (Gupta and Nilekani, 1977), in the build-up and penumbra region of a neutron field, or in the Bragg peak of a proton

beam. Also, the response to scattered radiation may depend on the size and nature of the dosimeter. A large proportion of scattered electrons have very low energies (Gupta and Nilekani, 1980), and as a result the effect of scattered radiation is underestimated in large ionization chambers. Thus liquid dosimeters are not only useful for small-volume dosimetry but are beneficial for large-volume applications, e.g. by mixing unsealed radionuclides intimately with the dosimeter. This is of special interest when assessing the radiation dose in radiopharmaceutical applications (Benedetto and Harris, 1985).

Chemical dosimeters are especially useful in neutron dosimetry since effects such as absorption, scattering and gamma production are optimally considered. Moreover, the dose in an aqueous medium is measured. Considering the relationship between radiation chemical yield (a measure of radiosensitivity) and linear energy transfer, chemical dosimeters enable not only the evaluation of the mean absorbed energy but also offer information regarding radiation quality (Axtmann and Licari, 1964). By quantifying radiation chemical yields in different radiation fields, certain models of radiation damage in biological systems can be tested. These models attempt to explain the observed biological damage by starting at the most fundamental radiochemical level, that is the production of ions (Freyer *et al.*, 1989).

If care is taken regarding the purity of the dosimeter solutions, the consistency between different laboratories is excellent (Green and Major, 1973). Since the uncertainties in spectrophotometeric calibrations are smaller in comparison with other systematic errors encountered in neutron dosimetry, chemical dosimeters have attractions for users at other centres, particularly because consistency between centres is often of greater interest than absolute doses.

A comparison using chemical dosimeters requires a choice of G-values (see below), whereas an ionometric comparison requires a choice of C_{λ} and C_{E} values appropriate to the type of radiation and class of ionization chamber used. In a report on a comparison of chemical and ionization dosimetry, Durocher *et al.* (1981) concluded that the higher experimental uncertainties associated with these parameters make ionometric comparison less reliable than a comparison based on chemical dosimetry.

The Fricke Dosimeter

In radiation dosimetry the ferrous ammonium sulphate (Fricke) solution is often chosen because of its advantages related to geometric and physical conditions (Fricke and Hart, 1966; Pejuan and Kühn, 1981). Unfortunately the Fricke dosimeter has a low radiation sensitivity in comparison to other dosimetric systems. Large doses of 40 Gy and more are required to use the dosimeter with reasonable accuracy (Chung, 1985). Although attempts have been made to extend the usefulness of the Fricke solution to lower doses, it is still at a disadvantage under some experimental conditions, for example under protracted irradiation conditions (Kartha, 1970). Wet chemical methods are in general less attractive for neutron dosimetry because of the lower sensitivity to higher LET radiations (Maughan *et al.*, 1983; Fregene, 1967).

The Ferrous Benzoic Xylenol Orange (FBX) Dosimeter

To overcome the limitations of the Fricke dosimeter a modified ferrous sulphate solution was developed by Gupta *et al.* (1974) and Gupta and Gomothy (1974). The essential difference is the addition of benzoic acid to promote the oxidation of Fe^{2+}, and the addition of xylenol orange to form an organo-metallic complex. In accordance with its constituents, the solution is known as the FBX dosimeter. A detailed description on the chemistry of the solution is given by Gupta *et al.* (1983, 1978). The net result of adding benzoic acid and xylenol orange is an increase in the molar absorbance coefficient of the solution and a higher radiation chemical yield (see below).

Radiation Chemical Yield and G-values

The radiation chemical yield, G(x), of a solution is the quotient of n(x) by ε, where n(x) is the amount of substance of a specified entity (x) which is produced, destroyed or changed by the imparted energy (ε) to the medium (ICRU 1980).

$$G(x) = n(x)/\varepsilon \, . \qquad [1]$$

A related quantity which is more commonly known as the G-value, is the amount of a molecular product formed for every 100 eV energy absorbed by the dosimeter. It follows that a higher G-value translates into a more radiosensitive dosimeter. The

relationship between dose (D), G-value and molar extinction coefficient (ε_λ) is given by:

$$D = \frac{1.602 \times 10^{-17} N_a \Delta(OD)}{G(x) \ell \rho \epsilon_\lambda}. \qquad [2]$$

where N_a is Avogadro's number, $\Delta(OD)$ the change in optical density of the solution at a specific wavelength (λ), ℓ the optical path length used to determine $\Delta(OD)$ and ρ the density of the dosimeter (Attix, 1986).

The origin of the molecular yield in question (Fe^{3+}) can be summarized as follows. Following the radiolysis of the solution, the primary radical yields are H, OH and H_2O_2. Each H_2O_2, OH and H radical leads to the oxidation of 8, 7 and 11 ferrous ions respectively (Gupta *et al.*, 1983). Therefore each of the individual G-values for H, OH and H_2O_2 will contribute to the G-value in equation [2].

The response of the FBX dosimeter is not expected to be influenced by the various dose rates used in this work. Gupta *et al.* (1981) found the dosimeter to be independent of dose rate and dose-fractionation effects.

Tissue Equivalence

Since the FBX solution is nearly tissue equivalent, the G-value (response) should directly reflect dose absorbed in tissue (Gupta and Nilekani, 1977; Upadhyay *et al.*, 1982). Compared to A-150 tissue-equivalent plastic which is used for neutron dosimetry, the FBX solution is a suitable substitute. The carbon and oxygen content in A-150 plastic is more or less reversed compared to muscle as defined by the ICRP (Uphadhyay *et al.*, 1982), and is shown in Table 1. For the dosimetry of low energy neutrons this discrepancy is relatively unimportant. However, for high energy neutron beams oxygen can be expected to play a more significant role in the transfer of energy to the medium (Smathers and Victor, 1977). In this respect the composition of the FBX solution appears to be more appropriate.

Table 1: *Percentage composition by weight of different elements present in the FBX solution, tissue-equivalent plastic (A-150) and muscle as defined by the ICRP.*

Elements	FBX	A-150	"ICRP Muscle"
C	0.050	76.8	12.3
N	0.001	3.6	3.5
O	88.8	5.9	72.9
H	11.1	10.2	10.2
S	0.082	-	-

Determination of Calibration Constants for the FBX Dosimeter

The following sections describe the determination of the molar extinction coefficient for the ferric-xylenol orange complex and G-values for the FBX dosimeter in a ^{60}Co γ-ray field and neutron fields generated via the d(16)/Be and p(66)/Be reactions.

Since the dosimeter is based on an oxidation process, the quality of the water used in the preparations of the solutions is critical. A major disadvantage in ferrous sulphate dosimetry is the high sensitivity of the solutions to organic impurities (Kartha, 1970). Chlorine ions largely inhibit the action of organic impurities and are the main reason why NaCl is added to the Fricke dosimeter (Fregene, 1967). In FBX solutions NaCl is not added and the presence of organic impurities are therefore more crucial. Water treatment is detailed in the Appendix.

Determination of the Molar Extinction Coefficient

The response of a wet chemical dosimeter depends on the G-value and the molar extinction coefficient of the ferric-xylenol orange complex. The latter must therefore be determined before one can establish the molecular yield in a radiation field. A number of factors need to be considered in the determination of the molar extinction coefficient.

In principle ε_λ should be measured for each spectrophotometer since its value depends in part on the specific instrument (Knowles and Burgess, 1984). Furthermore, the chemical purity of the constituents, particularly that of the complex-forming agent

xylenol orange, appears to influence the gradient of the standard calibration curve (ferric ion concentration versus absorbance) (Gupta and Narayan, 1985).

An additional problem arises in that the exact Fe^{3+} content of many ferric compounds that are potentially useful for determining ϵ_λ is not known. For example, Gupta and Narayan (1985) have used crystalline ferric ammonium sulphate but there is doubt as to the crystal water content of $NH_4Fe(SO_4)_2 \cdot 12H_2O$. This and other methods were at first tried by the author as part of a preliminary investigation but it was concluded that the use of inaccurate standards may lead to estimates of values of the coefficient of extinction and that it would be more accurate to use ϵ_λ values reported in the literature. Although ϵ_λ is theoretically a constant for a particular chemical species at a specific wavelength, possible variations in the instrumental response requires the construction of a calibration curve. With the use of a modern spectrophotometer, variations in ϵ_λ values due to instrumental response may well be smaller than variations in the extinction coefficient as measured with inaccurate Fe^{3+} concentrations. To prepare exact Fe^{3+} concentrations from a primary standard such as analytical grade iron wire is difficult and tedious. Although this was done as part of a preliminary investigation, such a procedure is not recommended.

Ferric Ion Standard

It is known that different commercial preparations of xylenol orange (XO) can influence the molar extinction coefficient. Because of this and the arguments presented above, it was decided to establish empirically the molar absorptivity for the FBX dosimeter. In view of the numerous questions surrounding the preparation of primary Fe^{3+} solutions, a commercial iron standard solution was used. (Eisen-Standardlösung, Titrisol, Merck). These were ampoules each containing 1.000 ± 0.002 gram of iron as $FeCl_3$ in diluted hydrochloric acid. The same approach was first followed by Pejuan and Kühn (1981) and later by Maughan *et al.* (1983). The details of preparation of standard FBX solutions to determine the molar absorptivity are given in the Appendix.

It was considered desirable to determine the molar extinction coefficient in the Fe^{3+} concentration range that was compatible with the range of photon and neutron doses used to the present work. The first step was to calculate the Fe^{3+} concentrations required for setting up the standard curve of expected absorbance of the FBX dosimeter.

The Fe^{3+} concentrations, $[Fe^{3+}]$, were calculated from equation [2] by substituting the ratio between $\Delta(OD)$ and $(\epsilon_\lambda \ell)$ with $[Fe^{3+}]$. Thus,

$$[Fe^{3+}] = \frac{\Delta(OD)}{\epsilon_\lambda \ \ell}. \qquad [3]$$

The expected Fe^{3+} concentrations for photon doses ranging from 0.5 to 5 Gy and neutron doses ranging from 1 to 10.2 Gy are listed in Table 2 . The G-values used in the calculation were 54.5 for photons and 26.5 for neutrons (Maughan *et al.*, 1983), assuming a molar extinction coefficient of 14207 $l \cdot mol^{-1} \cdot cm^{-1}$ (Pejuan and Kühn, 1981). Note that most of the expected optical densities fall between 0.2 and 0.8 absorbance units. This is fortunate because it is known from both theoretical calculations and experimental observations that absorbance measurements in this range are minimally influenced by instrumental errors (Knowles and Burgess, 1984).

Table 2: *Expected optical densities at 540 nm, and concentrations of Fe^{3+} resulting from photon and neutron irradiations.*

Physical Dose (Gy)		Δ(OD) at 540 nm	$[Fe^{3+}]$ (μM)
^{60}Co	neutrons		
0.5	1.0	0.04	2.86
1.0	2.0	0.08	5.73
1.5	3.1	0.12	8.60
2.0	4.1	0.16	11.46
2.5	5.1	0.20	14.32
3.0	6.1	0.24	17.19
3.5	7.2	0.28	20.05
4.0	8.2	0.33	22.92
4.5	9.2	0.37	25.78
5.0	10.2	0.41	28.65

Molar Extinction Coefficients Measured for the FBX Solution

The absorbance values (optical densities) measured at 540 nm for the standard solutions were plotted against the ferric ion concentrations listed in Table 1 (Fig. 1) Using linear regression through the origin, the slope of the curve which represents the molar extinction coefficient, was calculated. Three separate sets of absorbance measurements

were made for 3 sets of standard solutions. The calculated molar extinction values are given in Table 3.

Table 3: *Molar absorbance coefficient measured at 540 nm for standard ferric-xylenol orange solutions.*

Standard Solutions of $[Fe^{3+}]$ Set No.†		Slope ($l\ Mol^{-1}\ cm^{-1}$)
1		13801 ± 83
2		13926 ± 69
3		13837 ± 92
	Mean	13854 ± 64

†Each set consisted of a series of 10 standard $[Fe^{3+}]$ as listed in Table 2.

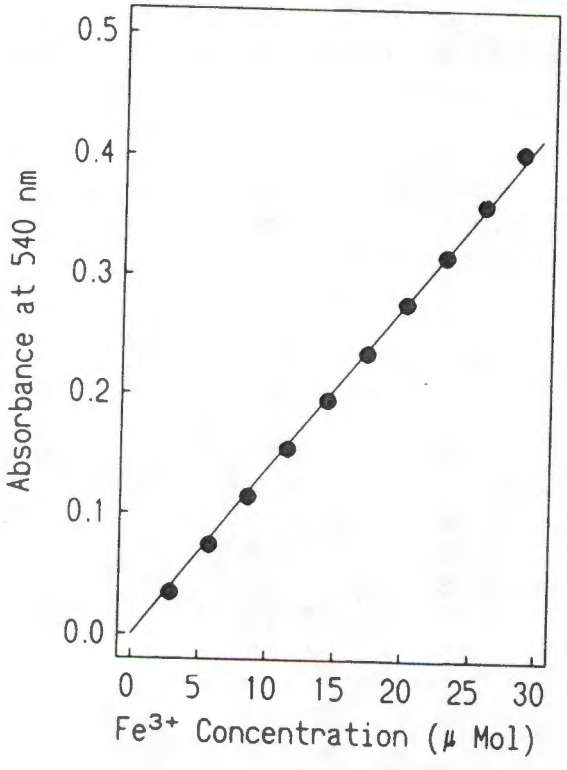

Figure 1: *Calibration curve for the ferric-xylenol orange dosimeter. The gradient of the curve is the molar absorbance coefficient (ε_λ) for the FBX dosimeter.*

The molar absorbtivity for the ferric-xylenol orange complex at 540 nm may change with different manufacturers (Gupta and Narayana, 1985). In Table 4 the present data is compared with those of other authors using xylenol orange from different manufactures.

The molar extinction coefficient measured in this work is therefore within 1% of the mean value in Table 4 and within 3% of the value reported by Pejuan and Kühn (1981), who also used the Merck product. It is also almost identical to the value reported by Benedetto *et al.* (1985).

Table 4: *Molar absorbance coefficients for the FBX dosimeter reported in the literature.*

ε_λ at 540 nm (l Mol^{-1} cm^{-1})	Manufacturer of xylenol orange	Reference
13400 ± 250	BDH	Gupta and Narayan (1985)
12500 ± 225	K and K Lab's	Gupta and Narayan (1985)
19134 ± 33	Labo Chemie	Gupta and Narayan (1985)
14290 ± 220	BDH	Maughan *et al.* (1983)
14207 ± 320	Merck	Pejuan and Kühn (1981)
13966 - a)	Not given	Benedetto *et al.* (1985)
13840 - b)	Not given	Benedetto *et al.* (1985)
13700 ± 667 (mean of above)†		
13854 ± 64	Merck	Present work (Table 3)

† The extremely high value of Gupta *et al.* (1985), obtained with Labo chemicals, was not used in the calculation of the mean.

a) Measured with a single-beam spectrophotometer.

b) Measured with a dual-beam spectrophotometer.

Preparation and Use of the FBX dosimeter

Details of the preparation procedure are given in the Appendix. Two liters of dosimeter were prepared at a time. The final concentration of each constituent is listed in Table 5. FBX solutions were prepared about 14 hours prior to irradiations. This was to allow the solutions time to stabilize. The optical density of the dosimeter at this time, measured at

540 nm against Millipore water, was about 0.2 absorbance units. Just prior to irradiations, polystyrene test tubes were rinsed with the solution and then filled with 5 ml of the solution.

Table 5: *Composition of the FBX dosimeter. Also listed is the concentration range of each component in the FBX solution between which the dosimetric response is reported to be stable.*

Chemical Composition	Concentration (mM)	Concentration range (mM)†	
		(below 10 Gy)	(10 - 20 Gy)
$(NH_4)_2Fe(SO_4)_2 \cdot 6H_2O$	0.2	0.1 - 0.3	0.2 - 0.3
$C_{31}H_{28}N_2Na_4O_{13}S$‡	0.2	0.1 - 0.3	0.2 - 0.3
H_2SO_4	25	15 - 45	25
C_6H_5COOH	5.0	3 - 9	5 - 9

† Adapted from Gupta 1974.

‡ 3′, 3″-Bis[bis(carboxymethyl)aminomethyl]cresolsulfonphthalein tetrasodium salt. (xylenol orange)

Spectrophotometric Readings

After irradiation the tubes were placed in a water bath at 25° C for at least 20 minutes. This was to allow for the completion of any post-irradiation oxidation (see below). The optical densities of the samples were then determined using an unirradiated dosimeter as reference. For certain samples both single wavelength (540 nm) and wavelength scans (200 - 800 nm) were recorded. The resolution of the scans was limited to 2 nm due to the limitations of the diode-array assembly in the spectrophotometer.

Optical densities were recorded using a diode-array spectrophotometer (Hewlett Packard model 8451A). It was considered important to maintain the position of the optical cell in the spectrophotometer (Feist, 1982). For this reason the spectrophotometer was equipped with a 80 μl flow cell (optical path length 1 cm). The flow cell was housed in

a thermostatable compartment which was maintained at 25° C throughout the measurements. Although the absorbance of FBX solutions are reported to be independent of temperature (Gupta and Gomathy, 1974), for consistency samples were maintained at the same temperature using a water bath.

A computer program written for the spectrophotometer facilitated the readings and data storage. The main advantage of the program was to control a peristaltic pump which moved sample volumes to the flow cell. With this arrangement multiple readings could be taken from the same sample. For practical reasons, such as flushing the connecting tubing and the flow cell compartment with the dosimeter before a measurement was taken, a minimum volume of FBX solution was needed (1 ml). It was, however, possible to obtain a spectrophotometric reading with as little as 0.2 ml when appropriate tubing was used in the peristaltic pump.

Time Course of Post-Irradiation Oxidation in the FBX Dosimeter

Because post irradiation oxidation takes place in the dosimetric solution, a delay is required between the end of irradiation and the spectrophotometer measurement. Gupta *et al.* (1978) reported that although the formation of the ferric-xylenol orange complex is immediate, the presence of hydroperoxides may be responsible for a delay in full colour development.

A special facility was devised to follow the response of the dosimeter during irradiation, and for some time thereafter (Fig. 2.). An indent was melted into the glass floor of a 10 ml round bottomed flask, the indent extending into the flask to reach the center of the boll part. A 5.5×10^3 MBq ^{60}Co source, fixed at the end of a Al rod, was placed inside the indent. The boll part of the modified flask was filled with FBX solution. With this arrangement FBX solutions could be irradiated more uniformly from the centre of the dosimeter. The entire assembly was shielded with lead blocks. The dose rate to the solutions was determined by Fricke dosimetry (G-value 15.5) and found to be 11.5 cGy/min (the method is detailed in the appendix). The spectrophotometer was positioned next to the radiation facility and connected to the dosimeter via thin tubing. A peristaltic pump moved small samples of the dosimeter at one minute intervals to the flow cell. After each measurement the sample was returned to the flask.

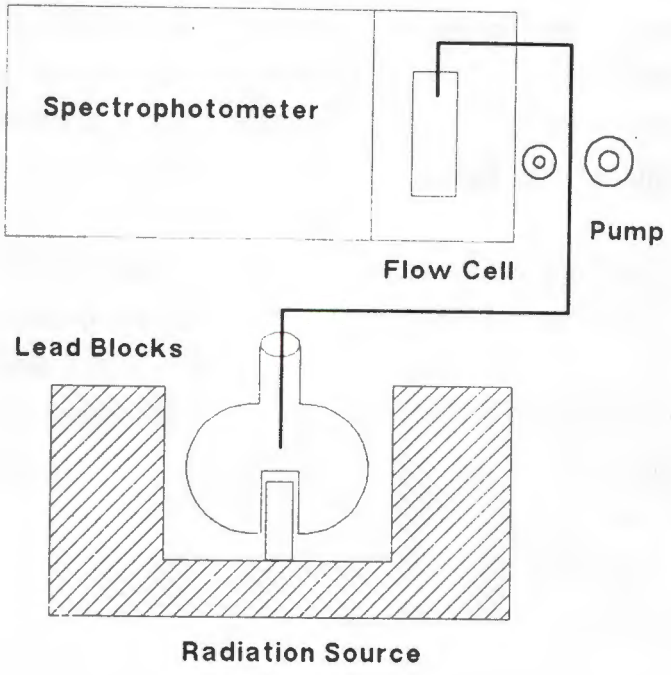

Figure 2: *Schematic diagram of irradiation facility used to investigate post irradiation oxidation and the low-dose response of the FBX dosimeter.*

Fig. 3. shows the results of the absorbance measurements. The first point in each data set was obtained immediately after the irradiation was completed. The absorbance continued to increase after termination of the irradiation, with the rate of increase diminishing with time. A delay was thus required before measuring the optical density. From the data in Fig. 3. it appeared that at least 20 minutes was required for the dosimeter to complete its response to a range of doses of radiation. Because of this, a waiting period of 20 minutes was strictly adhered to for all routine measurements. For maximum accuracy Matthews *et al.* (1978) considered a waiting period of 30 minutes too short and showed an increase in absorbance of greater than 1% per hour after this delay. Since the oxidation rate beyond 20 minutes is small, extended time periods were considered counter productive for the present study.

For doses below 1 Gy, a lag phase in the response of the FBX solution was evident. Although the response of the dosimeter is non-linear in this region, the molecular yield for a given dose was remarkably constant between solutions (Table 6).

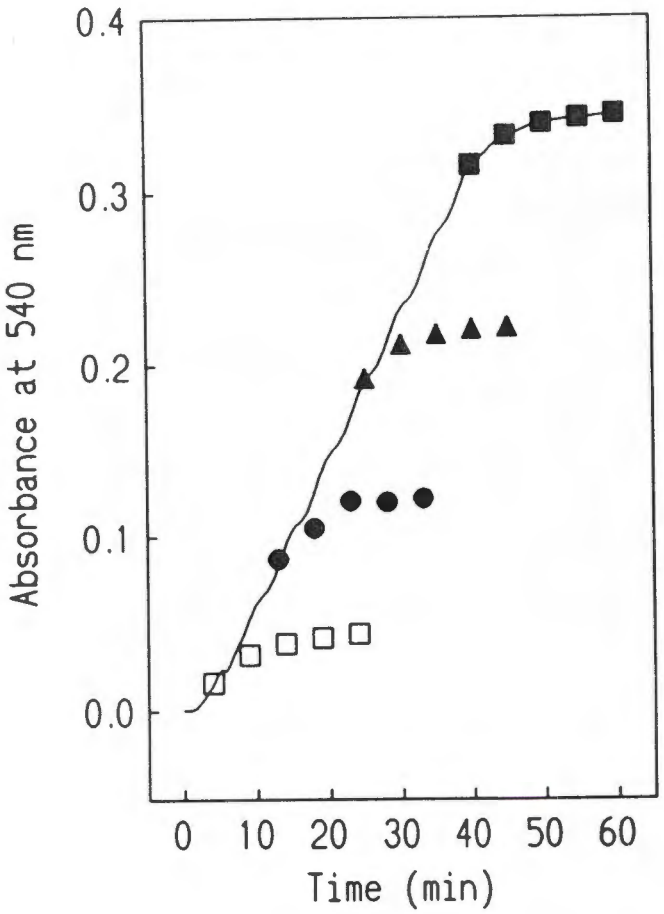

Figure 3: *Absorbance as a function of time (irradiation plus delay) for different FBX solutions respectively exposed to 0.46 (□), 1.5 (•), 2.87 (▲) and 4.6 (■) Gy of ^{60}Co γ-rays.*

Table 6: *Chemical yield (G-values) for FBX solutions exposed to ^{60}Co γ-rays and measured without allowing for post irradiation oxidation. The dose rate was 0.12 Gy min^{-1}.*

Irradation time (min)	2	5	10	24
Solution No.	G-values†			
1	17.1	27.8	36.1	44.1
2	17.2	26.5	35.9	44.9
3	16.9	27.9	37.5	46.8
4	17.0	26.4	35.6	44.6
mean	17.1	27.2	36.3	45.1
s.d.	0.1	0.8	0.8	1.2
cov (%)	0.6	2.9	2.2	2.7

† Calculated according to equation [4] below.

Neutron and Mixed-Field Irradiations of the FBX Dosimeter

FBX solutions were irradiated with p(66)/Be neutrons using a vertical beam. Polystyrene tubes containing 5 ml of the FBX solution were placed at an SSD of 150 cm on the central axis of a 29 × 29 cm field. Build-up consisted of 2 cm polyethylene and 15 cm of perspex was used for backscatter. Neutron dosimetry was performed with a TE ionization chamber and a graphite chamber used to assess the dose rate of the ^{60}Co source. The γ-component in the neutron beam for this arrangement was 7.8%. For the ^{60}Co irradiations a 20 × 20 cm field was used, also vertically orientated. Here build-up consisted of 5 mm of perspex and no backscatter material was used. The neutron and photon dose rates were respectively 0.35 and 0.45 Gy/min. In the mixed field exposures the neutron dose was applied first, and thereafter the samples were transported to the ^{60}Co source. The time interval between the two fractions was approximately one minute.

For measurements performed in the d(16)/Be field, FBX samples in polystyrene tubes were irradiated in a horizontal beam. The collimator head of the ^{60}Co unit was placed in tandem with the neutron collimator, facing the neutron beam as shown in chapter 4. The neutron field was 10 × 10 cm and the photon field 20 × 20 cm. For mixed-field irradiations the FBX solutions were exposed simultaneously to neutrons and photons. In order to apply the neutron and photon doses simultaneously so that the time of irradiation was the same for both radiation modalities, the neutron and photon dose rates were adjusted according to the mixture required. The neutron dose rate was altered by changing the beam current whilst lead slabs of varying thicknesses were placed in front of the ^{60}Co beam to modify the photon dose rate. Table 7 shows the various dose rates used to achieve the different neutron-photon mixtures.

G-values for the different neutron beams and their mixtures with ^{60}Co γ-rays

For each radiation type used in these measurements, i.e. ^{60}Co γ-rays, d(16)/Be or p(66)/Be neutrons, a series of absorbance measurements were made with the FBX dosimeter. The absorbance at 540 nm was plotted as a function of dose (Figs. 4, 5, 6, 7 and 8). For comparative purposes the results from the two different energy neutron beams are plotted together for similar n/γ mixtures. Some 300 tubes, each with 5 ml FBX solution, were irradiated. Four absorbance readings were made for each tube to check sample reproducibility. These readings were always within 0.01% of each other,

Table 7: *Beam current settings and photon dose rates used in simultaneous irradiations of d(16)/Be neutrons and ^{60}Co photons.*

D_γ/D_T (%)	Beam current (μA)	Dose rate (cGy min^{-1})	
		neutrons	photons
5.0†	9.4	29	-
28.0	4.2	14	40.3
51.8	6.5	22	22.1
76.4	8.0	26	8.2
100	-	-	61.4

†Inherent γ-contamination of the neutron beam.

so that only one absorbance reading from each sample was used in the calculations. The gradiant of each plot is proportional to the respective G-values. Equation [2] can be rewritten as:

$$G(x) = \Delta(OD)\, k/D\,, \qquad [4]$$

where

$k = 1.602 \times 10^{-17}\, N_a / \ell\, \rho\, \varepsilon_\lambda$,
$N_a = 6.023 \times 10^{23}$ mol^{-1} (Avogadro's number),
$\ell = 1.0$ cm (optical path length of flow cell),
$\rho = 1.02$ g/cm^3 (density of solution),
$\varepsilon_\lambda = 13854$ l mol^{-1} cm^{-1} (molar extinction coefficient), and
D = total dose (n+γ) absorbed by the solutions (Gy).

Then $k = 682.8$ and $G(x) = k \times \Delta(OD)/D$, i.e. the number of molecules of product formed for every 100 eV energy absorbed. The molecular product in this case is the Fe^{3+} - XO complex. G-values can be converted to units of moles/J. Therefore G(x) (moles/J) = G-value (molecules/100 eV) $\times$ 1.037×10^{-7} (Attix, 1986).

Equation [4] was used to calculate the G-values for d(16)Be neutrons, p(66)/Be neutrons, ^{60}Co γ-rays and various mixtures of each neutron beam with photons. Results are given in Table 8 below. G-values were calculated using the change in absorbance from 0 to 10 Gy, i.e. the initial part of the curves.

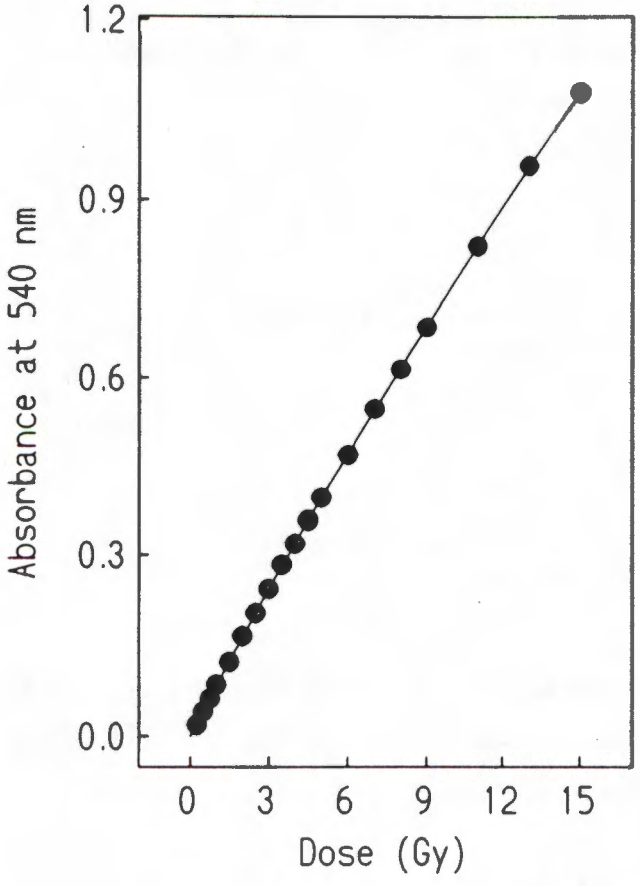

Figure 4: Change in absorbance for FBX solutions with dose following irradiation with ^{60}Co γ-rays.

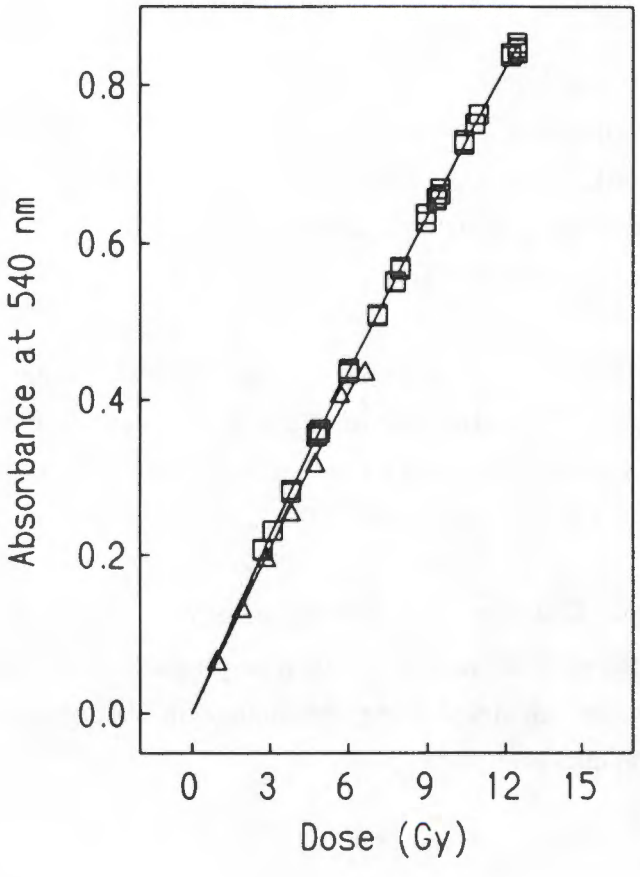

Figure 5: *Change in absorbance for FBX dosimeters with dose following irradiation with neutron - photon mixtures containing 31% p(66)/Be neutrons (□) or 28% d(16)/Be neutrons (△).*

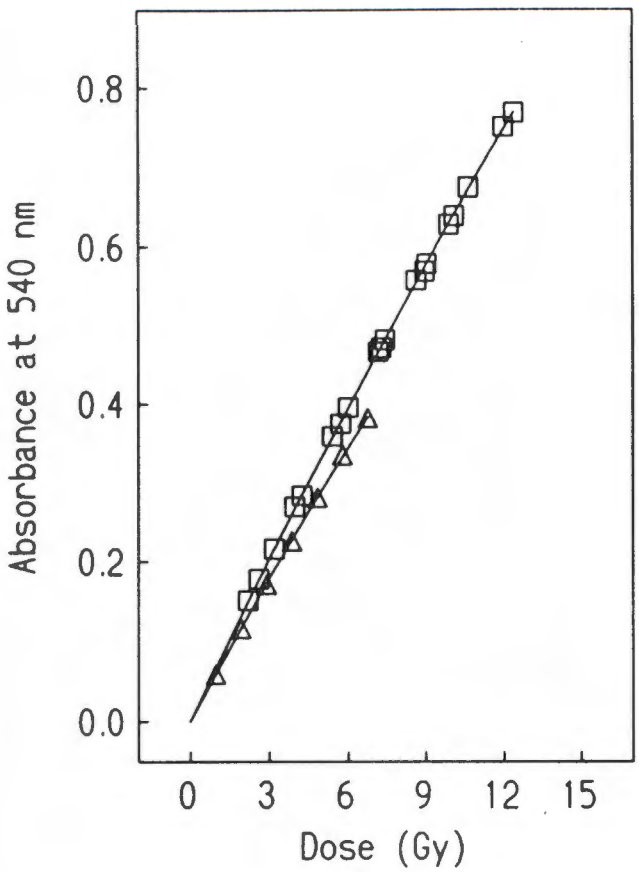

Figure 6: *Change in absorbance for FBX dosimeters with dose following irradiation with neutron - photon mixtures containing 54% p(66)/Be neutrons (□) or 52% d(16)/Be neutrons (△).*

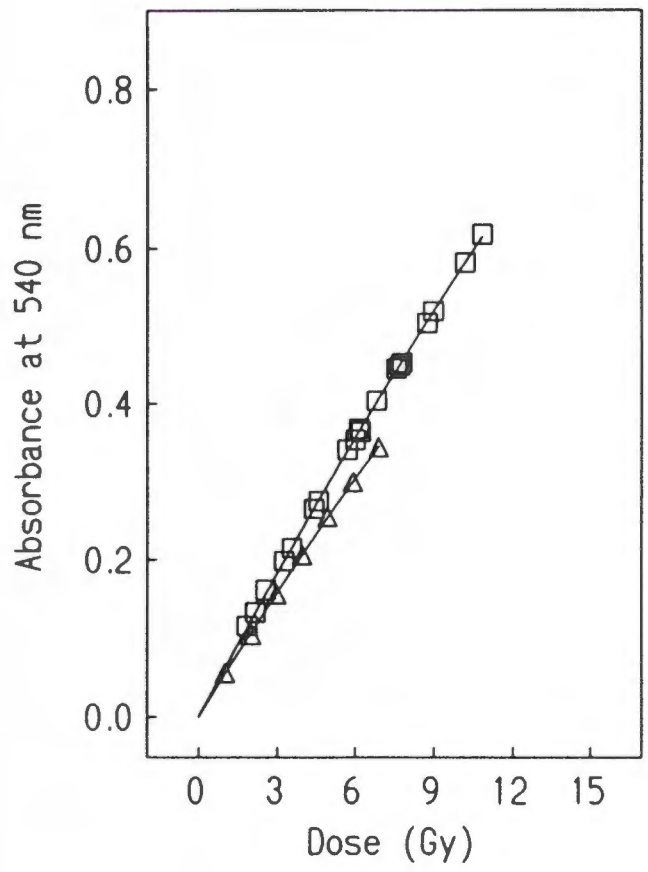

Figure 7: *Change in absorbance for FBX dosimeters with dose following irradiation with neutron - photon mixtures containing 69% p(66)/Be neutrons (□) or 72% d(16)/Be neutrons (△).*

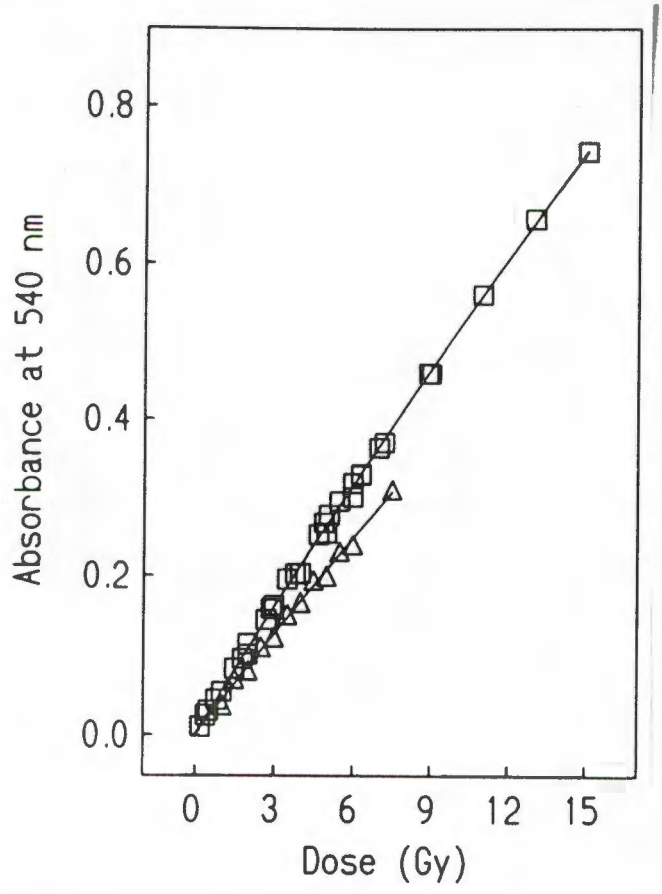

Figure 8: *Change in absorbance for FBX dosimeters with dose following irradiation with p(66)/Be neutrons (□) or d(16)/Be neutrons (Δ).*

G-value of the Neutron Component

The G-value for the neutron component in each of the beams was obtained in two ways. In the first procedure a neutron G-value was calculated for each of the n/γ mixtures using the expression:

$$G_n = \left[G_{(n+\gamma)} - G_\gamma f_\gamma\right]/f_n \,, \qquad [5]$$

where G_n is the molecular yield due to the neutron dose, $G_{(n+\gamma)}$ the G-value measured for the mixture, G_γ the yield in the ^{60}Co field and f_γ and f_n the photon and neutron dose fractions. Values obtained are given in Table 8. This method yielded mean G(n)-values of 27.2 (1.3) and 33.3 (1.3) $(100\ eV)^{-1}$ respectively for the d(16)/Be and p(66)/Be beams.

In the second procedure the $G_{(n+\gamma)}$ values obtained from the total dose measurements were plotted against the corresponding photon fractions of the particular mixture. The G_n value was then obtained by extrapolating to a zero γ-ray fraction using linear regression. The intercept represents the G-value for the neutron component of each

beam (Fig. 9). This method yielded a G_n-values of 27.3 ± 0.5 for d(16)/Be neutrons and 33.9 ± 0.3 for p(66)/Be neutrons. Here the derived uncertainties are far smaller than those estimated from the first method.

Table 8: *Gradients of absorbance at 540 nm versus radiation dose (measured) for FBX dosimeter and G-values (calculated) for different n/γ mixtures. Values are given ± S.E.*

Parameter	% of γ-rays in d(16)/Be beam				^{60}Co
	5.0	28.0	51.8	76.4	
slope × 10^3 (Gy^{-1})	41.249 (0.3)	51.071 (0.3)	57.754 (0.3)	68.303 (0.7)	76.596 (0.4)
G(n + γ)-value (100 eV)$^{-1}$	28.2 (0.2)	34.9 (0.2)	39.4 (0.2)	46.6 (0.5)	-
G(n)-value (100 eV)$^{-1}$	26.9 (0.2)	28.1 (0.2)	25.5 (0.1)	28.2 (0.3)	-
G(γ)-value (100 eV)$^{-1}$	-	-	-	-	52.3 (0.3)
	% of γ-rays in p(66)/Be beam				
	7.8	30.9	53.9	76.9	
slope × 10^3 (Gy^{-1})	52.175 (0.4)	58.489 (0.7)	63.974 (0.8)	69.854 (0.8)	76.974 (0.5)
G(n + γ)-value (100 eV)$^{-1}$	35.6 (0.6)	39.9 (0.5)	43.7 (0.5)	47.7 (0.2)	-
G(n)-value (100 eV)$^{-1}$	34.2 (0.6)	34.2 (0.4)	33.3 (0.4)	31.4 (0.1)	-
G(γ)-value (100 eV)$^{-1}$	-	-	-	-	52.6 (1.1)

A mean g(γ)-value of 52.5 ±1.1 was obtained from the above photon measurements. This is in reasonable agreement with the 54.0 ± 2.3 reported by Pejuan and Kühn (1981) for ^{60}Co γ-rays, and to the 54.4 ± 1.5 determined by Maughan *et al.* (1983) in a ^{137}Cs field.

To compare the variation in molecular yield of the FBX dosimeter with neutron energy, G-values for the standard Fricke dosimeter were determined for the d(16)/Be and p(66)/Be neutron beams and are compared with that reported for a d(4)/Be neutron beam in Table 9.

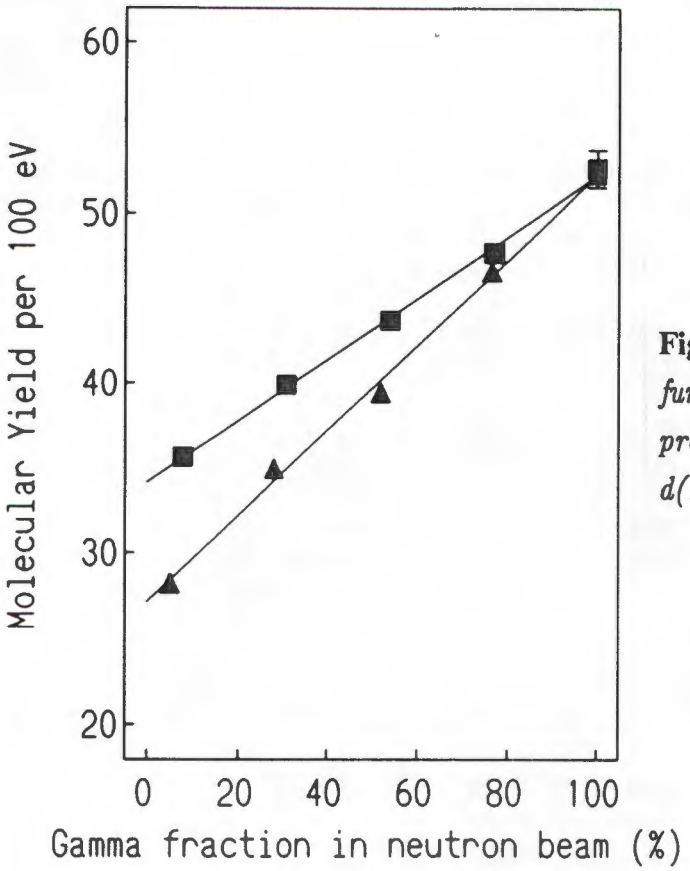

Figure 9: *$G_{(n+\gamma)}$-values as a function of the percentage ^{60}Co γ-rays present in a p(66)/Be (□) and d(16)/Be (△) neutron beams.*

Table 9: *Experimental FBX and Fricke G_n values for different neutron energies. Standard errors are indicated in brackets.*

Neutron Source	$\bar{E}_n$ (MeV)	D_γ/D_T (%)	G_n (per 100 eV)		References
			$FeSO_4$	FBX	
d(4)/Be	3.2	10.5	7.8†	23. (1.8)	Maughan *et al.*(1983)
d(16)/Be	6.3	5.0	8.7 (0.2)	27.3 (0.5)	This work
p(66)/Be	30.8	7.8	11.5 (0.1)	33.9 (0.3)	This work

† Theoretical value, Lawson and Porter (1975).

The ratio G_n (FBX)/G_n ($FeSO_4$) was found to be 3.0, 3.1 and 2.9 respectively for 3.2, 6.3 and 30.8 MeV neutrons. The consistency of this ratio with neutron energy is an indication of the accuracy of the molecular yields determined for the neutron component of different neutron sources.

Reproducibility of Measurements

Since the dosimeter was prepared *ab initio* each time, the reproducibility of different FBX solutions was checked. The G-values in Table 8 were computed from the combined data of sets of measurements. In Table 10 the $G_{(n+\gamma)}$-values obtained from 5 different FBX solutions are listed. The coefficients of variation for the parameters between the different FBX solutions were of the order of 2% or less. In Table 11 reproducibility in dosimetric response is shown for different mixtures of neutrons and γ-rays at an arbitrarily chosen total dose of 6 Gy. Again the variation between solutions was found to be less than 2%. In any one solution the variation in response was found to be within 1%.

Table 10: *Reproducibility of response between different ferrous-benzoic-xylenol orange solutions. The dosimeters absorbed a total dose of 6 Gy of either p(66)/Be neutrons, ^{60}Co γ-rays or various mixtures of neutrons and photons.*

Photon fraction (%)	7.8	30.9	53.9	76.9	100
Solution No.	$G_{(n+\gamma)}$-values				G_γ
1	34.3	-	-	-	52.5
2	35.9	40.2	44.3	50.2	53.8
3	35.7	40.9	45.2	49.5	51.7
4	35.8	40.8	44.9	49.1	53.7
5	34.8	-	-	-	-
Mean	35.3	40.6	44.8	49.6	52.9
S.D.	0.7	0.4	0.5	0.6	1.0
COV (%)	1.9	1.0	1.1	1.2	1.9

If the plasticware used with the dosimeter was "cured" before use, the results were reproducible to within 0.5% The plastic was "cured" by filling the container with FBX solution and then giving a high dose of photon radiation (10 Gy). The container was

then rinsed thoroughly with FBX solution before it was used. This procedure eliminated the slight increase in absorbance that occurred as a result of interaction between the plastic and solution. This increase in absorbance is a function of the surface to volume ratio (Kartha, 1970). Because of the many measurements performed it was not always practical to follow this procedure.

Table 11: *Reproducibility of $G_{(n+\gamma)}$-values calculated from dose vs. absorbance gradients. Different FBX solution prepared on separate occasions were each exposed to a series of doses of ^{60}Co photons, p(66)Be neutrons and various combinations of neutrons and photons.*

Photon fraction (%)	7.8	30.9	53.9	76.9	100
Solution No.	$G_{(n+\gamma)}$-values				G_γ
1	34.4 (0.2)	-	-	-	51.7 (0.3)
2	35.6 (0.1)	39.4 (0.3)	43.2 (0.3)	47.2 (0.3)	51.5 (0.5)
3	35.0 (0.3)	39.8 (0.3)	43.7 (0.4)	47.9 (0.3)	53.7 (0.3)
4	36.3 (0.2)	40.4 (0.4)	44.1 (0.4)	47.6 (0.4)	52.5 (0.2)
5	34.9 (0.1)	-	-	-	52.4 (0.2)
Mean	35.2	39.9	43.7	47.7	52.4
S.D.	(0.7)	(0.5)	(0.5)	(0.2)	(1.0)
COV (%)	2.0	1.3	1.1	0.4	1.9

It should be noted that for routine measurements using a 1 cm optical path length in the spectrophotometer, a minimum dose of 3 Gy photons or 5 Gy neutrons is described for accurate dose determinations. This corresponds to a change in absorbance of about 0.25 for each modality.

Absorbance Spectra of the FBX dosimeter following Irradiation

In Fig. 10 the dose response of the FBX dosimeter is shown for ^{60}Co photons and the two neutron fields as a function of wavelength. All three spectra were measured for an exposure of 6 Gy in each radiation field. The absorbance values were then normalized

to unit dose. The spectra showed two isometric points located at approximately 370 and 460 nanometers. At these wavelengths there is no response to the radiation. Absorbance values peaked at wavelengths slightly less than 540 nm which is the wavelength most generally used for FBX measurements. Both the standard ferric solutions and the FBX dosimeter indicated maximum absorbance values between 520 and 540 nm. Because of the broad character of the principle absorbance peak, all spectrophotometer readings were taken at 540 nm.

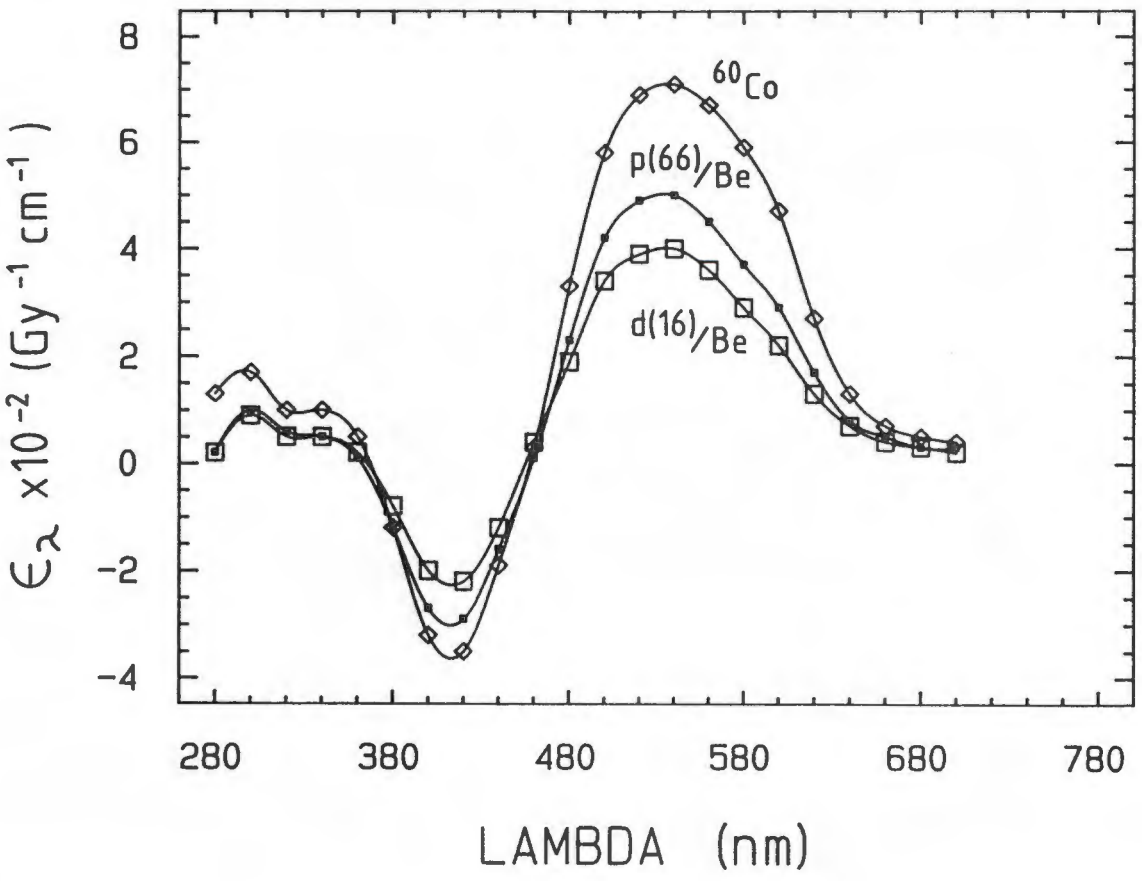

Figure 10: *Absorbed dose extinction values determined after exposing FBX solutions to radiation fields of varying quality.*

Molecular Yield and LET

It is evident from Fig. 9 and Table 8 that there is a reduction in the molecular yield per unit dose with an increase in LET. A higher LET is associated with lower energy [d(16)/Be] neutrons and/or having a lower fraction of photons in the mixture. The

decrease in the chemical yield with a higher LET can be accounted for by considering the concept of dose. Absorbed dose is a macroscopic quantity and is useful only in that it specifies in a single number the ambient energy concentration at the point of interest. Macroscopic dose as such cannot account for the different biological responses that are noted when a biological system is exposed to differing radiation qualities for the same absorbed dose. The biological effects of radiation are therefore attributed to the microscopic distribution of the energy (Rossi, 1968). These microscopic distributions can reflect the local energy density (energy/mass) in very small volumes. When this occurs in the FBX solution the following scenario can be applied.

Since the FBX dosimeter is a diluted solution, it can be assumed that the radiation interacts with the water, producing chemically active primary products in about 10^{-10} seconds after an ionizing event. These products are distributed heterogeneously and close to the charged-particle tracks (Attix, 1986). Some 10^{-4} seconds after the initial interaction the spatial distribution of these primary products, and other resultant chemical species that are formed, tend to homogenize due to diffusion (Pejuan, 1980). In the case of the FBX solution the formation of microscopic concentrations of Fe^{3+} is of prime interest, and is determined by the reaction rate of the oxidation process. In the period before the initial spatial distribution is obliterated these "packets" of high Fe^{3+} concentrations enhance competing back reactions, resulting in a reduction reaction, i.e. $Fe^{3+} \rightarrow Fe^{2+}$. With higher ionization densities the instantaneous concentration of Fe^{3+} ions is higher and reduction reactions are more pronounced. Thus, the radiation yield of a wet chemical dosimeter is inversely proportional to the LET (ICRU, 1980).

For this reason the denser tracks of ionizations formed by secondary particles during d(16)/Be neutron irradiations manifest in lower G-values. Likewise with an increase in the γ-fraction in the neutron beam, the net G-value of the mixture will increase.

Non-linearity in the Dose-Response Relationship

Examination of Figs. 4, 5, 6, 7 and 8 shows that the response of the dosimeter is not completely linear with dose. Benedetto *et al.* (1985) demonstrated this behaviour more clearly by following the response up to a dose of 50 Gy in a ^{137}Cs field. The non-linearity can be attributed to the low Fe^{2+} concentration with respect to the xylenol orange (Gupta, 1973). Two competitive reactions prevail. XO-transients react with both Fe^{2+} and with XO. In principle the XO and Fe^{2+} concentrations can be adjusted so

that sufficient Fe^{2+} ions are present to react with the XO-transients and that enough XO is present to complex with the Fe^{3+}. Such an adjustment, however, will result in a less responsive system and consequently the G-value will be lower.

Irradiations in the Build-up Region

Two milliliters of FBX solution was poured into polystyrene Petri dishes of diameter 51 mm. This resulted in a nominal depth of 1 mm (not taking surface tension into account). Because the surface to volume ratio of the sample configuration was relatively high, the Petri dishes were cured as previously discussed. The samples were positioned behind discs of nylon type 6 (density 1.14 g cm^{-3}). These discs ranged in thickness between 0.5 and 16 mm. Nylon type 6 is a good substitute for A150 TE-plastic (Binns and Hough, 1990).

Irradiations were from below. Circular openings were machined in a sheet of perspex and the Petri dishes supported by their rims over the openings. The 1 mm thick base of the polystyrene dishes also served as part of the build-up material. Further build-up in the form of nylon discs could be positioned beneath the dishes. Extrapolation chamber measurements with 1 mm thick nylon and polystyrene discs indicated a dose discrepancy of less than 1.5%.

Half the thickness of the dosimeter solution (0.5 mm), plus that of the nylon discs was taken as the effective build-up. For one set of measurements the irradiation was directed from above with no additional build-up between the neutron source and the dosimeter. Here an effective build-up of 0.5 mm was assumed. All samples received the same exposure. The selected level of exposure was equivalent to 6 Gy at 17 mm (D_{max}) in a phantom. Backscatter material was a block of 30 × 30 × 15 cm perspex positioned behind the samples. The neutron field size was 29 × 29 cm.

Chemical Yield in Response to Changes in the Spectral Character of the Beam

The relative response of the FBX solution in the build-up region is compared with extrapolation chamber measurements in Fig. 11. where all readings were normalized to those at D_{max}. Chemical and physical measurements appear to be in good agreement for most of the build-up profile.

Because of the rapid change in radiation quality with position in the build-up region, it is of interest to know whether the molecular yield (G-value) in the FBX solution reflects the change in ionization density. G-values were calculated from the absorbance measurements using equation [4]. In calculating the absorbed doses to the samples, cognizance was taken of the differences between kerma and absorbed dose in the build-up region, and the doses received by each sample were adjusted accordingly.

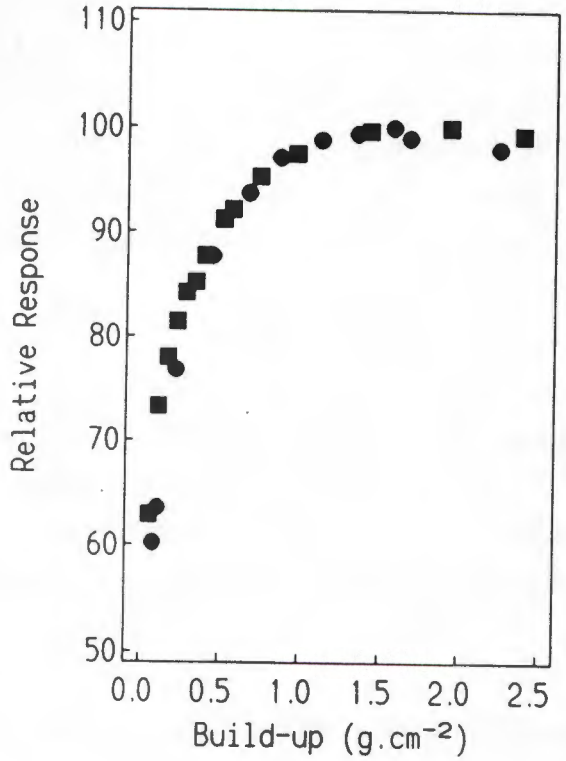

Figure 11: *Relative response of the FBX dosimeter (■) compared to that measured with an extrapolation chamber (•) in the build-up region of a p(66)/Be neutron beam.*

The $G_{(n+\gamma)}$-values are shown in Fig. 12. A sharp rise in the molecular yield was evident with less build-up. This is unexpected because the higher ionization densities previously indicated a reduction in the G-value. This was demonstrated in Table 8 where the G-values for p(66)/Be neutrons, d(16)/Be neutrons and ^{60}Co γ-rays are compared. Also, Freyer *et al.* (1989) reported a molecular yield of 5.01 per 100 eV in ferrous sulphate solutions irradiated with ^{238}Pu α-particles. This is less than half that measured in a Fricke solution exposed to the p(66)/Be neutrons (Table 9).

Because the samples did not receive the same dose it can be argued that the findings shown in Fig. 12 were the result of the non-linearity between dose and response in FBX solutions. However, inspection of the p(66)/Be data for a 29 × 29 cm field (Figs. 5 - 8) indicated that non-linearity would affect the G-values obtained in the build-up region by not more than 1.2%. This deviation is not enough to explain the sharp increase in G-values observed.

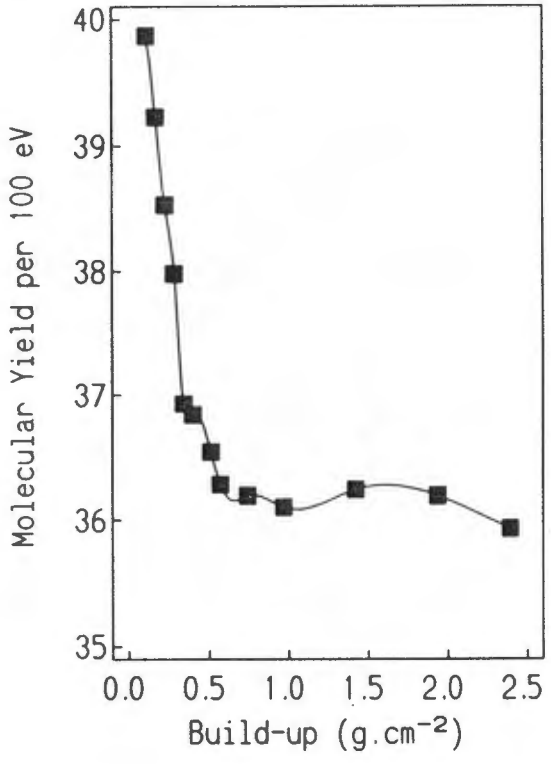

Figure 12: *Molecular yield of the FBX dosimeter exposed at various positions in the build-up region of a p(66)/Be neutron beam.*

Comparison between G-values and Microdosimetric Spectra

The radiation quality of the p(66)/Be beam used in the measurements presented here has been evaluated from single-event spectra measured with a tissue equivalent proportional counter (TEPC) (Binns and Hough, 1990). From these investigators' data it was clear that less build-up was associated with a decreased contribution to the dose from the recoil proton component. Using the microdosimetric data, a dose ratio B/A was reported for different positions in the build-up region. A and B was respectively defined as the dose contributions to the lineal energy region between 1 - 140 keVμm^{-1} and lineal energies larger than 140 keVμm^{-1}.

The noted trend in the measured G-values of the FBX dosimeter can be correlated with a similar trend in the dose ratios (Table 12). The same comparison is made in Table 13 but for neutron G-values determined at maximum build-up in different fast neutron beams.

Table 12: *Data obtained from measurements in the build-up region of the p(66)/Be neutron beam using a TEPC and the FBX dosimeter.*

Build-up ($g.cm^{-2}$)	B/A† ($\times 10^{-1}$)	G-value (Fe^{3+}/100 eV)
0.143	3.09	37.4
0.368	2.47	34.7
0.593	2.24	34.1
1.043	2.05	33.8
1.943 (D_{max})	1.93	33.3

†A: ($1 \leq y \leq 140$) $keV\mu m^{-1}$; B: ($y > 140$ $keV/\mu m^{-1}$)

Table 13: *Microdosimetric data and neutron G-values determined at maximum build-up in different fast neutron beams.*

Neutron source	B/A† ($\times 10^{-1}$)	G-value (Fe^{3+}/100 eV)
p(66)/Be	1.93	33.3
d(16)/Be	1.25	27.2
d(4)/Be	0.41‡	23.3

‡ Walker and Maughan (1986).

Whilst Table 13 appears to associate increasing neutron energies with larger G-values, this is not so in Table 12 where energy changes are minimal in the build-up region. The change in dose ratio B/A suggests that it is the relative magnitude of the proton and heavy recoil components in the secondary charged particle spectrum that determines the variation in the G-value.

CHAPTER 6

RADIOBIOLOGICAL PROPERTIES OF THE NEUTRON BEAMS USED IN THE STUDY

Introduction

As part of the pre-clinical calibration program at the NAC neutron therapy facilities, the basic radiobiological properties of the two neutron sources were evaluated. An assessment of the biological effectiveness of the neutron beams relative to ^{60}Co γ-rays (RBE) and the evaluation of their oxygen enhancement ratios (OER) were the principle properties of interest in the d(16)/Be and p(66)/Be beams. In the p(66)/Be field these investigations were limited to survival measurements using V-79 cells, whilst in the d(16)/Be field both survival measurements for V-79 cells and 10-day growth delay measurements using the root tips of the broad bean *Vicia faba* were performed. By comparing measured RBE and OER values to those reported by other investigators, the reliability of the experimental techniques was established.

Mammalian Cell Survival Studies in d(16)/Be and p(66)/Be Neutron Beams

Measurement of Radiobiological Effectiveness

V-79 cells were cultured and prepared for irradiation as detailed in the Appendix and irradiated under conditions of maximum dose build-up. Surviving fractions were determined and curves fitted using the method of Pike and Alper (1964). Fig. 1 shows survival curves that were fitted using the multi-target model. Linear quadratic expression was also used and these different procedures are described in the Appendix. The respective inactivation parameters are summarized in Table 1 together with ^{60}Co data.

The ratio D_o(photons)/D_o(neutrons) yielded RBE values of 1.90 and 1.67 respectively for the d(16)/Be and p(66)/Be beams. The RBE of 1.9 determined for the d(16)/Be beam is somewhat higher than the 1.6 determined for d(15)/Be neutrons at the University of Tokyo (Wakabayashi, 1983). A RBE value of 1.55 was determined for the p(62)/Be beam at Clatterbridge relative to 250 kV X-rays (Bewley *et al.*, 1989).

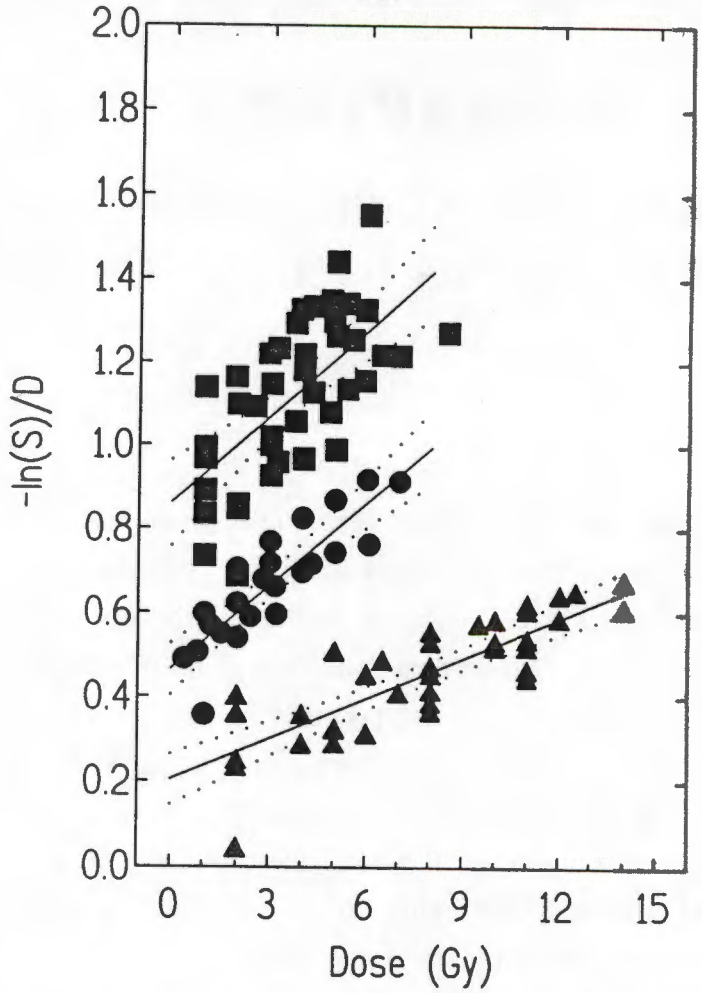

Figure 1: *$-Log_e$ of surviving fractions (s) divided by the dose (D) absorbed by V79 cells following exposure to p(66)/Be neutrons (●), d(16)/Be neutrons (■) and ^{60}Co γ-rays (▲).*

Table 1: *Inactivation parameters for the response of V-79 cells to d(16)/Be neutrons, p(66)/Be neutrons and ^{60}Co γ-rays. Parentheses indicate 95% confidence estimates.*

	Multi-target				Linear quadratic		
Radiation Source	D_0 (Gy)	n	D_q (Gy)	RBE	$\alpha \times 10$ (Gy^{-1})	$\beta \times 10$ (Gy^{-2})	$\bar{D}$ (Gy)
d(16)/Be	0.68 (0.05)	2.8	0.70	1.9 (0.2)	9.95 (1.3)	0.43 (0.2)	0.93
p(66)/Be	0.76 (0.07)	5.7	1.32	1.7 (0.2)	5.00 (0.6)	0.58 (0.1)	1.53
^{60}Co γ-rays	1.27 (0.1)	11.8	3.13	-	2.02 (0.7)	0.32 (0.07)	2.89

Assuming an X-ray vs γ-ray RBE of 1.13 (Winzel *et al.*, 1987), this translates to 1.75 which is compatible with the RBE determined for the p(66)/Be beam.

Accurate assessment of RBE-values using survival curves described by the coefficients α and β have previously been demonstrated in measurements where subtle variations in beam quality were correlated with changes in RBE and the microdosimetric parameter y* (Slabbert *et al.*, 1989).

Measurement of Oxygen Enhancement Ratios

Oxygen enhancement ratios for the d(16)/Be neutrons were determined by irradiating cells in suspension as detailed in the Appendix. Irradiations in a vertical p(66)/Be neutron beam were performed using circular shaped chambers (diameter 30 cm and 3 cm deep) constructed from aluminium. The chambers accommodated four 90 mm glass Petri dishes preplated with V-79 cells. In order to ensure good counting statistics at low doses, cells numbers were adjusted to give colony counts of about 400 per dose point. The polycarbonate cover of the chamber was clamped and sealed with a rubber O-ring. Anoxia was produced by flushing the chambers for one hour with a mixture of 5% CO_2 in ultra-pure N_2 (total oxygen concentration $<$ 10 ppm). Following irradiation the cells were incubated as detailed in the Appendix.

The OER for the d(16)/Be beam was found to be 1.6 (± 0.2). This agrees with the OER reported by McNally *et al.* (1982) for d(4)/Be neutrons and by Barendsen *et al.* (1966) for d(16)/Be neutrons. For the p(66)/Be beam, measurements covering two dose ranges (4 - 8 Gy) and (0.5 - 3.0 Gy) were performed. The respective inactivation parameters calculated are listed in Table 2. Since the low dose data did not permit the calculation of D_0 values, the OER in this instance was evaluated at 1 Gy in air and found to be 1.42. In the high-dose range the D_0 ratio yielded a value of 1.72 which is in agreement with an OER value of 1.7 determined at Fermilab (Hall *et al.* 1982). The observed reduction in OER at low doses underscores the results of studies conducted with CHO-K1 cells (Palcic *et al.*, 1984; Palcic 1984).

Growth Delay of *Vicia faba* Root Tips

The RBE and OER for the d(16)/Be neutron beam was determined using 10-day growth delay measurements on the primary root of the broad bean *Vicia faba*. Seedlings were cultured and root samples selected for irradiation as detailed in the Appendix.

Irradiations were performed using a perspex jig designed for the *Vicia faba.* The design of the jig is shown in the Appendix. To ensure full aerobic conditions, air

Table 2: *Inactivation parameters calculated for the response of V-79 cells to p(66)/Be neutrons under aerobic and anaerobic conditions. Parentheses indicate 95% confidence estimates.*

Cell Environment	Multi-target			Linear Quadratic		
	D_0 (Gy)	n	OER	$\alpha \times 10$ (Gy^{-1})	$\beta \times 10$ (Gy^{-2})	$\bar{D}$ (Gy)
High dose (Air)	0.45 (0.04)	64		0.87 (0.8)	2.72 (0.2)	1.55
High dose (N_2)	0.78 (0.08)	64	1.73 (0.2)	1.37 (0.7)	0.81 (0.1)	2.41
Low dose (Air)				4.41 (0.9)	0.98 (0.4)	1.50
Low dose (N_2)			1.42 (0.2)	3.18 (1.2)	0.39 (0.4)	2.17

was bubbled through the chamber before and during irradiations. For OER measurements, meristematic cells were rendered hypoxic by gassing the water in the target chamber of the radiation jig with high purity nitrogen for at least 30 minutes before, and during irradiation.

RBE Measurements

The inactivation parameters calculated from the 10-day growth delay measurements for two independent sets of data are given in Table 3. As growth delay is directly dependent on cellular survival, the G_{10} endpoint is assumed to represent a stochastic effect. Each data set constitutes a series of growth delay measurements following exposure to graded doses of d(16)/Be neutrons and ^{60}Co γ-rays delivered on the same day. The response of meristematic cells to the neutron irradiation was truely exponential (Fig. 2). Consequently a β-component could not be determined for this neutron beam. For the ^{60}Co irradiations a β-component was measured but found not significantly different from zero.

The RBE values calculated at the 50% level from each data set were in reasonable agreement. This underlines the importance of carrying out experiments in a so-called self contained manner (Hall and Kellerer, 1979). A mean RBE of 4.4 ± 0.2 was calculated. This compares favorably with an RBE value of 4.7 determined by Hall *et al.* (1973) for a similar ($\bar{E}_n$ = 6 MeV) neutron beam and as expected, is higher than the reported RBE values for 10-day growth delay measurements in more energetic neutron beams (Table 3).

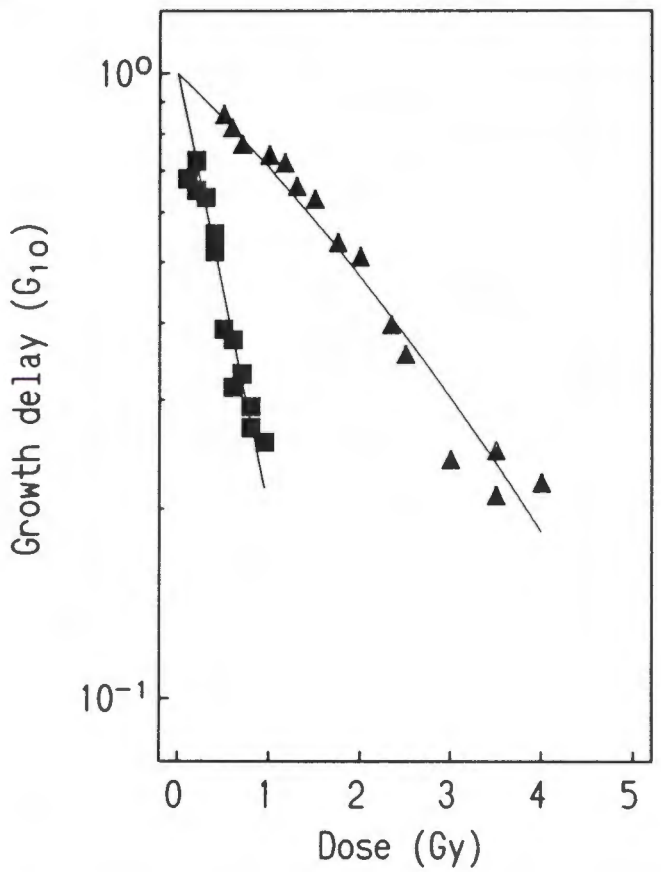

Figure 2: *10-Day growth delay measurements of the primary root of Vicia faba seedlings following exposure to d(16)/Be neutrons (■) and ^{60}Co γ-rays (▲).*

Oxygen Enhancement Ratios

The OER was also determined for meristematic cells exposed to d(16)/Be neutrons and ^{60}Co γ-rays. Results from one of the data sets are shown in Fig. 3. Inactivation parameters calculated from growth delay measurements following radiation under oxic and hypoxic conditions are listed in Table 4.

Table 3: *Inactivation parameters calculated from growth delay measurements following irradiation of Vicia faba root tips with d(16)/Be neutrons and ^{60}Co γ-rays. 95% Confidence intervals are indicated in brackets. RBE values were calculated at a level of 50% reduction in growth.*

Radiation Source	α (Gy^{-1})	$\beta \times 10^2$ (Gy^{-2})	$\bar{D}$ (Gy)	RBE
d(16)/Be	1.72 (0.76)	-	0.58	4.6
	1.51 (0.42)	-	0.66	4.2
^{60}Co γ-rays	0.34 (0.13)	2.26 (4.0)	2.35	-
	0.31 (0.08)	2.83 (3.0)	2.39	-

References			
d(16)/Be	Hall *et al.*	(1973)	4.7†
d(50)/Be	Van Dam *et al.*	(1980)	3.6
d(75)/Be	Van Dam and Wambersie	(1981)	3.2

† RBE value of 1.15 adopted for X-rays (Van Dam *et al.*, 1983)

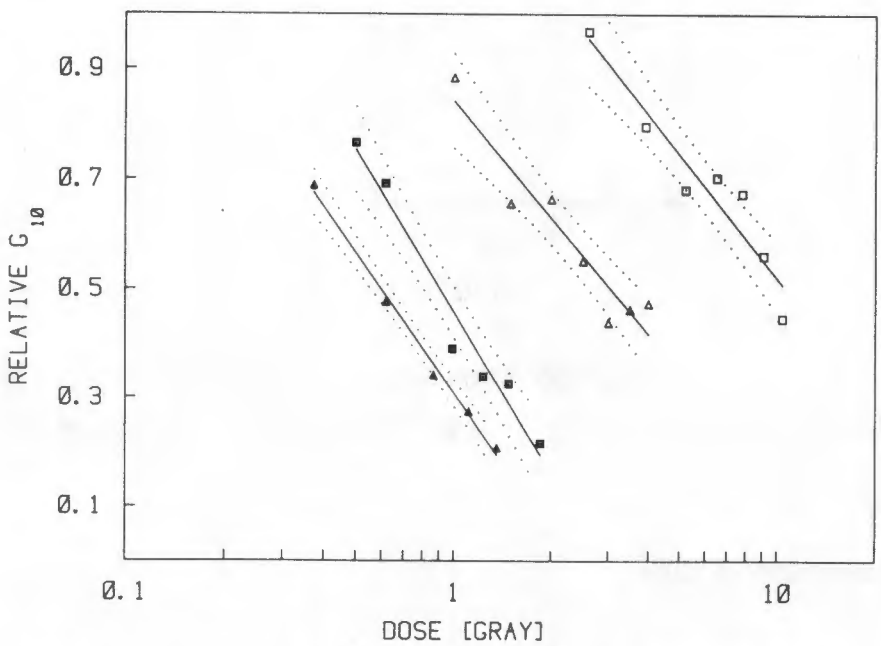

Figure 3: *10-Day growth delay measurements of the primary root of Vicia faba seedlings following exposure to d(16)/Be neutrons under aerated (▲) and hypoxic (■) conditions, and ^{60}Co γ-rays under aerated (△) and hypoxic conditions (□). Dotted lines indicate 95% confidence limits.*

Measured OER values are compared in Table 4. Reasonable agreement was observed for neutron OER values calculated from successive data sets and with values reported by other workers. The OER values for ^{60}Co irradiations were, however, consistently higher than that reported by van Dam *et al.* (1980, 1983) and Khokhar (1984) (Table 4).

Table 4: *Inactivation parameters calculated from growth delay measurements following irradiation of Vicia faba root tips with d(16)/Be neutrons and ^{60}Co γ-rays under aerobic and anoxic conditions. 95% Confidence intervals are indicated in brackets. OER values were calculated at a level of 50% reduction in growth.*

Cell Environment	α (Gy^{-1})	$\beta \times 10^2$ (Gy^{-2})	$\bar{D}$ (Gy)	OER
d(16)/Be neutrons				
Air	1.17 (0.2)	-	0.86	
N_2	0.74 (0.4)	5.19 (9.0)	1.18	1.5
Air	0.87 (0.7)	-	1.15	
N_2	0.55 (0.3)	-	1.82	1.6
References				
d+T	Van Dam (1983)			1.5
d(50)/Be	Van Dam *et al.* (1980)			1.5
d(16)/Be	Hall *et al.* (1976)			1.8

Cell Environment	α (Gy^{-1})	$\beta \times 10^2$ (Gy^{-2})	$\bar{D}$ (Gy)	OER
^{60}Co γ-rays				
Air	0.22 (0.1)	-	4.51	
N_2	0.03 (0.02)	0.39 (0.4)	11.1	3.1
Air	0.11 (0.2)	7.5 (6)	2.64	
N_2	0.03 (0.03)	7.4 (4)	8.51	3.3
References				
^{60}Co	Van Dam *et al.* (1980)			2.6
^{137}Cs	Van Dam *et al.* (1983)			2.7
X-rays	Khokhar (1984)			2.7

CHAPTER 7

SIMULTANEOUS AND SEQUENTIAL MIXED FIELD IRRADIATIONS OF MAMMALIAN CELLS

Introduction

In this chapter the influence of sequencing in mixed field exposures is investigated. As discussed in Chapter 1, the nature of lesions produced by one radiation type and subsequent interaction with those produced by another type may be determined by the irradiation protocol. Of particular interest is whether simultaneous or sequential irradiations of neutrons and photons can influence the level of synergistic interaction. Of added interest is the relevance of the order of sequential exposures, i.e. neutrons followed by photons or photons followed by neutrons.

Since synergistic interaction between different radiation types is founded on the induction of sublethal damage, the potential influence that the radiation protocol may have on cell death is based on the repair of these lesions. Higgins *et al.*, (1983) demonstrated that the simultaneous exposure of V-79 cells to 14.8 MeV neutrons and ^{60}Co γ-rays was more potent than sequential exposures for the same total dose. This was true irrespective of the order in which the irradiations were delivered. In these experiments low dose rates were used for both neutrons (0.05 Gy/min) and photons (0.08 Gy/min), consequently irradiations were protracted compared to the characteristic repair time of about one hour for V-79 cells. This led Zaider and Brenner (1984) to comment that under such conditions the synergistic interaction between neutrons and photons in the simultaneous exposure would be greater compared to that when the radiation types are delivered sequentially.

In a later set of measurements Higgins *et al.* (1984) eliminated the time difference between sequential and simultaneous irradiations by using a system of pulsed irradiations. As before, the authors demonstrated that simultaneous exposures were more potent than sequential irradiations. In contrast, McNally *et al.* (1985) did not find a difference between simultaneous and sequential irradiations of V-79 cells bombarded with combinations of X-rays and 3.2 MeV neutrons. These workers argued that because they had used dose rates about one order of magnitude higher than those used by Higgins *et al.* (1983), the role of reduced damage is less important. Consequently the

irradiation protocol should not affect the biological potency of a neutron-photon mixture. On the other hand, Ngo *et al.* (1981) reported that X-rays followed by Ne ions appeared to be more effective than the reverse sequence. This observation was made despite the fact that the dose rates for Ne-ions and X-rays were as high as 6 Gy/min and 2.7 Gy/min respectively.

Cell temperature and intercellular contact can also influence the repair of radiation damage. Stephens *et al.* (1987) suggested that temperature control during irradiations may explain the rapid split-dose recoveries observed in human cells types. Durand and Olive (1976) proposed that cell-to-cell contact is a strong modifier of repair of sublethal damage. Furthermore, Durand (1984) compared the repair of V-79 monolayers to that of V-79 spheroids during multifraction exposures and found that cells irradiated as spheroids had a greater potential for repair.

It is therefore necessary to examine the experimental configurations used by others to investigate simultaneous and sequential radiation exposures. Higgins *et al.* (1983; 1984) irradiated monolayers of cells at 37°C. In contrast, McNally *et al.* (1985) irradiated cell suspensions at room temperature. This may explain the inconsistencies.

In this chapter the combined effect of a mixture of 6.3 MeV neutrons and ^{60}Co γ-rays delivered either simultaneously or sequentially, is evaluated. In addition, investigations are described where mammalian cells in culture were exposed to p(66)/Be neutrons and ^{60}Co γ-rays, applied sequentially in different permutations.

Choice of neutron-photon mixture

Both Higgins *et al.* (1983; 1984) and McNally *et al.* (1985) compared simultaneous and sequential exposures using graded doses consisting of 40% neutrons and 60% photons. In the present work it was decided to use a mixture of approximately 25% neutrons and 75% photons. This mixture was selected because the percentage cell kill resulting from synergistic interaction between neutron and photon damage appears to reach a maximum when the combined dose consist of one part neutrons and 3 parts of photons. In Fig. 1 the percentage cells killed as a result of synergistic interaction is shown for different neutron-photon mixtures. The % of synergistic cell kill (%CK) shown in Fig. 1 was calculated using an expression described by Scott (1983).

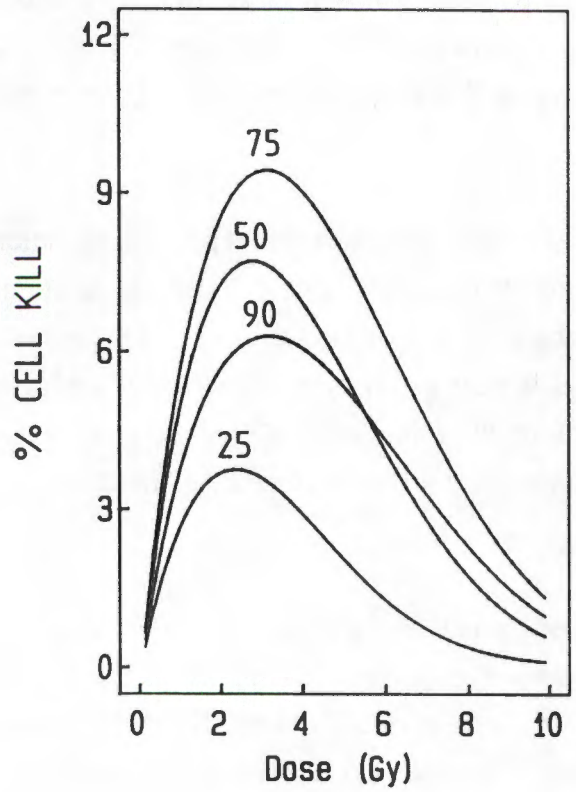

Figure 1: *The percentage of cells killed due to synergistic interaction between neutron and photon damage, as predicted for different mixtures of d(16)/Be neutrons and ^{60}Co γ-rays. The γ-ray percentage in each mixture is indicated. α and β values used in these calculations are listed in Table 1.*

$$\%\,CK = \frac{100\ e^{-(h_\gamma + h_n)}\ (1 - e^{-h_{n,\gamma}})}{1 - S}, \qquad [1]$$

where

$$h_\gamma = \alpha_\gamma D_\gamma + \beta_\gamma D_\gamma^2,$$

$$h_n = \alpha_n D_n + \beta_n D_n^2,$$

$$h_{n,\gamma} = -\ln S - h_n - h_\gamma,$$

and $$S = e^{-(\alpha_{n,\gamma} D_{n,\gamma} + \beta_{n,\gamma} D_{n,\gamma}^2)}.$$

In these calculations α- and β-values were used that describe the survival curves of V-79 cells in a d(16)/Be and ^{60}Co field. The α- and β-values for the different neutron-photon mixtures were estimated from surviving fractions calculated using the sequential synergistic equation of Zaider and Rossi (1980). Different sets of α- and β-values can

influence the level of synergistic cell kill. Even so, the pattern was always the same, with a 25% neutron and 75% photon mixture yielding the highest level of synergistic cell kill. Different models predict slight differences in the combined effect.

Irradiations With ^{60}Co γ-rays and d(16)/Be neutrons

Exponentially growing V-79 cells were irradiated as monolayers. Two days before irradiation 2×10^5 cells were plated in T 25 cm^2 growth flasks. This resulted in a culture density of about 1.2×10^5 cells/cm^2 at the time of irradiation. Care was taken to maintain the samples at 37° C before and during irradiation. The flasks were filled with complete medium and the samples irradiated in a small water phantom (10 × 10 × 3 cm) constructed of perspex.

Cells were irradiated using the tandem neutron-photon facility shown in Chapter 4. To ensure that the overall irradiation time was the same for both sequential and simultaneous exposures, the method of pulsed irradiation used by Higgins *et al.* (1984) was adopted. A schematic representation of the irradiation procedure is shown in Fig. 2. Simultaneous exposures were delivered in 3 minute intervals alternating with 3 minute beam off intervals. This procedure allowed one to keep the overall dose rate the same for both the simultaneous and sequential exposures. The neutron and photon dose rates were 0.20 and 0.63 Gy/min respectively.

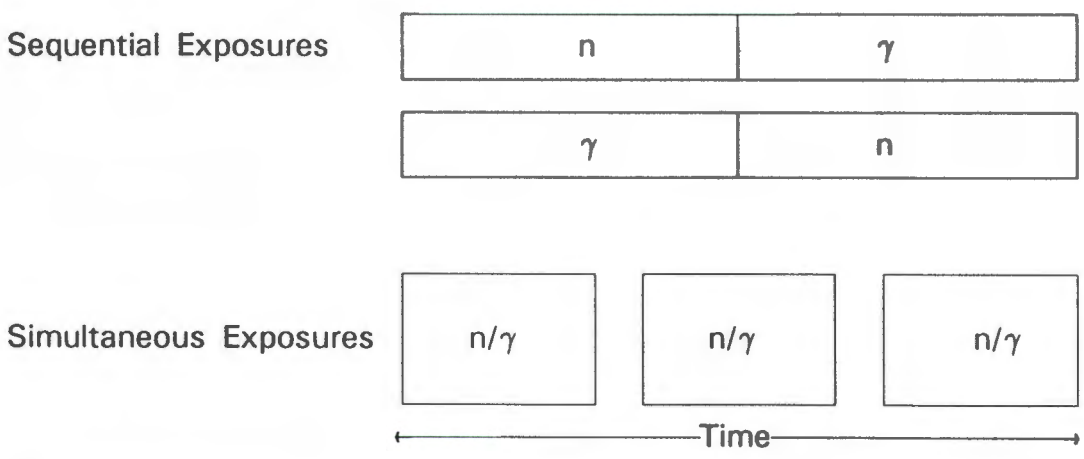

Figure 2: *Schematic representation of pulsed irradiation procedure employed to deliver a simultaneous and sequential radiation mixture consisting of 23% d(16)/Be neutrons and 77% ^{60}Co γ-rays in the same elapsed time.*

Survival following graded neutron doses (23%) and graded photon doses (77%), delivered either simultaneously or sequentially, were not significantly different. This is evident in Fig. 3 where the 95% confidence ellipses for the estimated α- and β-values are shown to overlap.

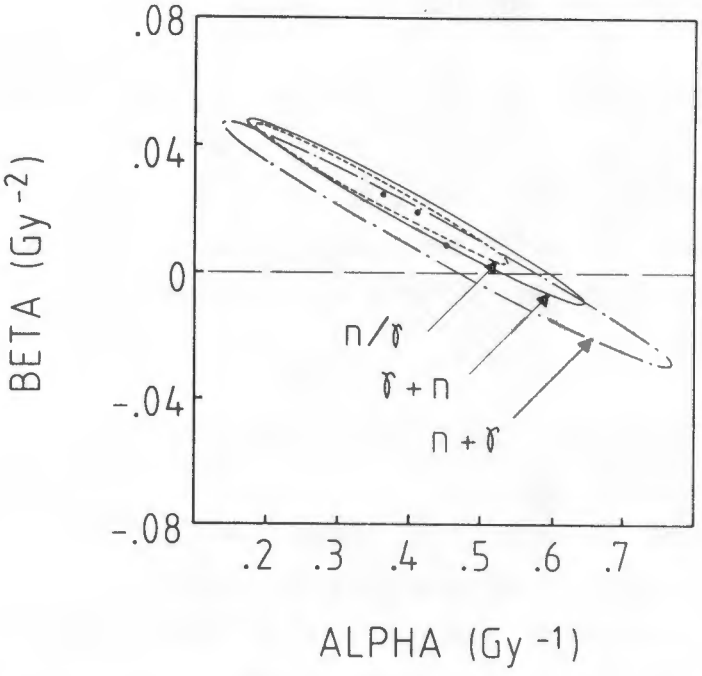

Figure 3: *95% Confidence ellipses for the inactivation parameters α and β describing the curves fitted to surviving fractions of V-79 cells following different irradiation procedures (see text).*

These observations disagree with the findings of Higgins *et al.* (1984) who reported an increase in the initial slope (α-value) of the survival curve following simultaneous exposures and an unchanged β-parameter when compared with sequential irradiations. These authors used a mixture of ^{60}Co γ-rays (60%) and 14.8 MeV neutrons (40%).

In spite of the lower neutron fraction used, the radiosensitivity of the V-79 cells was considerably higher compared to that observed by Higgins *et al.* (1983; 1984). The response measured here is also compatible to that measured by McNally *et al.* (1985), who did not observe a difference between simultaneous and sequential exposures. The higher doses (up to 16 Gy) of radiation used by Higgins *et al.* (1984) may have allowed these workers to resolve possible differences in the biological effect of different irradiation configurations.

From the presented data it was concluded that simultaneous and sequential irradiations yield essentially the same level of biological effect. Also, the ordering of sequential exposures did not significantly influence the evaluated dose-response parameters.

Sequential Exposures to ^{60}Co γ-rays and p(66)/Be Neutrons

The above consistancy observed between different sequences of d(16)/Be neutrons and photons delivered in close succession was also observed when CHO-K1 and B-16 cells were exposed to a series of doses consisting of 23% p(66)/Be neutrons and 77% ^{60}Co γ-rays (Fig. 4). These results are in agreement with those observed for V-79 cells irradiated with different sequences of d(16)/Be neutrons and ^{60}Co γ-rays (Fig. 3).

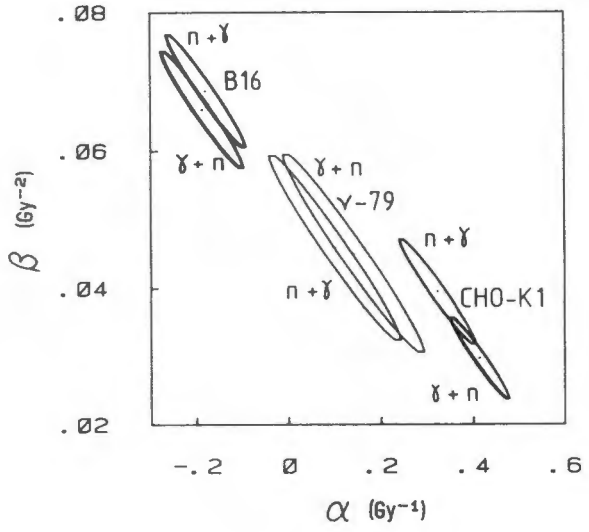

Figure 4: *95% Confidence ellipses for the inactivation parameters α and β describing the curves fitted to surviving fractions of V-79, CHO-K1 and B-16 cells following different irradiation procedures (see text).*

Simultaneous Mixtures and Fractionated Exposures

A fundamental question in mixed high-low-LET irradiations is whether the inherent γ-contamination of the neutron beam is responsible for the induction of reparable damage. This was investigated by exposing V-79 cells to split-doses of different neutron-photon mixtures [d(16)/Be neutrons and ^{60}Co γ-rays] separated by up to 3 hours. Between irradiations the cell samples were incubated at 37° C.

The neutron and photon doses used in each instance were chosen so that the first dose of each mixture would result in a surviving fraction of about 10%. The magnitude of repair can be expressed as a recovery ratio, i.e. the ratio S_t/S_0 where S_t is the surviving fraction at time t and S_0 is the surviving fraction when no time lapse was allowed between exposures. Recovery was observed between split doses of simultaneous mixtures containing 9% and 23% neutrons (Fig. 5). Recovery ratios obtained from split-dose exposures to photons only is shown for comparison. When the proportion of neutrons was 48%, no recovery was seen.

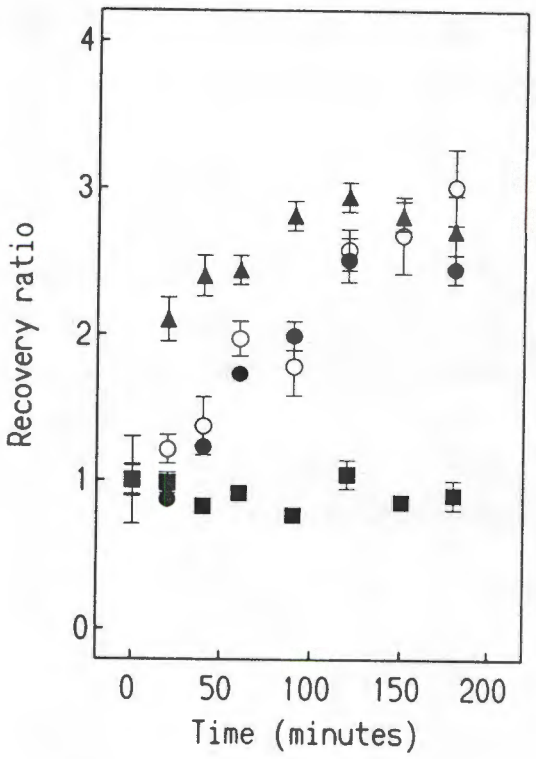

Figure 5: *Recovery ratios as a function of time for V-79 cells exposed to split doses of radiation mixtures containing d(16)/Be neutrons and ^{60}Co γ-rays: 10% neutrons (•), 23% neutrons (○) or 48% neutrons (■). Recovery ratios measured after a priming dose of 6 Gy photons followed by 6 Gy photons is also shown for comparison (▲). Standard deviations are indicated by error bars.*

Based on the above findings, it was concluded that reparable damage induced by the inherent γ-contamination, which is about 2% for the d(16)/Be beam (and not more than 7.8 % in the p(66)/Be beam), only contributes minimally to the induced reparable damage and is unlikely to play a significant role in any synergistic interaction.

Time Delayed Sequential Irradiations using p(66)/Be neutrons and ^{60}Co γ-rays

The synergistic interaction between different radiation types diminishes when the cells are allowed to repair sublethal damage between irradiations. In this section the recovery ratios obtained using split-dose exposures of neutrons and photons are shown. These

measurements had two objectives; firstly to demonstrate to what extent the p(66)/Be neutrons used in the study induced reparable damage, and secondly to follow the kinetics of recovery as a function of sequencing.

In general the repair measured in split-dose exposures is reflected in the size of the survival curve shoulder of the second radiation type. Rialton *et al.* (1974, 1975) reported a lack of repair in CHO cells exposed to ^{60}Co γ-rays followed by D-T neutrons. This is not surprising since the neutron dose response curve of these CHO cells had a small shoulder (D_q = 0.32 Gy). However, repair was also absent in V-79 cells irradiated with X-rays followed by d(16)/Be neutrons or neutrons followed by X-rays (Durand and Olive, 1976).

In Fig. 6 split dose recovery ratios are shown for V-79 cells exposed to a priming dose of 2 Gy p(66)/Be neutrons followed by 6 Gy photons, a priming dose of 6 Gy photons followed by 2 Gy neutrons and a priming dose of 3 Gy neutrons followed by 3 Gy neutrons. For comparison the recovery ratios from a priming dose of 6 Gy photons followed by 6 Gy photons is also shown. Recovery between dose fractions was evident, suggesting that the level of synergistic interaction between neutrons and photons will be reduced if time is allowed for the repair of sublethal damage. Also, recovery ratios of mixed field exposures followed over a period of 3 hours appeared to be independent of the radiation sequence. This is in contrast to the findings of Durand and Olive (1976). The repair noted in this study may be attributed to the higher neutron energies.

Neutron-Photon Interaction in the d(16)/Be Beam

The interaction between d(16)/Be neutrons and ^{60}Co γ-rays was determined by exposing V-79 fibroblasts, CHO-K1 and 3T3 cells to various neutron-photon mixtures. Simultaneous irradiations were performed in which the photon fraction was either 23%, 48% or 73% of the total dose. In addition to this, the cells were exposed to graded dose of photons only and neutrons only and to a series of neutron followed by photon exposures in which the neutron dose was 9%. The inherent γ-contamination of the neutron beam was 2%.

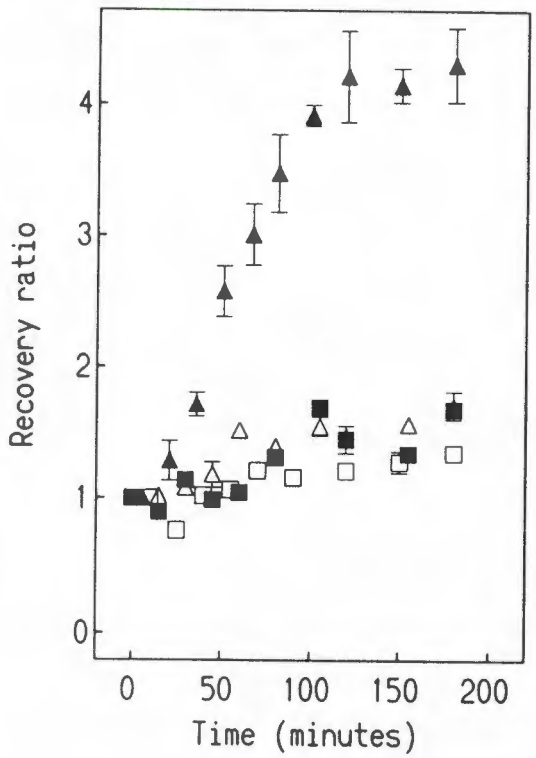

Figure 6: *Recovery ratios for V-79 cells exposed to a priming dose of 2 Gy p(66)/Be neutrons followed at various time intervals with a dose of 6 Gy ^{60}Co γ-rays (□), or a priming dose of 6 Gy photons followed by 2 Gy neutrons (△) or 3 Gy neutrons followed by 3 Gy neutrons (■). The recovery ratios from a 6 Gy priming dose of photons followed by 6 Gy photons is shown for comparison (▲). Error bars indicate standard deviations.*

The fitted survival curves to the V-79, CHO-K1 and 3T3 data are shown in Figs 7, 8 and 9 respectively. The various parameters describing the fitted curves to the survival data are listed in Table 1. Included in Figs. 7, 8 and 9 are the predicted surviving fractions for the different neutron-photon mixtures assuming independent action of the individual radiations types. The independent predictions were calculated from:

$$S = e^{-(\alpha_n D_n + \beta_n D_n^2 + \alpha_\gamma D_\gamma + \beta_\gamma D_\gamma^2)}, \qquad [2]$$

where

S = the surviving fraction,
D_n = the neutron dose and
D_γ = the photon dose.

α_n and β_n refer to inactivation parameters estimated from the neutron response curves and α_γ and β_γ are the coefficients for γ-ray inactivation.

The observed V-79 and CHO-K1 surviving fractions were lower than that predicted for independent actions, indicating synergistic interaction between neutron and

photon damage. In contrast, the response of the 3T3 cells to the different neutron-photon mixtures appeared to be antagonistic.

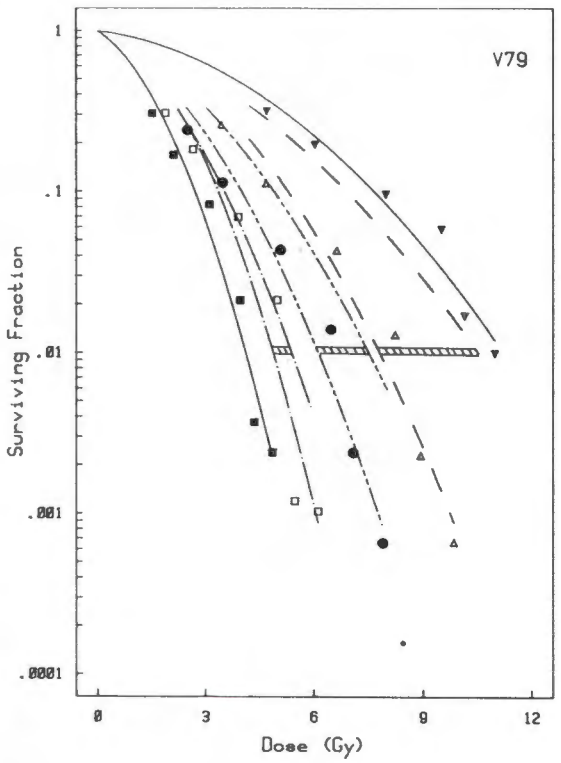

Figure 7: *Measured survival curves for V-79 cells following irradiation with d(16)/Be neutrons (■), ^{60}Co photons (▲), and simultaneous mixtures of neutrons and photons consisting of 23% neutrons (△), 48% neutrons (•) and 73% neutrons (□). The dashed lines indicate the expected surviving fractions for each radiation mixture if the individual modalities acted independently.*

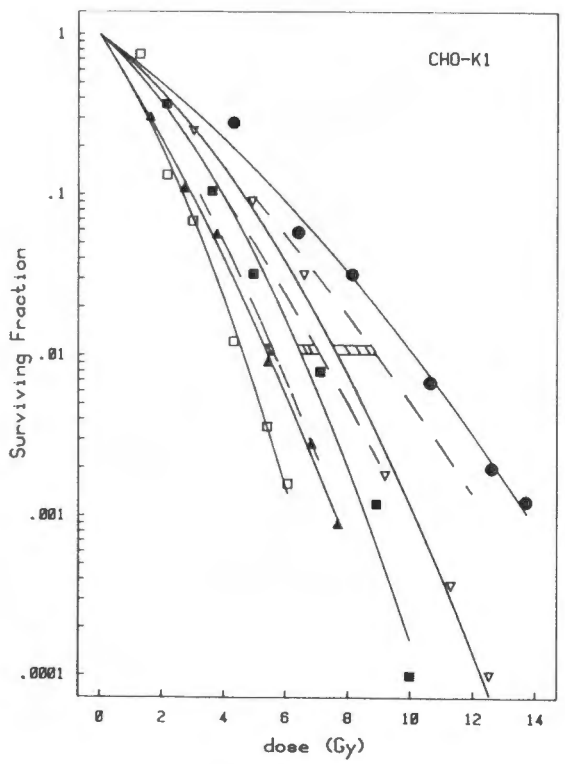

Figure 8: *Measured survival curves for CHO-K1 cells following irradiation with d(16)/Be neutrons (□), ^{60}Co photons (•), and simultaneous mixtures of neutrons and photons consisting of 23% neutrons (△), 48% neutrons (■) and 73% neutrons (▲). The dashed lines indicate the expected surviving fractions for each radiation mixture if the individual modalities acted independently.*

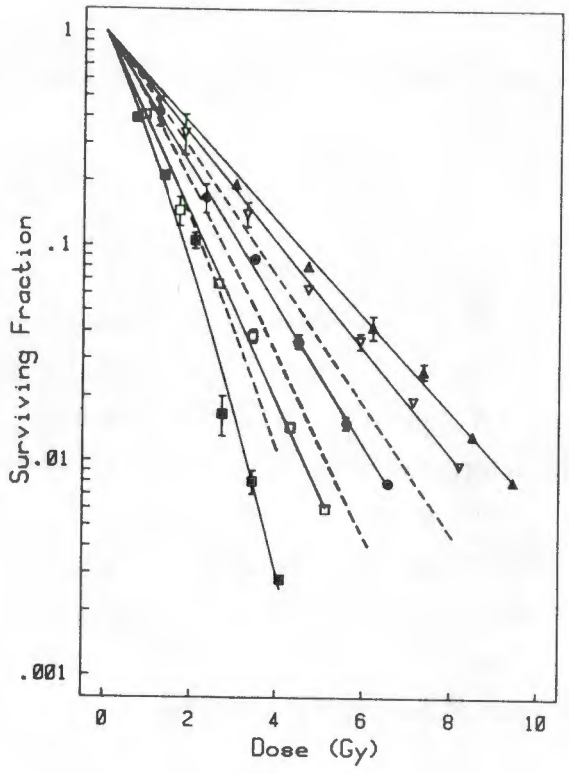

Figure 9: *Measured survival curves for 3T3 cells following irradiation with d(16)/Be neutrons (■), ^{60}Co photons (▲), and simultaneous mixtures of neutrons and photons consisting of 23% neutrons (△), 48% neutrons (•) and 73% neutrons (□). The dashed lines indicate the expected surviving fractions for each radiation mixture if the individual modalities acted independently. Standard deviations are indicated by error bars.*

Enhancement Ratios

In an attempt to quantify the level of interaction observed for the different mixtures, enhancement ratios (ER) were evaluated from the experimental data according to the method of Bird *et al.* (1983). The ER is the ratio of the dose assuming independent action to the experimentally observed dose which produces the same level of effect. Enhancement ratios were calculated at the 1% survival level and are shown in Fig. 10 as a function of the percentage neutrons present in each mixture. The V-79 and CHO-K1 cell types exhibit larger ER-values for smaller neutron fractions whilst the ER-values of the 3T3 cells were consistently less than unity. The latter finding indicates an antagonistic response for the 3T3 cells.

The different cell types used in these measurements had dissimilar radiosensitivities to radiation fields of varying quality. This is reflected in the changing $\bar{D}$-values (Table 1). There was a strong correlation between the photon sensitivity of a given cell type and mixtures containing various fractions of neutrons. The greater radiosensitivity of the 3T3 cells is manifested in smaller $\bar{D}$-values and is also evident in the larger α-values. With the exception of the neutron only irradiations, a significant β-parameter could not be detected using 3T3 cells in any of the other radiation fields.

This may explain the absence of synergy observed in this cell type. On the other hand the more radioresistant V-79 cells show larger β-values, facilitating a greater level of interaction between the neutrons and photons. This is reflected in the larger enhancement ratios (Fig. 10).

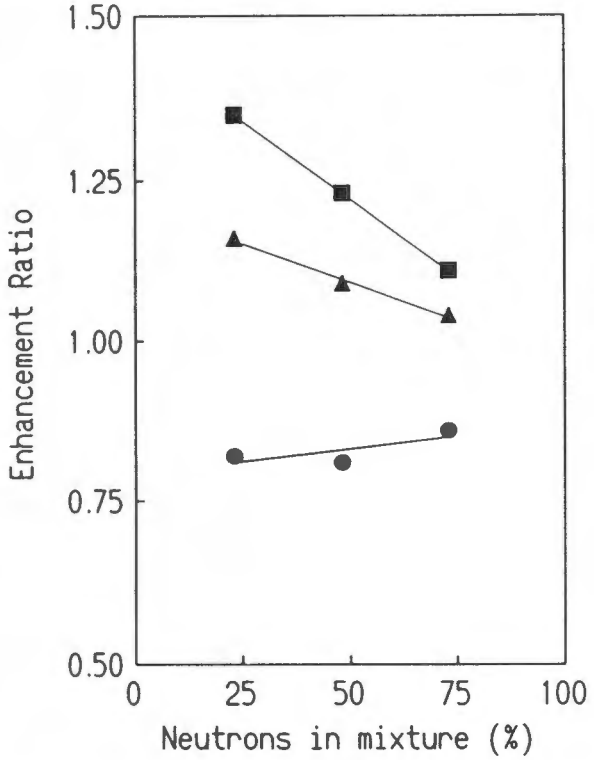

Figure 10: *Dose enhancement ratios calculated at the 1% survival level for the inactivation of V-79 cells (■), CHO-K1 cells (▲) and 3T3 cells (•) following exposure to various mixtures of d(16)/Be neutrons and ^{60}Co γ-rays.*

Ngo *et al.* (1988) reported that V-79 cells in the radioresistant S-phase showed a greater level of interaction compared to cells in other phases of the cell-cycle. A similar finding is presented here by comparing cell lines of different sensitivities. Should the cells in a tumour be more radioresistant than those of the surrounding normal tissue, these findings may indicate a therapeutic advantage for combined high-low-LET radiotherapy. The results are however not in agreement with expectations based on the findings of Peacock *et al.* (1988). These workers reported larger β-values (i.e. more intertrack interaction) in radiosensitive cell types.

Interaction In a n/γ Mixture Containing 9% d(16)/Be Neutrons

The trend in Fig. 10 indicating an increase in the enhancement ratios with a decreasing neutron fraction in the mixture may be misleading. The deduction that can be made is that very large enhancement ratios could be expected in beams where the neutron component is low. Predictions based on the Zaider and Rossi model(1980) indicate that

Table 1: *Inactivation parameters for different cell types following exposure to various mixtures of d(16)/Be neutrons and ^{60}Co γ-rays. 95% confidence limits are given in brackets.*

Neutron fraction in mixture (%)	α (Gy^{-1})	β (Gy^{-2})	$\bar{D}$ (Gy)	Enhancement Ratio
V-79				
98	0.331 (0.26)	0.189 (0.06)	1.39 (0.22)	
73	0.112 (0.36)	0.169 (0.07)	1.86 (0.53)	1.11
48	0.237 (0.21)	0.084 (0.03)	2.04 (0.40)	1.23
23	0.106 (0.15)	0.062 (0.02)	2.84 (0.53)	1.35
0	0.063 (0.09)	0.031 (0.01)	4.19 (0.58)	
CHO-K1				
98	0.678 (0.18)	0.067 (0.03)	1.22 (0.15)	
73	0.696 (0.09)	0.027 (0.01)	1.31 (0.09)	1.04
48	0.390 (0.13)	0.048 (0.02)	1.86 (0.26)	1.09
23	0.347 (0.11)	0.033 (0.01)	2.15 (0.29)	1.16
0	0.327 (0.07)	0.013 (0.01)	2.60 (0.28)	
3T3				
98	1.085 (0.22)	0.092 (0.06)	0.82 (0.08)	
73	0.993 (0.09)	-	1.00 (0.09)	0.86
48	0.738 (0.05)	-	1.36 (0.09)	0.81
23	0.568 (0.05)	-	1.76 (0.16)	0.82
0	0.509 (0.03)	-	1.96 (0.12)	

when the neutron dose in a mixture is below about 20%, the level of interaction diminishes dramatically.

A separate series of measurements was performed using V-79 cells to determine the enhancement ratio following sequential neutron-photon exposures in which the neutrons dose was 9% of the total dose. The data is shown in Fig. 11 and the inactivation parameters listed in Table 2. An enhancement ratio of 1.13 was calculated for this mixture. The decreased enhancement ratio compared to those in Fig. 10 is in agreement with the predictions based on the Zaider-Rossi model.

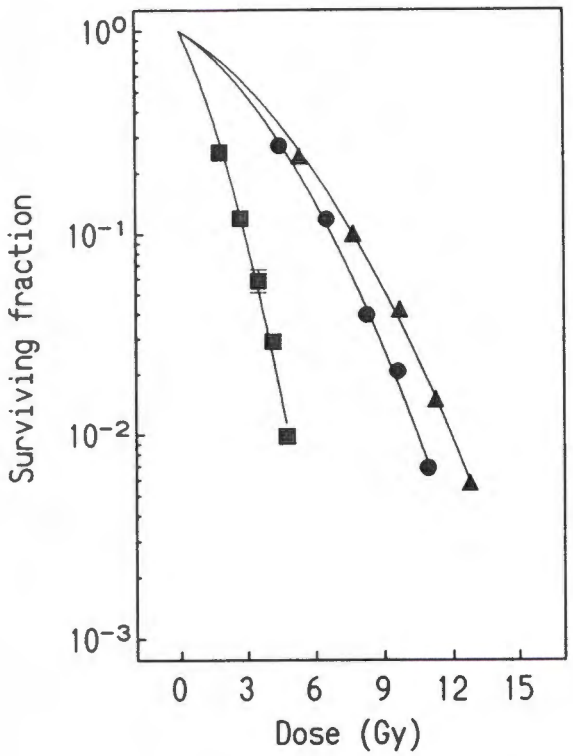

Figure 11: *Surviving fractions measured with V-79 cells following exposure to d(16)/Be neutrons (■), ^{60}Co γ-rays (▲) and a sequential mixture consisting of 9% neutrons followed by 91% photons (•).*

Combined Effect Predictions

Since the observed radiation damage produced by neutrons and photons was clearly not independent for the n/γ mixtures, it is of interest to determine whether the combined effects in the V-79 and CHO-K1 cells were in fact synergistic. For this purpose the envelope of additivity was calculated according to the procedures prescribed by Steel and Peckham (1979) and Streffer and Müller (1987).

Table 2: *Inactivation parameters calculated from observed surviving fractions of V-79 cells following exposure to d(16)/Be neutrons, ^{60}Co γ-rays and a sequential mixture containing 9% neutrons and 91% photons. Parentheses indicate 95% confidence limits.*

Radiation Type	α (Gy^{-1})	β (Gy^{-2})	$\bar{D}$ (Gy)	ER
d(16)/Be neutrons	0.548 (0.11)	0.0828 (0.028)	1.36 (0.09)	
^{60}Co γ-rays	0.145 (0.02)	0.0202 (0.003)	3.83 (0.17)	
9% n + 91% γ	0.163 (0.03)	0.0264 (0.004)	3.35 (0.16)	1.13

The neutron and photon doses required to reduce the surviving fraction of the V-79 cells to 1% is shown in Fig. 12. Three possible additive mechanisms are indicated. Mode I in Fig. 12 refers to hetero-additivity, assuming that the neutron and photon radiations cause cell killing by different mechanisms. This is the same as assuming the radiation types in a mixture act independently. The combination of neutron and photon doses required to reduce the surviving fraction to 1% was lower in all cases, again indicating an interaction of damage produced by a combination of radiation types.

Mode II refers to iso-additivity predictions where it is assumed that each agent in the mixture acts through a similar mechanism. Mode II was calculated in two ways. Firstly, the neutron and photon doses required to reduce the surviving fraction to 1% were calculated starting the addition procedure where neutrons are given first. Here the envelope of additivity encloses the experimental observations, classifying the combined effect as not more than additive, i.e. not synergistic. The second method of calculating mode II was based on giving the photons first, followed by neutrons. In this case the experimental points lie below the envelope of additivity, thus classifying the experimental observations as synergistic. Opposing conclusions can therefore be made using the same experimental data. Such a contradictory interpretation of mixed-field data has also been observed by Ngo *et al.* (1981). Therefore, constructing envelopes of additivity does not appear to be suitable for the interpretation of combined neutron-photon effects.

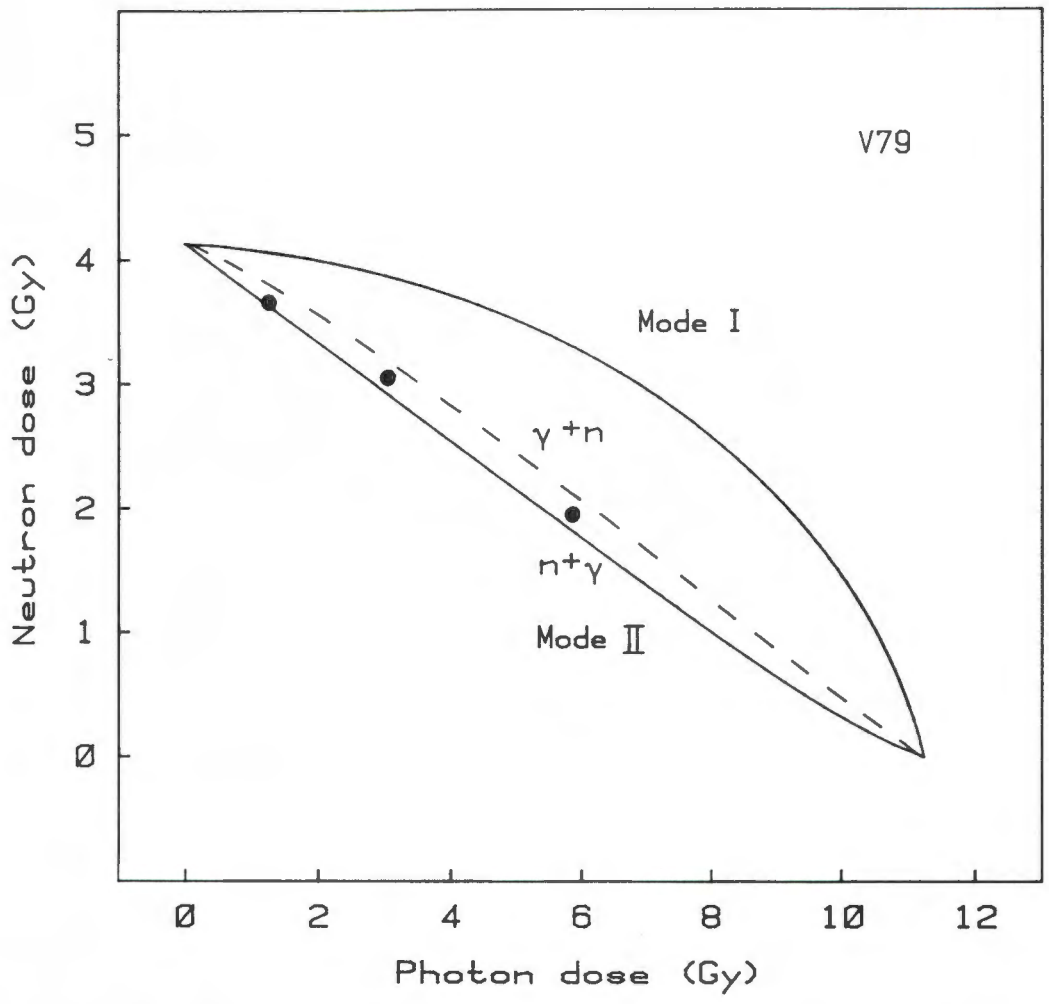

Figure 12: *Envelope of additivity calculated for V-79 cells at the 1% survival level for various mixtures of d(16)/Be neutrons and ^{60}Co γ-rays. The combinations of neutron and photon doses observed experimentally to reduce the surviving fraction to 1% are indicated (solid circles).*

An alternative method of analysis is that of linear isobolograms (Lam, 1989a) and is discussed below.

Predictions Based on the Lesion Additivity Model

In Chapter 3 the lesion additivity model (LAM) was discussed. The data for V-79 cells shown in Fig. 7 were analyzed according to the LAM and are presented in Fig. 13. The dose combination required to produce a given surviving fraction is well predicted by the model for the neutron-photon mixtures used. The solid line in Fig. 13 refers to the combination of neutron and photon doses required to produce zero-interaction. No systematic deviation between experimental data and predicted dose combinations was apparent at different levels of surviving fractions.

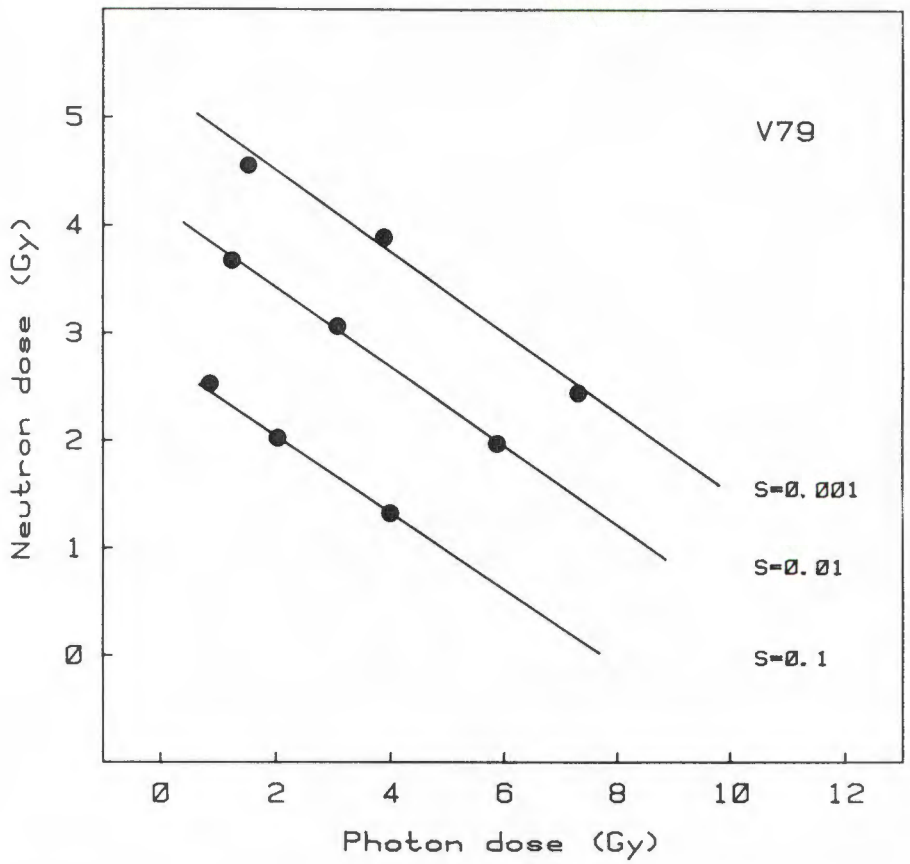

Figure 13: *Linear isobolograms for V-79 cells generated at different survival levels using experimentally measured d(16)/Be neutron and ^{60}Co γ-ray survival curves (solid lines). The combinations of neutron and photon doses observed experimentally to reduce the surviving fraction to various levels are indicated (solid circles).*

The data for the CHO-K1 cells (Fig. 8) were also analyzed using the LAM. According to this model the index of interaction (I) for a combination of neutrons and photons is predicted to be unity. The predictions were made using the dose responses to neutrons only and photons only. The indices of interaction calculated for CHO-K1 cells for different neutron-photon mixtures are shown in Fig. 14. An index of interaction smaller than one indicates that the lesion additivity model underestimates the level of biological effect observed for the dose of a particular neutron-photon mixture.

Included in Fig. 14 is the interaction index for the 23% neutron mixture calculated assuming that the neutrons and photons act independently. This is to illustrate that the concept of zero-interaction is different from that of independent action. Zero-interaction is a particular case of interaction where the individual dose relationships satisfy equation [7] in Chapter 3.

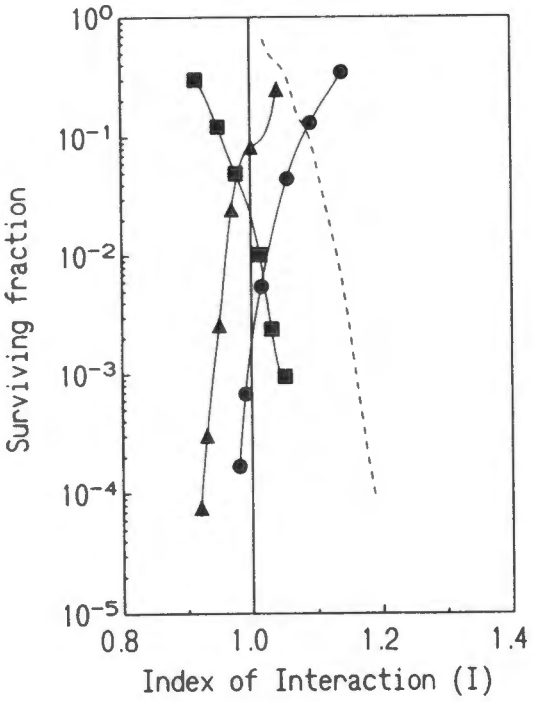

Figure 14: *Indices of interaction calculated for the lesion additivity model from the mean surviving fraction observed following exposure of CHO-K1 cells to simultaneous mixtures of d(16)/Be neutrons and ^{60}Co γ-rays consisting of 23% neutrons (▲), 48% neutrons (●) and 73% neutrons (■). The dashed line indicates interaction indices expected for a 23% neutron and 77% photon mixture if the damage produced by the different radiation types acted independently.*

By definition, synergy prevails when the index of interaction is less than one and antagonism is indicated by interaction indices larger than unity. As shown in Fig. 14 the experimentally determined indices cluster around the predicted value of 1. The calculated mean indices of interaction for surviving fractions observed with V-79, CHO-K1 and 3T3 cells are listed in Table 3.

The antagonistic interaction observed with 3T3 cells is reflected by indices of interaction larger than 1. Where synergistic interaction was evident (V-79 and CHO-K1 cells), indices of interaction were not different from unity for any of the mixed-field responses observed. The lesion additivity model appears to be suitable for predicting the synergistic interaction of various mixtures of neutrons and photons in mammalian cells.

Cell Kill due to Synergism

The proportion of cells in a targeted population which are inactivated by synergistic interaction between neutrons and photons are predicted to change with the total dose and the composition of the mixture. This was shown in Fig. 1. Irrespective of the neutron-photon mixture, the fraction of cells killed due to synergistic interaction reaches a maximum at total doses of about 3 - 4 Gy.

Table 3: *Mean indices of interaction (I) calculated according to the lesion additivity model for surviving fractions observed following exposure of V-79, CHO-K1 and 3T3 cells to various mixtures of d(16)/Be neutrons and ^{60}Co γ-rays. Standard deviations are shown in brackets.*

Interaction Index (I)			
	Cell Type		
% Neutrons in mixture	V-79	CHO-K1	3T3
9	1.00 (0.03)	-	-
23	1.00 (0.09)	0.99 (0.08)	1.22 (0.09)
48	0.99 (0.10)	1.04 (0.11)	1.22 (0.10)
73	0.98 (0.07)	0.99 (0.07)	1.09 (0.11)

The data presented in the previous section for V-79 cells were analyzed according to equation [1]. The synergistic cell kill for the various mixtures was predicted using the interaction function of Zaider and Rossi (1980). This was compared to the proportion of synergistic cell kill observed and is shown in Fig. 15. Experimental curves were generated using the best fit (α- and β-values) that described the responses to the different combinations of neutrons and photons. At higher doses (>4 Gy) there was good agreement between the experimental findings and the predicted responses. However, at the lower doses substantial disagreement between predicted and experimental findings was evident. This may be the consequence of extrapolating the experimental responses to low doses since surviving fractions were predominantly quantified at higher doses.

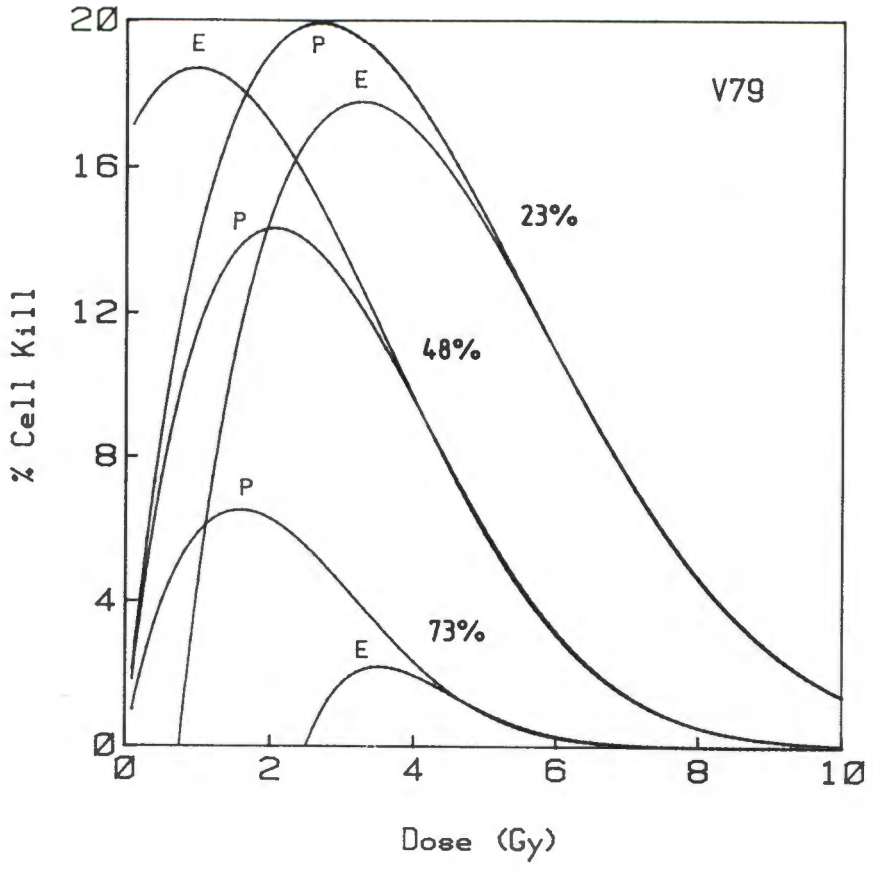

Figure 15: *Percentage cells killed due to synergistic interaction following exposure of V-79 cells to various mixtures of d(16)/Be neutrons and ^{60}Co γ-rays. Predicted responses and experimental responses are respectively indicated by P and E.*

In order to establish if the proportion of cells killed due to synergistic interaction is reduced at lower doses (less than 3 - 4 Gy), a separate experiment was performed. Surviving fractions were measured following the exposure of V-79 cells to various dose mixtures containing 23% neutrons and 77% photons (Fig. 16). The total doses were between 1 and 7 Gy. These doses were chosen to cover the entire range of expected responses. The fraction of cells killed as a result of synergistic interaction was calculated for this data set and is shown in Fig. 17 together with similar calculations for the data in Fig. 7 (23% neutron mixture). In spite of the large uncertainties encountered at low doses, the analysis indicated a maximum at about 5 Gy.

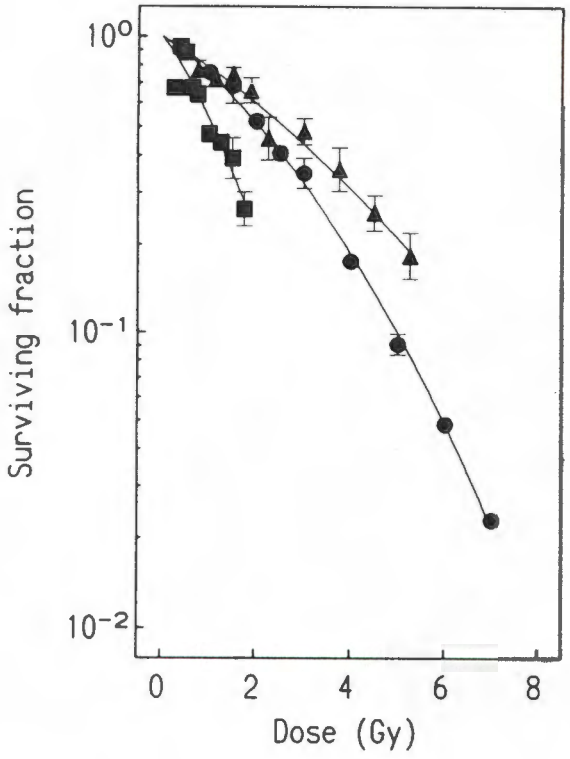

Figure 16: *Surviving fractions measured with V-79 cells following exposure to d(16)/Be neutrons (■), ^{60}Co γ-rays (▲) and a simultaneous mixture consisting of 23% neutrons and 77% photons (•). Standard deviations are indicated by error bars.*

These observations confirm that although the degree of interaction between damage produced by neutrons and photons increases monotonically with dose, the proportion of cells killed due to synergistic interaction relative to that inactivated by the individual radiation types reaches a maximum at about 5 Gy. A similar type of analysis for L5 cells exposed to 50% neutrons (14 MeV) and 50% X-rays indicated that a maximum of about 5% of these cells were killed due to synergism for a total dose of 1.5 Gy (Scott 1983). The higher dose at which the present data showed a maximum can in part be explained by the lower fraction of neutrons. There is a tendency for the percentage kill to peak at higher doses when the neutron contribution in the mixture is reduced (Fig. 15). The fact that synergistic cell kill is a maximum at relatively low doses may be important for the clinical use of neutron-photon mixtures.

Neutron-Photon Interaction in the p(66)/Be Beam

As shown in Table 1, which refers to neutron-photon interaction in a d(16)/Be beam, there is a trend for β-values to become smaller when the mean LET of the radiation field is reduced, i.e when there are more photons in the mixture. It would therefore be

expected that a first dose of relatively higher energy neutrons (lower LET) would result in lower levels of synergistic interaction with a subsequent dose of ^{60}Co γ-rays. In an attempt to verify this V-79 and CHO-K1 cells were exposed to various mixtures of p(66)/Be neutrons and ^{60}Co γ-rays given sequentially. The inactivation parameters calculated from the respective surviving fractions are listed in Table 4. Included are the inactivation parameters for B-16 cells also exposed to neutron-photon mixtures.

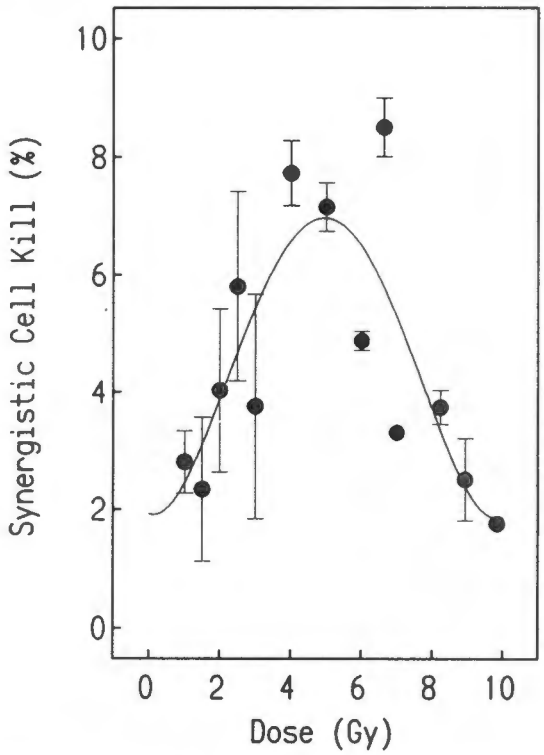

Figure 17: *Percentage cells killed due to synergistic interaction following exposure of V-79 cells to a mixture consisting of 23% d(16)/Be neutrons and 77% ^{60}Co γ-rays. Error bars indicate the standard error of the mean.*

The different radiosensitivities of the various cell types are indicated by their respective $\bar{D}$-values. The reduced potency of p(66)/Be neutrons relative to d(16)/Be neutrons is indicated by larger $\bar{D}$-values for neutron only irradiations (Tables 1 and 4). However, the calculated enhancement ratios were not significantly different from those observed in the same cell type exposed to mixtures of d(16)/Be neutrons and ^{60}Co γ-rays. The present approach aimed at demonstrating different levels of synergistic interaction with a change in LET was therefore inadequate. An alternative approach, comparing the induction of sublethal damage between high and low-LET radiation, is discussed in the following Chapter.

Table 4: *Inactivation parameters for different cell types exposed to various mixtures of p(66)/Be neutrons and ^{60}Co γ-rays. 95% Confidence limits are indicated in brackets.*

Neutron fraction in mixture (%)	α (Gy^{-1})	β (Gy^{-2})	$\bar{D}$ (Gy)	Enhancement Ratio
V-79				
92	0.468 (0.03)	0.053 (0.01)	1.63 (0.05)	
69	0.216 (0.1)	0.073 (0.01)	2.19 (0.24)	1.12
46	0.312 (0.11)	0.044 (0.01)	2.15 (0.30)	1.23
23	0.154 (0.05)	0.042 (0.01)	2.95 (0.20)	1.09
0	0.049 (0.05)	0.052 (0.01)	3.44 (0.60)	
CHO-K1				
92	0.432 (0.12)	0.102 (0.02)	1.48 (0.13)	
69	0.427 (0.04)	0.070 (0.01)	1.63 (0.10)	1.08
46	0.401 (0.03)	0.047 (0.01)	1.83 (0.07)	1.16
23	0.368 (0.04)	0.034 (0.01)	2.05 (0.11)	1.17
0	0.224 (0.06)	0.038 (0.01)	2.62 (0.25)	
B16				
92	0.241 (0.09)	0.074 (0.01)	2.10 (0.21)	
69	-	0.075 (0.01)	3.20 (0.52)	1.06
46	0.163 (0.08)	0.051 (0.01)	2.70 (0.31)	1.29
23	-	0.050 (0.01)	3.94 (0.50)	1.17
0	-	0.045 (0.01)	4.18 (0.53)	

CHAPTER 8

A COMPARISON OF SUBLETHAL DAMAGE INDUCED BY p(66)/Be NEUTRONS AND ^{60}Co γ-RAYS

Introduction

In the this Chapter the term sublethal damage is used in its operational sense (ICRU Report 30, 1979). The survival curves of cells exposed to high-LET radiation are characterized by larger β-values compared to those of the same cell type irradiated with photons (Fig. 1, Chapter 6). Also, Britten *et al.* (1992) found when determining the inherent neutron sensitivity of human cells exhibiting different photon sensitivities that larger β-values were inferred when the cells were exposed to p(62)/Be neutrons. Furthermore, there is a trend towards smaller β-values when d(16)/Be neutron beams with greater photon contamination are used (Table 1, Chapter 7). However, Joiner *et al.* (1983) using mouse skin reactions, reported similar β-values for neutrons and X-rays.

Considering that the β-value determined from a survival curve is a measure of cellular recovery (Peacock *et al.*, 1988; Steel 1991), the higher β-values observed following neutron irradiation therefore contradicts the expected trend. It is well established that biological damage from high-LET radiation offers less repair compared to photons. For example, lower recovery ratios for cells exposed to split doses of neutrons compared to photons have been reported by McNally *et al.* (1982) and Tubiana *et al.* (1990).

However, lower recovery ratios following neutron split doses and larger β-values for high-LET radiations are not necessarily contradictory. A β-value calculated from a survival curve represents a parameter based on the physical dose, whilst split-dose recovery ratios are compared at a level of iso-effect i.e., the biological effect of a lower neutron dose is compared with the same level of damage caused by a higher photon dose. This approach is based on an assumed single-hit, multitarget model of cell killing, which predicts that as the dose is increased the recovery ratio will rise to a maximum equal to the extrapolation number of the acute cell survival curve (Peacock *et al.*, 1988).

Split-dose recovery ratios are compared at a level of iso-effect occurring beyond the shoulder of both neutron and photon curves, usually at a surviving fraction of 10% or

less. It is assumed that a single value of the recovery ratio can be taken to represent the repair capacity of cells following exposure to a particular radiation type. However, Peacock *et al.* (1988) have pointed out that the recovery ratio does not reach a limiting value but continues to increase with dose. Consequently, should the split-dose recovery ratios of neutrons and photons be compared at a level of iso-dose rather than at a level of iso-effect, it is possible that repair compatible with the observed β-values could be demonstrated.

The induction of comparatively more sublethal damage by neutrons than photons is observed when the shoulder widths of survival curves following high- and low-LET radiation are compared. The smaller shoulder, i.e. less accumulation of sublethal damage following high-LET radiation, is the result of interaction of reparable damage (Ngo *et al.*, 1977). The induction of sublethal damage can thus be quantified by observing the rate at which D_q-values decrease for survival curves exposed to a priming dose of one radiation type followed by graded doses of a second type. McNally *et al.* (1981, 1984) have shown that D_q-values calculated from X-ray survival curves diminish at the same rate following equal priming doses of either X-rays or neutrons. This would imply that the same dose of different types of radiation induce comparable levels of sublethal damage. In contrast, when neutron and photon irradiations to a cell population are compared at a level of iso-effect, fewer neutron induced sublethal lesions were available for subsequent interaction with photons (Ngo *et al.*, 1977).

When the LET of the priming dose is further increased, such as with α-particles, there is either an equal or more effective induction of sublethal damage on a equal dose basis compared to neutrons or X-rays (McNally *et al.*, 1988). If the order of irradiations was reversed, i.e. for a priming dose of X-rays, then the D_q-value of the subsequent high-LET radiation either remains zero (31 MeV Ne-ions) or becomes zero (3.2 MeV neutrons) (Ngo *et al.*, 1981; McNally *et al.*, 1984).

Both the Ne-ion and the neutron beams used by Ngo *et al.* (1981) and McNally *et al.* (1984) respectively were high-LET radiation types that allowed either no or very little accumulation of sublethal damage. In contrast, the p(66)/Be beam used in the work presented here offers a broader shoulder for cell survival and therefore allows one to examine more readily the interaction of sublethal damage induced by high-LET radiation.

Irradiations

V-79 fibroblasts were exposed to a series of priming doses of either p(66)/Be neutrons or ^{60}Co γ-rays. The priming doses of neutrons were followed by graded doses of photons and photon priming doses were followed by graded doses of neutrons. The time interval between sequential irradiations of the two radiation types did not exceed 2 minutes. All the survival data for a given sequence were obtained by the irradiation of cell monolayers seeded from the same culture 4 hours previously (Figs. 1 and 2).

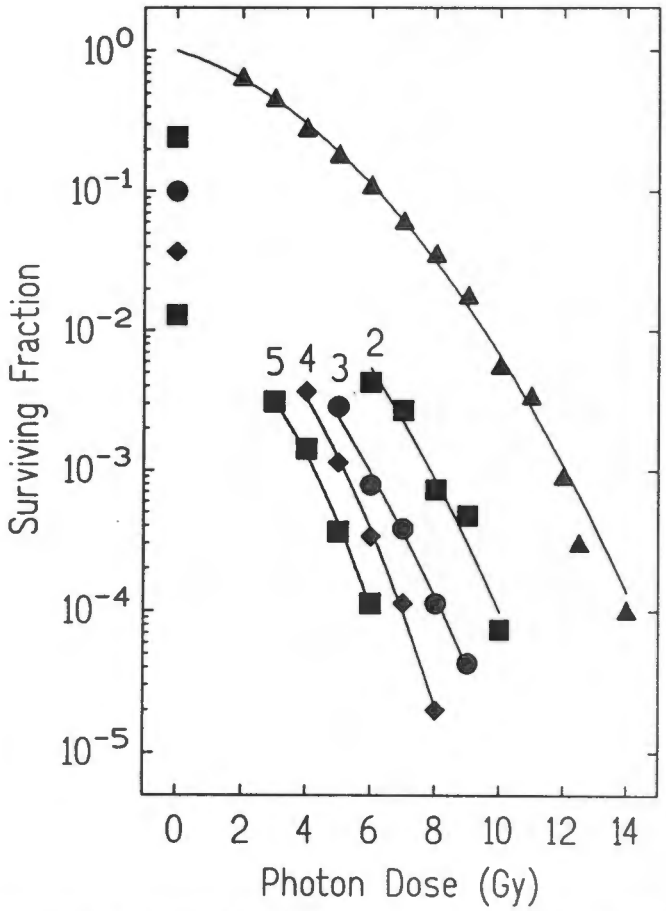

Figure 1: *Survival curves of V-79 cells exposed to graded doses of ^{60}Co γ-rays following exposure to priming doses of p(66)/Be neutrons. The size of the neutron priming dose used in each case is indicated.*

Influence of a Priming Dose on the Mean Lethal Dose (D_0)

The D_0 values of the photon survival curves where the priming dose was neutrons, were significantly smaller than those for photon survival in the absence of a priming dose (Fig. 3). This is in contrast to other authors who found no change in the D_0-value (Ngo *et al.*, 1981; McNally *et al.*, 1984). When neutron irradiations followed priming doses

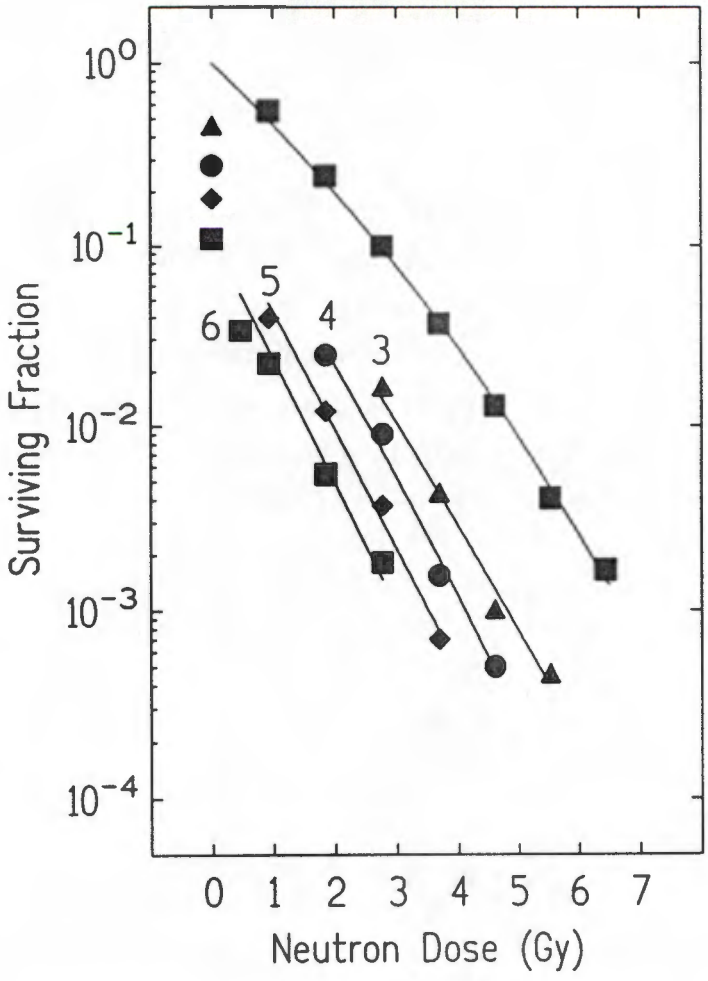

Figure 2: *Survival curves of V-79 cells exposed to graded doses of p(66)/Be neutrons following exposure to priming doses of ^{60}Co γ-rays. The size of the photon priming dose used in each case is indicated.*

of photons, no significant reduction in the mean lethal neutron dose was observed (Fig. 3). However, on average the D_0-values were slightly lower than those observed in the absence of a priming photon dose. The reduction in D_0-values can be interpreted as a manifestation of the synergistic interaction between sublethal damage induced by each of the two radiation types.

Effect of Priming dose on Shoulder Width (D_q).

D_q-values were calculated for each photon survival curve following a priming dose of neutrons. These calculations were performed in accordance with the method of McNally *et al.* (1984), using the average D_0-value.

The rate at which these D_q-values decrease as a function of the size of the neutron priming dose is shown in Fig. 4. Also shown in Fig. 4 is the rate at which the shoulder width of the photon only survival curve diminishes following a "priming" dose

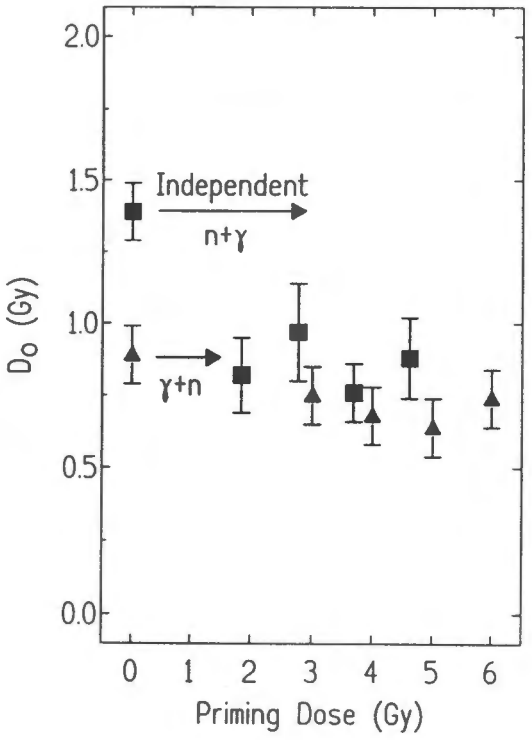

Figure 3: *Mean lethal dose values calculated for V-79 cells exposed to a priming dose of p(66)/Be neutrons followed by graded doses of ^{60}Co γ-rays (■), or exposed to a priming photon dose followed by graded doses of neutrons (▲). D_0-values assuming no interaction between neutron and photon damage are indicated for both radiation sequences. Error bars indicate 95% confidence limits.*

of ^{60}Co γ-rays. The latter was calculated by normalizing the surviving fractions of the photon only curve in Fig. 1 with respect to the effect of a given photon dose, i.e. a priming dose of ^{60}Co γ-rays. For each priming dose the mean lethal dose and extrapolation number (n) was estimated and the D_q-value calculated (Fig. 4). Adopting this approach, the D_q-values for equal neutron and photon priming doses were similar in most cases (Fig. 4). These observations are in agreement with the findings of Ngo *et al.* (1981) and McNally *et al.* (1984). Therefore the data in Fig. 1 can be interpreted as meaning that a priming dose of neutrons induces at least as much sublethal damage as the same dose of photons.

For the reverse sequence, i.e. photons followed by neutrons, a measurable reduction in the D_q-values for neutron irradiations was observed when compared with the D_q-values measured in the absence of a priming dose (Fig. 4). Except for the largest priming photon dose (6 Gy), all the neutron survival curves exhibited significant shoulders (Fig. 4). Using X-rays first followed by 3.2 MeV neutrons, McNally *et al.* (1984) observed only single-hit (exponential) survival curves, i.e. D_q = zero. This was interpreted to imply that the cells experienced the X-ray dose as an iso-effective neutron dose. In the present work a priming photon dose causes a reduction in the shoulder width of subsequent neutron survival curves. Following priming photon doses of as high as 4 Gy and 5 Gy, significant D_q-values were still observed with graded doses of

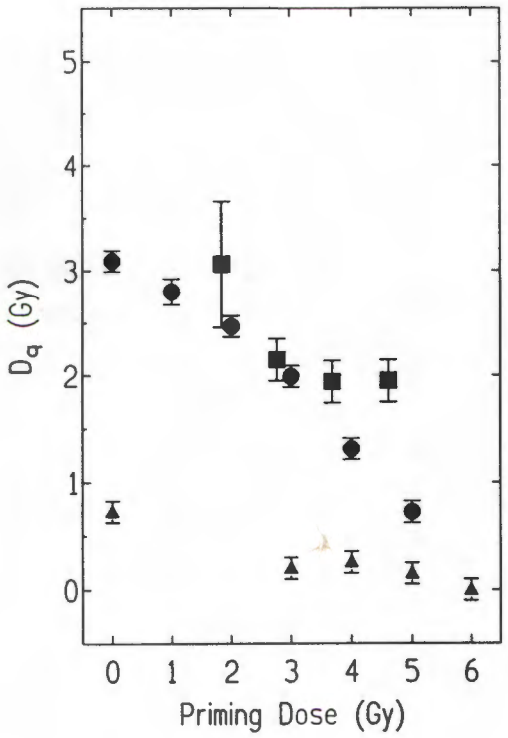

Figure 4: *D_q-values calculated for V-79 cells exposed to a priming dose of p(66)/Be neutrons followed by graded doses of ^{60}Co γ-rays (■), or exposed to a priming dose of photons followed by photons (•), or exposed to a priming dose of photons followed by graded doses of neutrons (▲).*

neutrons. Both these priming doses (4 Gy and 5 Gy) were large enough to reduce the surviving fraction of the cell population to a level beyond the shoulder of the photon-only curve (Fig. 1). The fact that the shoulder is still present in subsequent neutron curves following a priming dose of 4 Gy or 5 Gy photons suggests that the cells regarded the initial photon insult less than iso-effective compared to neutrons.

Non-Parametric Analysis

The analysis and interpretation of data presented above was reliant on D_q-values calculated from n and D_o-values estimated using the single-hit multitarget equation. This was done with the sole purpose of comparing the existing data to that of other authors who used the single-hit multitarget model. The estimation of the fitted parameters is sensitive to experimental data which deviates from the exponential portion of the surviving curve.

To eliminate the influence that model fitting might have on the interpretation of the data, it was decided to use a method of non–parametric analysis to evaluate the influence that different types of priming doses have on the induction of cellular damage.

The combined effect observed experimentally for a priming dose of one radiation type plus a subsequent (test) dose of the other radiation type, was compared to the combined effect calculated when the priming dose of a given type was replaced by an iso-effective dose of the other radiation type. Assume the observed surviving fraction (S) following a priming dose of neutrons (D_n) is $S(D_n)$, and that the observed surviving fraction following a combined exposure to a priming neutron dose plus a subsequent dose of photons (D_γ) is $S(D_n + D_\gamma)$. The photon dose required to reduce the surviving fraction to a level equivalent to $S(D_n)$ can then be calculated using the α- and β-parameters estimated for the photon only survival curve. This dose is the iso-effective photon dose (D'_γ). The same photon dose (D_γ) as added experimentally to a priming neutron dose, was added to D'_γ and the surviving fraction $S(D'_\gamma + D_\gamma)$ determined. $S(D'_\gamma + D_\gamma)$ was then compared to the combined effect obtained experimentally i.e. $S(D_n + D_\gamma)$. These surviving fractions are plotted in the lower part of Fig. 5 as the ratio $S(D'_\gamma + D_\gamma)/S(D_n + D_\gamma)$. This ratio is a relative measure of how the cell population experiences a priming dose of neutrons compared to an iso-effective dose of photons.

The ratio $S(D'_\gamma + D_\gamma)/S(D_n + D_\gamma)$ was consistently smaller than unity for all neutron priming doses followed by (test) doses of photons. The fact that the combined surviving fraction $S(D_n + D_\gamma)$ is larger than $S(D'_\gamma + D_\gamma)$ is an indication that the cells experienced a neutron priming dose as less potent than the iso-effective photon dose.

This phenomenon was confirmed by performing the same type of analysis using the surviving fractions obtained when the two modalities were applied in the reverse sequence, i.e. a priming dose of photons followed by graded doses of neutrons. In this case the effect of the initial photon dose (D_γ) is compared to an iso-effective neutron dose (D'_n), both followed by a subsequent (test) dose of neutrons. The ratio $S(D'_n + D_n)/S(D_\gamma + D_n)$ calculated in each case is shown in the upper part of Fig. 5. Surviving fractions $S(D_\gamma + D_n)$ were consistently smaller than $S(D'_n + D_n)$, implying that the initial photon doses were more damaging than so–called iso-effective neutron doses.

Based on the analysis presented above, the surviving fractions obtained using reverse sequences of neutron and photon irradiations lead to the same conclusion, i.e. neutron priming doses are less damaging to cells compared to iso-effective doses of photons. This may be due to the fact that neutrons induce more sublethal damage in the targeted cells compared to photons, as shown by figure 1, Chapter 6.

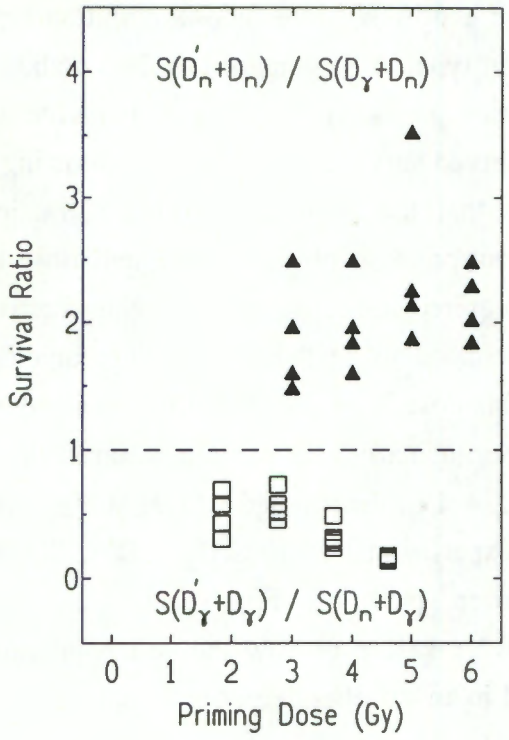

Figure 5: *Ratios of surviving fractions for V-79 cells calculated for different irradiation sequences and plotted as a function of the priming dose.*

Possible Role of Changes in Cellular Sensitivity

It is known that a dose of neutrons or other high-LET radiation types affect the age distribution of an exponentially growing cell population to a lesser degree than photons (Hall, 1988). It may therefore be argued that a redistribution of sensitive and radioresistant sub-populations of cells is the underlying mechanism that facilitates the results obtained in this work. However, it is difficult to reconcile a change in radiosensitivity induced by a priming dose of photons with the current observations. Relatively lower surviving fractions were observed for combined exposures following a priming dose of photons. Photon irradiation is more likely to make the population more radioresistant and consequently higher surviving fractions should be expected following an exposure to a second dose. If redistribution in cell sensitivity was involved then it is more likely that a larger level of synergistic interaction between the two radiation types is responsible for the lower surviving fractions. V-79 cells in late-S phase, known to be relatively radioresistant, experience more synergistic interaction when exposed to a combination of Bragg peak Ar-ions and X-rays (Ngo *et al.*, 1988).

CHAPTER 9

CELLULAR INACTIVATION AND VARIATIONS IN THE SECONDARY CHARGED PARTICLE SPECTRUM OF A p(66)/Be NEUTRON BEAM

The build-up zone of a high energy neutron beam offers a unique opportunity to investigate variations in radiation quality. In this chapter cells in culture are used to evaluate variations in the secondary charged particle spectrum of a p(66)/Be neutron beam. The RBE was quantified at different positions in the build-up region as it pertains to skin sparing in radiation therapy. Furthermore, the induction of sub-lethal damage was investigated by assessing the synergistic interaction between radiation damage in cells caused by priming doses of neutrons at different build-up positions, and that resulting from subsequent doses of ^{60}Co γ-rays.

Interaction of Fast Neutrons with Tissue

During neutron irradiation energy is transferred to biological samples by means of a range of secondary charged particles (Bewley *et al.*, 1974). These particles include recoil protons, the products of nuclear reactions (α-particles) and heavy recoils (C, N, O). The contributions made by each of these particle types to the total dose absorbed by the biological system depends on the neutron energy (Broerse and Zoetelief, 1978). The fractional dose due to a given energy transfer density is reflected in a microdosimetric spectrum of the beam. Examples of these are given by Hall *et al.* (1976), Zywietz *et al.* (1982) and Menzel (1990). Since the LET is different for each of these particles, both the type and the extent of the biological damage inflicted on the tissue will be determined by the spectral character of these charged particles.

The Build-up Region

The p(66)/Be beam used in this study has a build-up region which spans approximately 17 mm in tissue-equivalent material (Jones *et al.*, 1988). At the distal end of this region the physical dose absorbed by the medium attains a maximum (D_{max}). The range over which the various secondary particles cause ionizations in tissue varies over several

orders of magnitude. For the heavy nuclear recoils it can be as short as 5 micrometers, a distance which is comparable to the diameter of a mammalian cell, whilst recoil protons are projected in a forward direction for serveral millimeters (ICRU 1977). Because the range of the various secondary particles are different, the character of the charged particle spectrum changes in this transition zone or build-up region. The fractional dose contributed by densely ionizing particles peaks at shallow depths in the build-up region. At greater depths the contribution to the dose by recoil protons becomes progressively larger until a state of charged-particle equilibrium (CPE) is realised.

RBE in the Build-up Region

The motivation for measurements in this region was to quantify the level of biological damage that accompanies changes in the charged-particle spectrum. Of particular interest are changes in RBE and the induction of sub-lethal damage. Due to changes in the spectral character of the secondary charged particles, the RBE is expected to continuously decrease from the surface until a minimum value is realized at maximum build-up (17 mm). The build-up characteristics in terms of a biological effective dose was established by determinating the RBE at various positions in the build-up region.

Compared with lower energy neutrons, the build-up curve (as measured by ionometric methods) for the p(66)/Be is more gradual. For example, Bewley *et al.* (1974) calculated that the recoil proton component of a 7.5 MeV neutron beam travels only about 2.3 mm in water. When it is considered that the higher energy neutrons used in these measurements transfer far more energy to the recoil protons, the effect of a change in the secondary particle spectrum has greater bearing on the number of cells affected.

A neutron beam of higher mean energy is biologically less effective than a lower energy neutron field (Hall *et al.*, 1975) and it would be expected that the RBE of the p(66)/Be beam at D_{max} would be lower than, for example, a d(16)/Be neutron beam. Indeed this has been found to be the case as was demonstrated in Chapter 6. Therefore in a higher energy neutron beam a more dramatic change in the biologically effective dose can be expected in the build-up region.

On the other hand, a higher neutron energy also gives rise to a higher physical dose deposited by α-particles and heavy recoils (Menzel, 1990). Since the lineal energy of these particles is in the 200-1000 keV μm^{-1} range, cells at the surface are more likely to be "overkilled". It is known that the effectiveness of reproductive death of mammalian cells attains a maximum per unit dose at ionization densities of about 150 keV μm^{-1} and that the RBE becomes progressively smaller at higher lineal energies (Barendsen, 1990). The biological effectiveness of a higher energy neutron source might be lower at the surface compared to that at the surface in a less energetic neutron beam.

Changes in RBE in the build-up region of the p(66)/Be neutron beam were therefore investigated using mammalian cells in culture as a biological monitor.

Ionization Density and Induction of Sub-Lethal Damage

The range of radiation qualities encountered in the build-up region permit an investigation of the influence of ionization density and the induction of reparable damage. In addition, the synergistic interaction between sublesions generated by a priming dose of neutrons at different build-up positions and those induced by subsequent doses of ^{60}Co γ-rays was investigated.

Cell Sample Preparations

Two mammalian cell lines were used in this study, namely V-79 fibroblasts and Chinese hamster ovary cells (CHO-K1). These cell lines were routinely maintained in monolayer culture as detailed in the Appendix.

Cells in the exponential growth phase were harvested and varying numbers plated into 50 mm diameter Petri dishes 4 to 5 hours before irradiation. The number of cells plated was such that they would yield approximately 150 colonies per dish, irrespective of the dose and the radiation quality. In the case of the V-79 cells the dishes were returned to the incubator for 6 days after irradiation and for 8 days in the case of the CHO cells. Thereafter colonies were stained and counted as detailed in the Appendix and surviving fractions determined.

Irradiations

In order to expose some of the samples such that there was no build-up between the cells and the neutron source, the following procedure was adopted. Immediately before irradiation the medium covering the cell samples was decanted. The serum in the culture medium reduces surface tension, allowing the formation of an evenly spread thin film covering the monolayer. To prevent contamination from air-born particles, the open dishes were placed in a perspex jig which was then covered with a single layer of cling wrap (< 0.9 mg·cm^2). Monolayers kept "naked" in this way for up to one hour showed no change in plating efficiency. Irradiation time for these samples did not exceed 30 minutes. The surface dose samples (i.e. "naked" monolayers with no build-up) were irradiated from above with the dishes supported by backscatter material (30 × 30 × 15 cm perspex).

All other build-up positions were irradiated from below with the Petri dishes (containing growth medium) suspended in a 20 x 20 cm neutron field. Openings in a perspex sheet were machined to support the dishes at their rims. The set-up is shown in Fig. 1. Backscatter material was positioned above the dishes. Build-up of between 1 and 21 mm was obtained by placing nylon (type 6) discs between the beam and the samples. The use of different material types in the build-up arrangement, namely polystyrene and nylon 6, did not affect the dose absorbed by the samples. Measurements with an extrapolation chamber behind 1 mm thick nylon or polystyrene discs indicated a dose discrepancy of less than 1.5%.

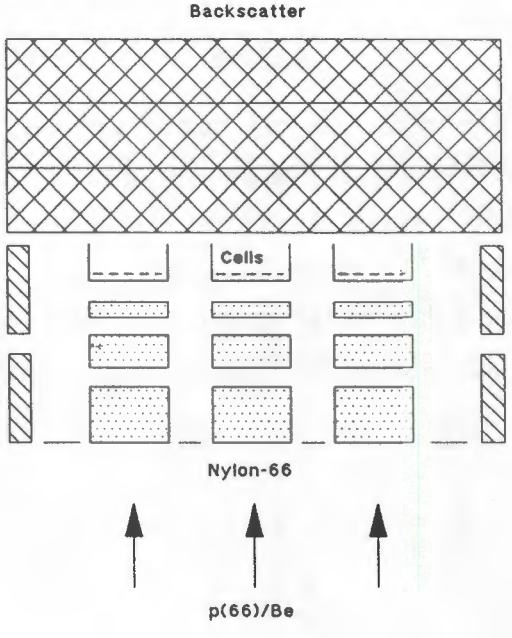

Figure 1: *Irradiation set-up used to expose cell monolayers to p(66)/Be neutrons at different positions in the build-up region.*

In the case of the mixed field exposures, the cells were first irradiated with neutrons followed by ^{60}Co γ-rays. The time interval between neutron and photon exposures did not exceed 2 minutes. For the photon exposures the monolayers were covered with medium. Irradiation was from below and 5 mm perspex ensured full build-up.

Surface Dose Samples

Repeated photon irradiations showed that V-79 cells moistened by only a thin film of medium, did not exhibit an increased sensitivity to radiation (Fig. 2). In fact a slight increase ($< 2\%$) in survival was observed when compared to cells covered with 1 mm of growth medium. However, this difference was not significant ($p < 0.07$). The small reduction in survival noted for cells covered with medium can be ascribed to backscatter.

Profile of Radiation Damage

A profile of biological damage in the build-up region was determined by exposing cell samples to fluence normalized neutron doses for various build-up thicknesses. The exposure level used was equivalent to that of an absorbed dose of 6 Gy at D_{max}. The resulting surviving fractions (Fig. 3) are a function of both a change in radiation quality and physical dose with different material thicknesses. To facilitate a comparison between the biological damage and physical dose, surviving fractions were normalized to that measured at 1 mm build-up.

Despite the scatter in the data, it would appear that beyond D_{max} the biological damage does not follow the trend suggested by physical dose measurements. The increase in survival in the build-up range 1.8 to 2.4 g cm^{-3} exceeds that ascribed to dose attenuation. The reason for this is not clear. The shape of the relative survival curve approximates that of a mirror image of the physical build-up curve and does not therefore reflect quality changes in this transition zone.

Relative Potency at Different Build-up Positions

To identify quality changes in the build-up region a second series of measurements was performed, from which complete survival curves were constructed following exposure

of cells for different build-up thicknesses, i.e. surface, 1 mm, 2.5 mm and 17 mm (D_{max}).

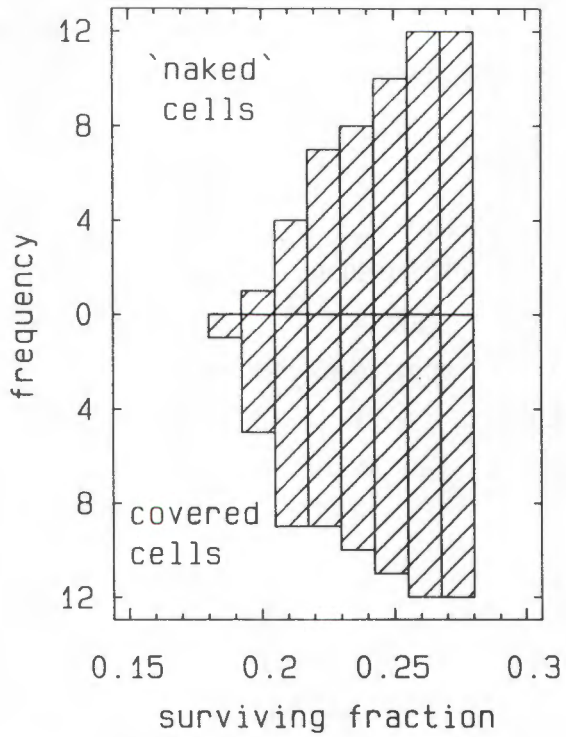

Figure 2: *The cumulative frequencies of surviving fractions for V−79 cells after repeated exposure to 6 Gy ^{60}Co γ-radiation. Monolayers were exposed either without medium (upper half) or covered with 1 mm growth medium (lower half).*

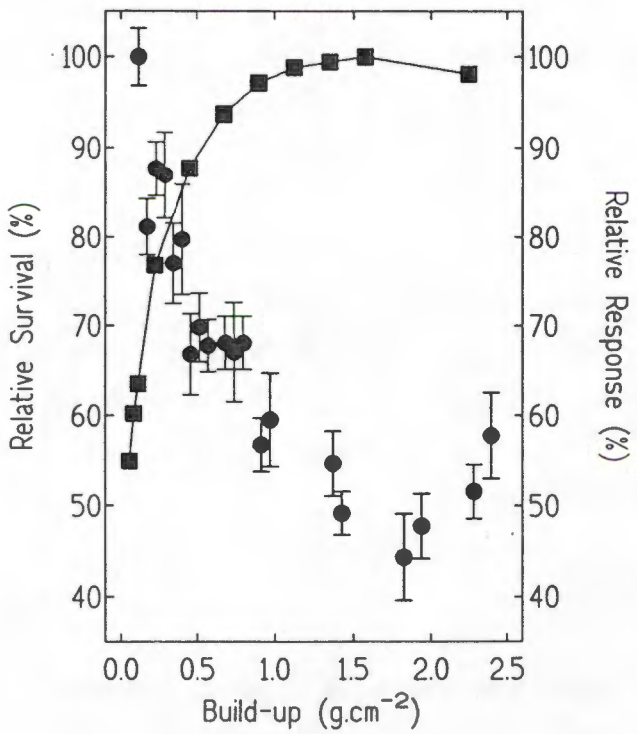

Figure 3: *The relative survival of V-79 cells (•) and relative dose (■) measured in the build-up region of a p(66)/Be neutron beam. The survival has been normalized to that at 1 mm build-up. Standard deviations are indicated by error bars.*

The exposures at each of these positions were adjusted to compensate for the associated lack in build-up and hence ensuring that the biological damage to the cells could be compared on a per gray basis. The correction factors used to calculate the exposures were determined by means of extrapolation chamber measurements in the build-up region (Jones *et al.*, 1988). The fractional physical doses are listed in Table 1.

Table 1: *Survival parameters for V-79 and CHO-K1 cells exposed to p(66)/Be neutrons at various build-up thicknesses. 95% confidence limits are given in brackets.*

V-79 CELLS						
t	α (Gy^{-1})	β (Gy^{-2})	$\bar{D}$ (Gy)	RBE	Fractional Dose	
					Physical	Biological
surface	0.875 (0.240)	0.145 (0.093)	0.91	1.72	0.40	0.68
1 mm	0.659 (0.073)	0.064 (0.017)	1.25	1.25	0.67	0.83
2.5 mm	0.616 (0.041)	0.051 (0.010)	1.36	1.15	0.80	0.92
17 mm	0.517 (0.061)	0.045 (0.015)	1.56	1.0	1.0	1.0
CHO-K1 CELLS						
t	α (Gy^{-1})	β (Gy^{-2})	$\bar{D}$ (Gy)	RBE	Fractional Dose	
					Physical	Biological
surface	0.758 (0.170)	0.153 (0.067)	0.99	1.73	0.40	0.68
1 mm	0.614 (0.081)	0.060 (0.019)	1.33	1.29	0.67	0.86
2.5 mm	0.547 (0.051)	0.058 (0.012)	1.45	1.18	0.80	0.95
17 mm	0.385 (0.064)	0.072 (0.016)	1.71	1.0	1.0	1.0

Figures 4 and 5 show results obtained with V-79 and CHO-K1 cells respectively. The parameters that characterize these survival curves were determined and are listed in Table 1. Included is the mean inactivation dose ($\bar{D}$), the integrated area under each survival curve. RBE-values are expressed as the ratio $\bar{D}_{max}$ / $\bar{D}_x$, where x is the position in the build-up thickness. An increase in RBE with less build-up is evident, with a relative potency of 1.7 measured at the surface. The RBE values of 1.25 and 1.29 measured with 1 mm build-up are in agreement with the 1.2 to 1.3 values reported for the UCLA [(p(45)/Be)], M.D. Anderson [(p(42)/Be)] and Seattle [(p(50)/Be)] neutron beams (Hall *et al.*, 1992).

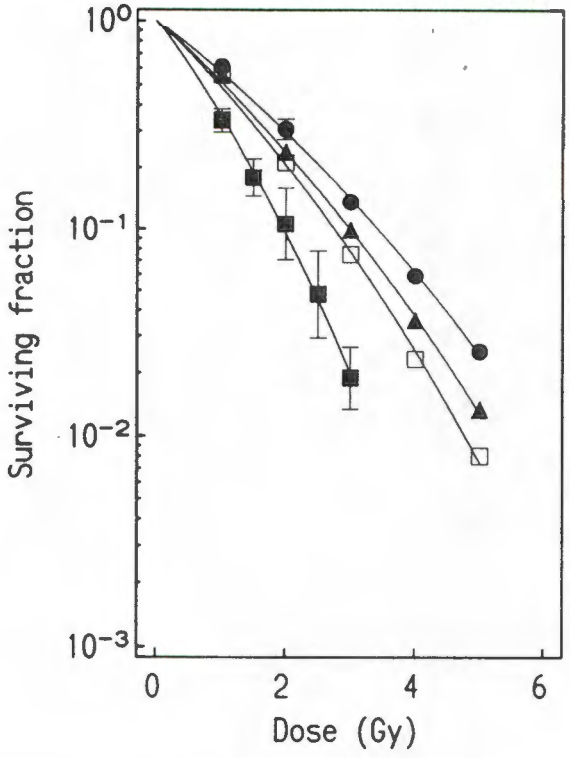

Figure 4: *Survival of V-79 cells at various positoins in the build-up region of a p(66)/Be neutron beam. Cells were irradiated without build-up (■) or with 1 mm (□), 2.5 mm (▲) and 17 mm (•) build-up. Standard deviations are indicated by error bars.*

The areas that demarcate a confidence level of 95% around the survival parameters (α and β) were calculated for each cell line and are shown in Fig. 6. Both cell types demonstrated a marked increase in the uncertainty associated with their respective α- and β-values when exposed without build-up. Because of the sharp increase in RBE at the surface, the inactivation parameters for these exposures were followed over a much smaller dose range. This results in an increased uncertainty in the estimates of α and β (Kellerer and Brenot, 1974).

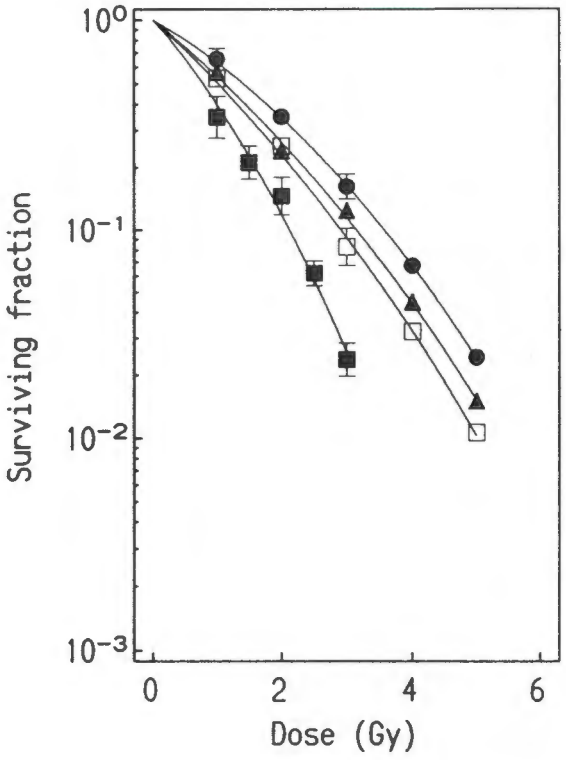

Figure 5: *Survival of CHO-K1 cells at various positions in the build-up region of a p(66)/Be neutron beam. Cells were irradiated without build–up (■) or with 1 mm (□), 2.5 mm (▲) and 17 mm (•) build-up. Standard deviations are indicated by error bars.*

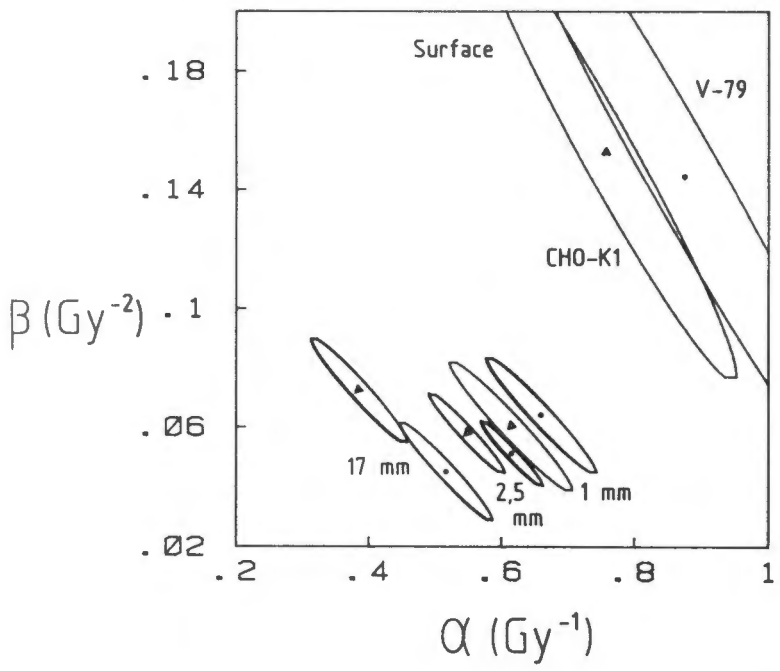

Figure 6: *Correlation between the co-variant survival parameters α and β, determined after irradiating V-79 (•) and CHO-K7 (▲) cells under varying build–up conditions in a p(66)/Be neutron beam.*

Comparison of Measured RBE values with Microdosimetric Data

The RBE-values determined above were correlated with microdosiemtric data obtained with a tissue equivalent proportional counter (Binns and Hough, 1992). This is shown in Fig. 7 where the dependent variables $\ln(RBE_n)$ and $\ln(y^*/y^*_{mb})$ are plotted as a function of the cube root of the material thickness. These transformations were done in order to find a linear correlation between material thickness and the varying radiation quality. A linear correlation was only possible at build-up thicknesses less than 3.5 mm.

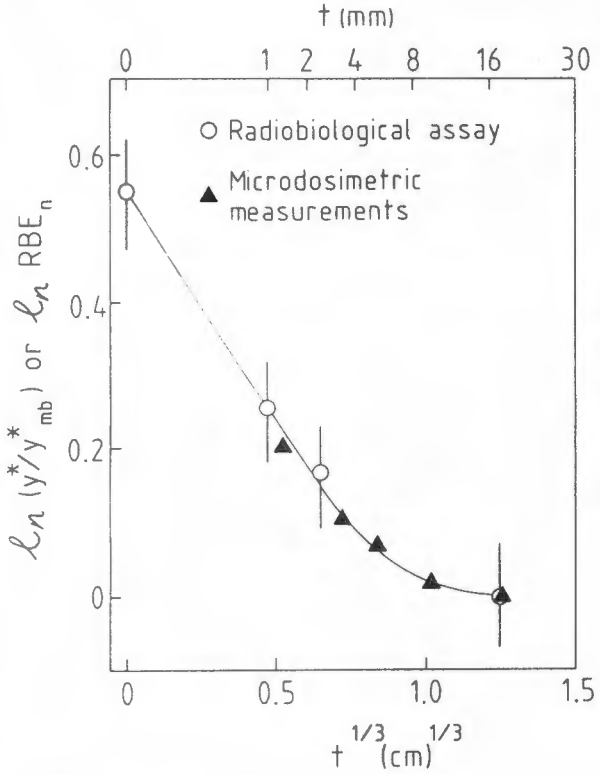

Figure 7: *Graph depicting the correlation between RBE or y^*/y^*_{mb} and $t^{1/3}$, as measured in a p(66)/Be neutron beam. Error bars indicate 95% confidence limits.*

Secondary Charged Particles and Cell Kill as a Result of the Accumulation of Sub-Lethal Damage

The reproductive death represented by the quadratic coefficients in Table 1 is the result of the accumulation of lesions produced by different tracks of ionizing particles (Barendsen, 1990). Inter-track actions are commonly interpreted to be responsible for sublethal damage that can accumulate to produce lethal lesions. Since the magnitude of this component is influenced by the time interval between fractionated doses, it is associated with the reparable component of radiation damage (Volkmer and Virsik-Peuckert, 1990).

In spite of the large uncertainties that are associated with the inactivation parameters for cells exposed at the surface, a marked increase in their β-values is evident. For example, the RBE_{∞} for V-79 cells exposed without build-up is 1.8 relative to cells exposed at D_{max}. Here, RBE_{∞} was calculated as:

$$RBE_{\infty} = \left[\frac{\beta(\text{at surface})}{\beta(\text{at } D_{max})} \right]^{\frac{1}{2}}$$

The fact that a significant β-component was observed for the surface measurement is noteworthy. Lunec *et al.* (1980) irradiated bacteria with 7 MeV neutrons in the presence and absence of secondary charged-particle equilibrium and compared their data with similar experiments using mammalian cells. These workers concluded that heavy-recoil nuclei, which are the secondaries most likely responsible for energy depositions near the surface, make a major contribution to damage in mammalian cells. The survival curves for high-LET radiation (100 - 1000 $keV \cdot \mu m^{-1}$) are usually characterized by an exponential response, i.e. a straight line on a semi-log plot without a "bending" component (β-value is zero). Examples of this are given by Broerse *et al.* (1967) who used human kidney cells and Bewley *et al.* (1974) who used rat fibrosarcoma cells. Both these investigators exposed the cells to neutron beams (15 and 7.5 MeV respectively) without build-up. The absence of a measurable oxygen effect in both studies, i.e. OER values not significantly different from unity, reflected the high-LET nature of the radiation at the surface. Since high-LET radiation gives rise to a relatively large α-component, the quadratic term for these conditions is comparatively small (Napolitano *et al.*, 1992).

This recovery-deficient behaviour is even more noticeable when the high RBE at the surface relative to that at D_{max} restricts the assay to the determination of surviving fractions from low radiation doses. The experimental protocols of other workers have placed a limit on the high-LET dose absorbed by the cells. Bewley *et al.* (1974) exposed cells at different build-up positions to compare kerma levels. Although kerma levels as high as 9 Gy were applied in their experiments, the cells at the surface absorbed only about 20% of the energy and thus the maximum dose due to α-particles and heavy recoil fragments was 1.8 Gy.

To account for the smaller doses in the transition zone, the exposure to cells at the different build-up positions was adjusted according to the fractional physical dose

shown in Table 1. As a result, cell survival at the surface was followed over a much larger dose window, i.e. up to 3 Gy. It is clear that if the surviving fractions at the surface were followed only up to 2 Gy, it would be difficult to determine a sizable β-component. The higher doses used in the present work were therefore selected to reveal significant β-values. The general trend indicated by the V-79 results is that β-values increase as build-up decreases.

Monte Carlo Simulations and Intertrack Damage

In an attempt to observe the likelihood of intertrack-damage, survival curves for the different build-up positions were simulated using a Monte Carlo method (Di Cera *et al.*, 1989). The simulations were based on the mean surviving fractions of the V-79 cells and the associated uncertainty empirically obtained at each dose point. The best fits to these simulated survival curves were calculated and the α-component plotted against the β-component for each simulation at each exposure position (Fig. 8). As expected the clusters of coordinates were well separated, thus confirming that the positions in the build-up region at which the cells were exposed to neutron irradiations were significantly different in terms of radiation quality. Of particular interest is the intertrack damage. In contrast to the component which increases linearly with dose (α-term), the cumulative type of damage described by the β-term usually shows only a small dependence on LET (Barendsen, 1989). Here the mean LET for the different build-up positions varies, with the greatest LET at the surface. Unlike the rest of the data in the current set, the β-values show a much stronger dependence on LET. Therefore, although α and β is covariant within a radiation type, there is a trend for β to increase with larger α–values.

Clinical Significance of Neutron Irradiation in the Build-up Region

The variation of the physical dose in the build-up region must be taken into account when evaluating the radiobiological data for application in clinical practice. When the measured RBE values at different build-up positions are corrected with respect to the fractional physical dose, the biological effective doses are obtained (Table 1). It is evident that skin sparing in terms of biological effective dose is considerably less than that indicated by the physical dose profile. At the surface for example, the biological effective dose is 68% of that at D_{max} compared to 40% indicated by physical measurements.

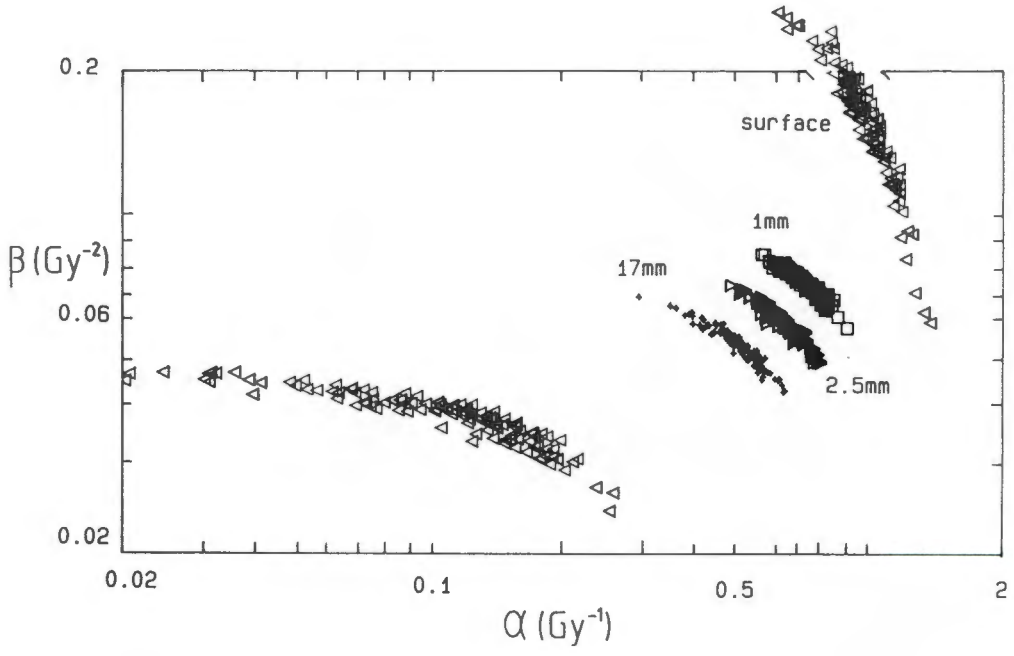

Figure 8: *Monte Carlo generated distribution of the inactivation parameters α and β for V-79 cells exposed to p(66)/Be neutrons at different positions in the build-up region. Also indicated is the distributon for ^{60}Co photons.*

The influence of the individual inactivation parameters, α and β, were also evaluated at different build-up positions with respect to the physical dose absorbed. Based on a total dose of 3 Gy at D_{max}, α-effect and β-effect values were determined.

Table 2: *The α-effect and β-effect on V-79 and CHO-K1 cells irradiated at different positions in the build-up region of a p(66)/Be neutron beam. 95% confidence limits in parenthesis.*

Irradiated position	α-effect		β-effect	
	V-79	CHO-K1	V-79	CHO-K1
Surface	0.349 (0.09)	0.402 (0.09)	0.811 (0.4)	0.802 (0.3)
1.0 mm	0.266 (0.03)	0.291 (0.04)	0.772 (0.21)	0.785 (0.25)
2.5 mm	0.228 (0.02)	0.269 (0.03)	0.745 (0.13)	0.716 (0.15)
17 mm	0.212 (0.03)	0.315 (0.05)	0.667 (0.22)	0.523 (0.12)
Ratio: surface/17 mm	1.6	1.3	1.2	1.5

The α-effect and β-effect (Steel and Peacock, 1989), i.e. surviving fractions caused respectively by the α- and β-actions are given in Table 2. It is clear that for all the build-up positions, α-damage is the major contributor to the total effect. However, the relative change in α-effect and β-effect between different positions in the build-up is more or less the same. Consequently, it can be expected that cells in the epidermal region of skin irradiated with neutrons are inflicted with relatively higher levels of reparable damage.

Reparable Damage in the Build-up Region of the p(66)/Be Beam

The influence of reparable damage induced at the surface was initially investigated by exposing V-79 cells to split doses (1.5 Gy + 1.5 Gy) of neutrons separated by various time intervals. The recovery ratio for each time interval is shown in Fig. 9 and is compared to recovery ratios obtained for cells exposed at D_{max} (3Gy + 3 Gy). Different doses were chosen so that the survival levels were comparable. Recovery ratios at D_{max} were found to be larger than unity. In contrast, split dose exposures at the surface consistently yielded recovery ratios less than 1, irrespective of the time between dose fractions. From this it is evident that the induction of reparable damage at the surface leads to "negative" repair which does not change significantly with increasing time between the two fractions. It is suggested that the synergistic interaction between sublethal lesions induced by split doses is responsible for this phenomenon.

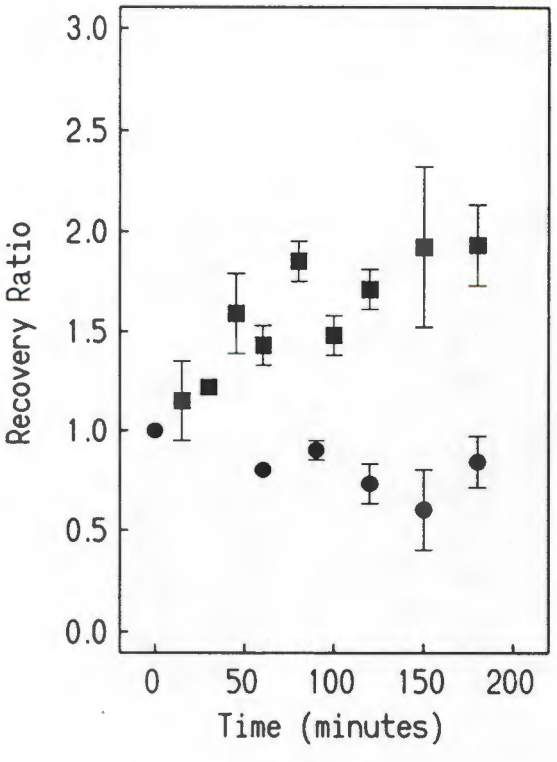

Figure 9: *Repair of sublethal damage as measured by split-dose recovery in V-79 cells. Cells were exposed to p(66)/Be neutrons (3 Gy + 3 Gy) under full build-up (■) and to (1.5 Gy + 1.5 Gy) without build-up (•). Standard deviations are indicated by error bars.*

All positions in the build-up region showed β-values that were significantly different from zero (Fig. 6), which infers the presence of reparable damage. There is some doubt as to how reliably a series of single doses, or even split-dose exposures, can reveal the true extent of sublethal damage induced by high-LET radiation. For example, a series of surviving fractions indicated no reparable damage when V-79 cells were exposed to split doses of Ne-ions (Ngo *et al.*, 1981). Nonetheless, further results by these authors clearly demonstrated that when these charged particles and X-rays were delivered in close succession, each radiation type produced damage which interacted with the other in a synergistic manner. These observations therefore imply that Ne-ions were capable of inducing damage that can be repaired.

Sequential Neutron and Photon Irradiations in the Build-up Region

With the above in mind, it was decided to initiate reparable damage with a priming dose of neutrons at different build-up positions in the p(66)/Be beam and to follow this with a series of ^{60}Co doses. Three positions were selected, the surface, 1 mm and 17 mm depth. The priming dose in all cases was 3 Gy. The time interval between the conclusion of the priming dose and a sequential dose of photons did not exceed 2 minutes.

The effect of the different high- and low-LET combinations are presented in Fig. 10. For comparison the predicted surviving fractions for independent action between the priming dose and the subsequent photon dose are also indicated. The prediction for independent action is the product of surviving fractions from the ^{60}Co-only irradiations and that from the priming dose. Therefore the dashed curves drawn in Fig. 10 are the fitted lines to the ^{60}Co-only measurements, but normalized (displaced downwards) with respect to the surviving fraction measured following the priming dose. The interaction between reparable damage induced by a priming dose and that induced by subsequent photon doses was evident for all the build-up positions. As expected, the β-type damage from a neutron priming dose interacted synergistically with the β-type damage from a subsequent photon dose. This resulted in surviving fractions that were lower than that predicted by assuming independent action.

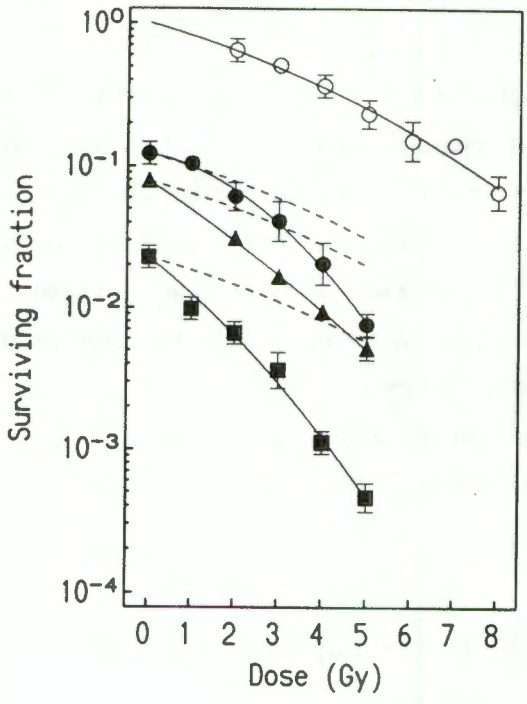

Figure 10: *^{60}Co survival curves for V-79 cells following exposure to a neutron priming dose of 3 Gy at the surface (■) and at depths of 1 mm (▲) and 17 mm (•), in the build-up region of a p(66)/Be beam. The upper curve (o) shows the photons-only survival. Standard deviations are indicated by error bars.*

Fig. 10 also shows that the degree of interaction between an equivalent priming dose (3 Gy in all cases) and a range of equal top-up doses is different at the various build-up positions. The interaction factor (ω), i.e. the extent of cell damage due to the interaction process, was calculated at various dose levels of photon irradiation to determine the combined effect of each mixture at each of the build-up positions. These are listed in Table 3. The interaction factor (ω) is the ratio:

$$\omega(D_n + D_\gamma) = \frac{S_\gamma(D_\gamma)\ S_n(D_n)}{S(D_n + D_\gamma)}$$

where $S(D_n + D_\gamma)$ is the surviving fraction following exposure to the neutron-photon mixture and $S(D_n)$ and $S(D_\gamma)$ are the surviving fractions following exposure to neutrons only and photons only respectively (UNSCEAR, 1982).

The synergistic interaction between high and low LET radiation was most pronounced at the surface position and decreased as build-up increased. This is in agreement with the trend of the β-values observed in Fig. 6. Since the likelihood of observing interaction of damage increases with dose, the interaction index increased when more photon radiation was added to the priming dose. This was the principle reason why equal priming doses were chosen for the different build-up positions.

Table 3: *The interaction factors ω for V-79 cells exposed at different build-up positions to a priming dose of p(66)/Be neutrons (3 Gy) and a series of ^{60}Co exposures. Standard deviations for mean ω/D_γ values are given in brackets.*

^{60}Co dose (Gy)	Position in build-up region		
	17 mm	1 mm	surface
2	1.28	1.68	2.26
3	1.47	2.44	3.15
4	2.03	3.18	7.77
5	3.86	3.65	11.69
ω/D_γ (Gy^{-1})	0.602 (0.1)	0.795 (0.1)	1.62 (0.6)

Included in Table 3 are the interaction factors per unit photon dose (ω/D_γ). This increases dramatically between the 1 mm and surface exposures. The difference between the 17 mm and 1 mm positions is also significant ($p < 0.033$).

Applicability to Neutron Therapy

Although the system of cell monolayers used in these investigations might not be directly transferable to the clinical situation, there are no other biological methods available to quantify radiation damage in the build-up region. Nevertheless, one important aspect has emerged that may be of relevance to clinical radiotherapy. It would be undesirable to apply a second neutron dose within 3 hours of the first. The interaction of reparable damage will augment radiation injury in the epidermal region of the skin. The skin is further at risk because the induction of sublethal damage by α-particles and heavy recoil fragments will lead to some synergistic interaction with the inherent γ-dose in the neutron beam. This is especially relevant to larger field sizes where γ-contamination is larger. In a 29 x 29 cm field the γ–contamination is as high as 7.8% (Jones *et al.*, 1988)

CHAPTER 10

INTERACTION DAMAGE INDUCED IN MERISTEMATIC CELLS BY d(16)/Be NEUTRONS AND ^{60}Co γ-RAYS

Introduction

Root meristems have been used frequently in radiobiological research because of their ease of handling and applicability of their response to general problems in radiobiology. Their use in radiation research has been reviewed by Marshall (1982). It is interesting to note that the first experiments were aimed at investigating the summation of the effects of radiation types with different ionization densities (Gray and Read, 1944). These workers investigated the effect of successive exposures of neutrons and γ-rays, and α-paricles and X-rays, and concluded that the combined effect in both cases were strictly additive. In contrast, Whitherspoon and Corney (1970) reported a greater than additive mortality for soyabean seedlings following exposure to a combination of γ-rays and fission neutrons.

Almost all the studies on the interaction of damage from different radiation types have been conducted in terms of stochastic effects, i.e. the endpoint which is monitored manifests itself as an all-or-nothing response, e.g. cellular survival. In this Chapter the interaction between high- and low-LET radiation is followed using both stochastic (10-day growth delay measurements) and non-stochastic (induction of micronuclei) endpoints. In the case of the latter the magnitude of the effect, rather than its probability, is followed as a function of dose.

Non-stochastic radiation damage is of particular interest in mixed-field interaction studies. It is appropriate since both the basic ideas of microdosimetry and the interaction of radiation-induced sub-lesions stem from visible chromosome aberrations (Bauchinger, 1983). The induced exchanges of material between different chromosomes observed in plant cells led to the suggestion that radiation damage in general is the result of separate effects at two or more locations in the cell that must interact to form a lethal event (Neary, 1965). Goodhead (1982) has summarized these ideas and has shown how they preceeded the theory of dual radiation action.

Apart from the historical connection between chromosome damage and the concept of interaction, investigations of this sort are of practical importance today. It is well established that chromosome damage is well suited to quantify the effects of low doses of radiation. For example, with cytogenetic dosimetry using human lymphocytes, doses as low as 5 cGy can be detected (Zoetelief and Broerse 1990). Mixed-field studies in the low dose region are important because they relate directly to biological dosimetry and radiation protection.

The experimental work described in this Chapter has been conducted on the meristematic cells of the main root tip of the broad bean *Vicia faba*. Meristematic cells were selected as a test system because of their characteristic responses to neutrons and photons. Firstly, the dose-response relationship for meristematic cells is strictly exponential following exposure to d(16)/Be neutrons (see Chapter 6). The quadratic component observed in repeated experiments was not significantly different from zero. This exponential behaviour of meristematic cells implies that a mixture of high- and low-LET radiation types would not be expected to produce damage that will interact. To verify the absence of interaction as predicted by the Zaider-Rossi model, meristematic cells were exposed to various mixtures of neutrons and photons.

Growth Delay Measurements

Two experiments were performed where growth delay was monitored to determine the combined effect of d(16)/Be neutrons and ^{60}Co photons. Growth delay was measured 10 days after irradiation (G_{10}). Roots were selected at random according to the procedure detailed in the Appendix. Root tips were secured for irradiation using a specially designed perspex jig described in the Appendix. Before and during irradiations the water surrounding the root tips was aerated using a diaphragm pump. Irradiations were performed with the tandem neutron-photon irradiation facility shown in Chapter 4.

For the first set of measurements, selected roots were exposed to d(16)/Be neutrons, ^{60}Co γ-rays and a mixture consisting of 40% neutrons and 60% photons. The purpose of the irradiation was twofold. Firstly, to establish if interaction can be observed in meristematic cells, and secondly to determine if a difference between simultaneous and

sequential exposures could be demonstrated. Both n+γ and γ+n sequences were investigated. All three mixed-fields comprised of 40% neutrons and 60% γ-rays. The dose response curves are shown in Fig. 1 and the inactivation parameters are listed in Table 1.

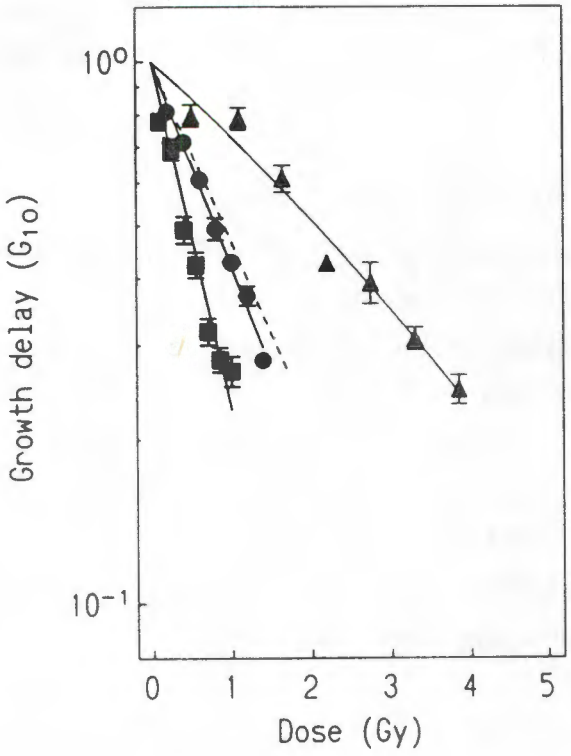

Figure 1: *Dose response curves plotted for experimental G_{10} measurements following exposure of Vicia faba seedlings to d(16)/Be neutrons (■), ^{60}Co γ-rays (▲) and a mixture of 40% neutrons and 60% photons (•). Also indicated is the predicted response if neutron and photon damage acted independently (dashed line). Standard deviations are indicated by the error bars.*

The neutron only and photon only measurements compare well to those conducted for the RBE measurements (Table 3, Chapter 6). The three modes of mixed-field exposures yielded inactivation parameters that were not significantly different and the overall response was very much the same. This is reflected in the $\bar{D}$-values which were almost identical. For this reason the data was collectively used to plot a single mixed-field curve (Fig. 1). Included is the data for the single modality exposures and the independent prediction based on the respective inactivation parameters.

Growth delay might intuitively be thought of as non–stochastic in nature. The endpoint is however treated here as a stochastic effect because it is directly dependent on the survival of a small number of meristematic cells and the dose–response shows no apparent threshold (ICRP 1984).

Analysis of the data indicated that the linear term dominates the response of meristematic cells. The absence of a significant quadratic component for the low-LET data is in agreement with observations made by others using photons. Herring (1980)

reported similar inactivation kinetics for both ^{192}Ir and ^{125}I irradiations. Also, Khokhar (1984) indicated an exponential response for 250 kVp X-rays using meristematic cells. This would account for the apparent absence of the accumulation of reparable damage.

Table 1: *Inactivation parameters for meristematic cells exposed to d(16)/Be neutrons, ^{60}Co γ-rays and a mixture consisting of 40% neutrons and 60% photons delivered simultaneously (n/γ) and sequentially (n+γ and γ+n). 95% confidence limits are givin in brackets.*

Radiation Type	α (Gy^{-1})	β (Gy^{-2})	$\bar{D}$ (Gy)
d(16)/Be	1.47 (0.3)	–	0.67
^{60}Co	0.295 (0.07)	0.0187 (0.02)	2.64
40% Neutrons and 60% Photons			
n/γ	0.78 (0.2)	0.067 (0.07)	1.09
n + γ	0.91 (0.2)	–	1.09
γ + n	0.69 (0.2)	0.14 (0.2)	1.07

On average however, the combined effect of a 40/60 neutron/photon mixture was found to be more than additive (Fig. 1). Because the response of meristematic cells to both neutron only and photon only exposures lacked a significant β-component, the observed synergy is unexpected. This is the first time that interaction has been demonstrated for two radiation types where each individualy exhibited an exponential dose response.

The 95% confidence ellipses were calculated for the experimental G_{10} data and are shown in Fig. 2. The α-component is particularly sensitive to the quality of the radiation field and this is exemplified by the clear separation of the ellipses calculated for the low-LET, mixed and high-LET data. Although the close grouping of the mixed-field ellipses infers only a marginal variation in beam quality, a tendency was observed for the α-values to decrease in the order; neutrons followed by photons, then simultaneous n/γ exposures and lastly photons followed by neutrons. This tendency is in agreement with the additive damage model of Scott (1983).

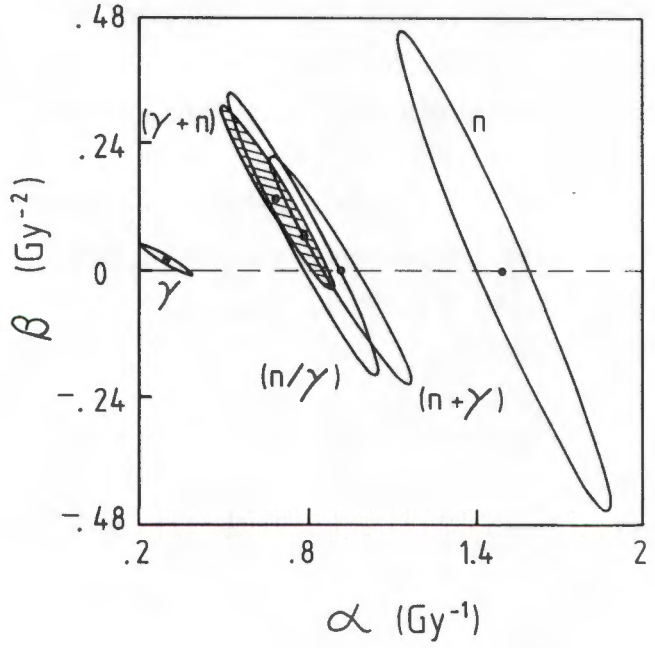

Figure 2: *95% Confidence ellipses for the inactivation parameters α and β determined from growth delay measurements in meristematic cells. Indicated are irradiations with d(16)/Be neutrons (n), ^{60}Co γ-rays (γ) and a mixture of 40% neutrons and 60% photons delivered simultaneously (n/γ) or sequentially as neutrons followed by photons (n+γ) or photons followed by neutrons (γ+n).*

Although only subtle differences seemed apparent, exposure to a mixture of neutrons and photons appeared to indicate synergistic interaction between these radiation types. In order to confirm this interaction phenomenon more rigorously, a second series of measurements was conducted in which the ratio of neutrons to photons was altered.

Influence of Different Neutron-Photon Mixtures

The dose response curves for mixtures containing 73% and 48% neutrons are shown in Fig. 3 and the dose responses for the mixture containing 23% neutrons is shown in Fig. 4. The respective inactivation parameters are listed in Table 2. Also shown in the figures are the dose responses for the various mixtures that can be expected for independent action.

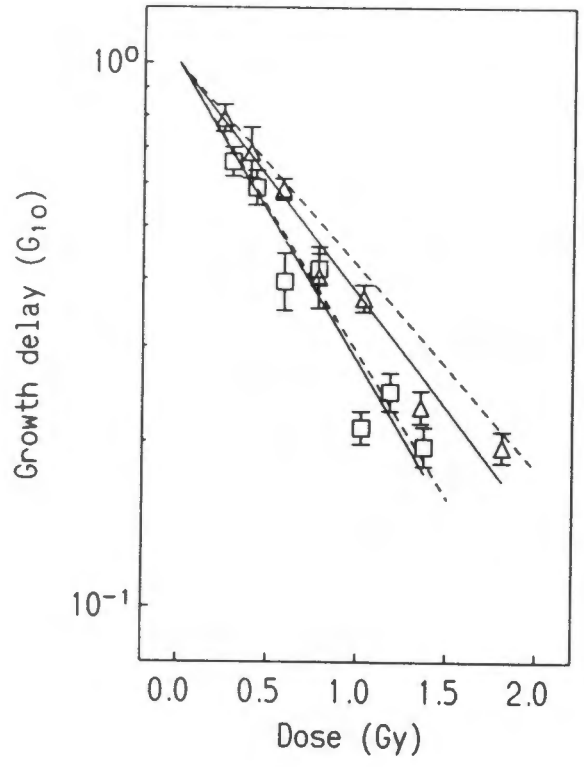

Figure 3: *Growth delay measurements for meristematic cells exposed to simultaneous mixtures of 48% d(16)/Be neutrons and ^{60}Co γ-rays (△) or 73% neutrons (□). Also indicated are the predicted responses for independent neutron and photon action (dashed lines). Error bars indicate standard deviations.*

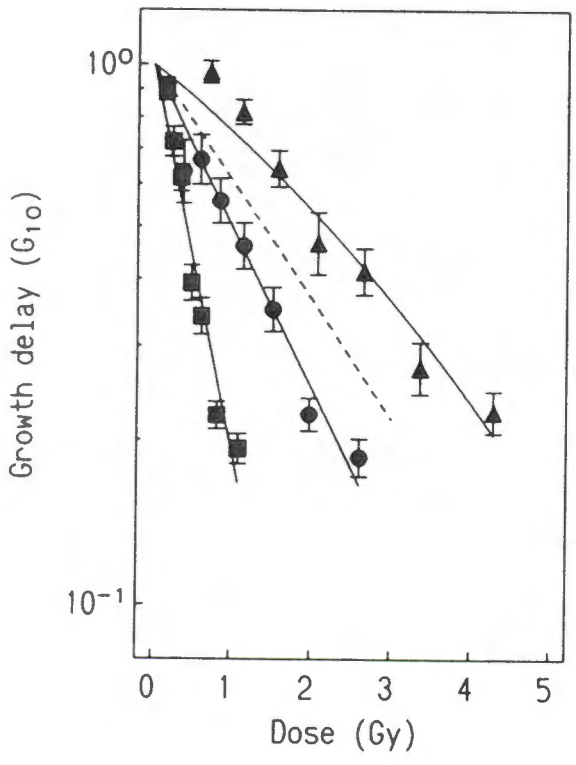

Figure 4: *Growth delay measurements for meristematic cells exposed to of d(16)/Be neutrons (■), ^{60}Co γ-rays (▲) and a simultaneous mixture containing 23% neutrons (●). Also indicated is the predicted response for independent neutron and photon action (dashed line). Standard deviations are indicated by the errors bars.*

Table 2: *Inactivation parameters calculated from growth delay measurements for meristematic cells exposed to d(16)/Be neutrons, ^{60}Co γ-rays and various mixtures of neutrons and photons delivered simultaneously. 95% Confidence limits are given in brackets.*

Radiation Type	α (Gy^{-1})	β (Gy^{-2})	$\bar{D}$ (Gy)
d(16)/Be	1.641 (0.3)	-	0.61 (0.2)
^{60}Co	0.263 (0.09)	0.0249 (0.02)	2.69 (1.0)
n/γ(73/27)	1.273 (0.3)	-	0.79 (0.2)
n/γ(48/52)	1.018 (0.2)	-	1.02 (0.2)
n/γ(23/77)	0.690 (0.2)	-	1.45 (0.3)

The observed dose response for the mixture containing 73% neutrons did not appear significantly different from the independent prediction. However, synergy was more evident for the mixtures containing 48% and 23% neutrons. Synergistic interaction was more noticeable when there were less neutrons in the mixture. These observations confirm the synergy observed in (Fig. 1) using 40% neutrons and 60% photons. These findings disagree with predictions based on the Zaider-Rossi model (1980). It is concluded here that synergistic interaction does occur between neutron and photon damage despite inferring truely exponential responses from the individual irradiations.

In view of the synergistic interaction observed with the growth delay measurements, the investigation was extended using the induction of micronuclei in meristematic cells.

Origin and Nature of Micronuclei

Following irradiation, a clearly visible abnormality in the cytoplasm of proliferating cells is the appearance of small round structures which resemble a nucleus in shape, structure and staining properties. Because these fragments are small in comparison to the size of the nucleus, they have been termed micronuclei or fragment nuclei (Evans

et al., 1959). The characteristic size and distribution of micronuclei is dependent on the cell type but not on the radiation dose (Kaffenberger *et al.*, 1990). It is interesting to note that the induction of micronuclei was first demonstrated by Evans *et al.* (1959) in broad bean root tips.

At first is was believed that the induction of micronuclei was solely due to the formation of acentric fragments. Because these structures lacked a centromere, they failed to be incorporated into one of the daughter nuclei during cell division (Heddle and Carrona, 1977). Later it was established that micronuclei formation is ascribed to both chromosomal damage and segregation errors (Geard and Yan Chen, 1990). Consequently some micronuclei are entire chromosomes that lag behind during mitosis due to defects in the mitotic spindle (Cornforth and Goodwin, 1991). Cornforth and Goodwin established that up to 14% of micronuclei in human fibroblasts contain one or more kinetochores, i.e. they are not acentric chromosome fragments. However, radiation induced micronuclei are predominantly derived from acentric fragments (Fenech and Morley, 1989; Littlefield *et al.*, 1989).

Acentric fragments are associated with dicentric formation in irradiated eukaryotic cells, a typical exchange type aberration (IAEA, 1986). Radiation-induced exchange aberrations require initial damage to chromatin at both locations involved in the exchange (Cornforth, 1989). Therefore two lesions are necessary for the formation of a micronucleus and thus the use of this endpoint is appropriate when studying the possible synergistic interaction between high- and low-LET radiation. Furthermore, dicentrics and micronuclei show a linear-quadratic dose-response (Lloyd *et al.*, 1986; Almassy *et al.*, 1987) indicating a contribution from two-track lesions (Countryman and Heddle, 1976). In addition, Vral *et al.* (1992) observed split-dose effects with micronuclei in human lymphocytes that could be attributed to the repair of sublethal damage.

The induction of micronuclei in meristematic cells was followed for two reasons. Firstly, the analysis of chromosome aberrations in meristematic cells is relatively easy because chromosomes of meristematic cells are large. The chromosome number is low ($2n=12$) and each cell contains about 46 pg of DNA (Kihlman, 1975). By comparison a Chinese hamster cell accommodates 8.3 pg of DNA which is distributed amongst 22 chromosomes, and a human lymphocyte has 7.3 pg of DNA in 46 chromosomes.

Secondly, the spontaneous aberration frequency of meristematic cells was reported to be very low (less than 2 micronuclei /1000 cells) by Marshall and Bianchi (1983). By contrast the background micronuclei frequency in mammalian cell culture lines is much higher. For example the spontaneous incidence of micronuclei in CHO-K1 cells was determined by the author and found to be in excess of 100 micronuclei/ 1000 cells. It was considered that a high incidence of micronuclei in unirradiated cells will obscure the demonstration of subtle synergism.

Identification Criteria for Micronuclei in Meristematic Cells

Criteria for scoring micronuclei were based on guidelines proposed by Almassy *et al.* (1987) and Krepinsky and Heddle (1983). These are:

1. A micronucleus must have the same structure as the nucleus and must be smaller.
2. It must be clearly separated from the nucleus.
3. The micronucleus must show a Feulgen-positive reaction and in contrast to non-nuclear particles, it must not show any light refractility.
4. Only cells with a well preserved cytoplasm can to be considered.
5. Scoring must to be restricted to cells in the meristematic region.

Examples of micronuclei are shown in Fig. 5.

Determination of Sampling Time

The meristem consists of an asynchronous population of actively dividing cells that exhibit a heterogeneous sensitivity to radiation. This, in concert with the mitotic delay that is induced by the radiation, raises uncertainties as to the correct fixation time. A single fixation time after radiation may not be representative of the aberration yield. The aim of the first set of measurements was to follow the effect of post irradiation intervals on micronuclei yield and thus determine which fixation times should be used in the measurement of dose-effect relationships.

Root tips were fixed at 6, 12, 18, 24, 30, 36, 42, and 48 hours after irradiation. This was done following a test dose of neutrons only, photons only, and a mixture of 48% neutrons and 52% photons. The data are presented in Fig. 6.

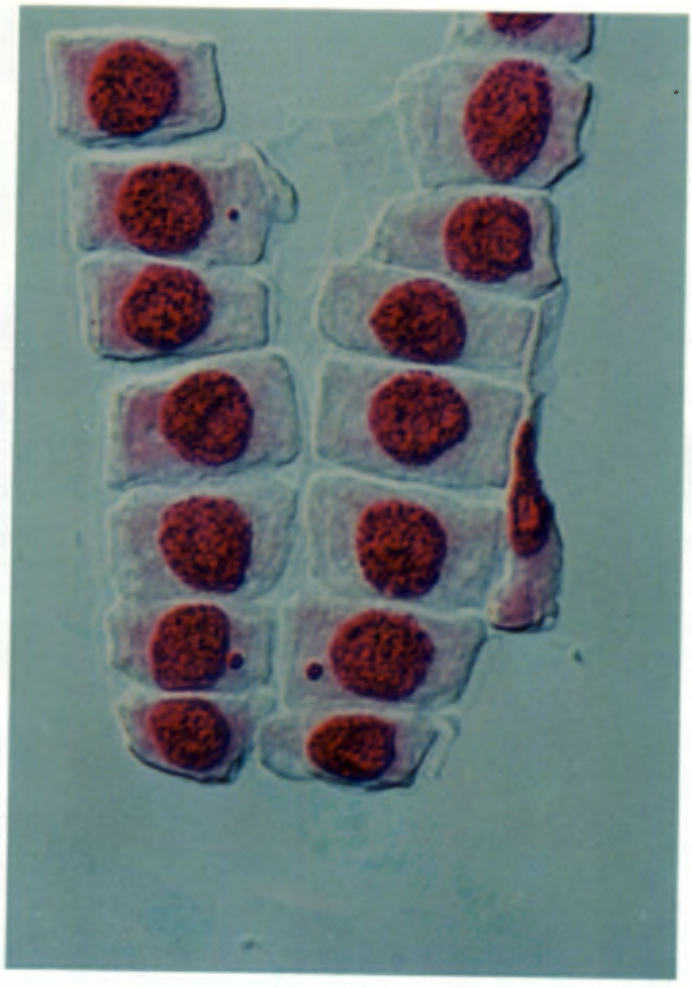

Figure 5: *Meristematic cells prepared and stained as detailed in the Appendix. Micronuclei are clearly visible in three of the cells.*

A similar pattern was observed for all the the radiation qualities applied. The induction of micronuclei became measurable at 12 hours followed by a sharp increase in frequency at 18 hours. Thereafter a relatively stable frequency of micronuclei was observed between 24 and 48 hours after irradiation. A possible exception was the response to neutrons only. In this case the maximum yield occured around 42 hours.
It is unlikely that this deviation is attributable to the radiation quality since the 48% neutron mixture conformed to the kinetics of photon only irradiation. Using 600 MeV neutrons Marshall (1982) found no definitive influence on the production rate of micronuclei. It was decided to use the mean value of micronuclei formation between 24 and 36 hours for the quantitative estimate of damage.

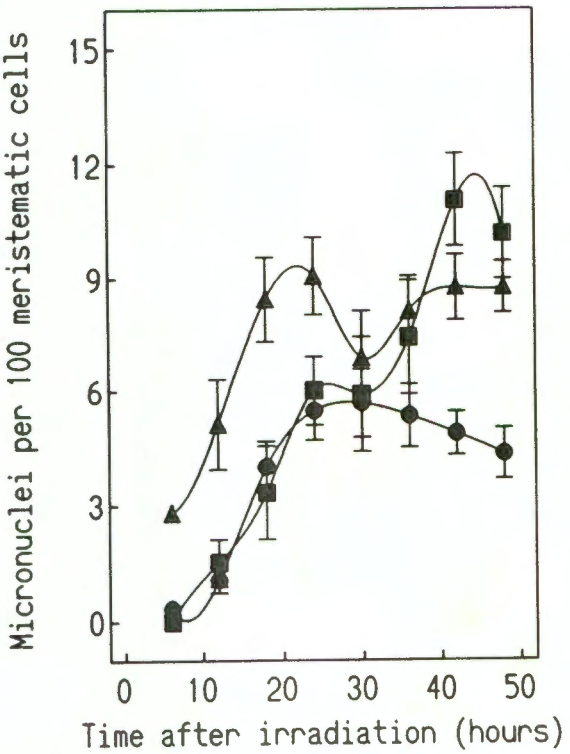

Figure 6: *Frequency of micronuclear formation in meristematic cells as a function of time after absorbing a dose of 40 cGy d(16)/Be neutrons (■), 180 cGy ^{60}Co γ-rays (▲), and 70 cGy of a simultaneous mixture consisting of 48% neutrons and 52% photons (•). Error bars indicate the Poisson error.*

Yield of Micronuclei Following Simultaneous Exposure to d(16)/Be Neutrons and ^{60}Co γ-rays

In Table 3 the micronuclei frequencies are listed for ^{60}Co γ-rays, d(16)/Be neutrons and a simultaneous exposure to 40% neutrons and 60% photons. The dose effect curves are depicted in Fig. 7 and a statistical analysis of the α- and β-coefficients is presented in Fig. 8. A larger covariance between α- and β-values is evident when the mean LET of the radiation is reduced. As expected, the α-values were well separated for the three radiation qualities but it was only the response to photons that exhibited a significant β-component. This is noteworthy since the dose range employed in these measurements was much lower than that for the G_{10} study. In principle it is more difficult to detect a significant β-component at lower doses (Watts *et al.*, 1986).

Table 3: *Micronuclei frequencies in meristematic cells exposed to d(16)/Be neutrons, ^{60}Co γ-rays and a simultaneous mixture of 40% neutron and 60% photons. Poisson errors are given in brackets.*

Dose (cGy)	Cells Scored	MN	MN per 100 cells
d(16)/Be neutrons			
5	3065	38	1.24 (0.2)
10	3223	68	2.11 (0.3)
20	3158	120	3.80 (0.4)
25	3054	131	4.29 (0.4)
30	3334	170	5.10 (0.4)
40	3329	293	8.80 (0.5)
50	3016	285	9.45 (0.6)
^{60}Co γ-rays			
0	3430	7	0.20 (0.1)
50	3459	46	1.33 (0.2)
70	3077	64	2.08 (0.3)
100	3263	124	3.80 (0.3)
130	3093	120	3.88 (0.4)
150	2690	170	6.32 (0.5)
200	3492	322	9.22 (0.5)
Simultaneous 40/60% n/γ mixture			
15	3001	36	1.20 (0.2)
30	3172	92	2.90 (0.3)
45	3211	183	5.70 (0.4)
60	3115	243	7.80 (0.5)
75	2707	222	8.20 (0.6)
90	3353	346	10.32 (0.6)
105	3098	412	13.30 (0.7)

Unlike the results from the G_{10} study, the calculated β-values show a small but steady increase with LET. Similar trends have been observed by Joiner *et al.* (1984) for neutron/X-ray mixtures using acute skin reactions in the mouse foot, by Raju *et al.* (1978) following irradiation of V-79 cells with various heavy particles and by Bauchinger *et al.* (1984) for chromosome aberrations in human lymphocytes following irradiation with slow and fast neutrons.

Using the data obtained from the individual photon and neutron irradiations, the response that might be expected if neutron and photon damage acted independently

was calculated and is indicated in Fig. 7. A synergistic effect is clearly demonstrated. The inactivation parameters determined for the different dose response curves are listed in Table 4.

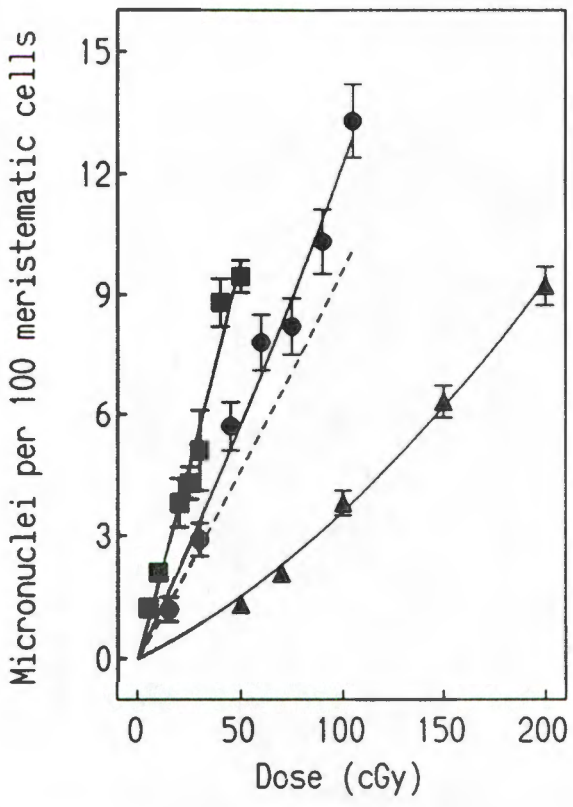

Figure 7: *Frequency of micronuclear formation in meristematic cells following exposure to d(16)/Be neutrons (■),^{60}Co γ-rays (▲) and a simultaneous mixture of 40% neutrons and 60% photons (•). The dashed line indicates the expected micronuclei frequencies if neutron and photon damage acted independently. Error bars indicate the Poisson error.*

Both the synergistic model of Zaider-Rossi and the lesion additivity model of Lam predict dose effect curves that were marginally lower than the experimental observations (Table 4). The fact that the Zaider-Rossi model is able to predict a dose response that is in reasonable agreement with the experimental observations illustrates a peculiar characteristic of the Zaider-Rossi interaction function. The Zaider-Rossi model is reliant on the determination of a dose-quadratic term for both neutron only and photon only responses. Although a β-component was determined in the micronuclei response to neutrons only, it was small and only amounted to 0.7 micronuclei per 100 cells for the neutron dose applied in the highest mixed field exposure (120 cGy). A quadratic

component of this magnitude does not lead to any significant deviations from linearity in the neutron dose-effect curve over the range of doses used. In spite of this, the Zaider-Rossi model predicted the experimental observations reasonably well. A similar observation was made by Scott (1984) using the additive damage model.

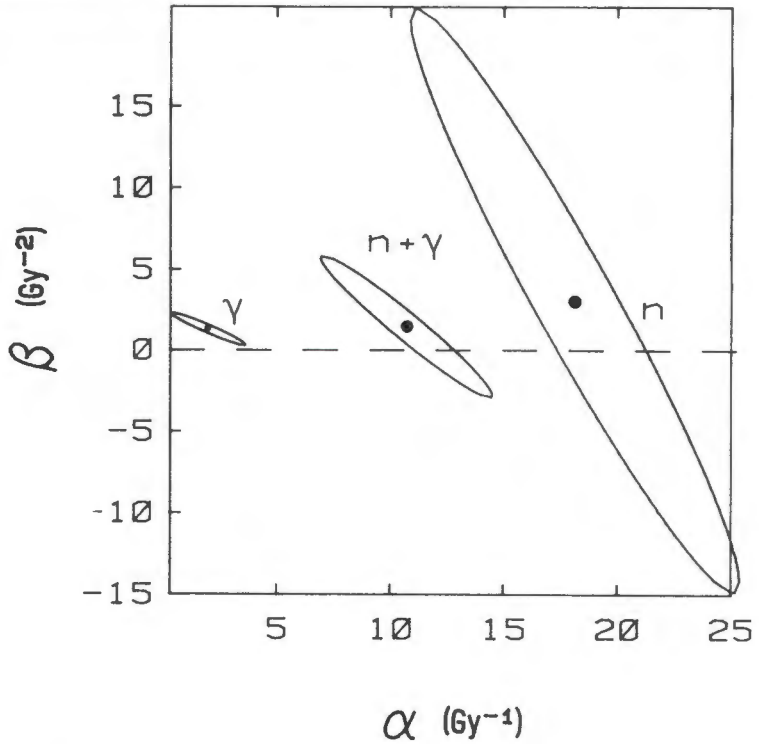

Figure 8: *95% Confidence ellipses for the inactivation parameters α and β determined from observed micronuclei formations in meristematic cells. Indicated are irradiations with d(16)/Be neutrons (n), ^{60}Co γ-rays (γ) and a mixture of 40% neutrons and 60% photons delivered simultaneously (n/γ).*

Although the mean frequency changes with dose, it was noted that the number of micronuclei formed in an individual cell rarely exceeded one. Out of the more than 60000 meristematic cells scored during this investigation, fewer than 100 cells contained more than one micronucleus. In contrast, other non-stochastic endpoints such as dicentric formation in human lymphocytes show a distribution of aberrations in the affected cells (Hellin *et al.*, 1990). Furthermore, the frequency distribution is influenced by the ionization density of the radiation. This is discussed in the following Chapter. The induction of micronuclei in meristematic cells does not exhibit a distribution that is expected of a non-stochastic endpoint. In view of this limitation it was decided to extend the interaction of radiation damage resulting from neutrons and photons to human lymphocytes.

Table 4: *Dose response parameters calculated from micronuclei formation in meristematic cells exposed to d(16)/Be neutrons, ^{60}Co γ-rays and a 40/60 n/γ mixture of neutrons and photons delivered simultaneously. 95% Confidence limit errors are given in brackets.*

Radiation Type	α (cGy^{-1})	$\beta \times 10^3$ (cGy^{-2})
d(16)/Be	0.181 (0.03)	0.304 (0.73)
^{60}Co	0.020 (0.01)	0.129 (0.04)
n/γ(40/60)	0.107 (0.02)	0.151 (0.17)
Predictions for n/γ mixture		
Independent	0.084	0.094
Zaider-Rossi	0.085	0.190
LAM	0.087	0.208

CHAPTER 11

INTERACTION OF NEUTRON AND PHOTON INDUCED DAMAGE IN HUMAN LYMPHOCYTES

Introduction

In the previous Chapter it was demonstrated that the micronuclei frequency yield was more than additive following exposure to mixed-field irradiations. This observation has implications for assessing the physical dose based on the quantification of radiation damage in human lymphocytes. In this chapter the effects of mixed-field exposures are investigated and the results related to biological dosimetry.

In cytogenetic dosimetry the dose absorbed by a radiation worker or a member of the public during a radiation accident is usually estimated from an analysis of chromosomal aberration frequencies. For this purpose calibration curves are constructed which relate the degree of chromosome damage observed in lymphocytes to the physical dose. Such calibration curves are available for a number of individual high- or low-LET radiation types (Fabry *et al.*, 1985; Hellin *et al.*, 1990). However, for mixtures of different radiation modalities, e.g. neutrons and photons, no such calibration curves are available.

To assess the absorbed doses where there has been an exposure to a mixed-field, the International Atomic Energy Agency (IAEA) has prescribed an iteration procedure based on the calibrated dose-effect relationships for the individual radiation types (IAEA, 1986). It is assumed that the ratio between neutron and γ-ray doses is known through some physical means. This approach is necessary since it is impractical to generate calibration curves for every mixed radiation field that may be encountered in radiation incidents.

However, this procedure can yield satisfactory dose estimates only if the different radiation types act independently of one another. The validity of this assumption in a radiation incident is questionable for two reasons.

Firstly, the dose-response curves for chromosome damage in fast neutron fields indicate a quadratic component (Lloyd *et al.*, 1976; Lloyd and Edwards 1983;

Matsubara *et al.*, 1988), suggesting that interaction with low-LET radiation is possible. Secondly, even if single hit kinetics prevail, e.g. following an exposure to fission neutrons in a criticality accident, interaction damage cannot be ruled out. In the previous Chapter it was established that failure to observe a quadratic component in the biological response to neutron irradiation does not prevent neutron induced lesions to interact with those resulting from low-LET radiation.

Takatsuji and Sasaki (1984) determined that the dose-quadratic component for dicentric formation in human lymphocytes irradiated with 23 MeV α-particles was not significantly different from zero. However, these authors also observed a change in the relative variances of distribution of dicentrics with mean dicentric yield. Such a change indicated the presence of inter-track interaction in the formation of dicentrics by α-particles. Consequently, interaction between high- and low-LET radiation in human lymphocytes is a real possibility when mixed fields are encountered, even when interaction is not inferred from the dose-effect relationship for the high-LET component.

If the accumulation of chromosome damage in a human lymphocyte is more than additive and this synergistic effect is not accounted for, it would lead to an overestimation of the dose absorbed in a mixed field radiation accident. It is therefore necessary to establish whether synergistic interaction is indeed realized when human lymphocytes are exposed to a mixed neutron-photon radiation field.

In this Chapter three experiments are described in which human lymphocytes were exposed to a mixture of high- and low-LET radiation. In the first experiment chromosome aberrations were followed in metaphase spreads following exposure to graded doses of d(16)/Be neutrons, ^{60}Co γ-rays and a mixture containing 23% neutrons and 77% photons. The neutrons and photons in the mixture were applied both sequentially and simultaneously. In the second experiment micronuclei frequencies were determined in binucleate lymphocytes following graded doses of p(66)/Be neutrons, ^{60}Co γ-rays and a mixture containing 46% neutrons and 54% photons. In the third experiment micronuclear formations were followed in binucleate lymphocytes following exposure to p(66)/Be neutrons without any build-up, i.e. not under conditions of secondary charged particle equilibrium. Here a mixture containing 47% neutrons and 53% ^{60}Co γ-rays was used.

Chromosome Aberrations following Simultaneous and Sequential Exposures to d(16)/Be Neutrons and ^{60}Co γ-rays

Whole blood samples were collected in glass tubes containing lithium heparin. All the samples for all the dose effect curves were collected from the same donor (a 35 year old healthy male) at the same time. Lloyd *et al.* (1975) suggested that for the construction of *in vitro* dose-response curves it is desirable to irradiate whole blood at 37° C. For this reason the appropiate measures were taken to maintain the blood at this temperature from the time of venepuncture until the cultures were fixed.

During irradiation the tubes were placed in a phantom made from perspex (7 × 8 × 3 cm). Water was circulated through the phantom using a thermostatically controlled water pump. Irradiations were performed between two and three hours after the samples were drawn using the neutron-photon facility described in Chapter 4. The 23% neutron 77% photon mixture was delivered both sequentially (γ+n) and simultaneously. After irradiation the blood cultures were prepared for chromosome analysis as detailed in the Appendix.

Chromatid Aberration Frequencies

For each dose point 100 metaphase spreads were analysed to determine the percentage of cells in the first mitotic division (M1) (Table 1). In a further 100 metaphases the frequency of different aberrations types were recorded for each dose point. These were: breaks, fragments, translocations, double minutes, dicentrics, tricentrics and ring formations (Table 1). These microscopic examinations were not undertaken by the author but performed in the Department of Human Genetics at the University of the Orange Free State) (Jansen, 1992). The total chromatid aberration frequency was calculated by weighting these aberration types respectively as 1, 2, 4, 4, 4, 8 and 4 chromatid aberrations (Savage, 1976).

Variations in the fraction of cells in M1 at the end of the culture time (50 hours) were evident (Fig. 1). Variations in the M1 fraction are attributable to different degrees of mitotic delay experienced by the different dose groups. This emphasized the importance of normalizing aberration frequencies accordingly. However, with the exception of the photon only irradiations, no significant correlation between physical dose and percentage cells in M1 could be established. Chromatid aberration frequencies were therefore normalized according to the mean fraction of cells in M1 (56.1%).

Table 1: *Frequency of different types of chromosomal aberrations observed in 100 lymphocyte metaphase spreads. Cells were irradiated with d(16)/Be neutrons, ^{60}Co γ-rays and a mixture containing 23% neutrons delivered either sequentially or simultaneously.*

Dose (Gy)	M1 (%)	Breaks	Frag-ments	Trans-loca-tions	Double minutes	Di-centrics	Tri-centrics	Rings
Neutrons								
0.00	64	-	1	-	-	-	-	-
0.15	50	4	4	-	-	3	-	-
0.40	62	3	14	-	2	2	-	1
0.80	70	3	21	-	10	11	-	1
1.25	71	10	49	1	6	17	1	1
1.90	67	3	88	1	3	33	2	5
2.50	71	3	112	2	17	55	3	4
^{60}Co								
0.50	55	6	2	-	-	-	-	-
1.00	63	4	13	-	1	5	-	-
1.50	72	2	21	-	1	7	-	1
2.50	63	7	51	-	4	19	-	1
3.50	72	13	59	-	4	28	-	1
4.5	84	10	156	2	3	57	2	4
Simultaneous								
0.00	45	-	1	-	-	-	-	-
0.45	70	5	6	-	-	3	-	-
0.80	48	4	23	-	1	12	-	-
1.77	54	5	28	2	10	26	-	6
2.59	66	4	76	6	7	33	1	1
3.47	78	7	156	3	9	43	1	6
4.38	64	10	149	6	26	66	2	3
Sequential								
0.45	68	4	9	-	-	1	-	-
0.80	52	4	17	1	1	6	-	3
1.77	63	2	36	-	-	10	-	4
2.59	64	-	66	2	4	17	-	6
3.47	78	4	54	1	34	27	1	4
4.38	82	1	167	-	15	54	2	9

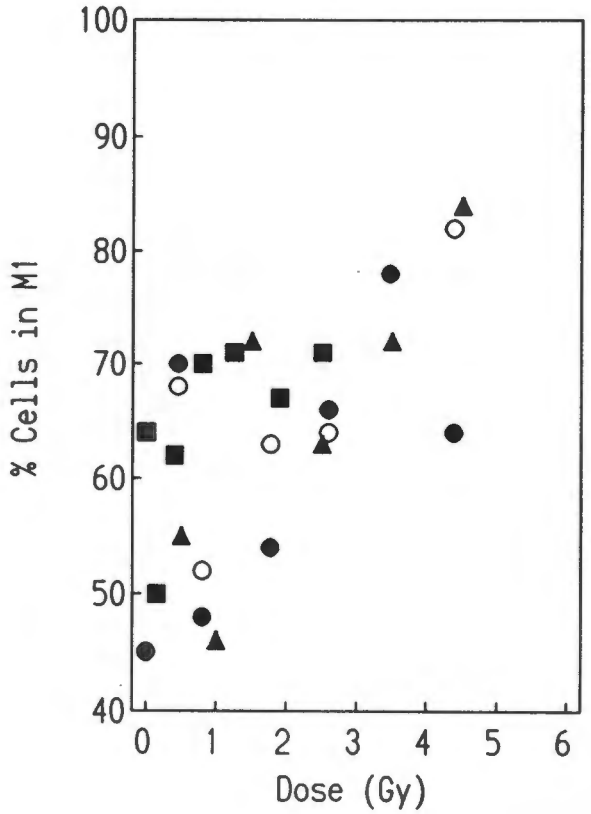

Figure 1: *The effect of radiation dose on the percentage lymphocytes in M1 after 50 hours in culture. Cells were irradiated with d(16)/Be neutrons (closed squares), ^{60}Co γ-rays (closed triangles) and a 23%/77% n/γ mixture applied either simultaneously (closed circles) or sequentially (open circles).*

The chromatid aberration frequency per cell is plotted in Fig. 2 as a funciton of dose for each radiation condition. A significant difference between sequential and simultaneous exposures is evident. Both mixed-field exposures yield aberration frequencies in excess of the sum predicted from the response of the individual radiations (Fig. 3). The latter was calcuated assuming no interaction between the damage induced by the neutrons and photons.

Dose response parameters calculated using the Zaider-Rossi interaction function and the lesion additivity model were almost identical (Table 2.). Thus the combined effect of the sequentially irradiated samples can be predicted reasonably well using either of these models (Fig. 3). However, the total damage following a series of simultaneous exposures was underestimated by both these models. This is unfortunate since only simultaneous exposures are likely to be encountered in accidents involving mixtures of neutrons and photons.

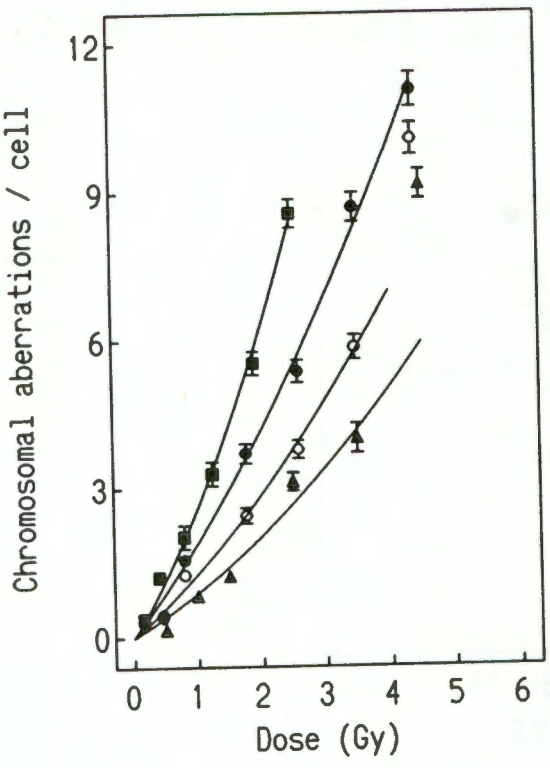

Figure 2: *Chromosomal aberration frequencies in lymphocytes following exposure to d(16)/Be neutrons (closed squares), ^{60}Co γ-rays (closed triangles), and a 23%/77% n/γ mixture applied sequentially (open circles) or simultaneously (closed circles). Poisson errors are indicated by the error bars.*

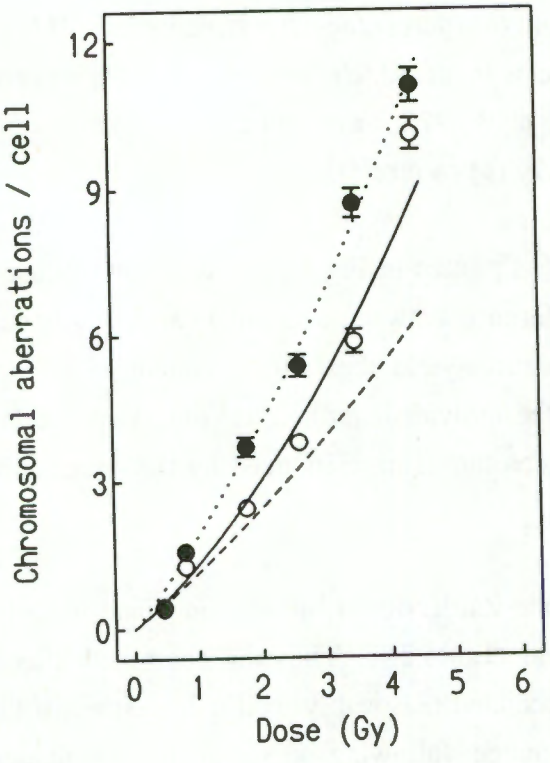

Figure 3: *Predictions for chromosomal aberration frequencies in lymphocytes following exposure to a mixture containing 23% d(16)/Be neutrons and 77% ^{60}Co γ-rays. Independent prediction (dashed line) and Zaider-Rossi model (solid line). Symbols for experimental data as in Fig. 2. The dotted line is the best fit to the data for the simultaneous exposure. Poisson errors are indicated by the error bars.*

Table 2: *Dose-response parameters calculated from the chromosomal aberration frequencies observed in Fig. 2 and predicted using the Zaider-Rossi and lesion additivity model (LAM).*

Radiation Type	α(± S.E.) (Gy-1)	β(± S.E.) (Gy-2)
d(16)/Be	1.995 (0.23)	.5502 (0.11)
60Co	0.754 (0.26)	0.126 (0.088)
n/γ	1.658 (0.209)	0.208 (0.057)
γ+n	1.098 (0.167)	0.163 (0.056)
Predictions for mixed field		
Independent	1.038	0.086
Zaider-Rossi	1.079	0.209
LAM	1.071	0.208

Previous results obtained using cell survival (V-79 cells), growth delay measurements (meristematic cells) and micronuclei frequencies (meristematic cells) indicated no difference in response between simultaneous and sequential mixed-field irradiations. The difference in response between simultaneous and sequential exposures seen in lymphocytes was unexpected. Unfortunately, due to the decommisioning of the cyclotron that provided the d(16)/Be beam, it was not possible to repeat these measurements. Even so, neutrons and photons delivered either simultaneously or sequentially appear to act in a non-independent manner in human lymphocytes. It is concluded that synergistic interaction plays a significant role in the formation of chromosome aberrations. Consequently, the estimation of dose in a mixed-field accident should incorporate a suitable interaction function.

Induction of Micronuclei in Binucleate Lymphocytes

It was considered necessary to attempt to confirm the synergistic interaction observed between neutron and photon damage using chromosome aberrations in human

lymphocytes by making use of a p(66)/Be neutron beam. The analysis of chromosome aberrations is however an extremely time consuming technique and the need arose for a less labour intensive method to assess radiation damage in human lymphocytes. It was further argued that the experimental value of this study would be enhanced if similar effects could be demonstrated employing a different biological endpoint.

An attractive option for rapid evaluations is the quantification of micronuclei in peripheral lymphocytes. This endpoint has proven to be a reliable indicator of chromosomal damage caused by ionizing radiation (Countryman and Heddle, 1976; Krepinsky and Heddle, 1983; Ramalho *et al.*, 1988). Compared to classical cytogenetic methods, the enumeration of micronuclei is relatively simple and allows for rapid scoring of large numbers of cells by personnel having undergone a brief training period (Thierens *et al.*, 1991). Micronuclei appear only in cells that have undergone nuclear division subsequent to irradiation, the frequency of which can vary according to culture conditions. Furthermore , lymphocyte proliferation kinetics varies between individuals (Gantenberg *et al.*, 1991), thus it is important to discriminate between dividing and non-dividing cells.

This discrimination problem was elegantly resolved by Fenech and Morley (1985, 1986) who introduced a cytokinesis blocking (CB) technique using Cytochalasin B (Cyt-B). Cyt-B is a inhibitor of the microfilament assembly and prevents cytoplasmic division after nuclear division has occurred. The addition of Cyt-B to the culture medium leaves some cells binucleated without interfering with the earlier part of mitosis (Carter, 1967). When scoring of micronuclei is limited to binucleate cells, enhanced precision and sensitivity is obtained (Fenech and Morley 1986).

Micronuclei and Cell Survival

A strong correlation exists between cell survival and micronucleus induction (Wandl *et al.*, 1989; Stap and Aten, 1990; Ono *et al.*, 1989). This relationship has been shown to hold for neutrons (Ono *et al.*, 1990) and photons (Masunaga *et al.*, 1991). Furthermore, the ratio of the inactivation parameters (α/β) for cell survival and micronucleus induction have been shown to be similar (Masunaga *et al.*, 1990).

Irradiations

Lymphocytes were exposed to the following irradiation configurations. Whole blood samples were positioned behind 2 cm of polyethylene and exposed to p(66)/Be neutrons under full charged particle equilibrium conditions (D_{max}). The field size for these irradiations was 29x29 cm and the dose from this field had an inherent γ-contamination of 7.8%. Whole blood samples were also exposed to ^{60}Co γ-rays alone as well as to a mixture containing 46% neutrons and 54% photons. Photon irradiation proceeded 2 minutes after completion of the neutron irradiation.

Some lymphocyte samples were first separated from other blood elements and centrifuged down onto the growth area of a petri dish. The method used is detailed in the Appendix. Once the medium was removed these samples were irradiated with p(66)/Be neutrons without any build-up material. The radiation effects observed under these conditions have been discussed in Chapter 9. These irradiations are referred to as $D_{surface}$ exposures and were delivered using a 20 × 20 cm field size. The inherent γ-ray contamination of this field was 6.7%. Lymphocytes were also exposed sequentially to neutrons (47%) and ^{60}Co γ-rays (53%).

Following irradiations, lymphocyte cultures were prepared as detailed in the Appendix. Cytochalasin B (3 μg/ml) was added to the growth medium 44 hours after mitogen stimulation of the cultures and cells were prepared for microscopic examination as detailed in the Appendix. Examples of binucleate cells are shown in Fig. 4.

Identification Criteria for Micronuclei in Human Lymphocytes

As with micronuclei in meristematic cells, the criteria for scoring micronuclei in human lymphocytes were largely based on the prescriptions set out by Almassy *et al.* (1987), Krepinsky and Heddle (1983) and Lasne *et al.* (1984). Using fluorescence microscopy, the following standards were adhered to:

1. Micronuclei were recorded only in cells containing two main nuclei with a well preserved cytoplasm.

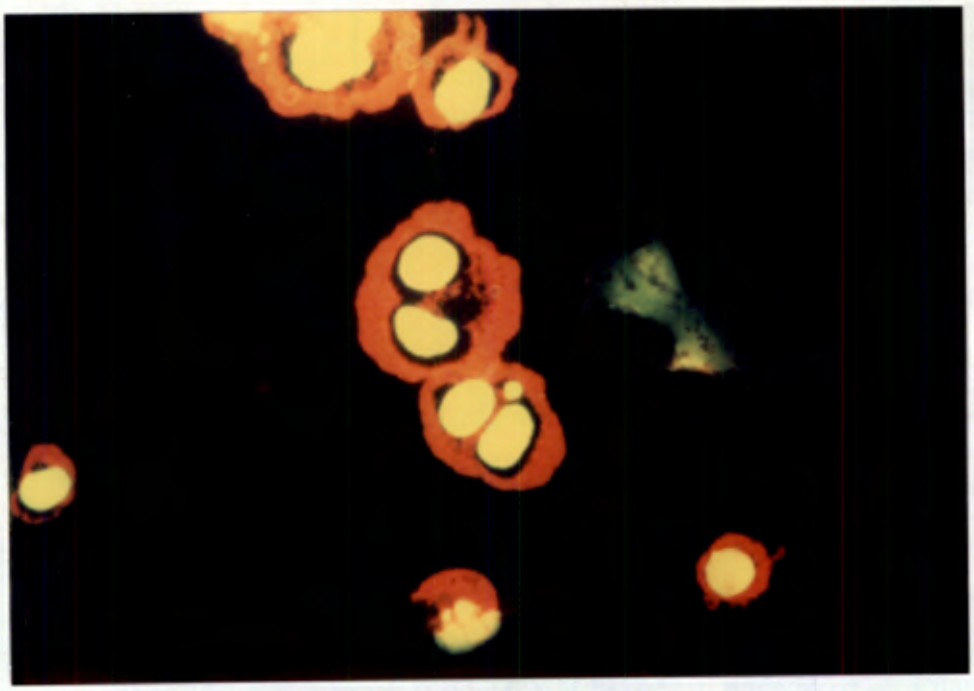

Figure 4: *Photomicrograph of two binucleate lymphocytes, one containing a micronucleus.*

2. Cells with three and four main nuclei were excluded from the count. These cells were not enumerated but have been reported to constitute less than 5% of the population (Gantenberg *et al.*, 1991). It was however noted that cells containing three or four nuclei frequently contained a micronucleus.

3. A micronucleus must show the same DNA-specific reaction as the two main nuclei. The latter fluoresces green-yellow with the acridine orange fluorochrome used for these observations (Hayashi *et al.*, 1983).

4. A micronucleus must show the same granular structure as the main nuclei. The staining intensity should be equal to that of a main nucleus.

5. The size of a micronucleus should not exceed about one third that of the main nucleus.

6. Micronuclei touching, but not overlapping each other or a main nucleus were counted (Huber *et al.*, 1992).

Influence of Cytochalasin B

Because the microfilament inhibitor is dissolved in pure dimethyl sulfoxide (DMSO) there is the possibility that the addition of Cyt-B might influence the micronuclei frequency in unirradiated cells (Cornforth and Goodwin, 1991). For this reason, some samples were initially cultured without Cyt-B for comparison. In these samples the spontaneous incidence of binucleate cells was found to be about 1.3% and a micronuclei frequency of 5.1 ± 1.7 per 500 cells was determined in the mononuclear population. Lymphocytes grown for the last 28 hours of the culture period in the presence of Cyt-B had a background frequency of 2.8 ± 0.8 micronuclei per 500 cytokinesis-blocked (CB) cells. About half the cells in these samples were binucleate (Table 3). It was concluded that the addition of Cyt-B to the culture medium did not significantly influence the spontaneous incidence of micronuclei in human lymphocytes.

Preliminary Measurements

To test whether the micronuclei frequencies observed were compatible with those reported by other investigators, tests were conducted using lymphocyte samples from five individuals. Two samples were obtained from each donor, one served as control for background measurements and the other was irradiated with a test dose of 1 Gy photons. The results are summarized in Fig. 5. Included in Fig. 5 is the mean and standard deviations of micronuclei frequencies observed in the lymphocytes of eight donors (Fenech and Morley, 1985).

There was good agreement between the present observations and those of Fenech and Morley (1985) regarding both background counts and test irradiated samples. This in spite of the fact that these authors used the May-Grünwald-Giemsa staining technique. Almassy *et al.* (1987) reported that about 20% more micronuclei can be recognized with acridine orange fluorescence compared to conventional staining.

Gantenberg *et al.* (1991) reported a higher mean background of 10 micronuclei per 500 lymphocytes and a mean value of 76 micronuclei per 500 binucleate cells was determined from their data for an absorbed dose of 1 Gy photons. However, these authors added Cytochalasin-B to the cultures at various times depending on the proliferation kinetics of the individuals lymphocytes.

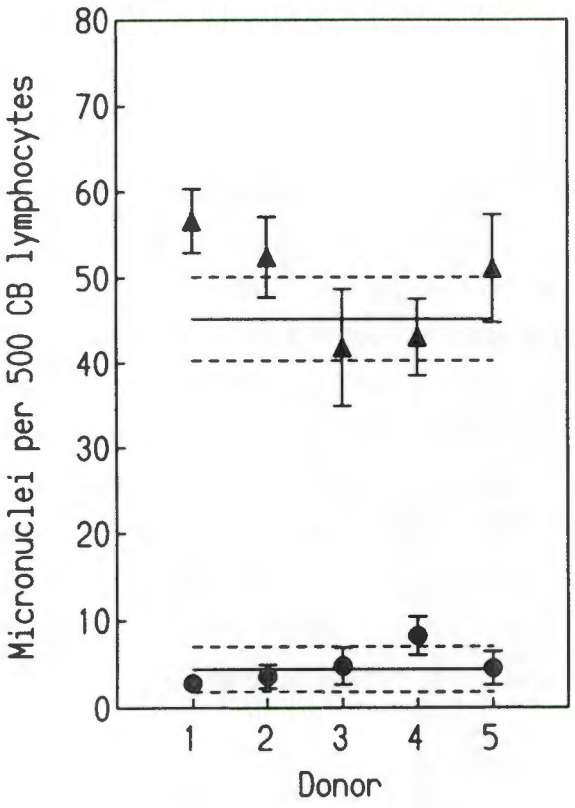

Figure 5: *Micronuclei frequencies in cytokinesis–blocked (CB) lymphocytes from five donors. Spontaneous formations (closed circles) and that from a test irradiation of 1 Gy ^{60}Co γ-rays (closed triangles) are shown. Poisson errors are indicated by the error bars. The solid and dashed lines indicate the mean and standard deviation of micronuclei frequencies obtained by Fenech and Morley (1985).*

Based on the average micronuclei frequency observed in samples from different individuals (Fig. 5), it was concluded that micronuclei could be identified in human lymphocytes with reasonable accuracy.

Single Modality Exposures

Micronuclei frequencies recorded following exposure of blood from one individual to graded doses of ^{60}Co γ-rays, p(66)/Be neutrons at D_{max} and p(66)/Be neutrons at the surface are listed in Table 3. Included are the percentage cells in each culture that contained two main nuclei. This is an indication of the proliferation kinetics of the lymphocytes. Variations were evident but no systematic change was noted between the different dose groups, irrespective of radiation quality applied. Micronuclei frequencies observed were therefore not influenced by variations in mitotic delay.

Table 3: *Mean micronuclei (MN) frequencies observed in cytokinesis-blocked (CB) lymphocytes following exposure to ^{60}Co γ-rays and p(66)/Be neutrons with and without build-up. Poisson error ($\sqrt{MN}$ /No. cell scored) is given in brackets. Included in the Table is the percentage of binucleate cells (BNC) observed in each culture.*

Dose (cGy)	No. CB cells observed	No. MN	MN per 500 BNC	BNC (%)
^{60}Co γ-rays				
0	1982	11	2.8 (0.8)	55
10	1349	22	8.2 (1.7)	54
25	1005	39	19.4 (3.1)	48
50	1229	72	29.3 (3.5)	52
100	2103	238	56.6 (3.7)	46
150	913	161	88.2 (6.9)	47
200	773	178	115.1 (8.6)	43
250	1536	400	130.2 (6.5)	46
300	873	246	140.9 (8.9)	45
400	640	285	222.7 (13.2)	50
p(66)/Be(D_{max})				
5	942	28	14.9 (2.8)	46
10	825	37	22.4 (3.7)	48
25	471	42	44.6 (6.8)	44
50	559	64	57.2 (7.2)	45
100	486	138	141.9 (12.1)	47
150	1306	465	178.0 (8.3)	45
p(66)/Be(D_{surf})				
5	940	46	24.5 (3.6)	45
10	1003	71	35.4 (4.2)	47
25	1054	214	101.5 (6.9)	50
50	706	230	162.9 (10.7)	46
75	708	284	200.6 (11.8)	46
100	936	596	318.4 (13.0)	47

The smallest photon and neutron doses in these measurements were respectively 10 and 5 cGy. In both instances the micronuclei yield was significantly different from the background.

The dose response curves from this study are plotted in Fig. 6. A linear relationship appears evident between dose and mean micronuclei frequency for all three radiation qualities. The mean background frequency was subtracted from the separate determinations and the slopes, calculated by means of regression analysis, were 0.525 ± 0.02 (^{60}Co γ-rays), 1.343 ± 0.09 (p(66)/Be neutrons at D_{max}) and 3.254 ± 0.23 (p(66)/Be neutrons without build-up). The RBE, given by the ratio of slopes, for neutrons under full charged particle equilibrium conditions and neutrons at the surface was found to be 2.6 and 6.2 respectively.

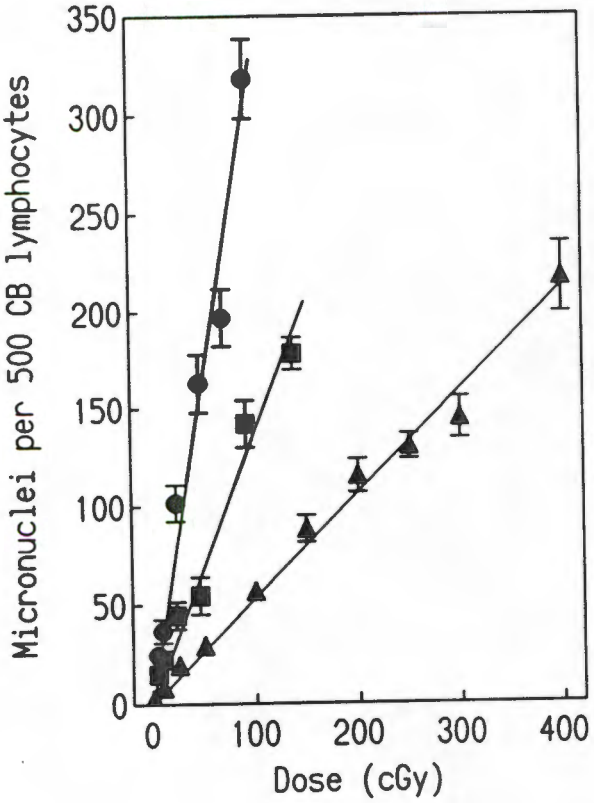

Figure 6: *Micronuclei frequencies observed in cytokinesis-blocked (CB) lymphocytes following exposure to graded doses of ^{60}Co γ-rays (closed triangles), p(66)/Be neutrons at D_{max} (closed squares) and without build-up (closed circles). Error bars indicate the Poisson error.*

Even though the photon doses extended up to 4 Gy, a linear response was noted for ^{60}Co irradiations. This behaviour is in agreement with X-ray studies performed by Fenech and Morley (1985, 1986) and Fenech *et al.* (1990). It is however different from the linear-quadratic responses noted by Almassy *et al.* (1987), Gantenberg *et al.* (1991) and Vral *et al.* (1992). There is no work to date with which the results from the neutron irradiations can be compared. The linear nature of these dose response curves is, however, in agreement with what is generally expected from high-LET radiation types (Lloyd *et al.*, 1976).

Micronuclear Formation and Radiation Quality

The response of a biological system to a particular radiation type is determined on the one hand by the initial physical damage and on the other hand by the inherent characteristics of the system. Radiation insult is manifested in the form of highly structured tracks and the microscopic features of these tracks vary considerably, both in distribution and magnitude when energy is deposited in cells (Goodhead, 1989). Low-LET tracks from γ-rays for example are relatively abundant (a dose of 1 Gy corresponds to about 1000 tracks) and cellular targets are thus more uniformly irradiated (Goodhead, 1989).

By contrast, a 1 Gy dose of α-particles corresponds to only about 4 tracks (highly dense ionizations) and the target area (cell) is not uniformly irradiated. These physical characteristics of radiation on a microscopic scale is analogous to dose absorption on a macroscopic scale when the irradiated object is non-uniformly exposed. Variations in the intracellular distribution of micronuclei can thus be expected with a change in ionization density.

Chromosomal aberration data is known to follow a Poisson distribution after exposure to low-LET radiation. For example, Lloyd *et al.* (1984) showed in an extensive study that the dicentric yield in human lymphocytes resulting from ^{60}Co γ-ray irradiations either conform to the Poisson distribution or is slightly under-dispersed (Lloyd *et al.*, 1986). In contrast, intracellular distribution of chromosomal aberrations following high-LET exposure has been shown to be over-dispersed. Examples of this have been reported for lymphocytes irradiated with 2.5 MeV neutrons (Hellin *et al.*, 1990), 14.5 MeV neutrons (Bauchinger *et al.*, 1983), fission neutrons (Bauchinger *et al.*, 1984) and 23 MeV α-particles (Takatsuji and Sasaki, 1984).

The distribution of micronuclei observed in single binucleate cells exposed to photons and neutrons, with and without build-up, are listed in Table 4. Over-dispersion of micronuclear formations is characterized by a ratio of the instrumental variance ($\hat{\sigma}^2$)

to statistical variance ($\bar{y}$) that exceeds unity (Edwards *et al.*, 1979). The ratio $\hat{\sigma}^2/\bar{y}$, known as the dispersion index. $\hat{\sigma}^2$, was calculated as:

$$\hat{\sigma}^2 = \sum_{\ell=1}^{N_i} (k_i - \bar{y})^2/(N_i - 1)$$

where k_i is the number of micronuclei in the ℓ^{th} of N cells and $\bar{y}$ the mean micronuclei frequency for a specific dose group (Huber *et al.*, 1992). To determine if the mean and the variance of the observed distributions were significantly different, the standard unit normal deviate of ($\hat{\sigma}^2/\bar{y}$) (μ-parameter in Table 4) was calculated according to Savage (1970).

$$\mu = d - (N - 1)/\sqrt{2(N - 1)(1 - 1/N\bar{y})}$$

where $d = (N - 1)\hat{\sigma}^2/\bar{y}$ (coefficient of dispersion), and N and $\bar{y}$ are as above.

A positive value of μ indicates an over-dispersion of the measured distribution relative to that of Poisson distributions, whereas a negative value of μ indicates under-dispersion. If the magnitude of μ exceeds 1.96, the over-dispersion is significant at the 95% confidence level. There is only a 5% chance that the magnitude of μ will exceed 1.96 when the underlying distribution is Poissonian.

For irradiations with ^{60}Co γ-rays the dispersion index was found to be close to unity (Table 4) with a mean value for all the dose points of 1.04. About half the distributions were slightly over-dispersed and about half were under-dispersed. The observed distributions deviated from a Poissonian distribution in only three of the nine dose groups studied. It was thus concluded that for photon irradiations, intracellular micronuclear formation conformed to the Poisson distribution. This is in contrast to the systematic over-dispersion of micronuclei noted by Vral *et al.* (1992) in lymphocytes following irradiations with X-rays.

Experimental distributions showed regular over-dispersion with a mean dispersion index of 1.11 following irradiation with p(66)/Be neutrons under conditions of full charged-particle equilibrium. Over-dispersion was significant at the 95% level in four of the six dose points observed. Under-dispersion was noted in only one sample but was not statistically significant.

Table 4: *Intracellular distribution of micronuclei in cytokinesis-blocked lymphocytes following exposure to graded doses of ^{60}Co γ-rays and p(66)/Be neutrons, with and without build-up. The dispersion index ($\hat{\sigma}^2/\bar{y}$) and standard unit normal deviate (μ) are also listed.*

No. of Cells with indicated number of MN								
Dose (cGy)	0	1	2	3	4	5	$\hat{\sigma}^2/\bar{y}$	μ
^{60}Co γ-rays								
0	1971	11					0.99	−0.16
10	1327	22					0.98	−0.41
25	966	39					0.96	−0.85
50	1157	72					0.94	−1.43
100	1885	205	10	1	1		1.17	5.61
150	771	127	13	1	-	1	1.15	3.16
200	611	149	11	1	1		0.99	−0.99
250	1201	278	50	6	1		1.11	3.06
300	665	174	30	4			1.06	1.27
400	415	174	42	7	2		1.08	1.49
p(66)/Be (D_{max})								
5	915	26	1				1.04	0.93
10	788	37					0.96	−0.89
25	433	35	2	1			1.15	2.32
50	507	43	7	1	1		1.39	6.48
100	378	85	17	5	1		1.27	4.20
150	929	307	53	16	1		1.10	2.68
p(66)/Be ($D_{surface}$)								
5	904	26	10				1.39	8.39
10	946	52	8	1			1.24	5.39
25	892	120	32	10			1.38	8.67
50	534	130	28	12	2		1.34	6.33
75	489	169	39	8	2	1	1.20	3.74
100	520	294	80	30	8	4	1.23	4.98

When lymphocytes were irradiated with neutrons in the absence of build-up material, the high-LET character of the heavy recoils and the α-particles was reflected in the comparatively large dispersion index noted in the samples (average 1.30). The μ-parameter was found to be in excess of 1.96 in all the dose groups studied.

Based on the progressive increase in the over-dispersion of the micronuclei yield per cell, from low-LET photon irradiations to high-LET neutrons (D_{max}) to very high-LET heavy charged particles ($D_{surface}$), it was concluded that micronuclear formation in lymphocytes could be correlated with the microscopic features of the various particle tracks.

Micronuclear Formation in Mixed high- and low-LET Radiation Fields

The linear nature of the dose responses for photon and neutron irradiations (with or without build-up) shown in Fig. 6, presents a unique data set for the study of synergistic interaction between high- and low-LET modalities. The interaction function of Zaider and Rossi (1980) excludes any interaction of damage between high- and low-LET radiation when one of the dose-response curves is truely linear. Moreover, the lesion additivity model of Lam (1988) also predicts independent action when both of the dose-response curves are linear.

The apparent absence of a two-track mechanism to induce micronuclei is not expected since it is well known that exchange aberrations follow a linear-quadratic behaviour with dose (Lloyd *et al.*, 1986). The bulk of acentric fragments arise from dicentrics in irradiated G_0 lymphocytes, and micronuclei are derived predominantly from acentric fragments (Vral *et al.*, 1992). It can be argued that synergistic interaction between neutron and photon damage could occur with micronuclei as endpoint, in spite of the fact that the responses for each individual modality does not indicate this.

There is evidence that the induction and repair of sublethal damage can be demonstrated with micronuclei, at least for lymphocytes irradiated with X-rays (Vral *et al.*, 1992). These authors performed split-dose irradiations and observed a continuous decrease in the micronuclei yield with increasing interfraction time.

In order to test whether the induction of reparable damage could be demonstrated with micronuclear formations in cells exposed to neutrons, lymphocytes were exposed to a priming dose of p(66)/Be neutrons followed by photon irradiations.

Table 5: *Mean micronuclei (MN) frequencies observed in cytokinesis-blocked (CB) lymphocytes following exposure to graded doses consisting of 46% p(66)/Be neutrons with build-up and 54% ^{60}Co γ-rays or graded doses consisting of 47% p(66)/Be neutrons without build-up and 53% ^{60}Co γ-rays. Poisson errors are given in brackets. Included in the table is the percentage of binucleate cells (BNC) observed in each culture.*

Dose (cGy)	No. CB cells observed	No. MN	MN per 500 BNC	BNC (%)
p(66)/Be neutrons (D_{max}) plus ^{60}Co γ-rays				
50	878	96	54.7 (5.6)	61
100	1360	338	124.3 (6.8)	58
150	1532	534	174.3 (7.5)	52
200	1734	802	231.3 (8.2)	51
250	1186	600	253.0 (10.3)	35
p(66)/Be neutrons ($D_{surface}$) and ^{60}Co γ-rays				
50	1000	226	113.0 (7.5)	57
100	710	342	240.9 (13.0)	55
150	852	598	350.9 (14.4)	51
200	854	669	391.7 (15.1)	53
250	632	507	401.1 (17.8)	38

The mean micronuclear yields observed in these samples are listed in Table 5. Data from Table 5 are plotted in Fig's 7 and 8. Saturation in the response of micronuclei was noted for the $D_{surface}$ mixed-field irradiations. One explanation for the observed saturation effect is that some samples were over dosed. Based on the measured RBE of 6.2 relative to ^{60}Co γ-rays for lymphocytes exposed to $D_{surface}$ neutrons only, the effective photon dose given to the 250 cGy dose point was calculated to be 8.6 Gy. Similar saturation effects were noted by Krepinsky and Heddle (1983) for lymphocytes irradiated with γ-rays at a dose of 4 Gy and by Pincu *et al.* (1984) at a dose of 6 Gy. Alternatively, the saturation effect can be explained by the lower percentage of cells containing two main nuclei observed for this dose point (Table 5).

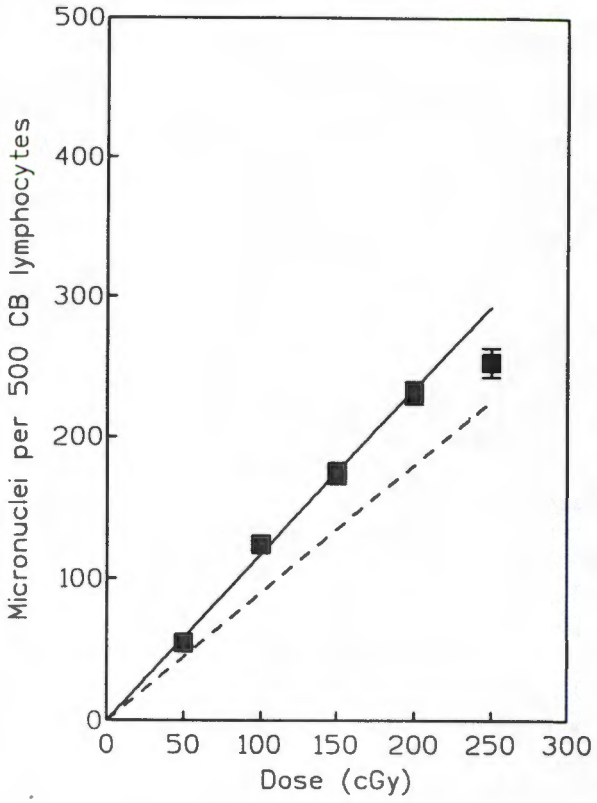

Figure 7: *Micronuclei frequencies observed in cytokinesis-blocked (CB) lymphocytes following exposure at D_{max} to graded doses consisting of 46% p(66)/Be neutrons and 54% ^{60}Co γ-rays (closed squares). The dashed line depicts the expected micronuclear yield if no interaction occurred between the neutron and photon damage.*

The distribution of micronuclei per cell for mixed-field irradiations is listed in Table 6. Over-dispersion was evident for both mixed-field experiments. With the exception of one dose point all the observed distributions deviated significantly from a Poissonian distribution. The mean dispersion indices were 1.22 (D_{max} mixture) and 1.16 ($D_{surface}$ mixture). These values are compatible with a dispersion index that can be expected for the applied radiation mixtures.

Synergistic interaction between lesions produced by a priming dose of D_{max} neutrons and photons as well as $D_{surface}$ neutrons and photons was clearly manifested (Fig's 7 and 8). The slope of the independent prediction for a mixture containing 46% neutrons (D_{max}) and 54% photons is 0.90. By contrast the slope of the micronuclei response observed for this mixture was 1.17 ± 0.05. The slope calculated for an independent prediction of a mixture containing 47% neutrons ($D_{surface}$) followed by photons (53%) is 1.81. The slope of the observed response (linear portion) was 2.35 ± 0.08.

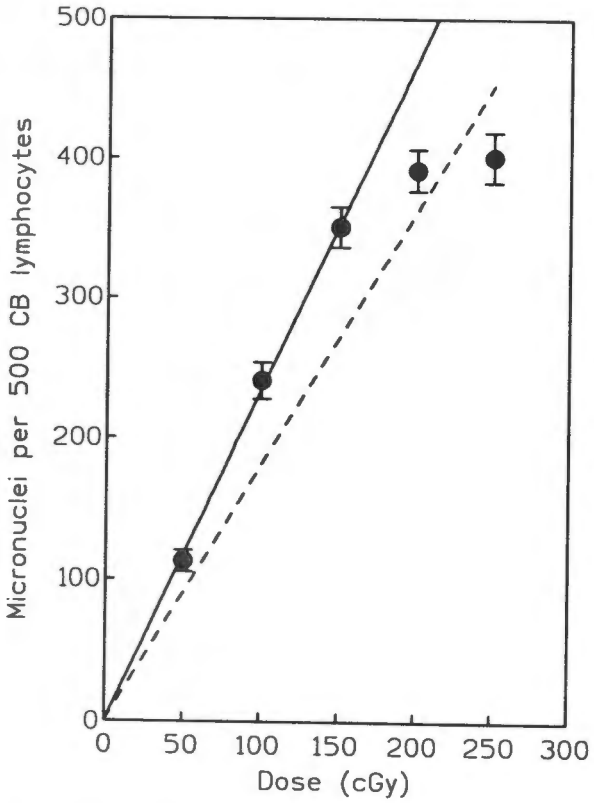

Figure 8: *Micronuclei frequencies observed in cytokinesis-blocked (CB) lymphocytes following exposure at the surface to graded doses consisting of 47% p(66)/Be neutrons and 53% ^{60}Co γ-rays (closed circles). The dashed line depicts the expected micronuclear yield if no interaction occurred between the neutron and photon damage. Poisson errors are indicated by the error bars.*

Although synergy was demonstrated for both mixed-field irradiations, no change in the level of sublethal damage induced by the diverse neutron irradiations (with or without build-up) could be discerned. The ratio of the observed slopes and the ratio of the predicted slopes was 1.3 in both instances.

Conclusion

The above data demonstrated that the physical nature of different radiation qualities is reflected in the MN frequency distribution of cytokinesis-blocked lymphocytes. In addition, the induction of reparable damage was illustrated through synergistic interaction observed between sublesions induced by neutrons and photons. Therefore, should biological dosimetry be based upon the enumeration of micronuclei, absorbed doses will be over-estimated in mixed high- and low-LET radiation fields. To date no interaction function or mixed-field model has been developed to account for the additional yield in micronuclei observed in mixed fields where the dose response to each single modality is linear.

Table 6: *Mean micronuclei (MN) frequencies observed in cytokinesis-blocked (CB) lymphocytes following exposure to graded doses consisting of 46% p(66)/Be neutrons with build-up and 54% ^{60}Co γ-rays or graded doses consisting of 47% p(66)/Be neutrons without build-up and 53% ^{60}Co γ-rays. The dispersion index ($\hat{\sigma}^2/\bar{y}$) and standard unit normal deviate (μ) are also listed.*

No. of Cells with indicated number of MN								
Dose (cGy)	0	1	2	3	4	5	$\hat{\sigma}^2/\bar{y}$	μ
p(66)/Be neutrons (D_{max}) and ^{60}Co γ-rays								
50	798	76	-	-	-	4	1.73	15.20
100	1076	238	40	4	2		1.13	3.42
150	1104	336	80	10	2		1.11	3.02
200	1110	484	110	22	8		1.10	2.85
250	716	366	82	18	4		1.02	0.69
p(66)/Be neutrons ($D_{surface}$) and ^{60}Co γ-rays								
50	822	136	36	6			1.25	5.66
100	460	174	62	12	2		1.16	3.07
150	454	242	122	26	6	2	1.16	3.21
200	406	290	107	41	8	2	1.11	2.25
250	302	202	89	31	6	2	1.13	2.46

SUMMARY

Of vital interest in radiation biology is the manner in which a particular type of ionizing radiation induces lethal and sublethal damage in cells. Of equal importance is the interaction between sublesions and how it affects the final level of biological damage. This study primarily concerns synergistic interaction between biological effects caused by mixtures of high energy neutrons [p(66)/Be and d(16)/Be] and ^{60}Co γ-rays. Findings are made that have bearing on both neutron therapy and the use of biological dosimeters for radiological protection.

Stochastic effects were quantified by means of dose-probability relationships that were obtained using various biological systems (mammalian cells of varying radiosensitivities, meristematic cells) and different endpoints (cells survival, growth delay). Also, non-stochastic effects (chromosome aberrations and micronuclear formation) were measured in human lymphocytes. The inactivation parameters determined from these relationships provided the data to test the validity of proposed biophysical models.

Whilst conventional physical dosimetry techniques were employed throughout to determine the neutron and photon doses in mixed fields, experimental conditions did arise where the molecular yield per unit dose of a ferrous sulphate xylenol orange solution could be usefully correlated with changes in radiation quality.

Survival of mammalian cells in culture were used to examine the influence of a mixture of d(16)/Be neutrons and ^{60}Co γ-rays delivered either simultaneously or sequentially. Different irradiation protocols proved to be inconsequential the final level of biological effect. This is in part expected as the time necessary to deliver a

dose of either neutrons and photons was less than 1/5 that of the characteristic repair time for the cells used ($T_1/_2 \approx 70$ min.) It should be noted however, that the dose rates used in this study is slow compared to the fast component of DNA repair which have a $T_1/_2 \approx$ 3-5 min. (Sakai *et al.*, 1987). Therefore, the true level of synergistic interaction is consistently underestimated by these observations. As a consequence the potential influence of the irradiation protocol on this phenomenon can not be completely ignored. Synergistic interaction was observed in different neutron-photon mixtures but appeared to be most pronounced when the radiation mixture consisted of about one part neutrons and three parts photons. The percentage of cells killed due to synergistic interaction varied with the total dose absorbed and reached a maximum at approximately 5 Gy. It was furthermore noted that enhancement ratios increased with greater radioresistance, indicating that synergistic interaction may constitute therapeutic gain for mixed beam protocols.

A basic assumption of the Theory of Dual Radiation Action (TDRA) is that sublesions are produced at a rate proportional to the specific energy of the radiation. Therefore it could be expected that the level of synergistic interaction between neutron and photon damage would increase as the energy of the particle beam is reduced, i.e. an increase in LET. Enhancement ratios observed were however very similar for the two neutron beams used in this study.

Furthermore, calculations based on inactivation parameters determined from repeated surviving fraction measurements in each beam, indicated that the proportion of cell kill as a result of synergistic interaction, can be expected to increase when the energy of the neutron source is higher. As the intertrack (reparable) damage per unit dose was found to be very similar for the two neutron fields, higher levels of synergy with neutron energy must be ascribed to the noted reduction in the lethal component

of the p(66)/Be beam. In fact it has been suggested that the initial slope of a survival curve is not independent of the repair capacity of a cell (Barendson, 1990). Therefore, if the smaller lethal component associated with the higher energy neutron source is in part due the induction of more reparable damage it might explain the expected increase in synergistic cell kill between p(66)/Be neutrons and photons.

Enhanced synergy between photon damage and that caused by more energetic neutrons can also be rationalized based on the size of the penumbra radii of δ-rays associated with each ionization track. An increase in the energy of the particle in a track result in more energetic electrons, thus a larger volume of the cell nucleus is irradiated with low-LET δ-rays (Belli *et al.*, 1992). Therefore, a greater proportion of reparable damage is induced by the p(66)/Be beam compared to the d(16)/Be beam, leading to more synergistic interaction with ^{60}Co γ-rays.

Sublethal damage induced by p(66)/Be neutrons and ^{60}Co γ-rays were compared using a priming dose of one radiation type followed by test doses of the other. Analysis of the data in terms of the multi-target model indicated that on a per gray basis, neutrons induce as much sublethal damage as photons. However, non-parametric analysis of the data showed that mammalian cells regard a priming dose of neutrons as somewhat less effective than an iso-effective photon dose. Conversely, a priming dose of photons was found to induce a type of radiation damage, that when combined with subsequent doses of neutrons, led to lower levels of survival noted when an iso-effective neutron dose was substituted for the priming photon dose.

With progressively less build-up, sublethal damage induced by a priming dose of p(66)/Be neutrons resulted in greater levels of synergistic interaction when combined

with photons. The level of interaction between different secondary charged particles and ^{60}Co γ-rays is however influenced more by the severity of biological damage than radiation quality. A comparison of interaction factors (ω) at similar levels of combined damage, suggests less synergy when the overall LET of a priming dose is increased. This finding is in agreement with more synergistic cell kill that can be expected when the neutron energy is higher.

Interaction between neutron and photon damage was also followed in meristematic cells because the response of this cell type to the neutron irradiation shows an apparent absence of intertrack damage. The investigations included the quantification of growth delay and micronuclei formations. Synergistic interaction was observed for both endpoints.

Chromosome aberrations in human lymphocytes indicated synergistic interaction between neutron and photon damage. Because the noted effects have implications for biological dosimetry, the formation of micronuclei in binucleate lymphocytes were quantified as a function of radiation quality in mixed n/γ radiation fields. Synergy was again observed, contrary to the predictions of biophysical models. This is not surprising since the induction of a micronucleus in a pure diploid cell constitutes a lethal event (Revell, 1983). Even so, high-LET irradiations (p(66)Be neutrons under full build-up conditions) and very high-LET irradiations (neutrons without build-up) showed similar levels of synergistic interaction with photons. This in spite of the fact that the number of particle tracks per unit dose are very different as defined by the dispersion index of micronuclei observed.

Although the mechanism of synergy is instinctively thought of as a binary interaction between sublesions caused by different radiation types, enhanced effects may be the result of composite interactions generated at critical points in the genome. The exact target for cellular inactivation by ionizing radiation is still obscure but it has been suggested that locally multiply damage sites (LMDS) on both strands in a small region of DNA might constitute an effective lesion (Ward 1985). Monte Carlo simulations based on a stochastic track-structure model suggests that the basic lesion for cellular inactivation is the interaction between two double strand breaks in an encounter radius of about 0.5 nm (Brenner, 1990).

APPENDIX

DETAILS OF METHODS USED IN THE EXPERIMENTAL INVESTIGATIONS

PART A: MATHEMATICAL AND STATISTICAL ANALYSIS OF DOSE RESPONSE DATA

Both stochastic (cell survival) and non-stochastic (micronuclei formation) dose response data generated in this study can be adequately described by a linear-quadratic relationship. As early as 1966 Sinclair found that a linear-quadratic expression gave the best fit to this type of data. However, it is only in the past 12 years that the linear quadratic model has gained favour amongst the numerous models proposed to describe radiation dose-effect data. The linear-quadratic, or α-β model as it has also become known, was first formally proposed by Kellerer and Rossi (1972). The model was derived from their Theory of Dual Radiation Action (TDRA) and considered the stochastic nature of energy depositions in spherical regions (sensitive sites) of μm dimensions. Although it is based on microdosimetric principles, the prediction that can be made that:

$$LOG_e(RBE) = -1/2\ LOG_e\ (Dose\ neutrons), \qquad [1]$$

has proved to be true for a number of biological systems and endpoints (Goodhead 1982). Further experimental justification for the site model was described by Goodhead (1982) and included the inference that the diameters of the sensitive sites were approximately the same for different biological systems (0.2 - 2 μm). The TDRA proposed that radiation injury to cells arose from pairs of sub-lesions and the resulting biological effects depended on the square of the specific energy i.e. the absorbed dose divided by the mass of spherical microscopic tissue regions. The total effect (E) for a given endpoint was related to the macroscopic dose (D) as follows:

$$E = \alpha D + \beta D^2. \qquad [2]$$

From this the fraction of single cells (S) that will survive a dose (D) is

$$S = EXP [(-(\alpha D + \beta D^2)]. \quad [3]$$

A similar equation for cell survival was proposed by Chadwick and Leenhouts (1981).

From a statistical point of view, the analysis of Fertil et al. (1980) showed that the α-β model is preferred for at least five out of six human cell lines tested. More important is that when these authors compared the confidence intervals of various parameters predicted from fitting different models to the same data, only the linear-quadratic model corresponded to the shape of all the dose-survival data, irrespective of which part of the survival curve was under consideration. Unlike the mean lethal dose (D_0) and extrapolation number (n) calculated from multitarget model, the two component models gave a description of the entire survival curve. Moreover, the validity of the α and β parameters has been tested for mammalian cells exposed to high energy neutrons (Fertil et al., 1982) and found to explain neutron action as adequately as when cell kill is accounted for in a photon radiation field.

The confidence ellipses of the fitting parameters for the one hit, two hit, and one-hit multitarget with initial slope models are different for different sections of the survival curve. These sections thus need different pairs of coefficients for suitable description. The linear-quadratic model, however, determine survival fractions within the 95% confidence interval of the experimental data over the entire dose region.

Estimation of the parameters α and β

For n data points, denoted by (D_1,S_1), (D_2,S_2),.....,(D_n,S_n), estimates of α and β can be obtained by means of regression through the origin after linearising the equation by taking natural logarithms on both sides of equation [3] to give

$$\ln(S) = -\alpha D - \beta D^2, \quad [4]$$

for D_i (dose) and $Y_i = \ln(S_i)$.

A possible problem occurs regarding whether the variability of the data about the true survival curve can be assumed to be additive or relative in the model. The data showed that the assumption of relative errors was justified, which thus made the use of linearising the dose-response equation correct in estimating α and β.
The least squares estimate of α and β are

$$\alpha = \left\{(\Sigma D_i^4)\cdot(\Sigma D_i Y_i) - (\Sigma D_i^3)\cdot(\Sigma D_i^2 Y_i)\right\} / \left\{(\Sigma D_i^2)\cdot(\Sigma D_i^4) - (\Sigma D_i^3)^2\right\} \qquad [5]$$

$$\beta = \left\{(\Sigma D_i^2)\cdot(\Sigma D_i^2 Y_i) - (\Sigma D_i^3)\cdot(\Sigma D_i Y_i)\right\} / \left\{(\Sigma D_i^2)\cdot(\Sigma D_i^4) - (\Sigma D_i^3)^2\right\} \qquad [6]$$

The variance of α and β and the covariance between α and β are given by:

$$\text{var}(\alpha) = \sigma^2(\Sigma D_i^4) / \left\{(\Sigma D_i^2)\cdot(\Sigma D_i^4) - (\Sigma D_i^3)^2\right\} \qquad [7]$$

$$\text{var}(\beta) = \sigma^2(\Sigma D_i^2) / \left\{(\Sigma D_i^2)\cdot(\Sigma D_i^4) - (\Sigma D_i^3)^2\right\} \qquad [8]$$

$$\text{covar}(\alpha,\beta) = -\sigma^2(\Sigma D_i^3) / \left\{(\Sigma D_i^2)\cdot(\Sigma D_i^4) - (\Sigma D_i^3)^2\right\} \qquad [9]$$

where σ^2 is the estimate of the error variance obtained from the residual sum of squares (RSS) as RSS/(n-2).

A separate 100 $(1-\delta)$% confidence interval for each of the parameters is then given by

$$\alpha \pm t_{n-2,1-\delta/2}\,\sigma^2\sqrt{\text{var}(\alpha)} \qquad [10]$$

$$\beta \pm t_{n-2,1-\delta/2}\,\sigma^2\sqrt{\text{var}(\beta)} \qquad [11]$$

Here $t_{n-2,1-\delta/2}$ is obtained either from tables of the t distribution, or as $\sqrt{F_{1,n-2,\sigma/2}}$ from tables of the F distribution (Sachs, 1982).

Joint 100 (1-δ)% confidence ellipsoid for α and β

Because the two coefficients α and β are related to each other in the fitting of an experimental set of data, it is necessary to take this relationship into account when the statistical errors of a survival curve are estimated. A joint 100(1-δ)% confidence for α and β can be obtained as

$$(\alpha-\hat{\alpha}\ \ \beta-\hat{\beta}) \begin{bmatrix} \Sigma D_i^2 \Sigma D_i^3 & \alpha-\hat{\alpha} \\ D_i^3 \Sigma D_i^4 & \beta-\hat{\beta} \end{bmatrix} \begin{bmatrix} \alpha-\hat{\alpha} \\ \beta-\hat{\beta} \end{bmatrix} \leq 2\sigma^2 F_{2,n-2,1-\delta} \qquad [12]$$

where $F_{2,n-2,1-\sigma}$ is obtained from tables of the F distribution with 2 and n-2 degrees of freedom, at the 1-σ level of significance. This leads to a confidence ellipse around α and β. The ellipse encloses a surface such that each point on that surface reflects a coordinate pair of α and β values which can be used to describe the shape of the dose-effect curve within the selected level of significance.

The confidence ellipse was obtained using a method described by Sokal and Rohlf (1969). This sophisticated method is not often used in radiobiology, hence it is discussed in detail.

The first step is to find eight strategic coordinates of (α,β) values which lie on the ellipse. These eight points are determined from $\lambda\alpha$ and $\lambda\beta$, that is, the characteristic roots (eigenvalues) and the slopes of the major and minor axes of the ellipse. The eigenvalues are measures of the variability along the major and minor axes of the ellipse. They were obtained as follows:

$$\text{LET L} = \sqrt{(\text{var}(\alpha) + \text{var}(\beta))^2 - 4(\text{var}(\alpha)\cdot\text{var}(\beta)-(\text{cov}(\alpha,\beta))^2} \qquad [13]$$

$$\text{then} \quad \lambda_\alpha = \frac{\text{var}(\alpha) + \text{var}(\beta) + \text{L}}{2} \qquad [14]$$

$$\text{and} \quad \lambda_\beta = \frac{\text{var}(\alpha) + \text{var}(\beta) - \text{L}}{2}. \qquad [15]$$

The slope of the principle axis is:

$$b_1 = \frac{\text{cov}\ (\alpha,\beta)}{\lambda_\alpha - \text{var}(\alpha)} \qquad [16]$$

and that of the minor axis is given by

$$b_2 = \frac{1}{b_1} \qquad [17]$$

The eight points describing a particular confidence region are computed as follows:

$$\text{LET } C_{1-\sigma} = \frac{\lambda_\alpha \lambda_\beta (n-1)^2}{(n-2)} F_{2,n-2,1-\delta} \qquad [18]$$

(1) $\alpha_1 = \alpha + \sqrt{\dfrac{c_{1-\sigma}}{\text{var}(\beta)}}$, $\beta_1 = \beta$

(2) $\alpha_2 = \alpha - \sqrt{\dfrac{c_{1-\sigma}}{\text{var}(\beta)}}$, $\beta_2 = \beta$

(3) $\alpha_3 = \alpha$, $\beta_3 = \beta + \sqrt{\dfrac{c_{1-\sigma}}{\text{var}(\beta)}}$

(4) $\alpha_4 = \alpha$, $\beta_4 = \beta - \sqrt{\dfrac{c_{1-\sigma}}{\text{var}(\beta)}}$

(5) $\alpha_5 = \alpha + \beta_1 \sqrt{\dfrac{c_{1-\sigma}}{\lambda_\beta(1+b_1^2)}}$, $\beta_5 = \beta + \sqrt{\dfrac{c_{1-\sigma}}{\lambda_\beta(1+b_1^2)}}$

$$(6)\quad \alpha_6 = \alpha - b_1\sqrt{\frac{c_{1-\sigma}}{\lambda_\beta(1+b_1^2)}}\ ,\quad \beta_6 = \beta - \sqrt{\frac{c_{1-\sigma}}{\lambda_\beta(1+b_1^2)}}$$

$$(7)\quad \alpha_7 = \alpha + b_2\sqrt{\frac{c_{1-\sigma}}{\lambda_\beta(1+b_2^2)}}\ ,\quad \beta_7 = \beta + \sqrt{\frac{c_{1-\sigma}}{\lambda_\alpha(1+b_2^2)}}$$

$$(8)\quad \alpha_8 = \alpha - b_2 - \sqrt{\frac{c_{1-\sigma}}{\lambda_\beta(1+b_2^2)}}\ ,\quad \beta_8 = \beta - \sqrt{\frac{c_{1-\sigma}}{\lambda_\alpha(1+b_2^2)}}$$

To draw the complete ellipse, the above coordinates were used in a series of linear equations to solve for the five unknowns in a general equation describing a cone. The general equation used was

$$A\,\beta_j^2 + B\,\alpha_j\beta_j + C\,\alpha_j^2 + D\,\beta_j + E\,\alpha_j + 1 = 0 \qquad [19]$$

for $\beta_6 \le j \le \beta_5$.

The five unknowns (A, B, C, D and E) are read from the solution matrix determined by Gaussian elimination. This general equation (equation 19) can be rewritten in the form of a simple quadratic expression.

Let $$F = B\,\alpha_j\cdot\beta_j + E \qquad [20]$$

and $$G = 1 + D\,\beta_j + A\,\beta_j^2 \qquad [21]$$

then $$C\,\alpha_j^2 + F\,\alpha_j + G = 0 \qquad [22]$$

The complete ellipse is then drawn in two parts, an upper half and a lower half. For each selected value of β between a minimum given by β_6 and a maximum given by β_5, there are two solutions for α. The upper half is given by

$$-F + \frac{\sqrt{F^2 - 4GC}}{2C} \qquad [23]$$

and the lower half is given by

$$-F-\frac{\sqrt{F^2-4GC}}{2C} \qquad [24]$$

The Mean Inactivation Dose ($\bar{D}$)

Although the parameters α and β are frequently used to characterise cell radiosensitivity, it is sometimes preferred to specify the overall dose response of a cell type by a single parameter (Fertil et al., 1982; Malaise et al., 1987; Deschavanna et al., 1990). For comparative purposes this parameter should represent a measure of the radiosensitivity of the cell population. It should also keep the scatter of the data small and be readily computed from survival curves. $\bar{D}$, as recommended by the ICRU Report 30 (1979), is such a parameter and has been shown to represent the radiosensitivities of different cell lines (Malaise et al., 1987).

In terms of the linear-quadratic model, the mean inactivation dose is given by

$$\bar{D} = -\int_0^{\infty} D \cdot \frac{d(S(D))}{dD} \cdot dD \qquad [25]$$

$$= \int_0^{\infty} e^{-\alpha D-\beta D^2} \cdot dD. \qquad [26]$$

There are several different cases to be considered for the explicit evaluation of $\bar{D}$, depending on whether α and β are negative, zero or positive.

If $\beta < 0$ there is no solution for this integral.

If $\beta = 0$ and $\alpha = 0$, $\bar{D} = \infty$ [27]

If $\beta = 0$ and $\alpha \neq 0$, $\bar{D} = 1/\alpha$. [28]

This is the same as D_0, the mean lethal dose.

If $\beta > 0$ and $\alpha = 0$, $\bar{D} = \frac{1}{2}\sqrt{\frac{\pi}{\beta}}$ [29]

If $\beta > 0$ and $\alpha \neq 0$, then $\bar{D} = \sqrt{\frac{\pi}{2}} \cdot e^{\alpha^2/4\beta} \cdot \left[1 - \Phi\left(\alpha / \sqrt{2\beta}\right)\right]$ [30]

Let $x = \alpha / \sqrt{2\beta}$. Then the term $\Phi(x)$ can be approximated to within 0.000025 as follows:

For $\alpha > 0$,

$$\Phi(x) = 1 - \frac{1}{2}(a_1 t + a_2 t^2 + a_3 t^3) \cdot e^{-x^2/2} \quad [31]$$

where $t = 1 / (1 + 0.47047 / \sqrt{2})$ [32]

Then $a_1 = 0.3480242$ [33]

$a_2 = 0.0958798$ [34]

$a_3 = 0.7478556$ [35]

For $\alpha < 0$,

$$\Phi(x) = \frac{1}{2} \cdot (a_1 s + a_2 s^2 + a_3 s^3)\, e^{-x^2/2} \quad [36]$$

where α_1, α_2 and α_3 are as above, and

$s = 1 / \left[1 - 0.47047 / \sqrt{2}\right]$ [37]

$\text{var}(D) = n\left\{g_1^2 \text{var}(\alpha) - g_1 g_2 \text{cov}(\alpha,\beta) + g_2^2 \text{var}(\beta)\right\}$ [38]

PART B: CULTURE OF MAMMALIAN CELLS

Four mammalian cell types were used in the experimental work. These were Chinese hamster fibroblasts (V-79 379A), *Chinese hamster ovary (CHO-K1), murine 3T3 and* B16 melanoma cells. Although the tissue culture procedures were in many ways the same for the different cell lines, there were minor differences in cell handling between the different cell types. These are detailed in the relevant sections. Most experimental data were generated using the V-79 cell line, thus a detailed description of pertinent tissue culture techniques for this cell type is given.

The aim of the culture program was to supply throughout the course of experimentation, cells that would be as far as possible uniformly sensitive to ionizing radiation. To meet this demand on uniformity, cells from only up to 10 passages of subculturing were used in the experiments.

Chinese hamster fibroblasts (V-79 379A)

Source and Storage

The V-79 379A cell line was obtained from the CRC Gray Laboratories, Middlesex, England. At the time the cells were received they were labelled as passage 8. From this stock subcultures were prepared (as described below) and stored in liquid nitrogen.

Routine Subculture

The fibroblasts were cultivated as monolayers in rectangular 25 cm^2 polystyrene tissue culture flasks (Nunc). The growth medium was Eagle's Minimum Essential Medium (MEM) (Gibco) supplemented with Earle's salts, L-glutamine, sodium bicarbonate (2.2 g/litre), penicillin (Crystapen 0.06 g/litre) and streptomycin (Novastrep 0.1 g/litre). Foetal calf serum (FCS) (Highveld Biological) was added to obtain complete growth medium [10% in FCS (v/v)].

Incubation took place at 37° C in a water jacketed incubator (Forma Scientific). During incubation periods the caps of the growth flasks were loosened to allow venting. The incubator was equipped with a humidity reservoir and electronically controlled

gas-processors to maintain a mixture of 5% CO_2 in air throughout the chamber. The incubator was free standing on a laboratory bench to eliminate any vibrations.

Trypsinization

The so called "dry" trypsinization method was followed. Cell monolayers which were near-confluent were detached from the growth surface using a 1:1 mixture of trypsin (0.25% in phosphate buffered saline (PBS)) and EDTA (0.1% in PBS). After decanting the growth medium, the cell surface was rinsed twice with approximately 3 ml of trypsin mixture previously heated to 37° C. Following the second rinse, the cells were left almost dry with only a thin film of trypsin covering them. The flask was then capped and incubated for three to four minutes after which it was firmly tapped against the palm of the hand to loosen the cells from the growth surface. 10 ml of complete medium was immediately added and the suspension vigorously pipetted up and down using a 10 ml pipette to ensure the formation of single cells. An estimate of the cell concentration was then made using a bright lined haemacytometer (Neubauer). Approximately 2×10^5 cells were transferred in duplicate from the suspension to 25 cm^2 tissue culture flasks. Growth medium was added to obtian a final volume of 5 ml in each flask. In addition, 4 ml of the cell suspension was "back seeded" into the original flask to act as a backup in case of contamination.

The cells were subcultured three times a week, on Mondays, Wednesdays and Fridays, with each split representing the end of a passage. On Mondays and Wednesdays 2×10^5 cells were plated into 25 cm^2 tissue culture flasks. To prevent overgrowing over weekends, only 1×10^5 cells were plated on Fridays.

Subculture for Experimental Work

Two days before scheduled irradiations, cells were subcultured in much the same way as that for the maintenance of the line, although stricter control over cell numbers was exercised. Growth curve measurements showed that the doubling time for the fibroblasts was about 10.5 hours. Therefore 2 days after seeding the cells, the culture had progressed through four to five doublings. The fibroblasts would thus be out of there initial lag phase and in a state of exponential growth on the day of irradiation.

The status of the cells was always confirmed by a microscopic examination of the monolayers which showed some of the cells progressing through mitosis, i.e. rounded and loosely attached to the surface. Although the cells covered most of the growth surface at this time, there were still some open spaces. The average cell density was approximately $1.5 \times 10^5/cm^2$.

Hereafter the cells were trypsinized and suspended in 10 ml complete medium. Thus usually yielded between 3×10^5 and 4×10^5 cells per ml. An important criterion at this stage was that of cell singularity. If cell clusters were observed in the suspension then the preparation was either disregarded, in which case the trypsinization procedure was repeated using one of the backup flasks, or the suspension was put through a 20 gauge needle using a 10 ml disposable syringe.

Irradiation of Cell Suspensions in a Horizontal Radiation Field

Suspensions prepared as above were transferred to a flat bottomed 25 ml glass vessel for irradiation. The glass vessel was equipped with ground glass stopper and two gas ports for the manipulation of physiological conditions. This included the flushing of cell suspensions with either 5% CO_2 in air or 5% CO_2 in ultra pure nitrogen. Before and during irradiations the cell suspensions were gassed and also gently stirred using a Teflon coated magnetic stirring bar. The stirring was set to a slow speed (100 rpm) with intermittent reversing periods. Measurements showed that this stirring action did not affect the plating efficiency in any way. Unless otherwise stated, all horizontal irradiations were performed using this technique.

Following irradiation, 1.5 ml aliquotes of cell suspensions were drawn from the gas exit port using a 2 ml syringe fitted with a 19 gauge needle. The samples were then divided into two for repeated counting in the haemacytometer and for appropriate dilution, depending on the magnitude of the radiation dose received. Dilution routes were followed that would assure the formation of about 200 colonies irrespective of the dose received.

Seeding of Irradiated Cells

Before the start of each experimental run 3 ml of complete medium was added to 60 mm diameter Petri dishes for cell culture (Nunclon). The dishes were kept in the incubator

at 37° C and removed before the seeding of cells from the final dilution. The cells were seeded into warm medium, the pH of which had already reached equilibrium. The final volume was 3.5 to 4 ml. Three or four replicates from the final dilution were seeded for each dose point. The cells were then incubated at 37° C in a 5% CO_2 environment for six days.

Colony Staining and Counting

At the end of the incubation period colonies were stained for counting as follows. First the growth medium was decanted and the dishes rinsed with 3 ml of phosphate buffered saline. The colonies were then fixed for 20 minutes using a mixture of 20% acetic acid, 20% methanol and 60% distilled water. The fixative mixture was replaced with 0.01% Amido Black 10 B which was made up in methanol, acetic acid and water in the ratio 1:1:3 (v/v). The colonies were exposed to this mixture for 30 minutes, after which the dishes were rinsed once with 3 ml fixative. They were then over-turned for drying. Colonies constituting more then 50 cells were counted.

Irradiation of Cells in a Vertical Beam

When a vertical radiation field was available it was preferable to seed the cells into the Petri dishes before irradiation. This allowed one to deal only with unirradiated cells during the dilution steps. Furthermore, this approach allowed for the seeding of appropriate cell numbers following a single dilution route for all dose points. Not only did this reduce the amount of work involved, but the single dilution route technique also produced survival curves of higher precision because the method was less prone to pipetting errors. Where appropriate, cells were seeded not more than one hour before irradiations so that they were still in a state of suspension, although they had by then settled to the bottom of the dish. This approach was also used in the characterization and periodic checking of cell radiosensitivity.

Chinese Hamster Ovary (CHO-K1) cells

The CHO-K1 cell line was obtained from the Department of Microbiology, MEDUNSA, Pretoria. The cells were labelled as passage 6. Subcultures were prepared in the same manner as described for the V-79 cells and stored in liquid nitrogen. For routine maintenance the cells were cultured in Ham's F-12 medium supplemented with 10%

foetal calf serum. The cells were maintained by subculture 3 times a week, 1/5 of a near confluent monolayer was transferred each time. Thereafter, the cells were prepared for irradiation using the same procedure as adopted for the V-79 cells.

Murine (3T3) Fibroblasts

The 3T3 cell line was obtained from Highveld Biological (Johannesburg). The cells were labelled arbitrary as passage 1. Subcultures were prepared in the same manner as for V-79 cells and stored in liquid nitrogen. For routine maintenance cells were cultured in MEM supplemented with 10% foetal calf serum. Subculturing was as for CHO-K1 cells. Cells were prepared for irradiation using the same procedure as adopted for V-79 cells. Ten days were allowed for colony formation.

Murine (B16) Melanoma

These cells were obtained from the Radiotherapy Department of the University of Cape Town. They were routinely cultured in MEM supplemented with 10% foetal calf serum. The cells were maintained by subculturing as for CHO-K1 cells. Cells were prepared for irradiation using the same procedure adopted for the V-79 cells. Twelve days were allowed for colony formation.

Freezing and Storage of Cells

The same procedure was followed for all the cell lines used in the laboratory. A monolayer of cells was grown to sub-confluence in a 25 cm^2 tissue culture flask. The cells from this stock culture were then trypsinized and resuspended in 10 ml complete growth medium. From the suspension aliquots were seeded into 25 cm^2 flasks, growth medium added and cells allowed to propagate until they covered the growth area. These monolayers were then detached from the growth surface using trypsin-EDTA, resuspended in 10 ml complete medium and centrifuged in sterile test tubes for 5 minutes at 1000 rpm. The medium was then decanted and the cell pellet resuspended in 1.8 ml complete medium. To this cell suspension was added, 0.2 ml dimethyl sulphoxide (DMSO - Merck). Thereafter, the suspensions well mixed and placed in 2 ml cryotubes (Nunc).

The samples were allowed to cool at a rate of approximately 1° C per minute by placing

the cryotubes in a polystyrene box which was placed in the laboratory freezer. Here the cells reached a minimum temperature of -20° C. The cryotubes were then wrapped in paper towelling and suspended in the gas phase of the liquid nitrogen container. The following day the cryotubes were clipped into canes and stored in the liquid nitrogen.

Thawing of Cells

A cryotube was removed from the liquid nitrogen and placed immediately into a 37° C water bath. As soon as the suspension had thawed, it was mixed with 8 ml of complete medium, centrifuged for 5 minutes at 1000 rpm and the supernatant discarded. The cell pellet was resuspended in 6 ml complete medium and seeded in a growth flask. The next day the cells had attached to the growth surface and in most instances filled the growth area so that subculturing was required.

MERISTEMATIC CELLS

Another cell type used in the investigations was meristematic cells in the root tip of seedlings from the broad bean *Vicia faba* (Fiord variety). The beans were obtained from the Department of Agriculture's Research Institute for Winter Rainfall Region at Stellenbosch. In this test system both the inhibition of root growth and the induction of micronuclei were followed. The method of culture was in general the same as that described by Marshall (1982).

***Vicia faba* Culture**

About 3 times the number of beans that were finally needed for the experiment were soaked in a tray filled with filtered tap water. A steady flow of water of about 1 litre/min was maintained for 2 days. During this time the beans swelled under osmotic pressure and the root-tips started to break through the outer skin. The beans were then planted in moist Vermiculite at a depth of 1 cm. After a growth period of 3 days the beans were taken out of the Vermiculite and rinsed in fresh water. The length of each primary root was measured from the cotyledon to the tip. The testa and plumule were removed and seedlings that were damaged or shorter than 20 mm were discarded. A minimum length of 20 mm was necessary for the roots to reach the water level in the culture-tank. The latter was a water filled glass tank equipped with a thermostatically controlled heater and a water pump running at 14 litre/min. The water

temperature was maintained at 19° C ± 0.5. In addition, the water was continuously aerated using a diaphragm pump.

The beans were suspended over the water such that the roots were submerged but the cotyledons remained dry. This was accomplished by using 3 mm thick Perspex plates perforated with holes through which the roots could pass. The holes formed a grid pattern which allowed each hole to be labelled with a set of coordinates representing the number and the row. In this manner each root was assigned an identification number and could easily be tracked in the culture-tank.

Root Selection

After 3 days the beans were measured for the second time in order to determine the growth rate during this initial test period. The germination and subsequent growth of seedlings was always planned so that the end of the test growth period coincided with the day of irradiation. Because a large quantity of root-tips (up to 1000) was involved in certain experiments, a program was developed on a Hewlett-Packard series 85 computer to facilitate the handling of data. Length measurements were directly entered into a memory matrix, the coordinates of which corresponded to that of the grid on the tank. The data was then stored on a disk file.

At the end of the second set of measurements an algorithm calculated the mean and standard deviation of firstly the growth rate during the first 3 days and secondly the total lengths at the end of this test period. Only those beans that were within one standard deviation of the mean of both these populations were selected for irradiation. The selected seedlings were then ranked in an array progressing from short to long.

Sub-groups of beans were selected from the above population as follows. An array of beans were randomly sub-divided according to the number of dose points to be used in the construction of a particular dose-effect relationship. These sub-populations were again sub-divided at random according to the number of arms in the experiment. In each of these groups there was thus a number of beans that were to be used to determined a specific radiation effect for a specific dose. A minimum of 10 beans was considered essential for each dose point. By virtue of the ranking procedure, the 10 beans in each of the dose groups were essentially of equal length and rarely differed by more than 2 mm.

Irradiation of *Vicia faba* Roots

In order to irradiate the root tips, the seedlings were taken from the grid and placed sequentially into specially constructed Perspex jigs (Fig. 1). To facilitate the loading of these jigs, the computer program provided a printout listing the grid coordinates or each bean in each group.

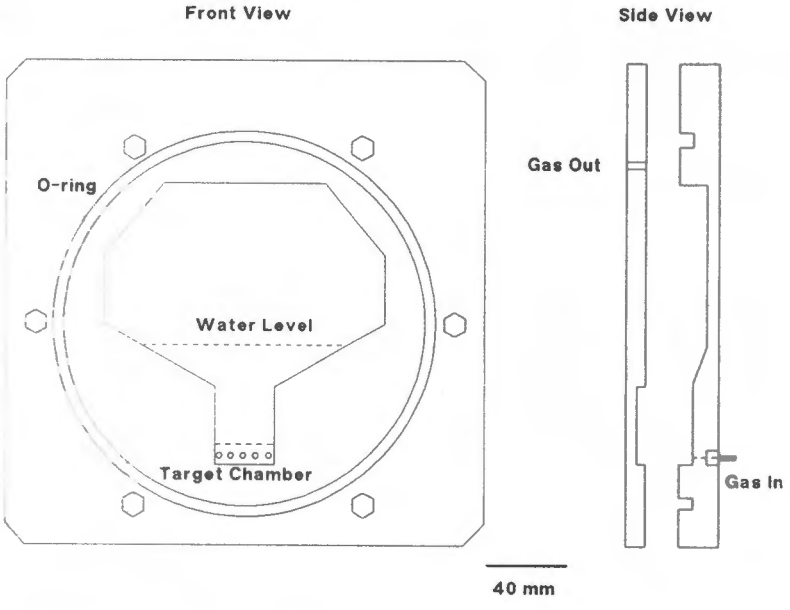

Figure 1: Perspex jig used to irradiate *Vicia faba* seedlings.

The design of the jig was such that the roots remained wet throughout the duration of the irradiation. Not only were the chambers water-tight but the large O-rings sealed the interior from the atmosphere. The nipple at the back was used to pass gas through the chamber, the type of gas being determined by the physiological condition required. For irradiations under aerobic conditions, air bubbling at a flow rate of 2 litre/min was maintained before and during irradiations using a diaphragm pump. Meristematic cells in the root tips were made hypoxic by gassing the water in the chambers with ultra high-purity nitrogen (Afrox) at 2 litres/min for at least 30 minutes before and during irradiations. Each cylinder of ultra high-purity nitrogen was tested and certified by the supplier and never contained more than 8 ppm oxygen.

At the end of the irradiation the beans were removed from the jigs in the same sequences as they were packed, and returned to the growth-tank. Depending on the specific endpoint under investigation, the beans were then allowed to grow for various time intervals. Any side roots that formed were removed during daily inspection. In

the growth delay studies the root lengths were measured after 10 days and the relative growth over this period calculated by normalizing each measurement to the mean length of the controls. For the micronuclei assay 3 different periods of growth were observed, as detailed in the next section.

Micronuclei Assay

Since the formation of micronuclei is a time dependent process which is further complicated by mitotic delay as a result of radiation, it was necessary to fix the root-tips at various time intervals after irradiation (Evans *et al.*, 1959). Twenty four, 36 and 48 hours after irradiation of the seedlings the terminal 3 cm of the root-tips were cut off and fixed in a 1:3 (v/v) mixture of acetic acid and ethyl alcohol. The tubes containing the root-tips were marked with information on dose, radiation quality and fixation time. The root-tips were left in the fixative for 3 hours after which the solution was replaced with 70% ethyl alcohol. To minimize breakage, it was found preferable to remove the solutions using a Pasteur pipette connected to a vacuum pump. Because it was not possible to process all the tips within the following few weeks, the 70% alcohol was replaced with a preservative which consisted of:

1. 70% ethyl alcohol (2 parts).
2. Acetic acid (concentrated, 1 part).
3. 50% glycerol in ethyl alcohol (1 part).

The tissue remained stable in this solution for several months (Marshall, 1982).

Preparation of Permanent Slides of Meristematic Cells

Initially the cells were stained to highlight the nuclear material. Using a water bath, the root-tips were hydrolized in 1 M HCl at 60° C for 12 minutes. The time was important and hydrolysis of the different samples was staggered in order not to deviate from this period by more than 2 minutes. The acid was then promptly sucked from the sample tubes and replaced with a stain mixture prepared as follows:

1. 0.5 g basic fuchsin (PAL Chemicals).
2. 100 ml distilled water.

3. 10.5 g potassium disulfite (Merck).
4. 15 ml 1 M hydrochloric acid (Merck).

Using the above solution, good staining of both nuclei and micronuclei was obtained, provided that the cells were exposed to the stain no longer than 2 hours. Further staining tended to spill into the cytoplasm. The meristematic region was easily recognizable after the staining procedure thus facilitating dissection.

Permanent slides were made from the terminal 1.5 mm portion of the root-tip (excluding the root cap). The meristem region was macerated and squashed, one per slide, and covered with a pre-treated cover slip. This pre-treatment consisted of coating the cover slip with a very thin layer of a albumin-glycerin sodium salicylate mixture, followed by heating over a flame. The cover slip was pressed onto the slide. Thereafter the microscope slide and attached cover slip were placed in a 15% acetic acid solution. In the solution the cover slip was allowed to detached from the slide.

Dehydration took place by exposing the cover slips for 1 minute to each of the following solutions in the stated sequence:

70% ethanol, 80% ethanol, 90% ethanol, 96% ethanol, absolute ethanol, 50% xylene/50% ethanol and 100% xylene.

The cover slips were mounted on top of a clean microscope slide using Entellan (Merck).

From each slide at least 2000 cells were scored for the presence of micronuclei using a Zeiss microscope, model IM 35. The settings used were for bright field illumination and with 400x magnification.

LYMPHOCYTE CULTURES FOR CHROMOSOME ANALYSIS

Blood samples were prepared for chromosome analysis using a microculture method which was in general in accordance to that proposed by the IAEA (1986). The specific details of the method used here is that employed routinely at the Department of Human Genetics, University of the Orange Free State.

Lymphocyte cultures were setup in duplicate for each sample in a 50 ml universal specimen container. Each culture consisted of:

1. 8 ml Ham's F-10 medium (Highveld Biological), supplemented with penicillin (Crystapen 0.06 g/litre) and streptomycin (Novastrep 0.1 g/litre).
2. 1 ml Foetal calf serum.
3. 0.4 ml Whole blood.
4. 0.5 ml Phytohaemagglutinin (PHA-M Form, Gibco).
5. 0.1 ml Bromodeoxyuridine (BrdU, Boehringer Manhiem), from a stock solution consisting of 0.04 g BrdU dissolved in 50 ml saline.

The cells were incubated at 37° C for 47 hours, then colcemid was added to a final concentration of 3 μg/ml. The cells were arrested in mitosis by incubating the cultures for an additional 3 hours at 37° C.

Cell Harvest

Lymphocytes were harvested from the cultures by strictly following these procedures:

1. Cultures were centrifuged for 10 minutes at 1000 rpm (190 g).
2. All but 1 ml of the supernatant was removed by suction.
3. Using a vortex mixture, the cells were resuspended in 5 ml KCl (0.075 M), pre-warmed to 37° C and left in the incubator for 14 minutes.
4. Repetition of steps 1 and 2.
5. The cells were resuspended in 5 ml cold (-20° C) fixative (methanol:acetic acid, 3:1).
6. Repetition of steps 1 and 2.
7. Repetition of step 5, but with a fixative consisting of 6 parts methanol and 1 part acetic acid.
8. Cell suspensions were left in the laboratory refrigerator overnight. The next day the suspensions were centrifuged as in step 1 and all but 0.5 ml of the fixative removed.
9. The cell button was resuspended in the remaining fluid.
10. Using a Pasteur pipette, droplets of cell suspensions were dropped onto a microscope slide from a height of about 20 cm. The metaphase spreads were left to dry on the laboratory bench.

Chromosome Staining

Chromosomes were stained for fluorescence microscopy using acridine orange. A stock solution was prepared by dissolving 0.1 acridine orange (BDH) in 100 ml distilled water. The working staining solution consisted of 1 ml stock solution diluted in 50 ml phosphate buffer (pH 6.8). Slide preparations were left in this solution for 20 minutes, the excess stain removed and then eestained for 10 minutes in phosphate buffer. About 3 drops of buffer were dripped onto a slide and a coverslip mounted. The sides of the coverslip were sealed using Entellan (Merck).

Preparation of Cytokinesis-Blocked Lymphocytes

Samples were prepared for culture by first separating the lymphocyte population from the other blood elements.

Lymphocyte Separation

Whole blood samples (5-7 ml) were centrifuged for 10 minutes at 1000 rpm and the serum removed so that only about 1 cm of serum remained above the cell component. The cells were diluted (approximately 1:1) with phosphate buffered saline (PBS) and layered on 3 ml Histopaque (Sigma). The layers were then centrifuged for 30 minutes at 1000 rpm. Following centrifugation, the white ring of lymphocytes was clearly visible. The supernatant was removed so that about 1 cm remained above the cloud of lymphocytes. Using a Pasteur pipette, the lymphocytes were selectively transferred to a clean centrifuge tube, diluted with an equal volume of PBS and centrifuged for 10 minutes at 1000 rpm. The supernatant was discarded and the button of cells resuspended in 10 ml growth medium (RPMI-1640).

Cell Culture

The growth medium was supplemented with penicillin (0.1 mg/l), streptomycin (0.1 mg/l) and 15% heat inactivated foetal calf serum. The isolated lymphocytes were stimulated to divide using 100 μl PHA and incubated at 37° C in an upright 25 cm^2 an upright growth flask. Following 44 hours of incubation, cytochalasin B was added to yield a final concentration of 3 μg/ml. The cultures were then incubated for an additional 28 hours.

Cell Harvest

Cell suspensions were centrifuged at 700 rpm (100 G) for 5 minutes. All but 0.5 ml of the supernatant was removed and the lymphocytes resuspended in the remaining medium using a vortex mixture. About 20 drops of the cell concentrate were spaced on a microscope slide which was then centrifuged for 7 minutes at 700 rpm. Because a cytospin was not available, the slides were placed on filter paper at the bottom of the centrifuge bucket (Heraeus Christ, Digifuge model). The slides were left to dry on the laboratory bench, then the lymphocytes fixed by flooding the slides with methanol:acetic acid (3:1).

Nuclear Staining

Lymphocytes were stained for fluorescence microscopy in a working solution of acridine orange that consisted of 0.5 ml stock solution diluted in 50 ml phosphate buffer (pH 6.8). Slide preparations were left in this solution for 3 minutes, washed in distilled water and then destained for 2 minutes in phosphate buffer. A coverslip was mounted on a thin layer of phosphate buffer and the sides of the coverslip were sealed using Entellan (Merck).

Fluorescence Microscopy

Fluorescence microscopy was performed using a Zeiss microscope, model IM 35. The microscope was fitted with blue epi-fluorescence, exciter filter 450-490 nm and barrier filter 520 nm. All observations were made using a 100x objective (oil) giving a final magnification of 1000x.

WATER PREPARATION FOR USE WITH THE FBX DOSIMETER

Tap water feeding a still was pre-filtered through a sponge. Following a single distillation the water was stored in a clean plastic container. Once cooled, the water was fed through a series of filters and de-ionizers (Milli-Q water system - Millipore). This consisted of a carbon cartridge, 2 ion exchangers, an Organex-Q cartridge and finally a Milli-Stak filter. The water was continuously run through these filters until the conductivity meter read 10^{-18} ohm. Both the carbon filter and the Organex-Q cartridge ensured the removal of organic impurities.

Even with the most stringent quality control for water purification, contamination can still occur unless all glassware is cleaned with equal care. The glassware used in the preparation and storage of the dosimeter was soaked overnight in a dichromate - sulphuric acid solution, followed by rinsing several times with purified water. Extreme care was exercised to avoid contamination of the FBX solution during preparation, storage and handling.

Preparation of Standard FBX Solutions

Primary Fe^{3+} concentrations were prepared by diluting a commercial iron standard (Eisen-Standardlosüng, Titrisol, Merck). This was an ampoule containing 1.000 ± 0.002 g of iron as $FeCl_3$ in diluted hydrochloric acid. At least 5 liters of a diluting solution was needed for the procedure. The diluting solution was prepared using the same constituents required for the FBX dosimeter but without the ferrous ammonium sulphate. Because it was convenient to work with two-liter volumetric flasks, the following amounts of chemicals were disolved to make up this volume:

1.	H_2SO_4 (98% Merck AR)	2.72 ml.
2.	C_6H_6.COOH (BDH Analar)	1.2212 g.
3.	Xylenol orange (Merck)	0.3042 g.

The sulphuric acid was added to about 1 litre of water. The benzoic acid was then added and the mixture heated to ~ 60° C on a hotplate and maintained at this temperature for approximately 15 minutes. Heating was necessary because the benzoic acid has a low solubility in water. After the benzoic acid was dissolved, the solution was cooled by running tap water onto the side of the flask. Thereafter the xylenol orange was added and the volumetric flask filled to the mark with more de-ionized water.

The membrane of the ampoule containing the standard iron solution was pierced with a glass rod and the contents emptied into a 1 litre volumetric flask. The rod and ampoule were rinsed with the diluted solution and the flask filled to the mark. The concentration of Fe^{3+} was then 1.79×10^{-2} N. Of this solution, 40 ml was buretted and then diluted to 1 litre. From this, aliquots of 1, 2, ... 10 ml were extracted with a 10 ml burette and each standard further diluted to 250 ml. The solutions with the reference solution (diluting medium), were allowed to stand for 1 hour in a waterbath at 25° C before absorbance measurements were performed.

Preparation of the Fricke Dosimeter

Two litres of the dosimeter were prrepared at a time. The following constituents were dissolved in de-ionized water and diluted to the mark in a volumetric flask.

1.	H_2SO_4 (98 %)	44 ml
2.	$(NH_4)_2Fe(SO_4)_2.6H_2O$	0.7843 g
3.	NaCl	0.1169 g

After irradiation the solutions were allowed at least 5 minutes to stabilize before absorbance measurements were performed at 304 nm. A molar extinction coefficient of 2066 ± 20 l mol^{-1} cm^{-1} was determined for the Fricke solution. Dose measurements in a ^{60}Co field were based on a G-value of 15.4 (Attix, 1986).

REFERENCES

Aberchrombie M., Hickman C.J. and Johnson M.L. (1973). A Dictionary of Biology. Penguin Books.

Ager D.D. and Haynes R.H. (1987). Mathematical description of the interaction between cellular inactivating agents. Radiat. Res. 110, 129 – 141.

Almassy Z., Krepinsky A.B., Bianco A. and Köteles G.J. (1987). The present state and perspectives of micronucleus assay in radiation protection. A review. Int. J. Appl. Radiat. Isot. 38, 241 – 249.

Ando K., Koike S., Fukuda N., Kanehira C. (1984). Independent effect of a mixed–beam regimen of fast neutrons and gamma rays on a murine fibrosarcoma. Radiat. Res. 98, 96 – 106.

Attix F. (1986). Introduction to radiological physics and radiation dosimetry. John Wiley & Sons, New York. p 422.

Axtmann R.C. and Licari J.A. (1964). Yield of the Fricke dosimeter to 14.6 MeV neutrons Radiat. Res. 22, 511 – 518.

Barendsen G.W., Beusker I.L.J., Vergroesen A.J. and Budke L. (1960). Effects of different ionizing radiations on human cells in culture. II. Biological experiments. Radiat. Res. 13, 841 – 849.

Barendsen G.W., Koot C.J., and van Kersen G.R. (1966). The effect of oxgygen on impairment of the proliferative capacity of human cells in culture by ionizing radiations of different LET. Int. J. Radiat. Biol. 10 , 317 – 327

Barendsen G.W. (1989). Cell survival curve shapes and radiation responses of tumors. The significance of the linear term in the linear–quadratic model. In. The Scientific Basis of Modern Radiotherapy. Ed. N.J. McNally. BIR Report 19. British Institute of Radiology. London, p 10.

Barendsen G.W. (1990). Mechanisms of cell reproductive death and shapes of radiation dose–survival curves of mammalian cells. Int. J. Radiat. Biol. 57, 885 – 896.

Barendsen G.W. (1990). A hypothesis concerning the interaction of DNA double–stranded breaks as mechanism for cell reproductive death as a function of LET.(Abstract) Int. J. Radiat. Biol. 58, 1046 – 1046.

Battermann J.J., Breur K., Hart G.A.M. and Pepenzeel H.A. (1981). Observations on pulmonary metastases in patients after single doses and multiple fractions of neutrons and cobalt–60 gamma rays. Eur. J. Cancer 17, 539 – 548.

Bauchinger M. (1983). Microdosimetric aspects of the induction of chromosome aberrations In Radiation Induced Chromosome Damage in Man, eds T. Ishihara and M.S. Sasaki (New York: R. Liss) p 1.

Bauchinger M., Kühn H., Dresp J., Schmid E. and Streng S. (1983). Dose–effect relationship for 14.5 MeV (d+T) neutron–induced chromosome aberrations in human lymphocytes irradiated in a man phantom. Int. J. Radiat. Biol. 43, 571 – 578.

Bauchinger M., Koester L., Schmid E., Dresp J. and Streng S. (1984). Chromosome aberrations in human lymphocytes induced by fission neutrons Int. J. Radiat. Biol. 45, 449 – 457.

Belli M., Goodhead D.T., Ianzani F., Simone G. and Tabocchini M.A. (1992). Direct comparison between protons and alpha–particles of the same LET: II. Mutation induction at the HPRT locus in V79 cells. Int. J. Radiat. Biol. 61, 625 – 629.

Benedetto A.R. and Harris C.R. (1985). Measurement of absorbed dose from radionuclide solutions mixed intimately with the FBX dosimeter. Health Phys. 49, 455 – 477.

Berenbaum M.C. (1981). Criteria for analyzing interactions between biologically active agents. Adv. Cancer Res. 35, 269 – 335.

Berenbaum M.C. (1985). The expected effect of a combination of agents: the general solution. J. Theor. Biol. 114, 413 – 431.

Berenbaum M.C. (1991). Concepts for describing the interaction of two agents. Radiat. Res. 126, 264 – 265.

Bewley D.K. and Fowler J.F. (1972). Fast neutron beams for radiotherapy. In Peaceful uses of atomic energy. IAEA Vienna 13, 137 – 146.

Bewley D.K., McNally N.J. and Page B.C. (1974). Effect of the secondary charged–particle spectrum on cellular response to fast neutrons. Radiat. Res. 8, 111 – 121.

Bewley D.K., Cullen B.M., Astor M., Hall E.J., Blake S.W., Bonnett D.E. and Zaider M. (1989). Changes in biological effectiveness of the neutron beam at Clatterbridge (62 MeV p on Be) measured with cells in vitro. Brit. J. Radiol. 62, 344 – 347.

Binns P.J. and Hough J.H. (1987). Spectral energy measurements in a fast neutron therapy field. Nucl. Instr. & Meth. A255, 330.

Binns P.J. and Hough J.H. (1988). Lineal energy measurements in two fast neutron beams: d(16) + Be and p(66) + Be. Radiation Protection Dosimetry 23, 385 – 388.

Binns P.J. and Hough J.H. (1990). Build–up measurements using a 1/2 inch TEPC. NAC Annual Report NAC/AR/90–01. p 204.

Bird R.P., Zaider M., Rossi H.H., Hall E.J., Marino S.A. and Rohrig N. (1983). The sequential irradiation of mammalian cells with X–rays and charged particles of high LET. Radiat. Res. 93, 444 – 452.

Brenner D.J. (1990). Track structure, lesion development and cell survival. Radiat. Res. 124, 529 – 537.

Blake P.K., DeLuca P.M., Pearson D.W., Meisner L.F. and Gould M.N. (1986). The effects of mixed neutron–gamma beams in both sequential and simultaneous irradiation modalities on chromosomal aberrations. USDOE Report No. DOE/EV/01105–317.

Britten R.A., Warenius H.M., Parkins C. and Peacock J.H. (1992). The inherent cellular sensitivity to 62.5 MeV (p+/Be) neutrons of human cells differing in photon sensitivity. Int. J. Radiat. Biol. 61, 805 – 812.

Broerse J.J., Barendsen G.W. and Van Kersen G.R. (1967). Survival of cultured human cells after irradiation with fast neutrons of different energies in hypoxic and oxygenated conditions. Int. J. Radiat. Biol. 13, 559 – 572.

Broerse J.J. and Zoetelief J. (1978). Dosimetric aspects of fast neutron irradiations of cells cultured in monolayer. Int. J. Radiat. Biol. 33, 383 – 385.

Broerse J.J., Lyman J.T. and Zoetelief J. (1985). Dosimetry of external beams of particles. In The Dosimetry of Ionizing Radiation, Vol. I (K.R. Case, B.E. Bjärngard and F.H. Attix eds.). Academic Press, London.

Brooks A.L., Newton G.J., Shyr L.J., Seiler F.A. and Scott B.R. (1990). The combined effects of ‘–particles and X–rays on cell killing and micronuclei induction in lung epithelial cells. Int. J. Radiat. Biol. 58, 799 – 811.

Bukowski R.M., Gahbauer R., Rodriquez–Antunez A. and Hermann R. (1982). Mixed beam radiotherapy and combination chemotherapy in localized pancreatic adenocarcinoma – preliminary results. Int. J. of Radiat. Oncol. Biol. Phys. 8, 1231 – 1233.

Carl U.M., McNally N.J. and Joiner M.C. (1987). a) The effect of mixed fractionation with X–rays and neutrons on tumor growth delay and skin reactions in mice. Brit. J. Radiol. 60, 583 – 588.

Carl U.M., McNally N.J. and Joiner M.C. (1987). b) Change in therapeutic gain with photon contamination in a neutron beam. Brit. J. Radiol. 60, 937 – 938.

Carter S.B. (1967). Effects of cytochalasins on mammalian cells. Nature 213, 261 – 264.

Chadwick K.H. and Leenhouts H.P. (1981). The Molecular Theory of Radiation Biology. Springer–Verlag, Berlin.

Chapman J.D., Blakely E.A., Smith K.C. and Urtasun R,C. (1977). Radiobiological characterization of the inactivating events produced in mammalian cells by helium and heavy ions. Int. J. of Radiat. Oncol. Biol. Phys. 3, 97 – 102.

Chung W.H. (1985). In Techniques of Radiation Dosimetry. Eds. K. Mahesh and D.R. Vij.

Cohen L. (1986). Calculation of clinical r.b.e. values for neutrons. Int. J. Radiat. Biol. 50, 147 – 154.

Cornforth M.N. (1989). On the nature of interactions leading to radiation–induced chromosomal exchange. Int. J. Radiat. Biol. 56, 635 – 643.

Cornforth M.N. and Goodwin E.H. (1991). Transmission of radiation–induced acentric chromosomal fragments to micronuclei in normal human fibroblasts. Radiat. Res. 126, 210 – 217.

Countryman P.I. and Heddle J.A. (1976). The production of micronuclei from chromosome aberrations in irradiated cultures of human lymphocytes. Mutat. Res. 41, 321 – 332.

Curtis S.B. (1976). The OER of mixed high– and low–LET radiation. Radiat. Res. 65, 566 – 572.

Curtis S.B. (1986). Lethal and potentially lethal lesions induced by radiation. A unified repair model. Radiat. Res. 106, 252 – 270.

Deschavanne P.J, Fertil B., Chavaudra N. and Malaise E.P. (1990). The relationship between radiosensitivity and repair of potentially lethal damage in human tumor cell lines with implications for radioresponsiveness. Radiat. Res. 122, 29 – 37.

Di Cera E., Andreasi Bassi F. and Arcovito G. (1989). Parameter resolution in two models for cell survival after radiation. Radiat. Environ. Biophys. 28, 265 – 271.

Duncan W., McLelland J., Jack W.J.L., Arnott S., Davey P., Gordon A., Kerr G.R. and Williams J.R. (1986). The results of a randomised trial of mixed schedule (neutron/photon) irradiation in the treatment of supratentorial grade III and grade IV astrocytoma. Brit. J. Radiol. 59, 379 – 383.

Durand R.E. and Olive P.L. (1976). Irradiation of multi–cell spheroids with fast neutrons versus X–rays: A qualitative difference in sub–lethal damage repair capacity or kinetics. Int. J. Radiat. Biol. 30, 589 – 592.

Durand R.E. (1984). Repair during multifraction exposures: Spheroids versus monolayers. Brit. J. Radiol. 49, 203 – 206.

Durocher J.J.G., Boese H., Cormack D.V. and Holloway A.F. (1981). A comparison of chemical and ionization dosimetry for high–energy X–ray and electron beams. Med. Phys. 8, 197 – 202.

Edwards A.A., Lloyd D.C., Purrott R.J. (1979). Radiation–induced chromosome aberrations and the poisson distribution. Radiat. Environ. Biophys. 16, 89 – 100.

Engenhart R., Kimmig B., Marin Grez M, Hover K.H., Flentje M. and zum Winkel K. (1987). Combined neutron–photon therapy of locally recurrent recto–sigmoidal tumors. Workshop on fast neutron radiotheapy. EORTC.Gesellschaftfür Strahlen– und Umweltforschung Munchen. p 5.

Evans H.J., Neary G.J. and Williamson F.S. (1959). The relative biological efficiency of single doses of fast neutrons and gamma–rays on Vicia faba roots and the effect of oxygen. Part II. Chromosome damage: the production of micronuclei. Int. J. Radiat. Biol. 3, 216 – 229.

Fabry L., Leonard A. and Wambersie A. (1985). Induction of chromosome aberrations in Go human lymphocytes by low doses of ionizing radiations of different quality. Radiat. Res. 103, 122 – 134.

Feist H. (1982). Determination of the absorbed dose to water for high–energy photons and electrons by total absorption of electrons in ferrous sulphate solotion. Phys. Med. Biol. 27, 1435 – 1447.

Fenech M. and Morley A.A. (1985). Measurements of micronuclei in lymphocytes Mutation Res. 147, 29 – 36.

Fenech M. and Morley A.A. (1986). Cytokinesis–block micronucleus method in human lymphocytes: effect of in vivo ageing and low dose X–irradiation. Mutation Res. 161, 193 – 198.

Fenech M. and Morley A.A. (1989). Kinetochore detection in micronuclei: an alternative method for measuring chromosome loss. Mutagenesis 4, 98 – 104.

Fenech M, Denham J., Francis W. and Morley A. (1990). Micronuclei in cytokinesis–blocked lymphocytes of cancer patients following fractionated partial body radiotherapy. Int. J. Radiat. Biol. 57, 373 – 383.

Fertil B., Deschavanne P.J., Lachet B. and Malaise E.P. (1980). In vitro radiosensitivity of six human cell lines. A comparative study with different statistical models. Radiat. Res. 82, 297 – 309.

Fertil B., Deschavanne P.J., Gueulette J. et al (1982). In vitro radiosensitivity of six human cell lines. II. Relation to the RBE of 50–MeV neutrons. Radiat. Res. 90, 526 – 537.

Fertil B., Dertinger H., Courdi A. and Malaise E.P. (1984). Mean inactivation dose: A usefull concept for intercomparison of human cell survival curves. Radiat. Res. 99, 73 – 84.

Franke H.D. and Schmidt R. (1985). Clinical results with fast neutrons (DT, 14 MeV) Radiation Medicine 3, 151 – 160.

Freeman M.L., Sierra E. and Hall E.J. (1983). The repair of sublethal damage in diploid human fibroblasts: A comparison between human and rodent cell lines. Radiat. Res. 95, 382 – 391.

Fregene A.O. (1967). Calibration of the ferrous sulfate dosimeter by ionometric and calorimetric methods for radiations of a wide range of energy. Radiat. Res. 31, 256 – 272.

Freyer J.P., Schillaci M.E. and Raju M.R. (1989). Measurement of the G–value for 1.5 keV X–rays. Int. J. Radiat. Biol. 56, 885 – 892.

Fricke H. and Hart E.J. (1966). In Radiation Dosimetry, Vol II. Eds, F.H. Attix and W.C. Roesch (Academic Press, New York) p.167.

Gahbauer R.A., Horton J., Ngo F.Q., Roberts W. and Blue J. (1985). Biological considerations for treating alternate fields versus all fields daily with high and low LET radiation. Strahlentherapie 161, 771 – 774.

Gantenberg H.W., Wuttke K., Streffer C. and Mu?ller W.U. (1991). Micronuclei in human lymphocytes irradiated in vitro or in vivo. Radiat. Res. 128, 276 – 281.

Geard C. and Yan Chen C. (1990). Micronuclei and clonogenicity following low– and high–dose–rate: irradiation of normal human fibroblasts. Radiat. Res. 124, 56– 6.

Goodhead D.T. (1982). An Assessment of the Role of Microdosimetry in Radiobiology. Radiat. Res. 91, 45 – 76.

Goodhead D.T. and Brenner D.J. (1983). Estimation of a single property of low LET radiations which correlates with biological effectiveness. Phys. Med. Biol. 28, 485 – 492.

Goodhead D.T. (1989). The initial physical damage produced by ionizing radiations. Int. J. Radiat. Biol. 56, 623 – 634.

Goodhead D.T. and Nikjoo H. (1989). Track structure analysis of ultrasoft X–rays compared to high– and low–LET radiation. Int. J. Radiat. Biol. 55, 513 – 529.

Goodhead D.T., Belli M., Mill A.J., Bance D.A., Allen L.A., Hall S.C., Ianzani F., Simone G., Stevens D.L., Stretch A., Tabocchini M.A. and Wilkinson R.E. (1992). Direct comparison between protons and alpha–particles of the same LET: I. Irradiation methods and inactivation of asynchronous V79, HeLa and C3H 10T1/2 cells. Int. J. Radiat. Biol. 61, 611 – 624.

Gray L.H. and Read J. (1944). The effect of ionizing radiations on the broad bean root. VI: Summation of the effects of radiation of different ion density. Brit. J. Radiol. XVI, 271 – 273.

Green D. and Major D. (1973). The G–value for the ferrous sulphate dosemeter for 14 MeV neutrons. Phys. Med. Biol. 18, 369 – 378.

Griffin T.W., Pajak T.F., Maor M.H., Laramore G.E., Hendrickson F.R., Parker R.G., Thomas F.J. and Davis L.W. (1989). Mixed neutron/photon irradiation of unresectable squamous cell carcinomas of the head and neck: The final report of a randomized cooperative trial. Int. J. of Radiat. Oncol. Biol. Phys. 17, 959 – 965.

Gupta B.L. and Gomathy K.R. (1974). Consistency of Ferrous Sulphate–Benzoic Acid–Xylenol Orange Dosimeter. Int. J. Appl. Radiat. Isot. 25, 509 – 513.

Gupta B.L., Dvornik I. and Zec U. (1974). New chemical systems for low–level fast neutron dosimetry. Phys. Med. Biol. 19, 843 – 852.

Gupta B.L. and Nilekani S.R. (1977). Build–up dose measurement in 6OCo irradiations using the ferrous sulfate–benzoic acid–xylenol orange dosimeter. Int. J. Appl. Radiat. Isot. 28, 805 – 808.

Gupta B.L., Bhat R.M., Gomathy K.R. and Susheela B. (1978). Radiation Chemistry of the ferrous sulfate–benzoic acid–xylenol orange system. Radiat. Res. 75, 269 – 277.

Gupta B.L. and Nilekani S.R. (1980). Scatter effects in electron dosimetry. Int. J. Appl. Radiat. Isot. 31, 41 – 43.

Gupta B.L., Kini U.R. and Bhat R.M. (1981). Dose–rate and fractionation studies with FBX dosimeter. Int. J. Appl. Radiat. Isot. 32, 701 – 704.

Gupta B.L. , Kini U.R., Bhat R.M. and Madhvanath U. (1982). Use of the FBX dosimeter for the calibration of cobalt–60 and high–energy teletherapy machines. Phys. Med. Biol. 27, 235 – 245.

Gupta B.L., Bhat R.M., Narayan G.R. and Susheela B. (1983). Acid and xylenol orange effects in the FBX dosimeter. Int. J. Appl. Radiat. Isot. 34, 887 – 890.

Gupta B.L. and Madhvanath U. (1985). G(Fe3+) values in the FBX dosimeter at low dose–rates. Int. J. Appl. Radiat. Isot. 36, 985 – 987.

Gupta B.L. and Narayan G.R. (1985). G(Fe3+) values in the FBX dosemeter. Phys. Med. Biol. 30, 337 – 340.

Hall E.J., Rossi H.H., Kelllerer A.M. Goodman L.J. and Marino S. (1973). Radiobiological studies with monoenergetic neutrons. Radiat. Res. 54, 431 – 443.

Hall E.J., Novak J.K., Kelllerer A.M., Rossi H.H., Marino S. and Goodman L.J. (1975). RBE as a function of neutron energy. I. Experimental Observations. Radiat. Res. 64, 245 – 255.

Hall E.J., Roizin–Towle L and Attix F.H. (1976). Radiobiological studies with cyclotron–produced neutrons currently used for radiotherapy. Int. J. of Radiat. Oncol. Biol. Phys. 6, 33 – 40.

Hall E.J. and Kellerer A. (1979). Review of RBE data for cells in culture. In High LET Radiations in Clinical Radiotherapy, eds. G.W. Barendsen, J. Broerse and K. Bruer (Pergamon Press, Oxford) p. 171.

Hall E.J., Kellerer A.M. and Friede H. (1982). Dependence on neutron energy of the OER and RBE Int. J. of Radiat. Oncol. Biol. Phys. 8, 1567 – 1572.

Hall E.J. (1988). Radiobiology for the Radiobiologist. Third Edition, J.B. Lippincott Company. Philadelphia.

Hall E.J., Astor M. and Brenner D. (1992). Biological intercomparisons of neutron beams used for radiotherapy generated by p+/Be in hospital–based cyclotron. Brit. J. Radiol. 65, 66 – 71.

Halpern J.H., Maor M.H., Hussey D.H., Henkelmann G.C., Sampiere V. and McNeese M.D. (1990). Locally advanced breast cancer treated with neutron beams: long–term follow–up in 28 patients. Int. J. of Radiat. Oncol. Biol. Phys. 18, 825 – 831.

Hayashi M. Sofuni T. and Ishidate M. (1983). An application of Acridine Orange fluorescent staining to the micronucleus test. Mutat. Res. 120, 241 – 247.

Heddle J. A. (1965). Lack of interaction of X–ray– and neutron–induced chromosome breaks in barley Mutation Res. 2, 149 – 155.

Heddle J. A. and Carrano (1975). The DNA content of micronuclei induced in mouse bone marrow by γ–irradiation: Evidence that micronuclei arise from acentric chromosomal fragments. Mutat. Res. 44, 97 – 104.

Hellin H., Paulsen A. Liskien H., Decat G., Wambersie A., Leonard A. and Baugnet–Mahieu L. (1990). Chromosome aberrations induced in vitro in human lymphocytes by monoenergetic 2.5 MeV neutrons and ^{60}Co gamma rays. Strahlenther. Onkol. 166, 549 – 553.

Hendry J.H., Rosenberg I. and Green D. (1976). Addition of neutron and gamma–ray fractions for intestinal damage. Radiol. 121, 483 – 486.

Hering E.R. (1980). A comparison of the biological effect of ^{125}I and ^{192}Ir gamma rays on the roots of Vicia faba using a specially designed applicator. Brit. J. Radiol. 53. 255 – 258.

Higgins P.D. (1984). The effect of simultaneous versus sequential mixtures of high and low LET radiation. A paper presented at the "Optimization of cancer radiotherapy: Second Int. Conf. on dose, time and radiation fractionation in radiation oncology. Univ. of Wisconsin, Madison, Wisconsin.

Higgins P.D., DeLuca P.M. and Pearson D.W. (1983). V79 Survival following simultaneous or sequential irradiation by 15–MeV neutrons and 6OCo photons. Radiat. Res. 95, 45 – 56.

Hornsey S., Andreozzi U. and Warren P.R. (1977). Sublethal damage in cells of the mouse gut after mixed treatment with x–rays and fast neutrons. Brit. J. Radiol. 50, 513 – 517.

Huber R. Braselmann H. and Bauchinger M. (1992). Intra– and inter–individual variation of background and radiation–induced micronucleus frequencies in human lymphocytes. Int. J. Radiat. Biol. 61, 655 – 661.

Hussey D.H., Jardine J.H., Raulston G.L., Stephens L.C., Gray K.N., Maor M.H. and Withers H.R. (1982). 50 Mev d/Be neutrons: A comparison of normal tissue tolerance in animals with clinical observations in patients. Int. J. of Radiat. Oncol. Biol. Phys. 8, 2083 – 2088.

ICRP (1984). International Commission on Radiological Protection. Report 41. Nonstochastic Effects of Ionizing Radiation. (Pergamon Press, Oxford).

ICRU (1977). International Commision on Radiation Units and Measurements. Report 26. Neutron Dosimetry for Biology and Medicine. (ICRU, Washington D.C.).

ICRU (1979). International Commision on Radiation Units and Measurements. Report 30. Quantitative Concepts and Dosimetry in Radiobiology. (ICRU, Washington D.C.).

ICRU (1989). International Commision on Radiation Units and Measurements. Report 45. Clinical Neutron Dosimetry Part I. (ICRU, Washington D.C.).

IAEA (1986). International Atomic Energy Agency. Report 260. Biological Dosimetry: Chromosomal Aberrations Analysis for Dose Assessment. (IAEA, Vienna)

Jansen S. (1992). Personal communication.

Joiner M.C., Maughan R.L., Fowler J.F. and Denekamp J. (1983). The RBE for mouse skin irradiated with 3–MeV neutrons: Single and fractionated doses Radiat. Res. 95, 130 – 141.

Joiner M.C., Bremner J.C., Denekamp J. and Maughan R.L. (1984). The interaction between X–rays and 3 MeV neutrons in the skin of the mouse foot. Int. J. Radiat. Biol. 46, 625 – 638.

Jones D.T.L., Yudelev and Hendrikse W.L.J. (1988). Physical characteristics of the South African high energy neutron therapy facility. Radiat. Protec. Dosimetry 23, 365 – 368.

Jones D.T.L., Symons J.E., Fulcher T.J., Brooks F.D., Nchodu M.R., Allie M.S., Buffler A. and Oliver M.J. (1992). Neutron fluence and kerma spectra of a p(66)/Be(40) clinical source. Med. Phys. 19, 1285.

Kaffenberger W., Becker K. and Van Beuningen D. (1990). Comparison of micronucleus frequencies and proliferation kinetics in three X–irradiated cell lines. Strahlenther. Onkol. 166, 617 – 625.

Kartha M. (1970). A ferrous sulfate mini–dosimeter. Radiat. Res. 42, 220 – 231.

Katz R. and Sharma S.C. (1974). Cellular survival in a mixed radiation enviroment. Int. J. Radiat. Biol. 26, 143 – 146.

Kellerer A. and Rossi H.H. (1978). A generalize formulation of dual radiation action. Radiat. Res. 75, 471 – 488.

Kellerer A.M. and Brenot J. (1974). On the statistical evaluation of dose–response functions. Rad. and Environm. Biophys. 11, 1 – 13.

Kellerer A.M. and Hug O. (1972). A theory of dose–effect relations. Encyclopaedia of medical radiology. (Publ. Springer, Berlin) 3, 1 42.

Kellerer A.M. and Rossi H.H. (1972). The theory of dual radiation action. Current Topics in Radiation Research Quarterly. 8, 85 – 158.

Khokhar M.T. (1984). Dose–independent effect of misonidazole in fractionated irraditions of hypoxic Vicia faba bean roots. Int. J. Radiat. Biol. 45, 311 – 320.

Kihlman B.A. (1975). Root tips of Vicia faba for the study of the induction of chromosomal aberrations. Mutat. Res. 31, 401 – 412.

Knowles A. and Burgess C. (1984). Practical Absorption Spectrometry. Chapman and Hall Ltd, London.

Krepinsky A. B. and Heddle J.A. (1983). Micronuclei as a Rapid and Inexpensive Measure of Radiation–Induced Chromosomal Aberrations In Radiation Induced Chromosome Damage in Man, eds T. Ishihara and M.S. Sasaki (New York: R. Liss) p 93.

Lam G.K.Y. (1987). a) The survival of a biological system to mixed radiations. Radiat. Res. 110, 232 – 243.

Lam G.K.Y. (1987). b) The interaction of radiations of different LET. Phys. Med. Biol. 32, 1291 – 1309.

Lam G.K.Y. (1988). a) The combined effects of mixtures of ionizing radiations. J. theor. Biol. 134, 531 – 546.

Lam G.K.Y. (1988). b) On the general validity of linear summation of dose equivalents for mixed radiations. Health Physics 54, 57 – 61.

Lam G.K.Y. (1989). a) Analysis of interaction for mixtures of agents using the linear isobole. Bul. Math. Biol. 51, 293 – 309.

Lam G.K.Y. (1989). b) On the use of effective dose in the treatment planning of high linear–energy–transfer radiation. Med. Phys. 16, 687 – 691.

Lam G.K.Y. (1989). c) An isoeffect approach to the study of combined effects of mixed radiations – the nonparamatric analysis of in vivo data. Radiat. Res. 119, 424 – 431.

Lam G.K.Y. (1990). a) On the biophysical interpretation of the mathematical product of dose and relative biological effectiveness. Phys. Med. Biol. 35, 481 – 488.

Lam G.K.Y. (1990). b) The use of the pion stopping distribution and lesion additivity concept for the calculation of effective doses in pion treatment planning. Phys. Med. Biol. 35, 731 – 740.

Laramore G.E., Krall J.M., Thomas F.J., Griffin T.W., Maor M.H. and Hendrickson F.R. (1985). Fast neutron radiotherapy for locally advanced prostate cancer. Results of an RTOG randomized study. Int. J. of Radiat. Oncol. Biol. Phys. 11, 1621 – 1627.

Lasne C. Gu Z.W. Venegas W. and Chouroulinkov I. (1984). The in vitro micronucleus assay for detection of cytogenetic effects induced by mutagen–carcinogens: comparison with the in vitro sister–chromatid exchange assay. Mutat. Res. 130, 273 – 282.

Lawson R.C. and Porter D. (1975). The response of the ferrous sulphate dosemeter to neutrons. Phys. Med. Biol. 20, 420 – 430.

Leenhouts H.P., Sijsma M.J., Cebulska–Wasilewska A. and Chadwick K.H. (1986). The combined effect of DBE and X–rays on the induction of somatic mutations in Tradescantia. Int. J. Radiat. Biol. 49, 109 – 119.

Ling C.C., Spiro I.J. and Stickler R. (1984). Dose–rate effect between 1 and 10 Gy/min in mammalian cell culture. Brit. J. Radiol. 57, 723 – 728.

Littlefield L.G., Sayer A.M. and Frome E.L. (1989). Comparisons of dose–response parameters for radiation induced acentric fragments and micronuclei observed in cytokinesis arrested lymphocytes. Mutagenesis 4, 265 – 270.

Lloyd D.C., Purrott R.J., Dolphin G.W.,Bolton D., Edwards A.A. and Corp M.J. (1975). The relationship between chromosome aberrations and low LET radiation dose to human lymphocytes. Int. J. Radiat. Biol. 28, 75 – 90.

Lloyd D.C., Purrott R.J., Dolphin G.W. and Edwards A.A. (1976). Chromosome aberrations induced in human lymphocytes by neutron irradiation. Int. J. Radiat. Biol. 29, 169 – 182.

Lloyd D.C. and Edwards A.A. (1983). Chromosome Aberrations in Human Lymphocytes: Effect of Radiation Quality, Dose and Dose Rate. In Radiation Induced Chromosome Damage in Man, eds T. Ishihara and M.S. Sasaki (New York: R. Liss) p 23.

Lloyd D.C., Edwards A.A., Prosser J.S. and Corp M.J. (1984). The dose response relationship obtained at constant irradiation times for the induction of chromosome aberrations in human lymphocytes by cobalt–60 gamma rays. Radiat. Environ. Biophys. 23, 179 – 189.

Lloyd D.C., Edwards A.A. and Prosser J.S. (1986). Chromosome aberrations induced in human lymphocytes by ?in vitro acute X and gamma radiation. Rad. Protect. Dosimetry 15, 83 – 88.

Loew S. (1953). The problem of synergism and antagonism of combined drugs. Arzneimittelforschung 3, 285 – 290.

Lunec J., Cramp W.A. and Hornsey S. (1980). Neutron irradiation of bacteria in the presence and absence of secondary charged–particle equilibrium. Radiat. Res. 83, 607 – 620.

Magnien E., Dalschaert X. and Coppola M. (1981). Dose–effect relationships, rbe and split–dose effects after gamma and fast neutron irradiation of protoplasts from wild Nicotiana species. Int. J. Radiat. Biol. 40, 463 – 474.

Malaise E.P., Fertil B., Deschavanne P.J., Chavaudra N. and Brock W.A. (1987). Initial slope of radiation survival curves is characteristic of the origin of primary and established cultures of human tumor cells and fibroblasts. Radiat. Res. 111, 319 – 333.

Maor M.H., Hussey D.H., Barkley Jr. H.T. and Peters L.J. (1983). Neutron therapy for head and neck cancer: I. A final report of the MDAH–TAMVEC pilot studies. Int. J. of Radiat. Oncol. Biol. Phys. 9, 1255 – 1260.

Marshall I. (1982). The effects of low doses of different radiation qualities on Vicia faba bean root meristems. Thesis. Kernforschungszentrum Karlsruhe GmbH, ISSN 0303–4003.

Marshall I. and Bianchi M. (1983). Micronucleus induction in Vicia faba roots. Part 1 Absence of dose–rate, fractionation and oxygen effect at low doses of low LET radiation. Int. J. Radiat. Biol. 44, 151 – 162.

Maruyama Y., Feola J. and Berner B. (1988). Mixed schedules for neutron therapy. Brit. J. Radiol. 61, 423 – 424.

Masuda K. (1970). Effects of 14–MeV neutrons and X–rays, single or combined, on the reproductive capacity of L cells. J. Radiat. Res. 11, 107 – 112.

Masunaga S., Ono K., Wandl E.O., Fushiki M. and Abe M. (1990). Use of micronucleus assay for the selective detection of radiosensitivity in BUdR–unincorporated cells after pulse–labelling of exponentially growing tumours cells. Int. J. Radiat. Biol. 58, 303 311.

Masunaga S., Ono K. and Abe M. (1991). A method for selective measurement of radiosensitivity of quiescent cells in solid tumors – combination of immunofluorescence staining to BrdU and micronucleus assay. Radiat. Res. 125, 243 – 247.

Matsubara S., Kuwabara Y., Horiuchi J., Suzuki S. and Ito A. (1988). Dose distribution of neutron beam and chromosome analysis. Int. J. of Radiat. Oncol. Biol. Phys. 14, 503 – 509.

Matthews R. W., Barker N.T. and Sangster D.F. (1978). A comparison of some aqueous chemical dosimeters for absorbed doses of less than 1000 rads. Int. J. Appl. Radiat. Isot. 29, 1 – 8.

Maughan R.L., Slabbert J.P. and Roper M.J. (1983). Use of the modified Fricke solution (FBX) for neutron dosimetry. In Proc. 7th Cong. of Radiation Research (Amsterdam). Hague: Martinus Nijhoff.

McNally N., de Ronde J. and Hinchliffe M. (1981). Interaction between X–rays and neutrons. (Abstract) Radiat. Res. 87, 409 – 410.

McNally N.J., Maughan R.L., de Ronde J., and Roper M.J. (1982). Measurements of some radiobiological and physical properties of neutrons produced by a 4 MV Van de Graaff accelerator. Radiat. Res. 89, 227 – 237.

McNally N.J., de Ronde J. and Hinchliffe M. (1984). The effect of sequential irradiation with X–rays and fast neutrons on the survival of V79 Chinese hamster cells. Int. J. Radiat. Biol. 45, 301 – 310.

McNally N.J., de Ronde J. and Hinchliffe M. (1985). Survival of V79 cells following simultaneous irradiation with X–rays and neutrons in air or hypoxia. Int. J. Radiat. Biol. 48, 847 – 855.

McNally N.J., de Ronde J. and Folkard M. (1988). Interaction between X–ray and α–particle damage in V79 cells. Int. J. Radiat. Biol. 53, 917 – 920.

Menzel H.G., Pihet P. and Wambersie A. (1990). Microdosimetric specification of radiation quality in neutron radiation therapy. Int. J. Radiat. Biol. 57, 865 – 883.

Mijnheer B.J., Wootton P., Williams J.R., Eenma J. and Parnell C.J. Uniformity in dosimetry protocols for therapeutic applications of fast neutron beams. Med. Phys. 14, 1020.

Murthy M.S.S., Madhvanath U., Subrahmanyam P., Rao B.S. and Reddy N.M.S. (1975). Synergistic effect of simultaneous exposure to ^{60}Co gamma rays and ^{210}Po α–rays in diploid yeast. Radiat. Res. 63, 185 – 190.

Napolitano M., Durante M., Grossi G.F., Pugliese M. and Gialanella G. (1992). Inactivation of C3H 10T1/2 cells by monoenergetic high LET alpha–particles. Int. J. Radiat. Biol. 61, 813 – 820.

Neary G.J. (1965). Chromosome aberrations and the theory of RBE. Int. J. Radiat. Biol. 9, 477 – 503.

Nelson J.S.R., Carpenter R.E. and Parker R.G. (1975). Response of mouse skin and the C3HBA mammary carcinoma of the C3H mouse to X–rays and cyclotron neutrons: effect of mixed neutron–photon fractionation schemes. Eur J. Cancer 11, 891 – 901.

Ngo F.Q.H., Han A. and Elkind M.M. (1977). On the repair of sub–lethal damage in V79 Chinese hamster cells resulting from irradiation with fast neutrons or fast neutrons combined with X–rays. Int. J. Radiat. Biol. 32, 507 – 511.

Ngo F.Q.H., Blakely E.A. and Tobias C.A. (1978). Does an exponential survival curve of irradiated mammalian cells imply no repair ?. Radiat. Res. (abstract) 74, 588 – 598.

Ngo F.Q.H., Blakely E.A. and Tobias C.A. (1981). Sequential exposures of mammalian cells to low– and high–LET radiations. I. Lethal effects following X–ray and neon–ion irradiation. Radiat. Res. 87, 59 – 78.

Ngo F.Q.H., Blakely E.A., Tobias C.A., Chang P.Y. and Lommel L. (1981). The effects of mixed–LET radiation fields. (Abstract) Radiat. Res. 87, 407 – 408.

Ngo F.Q.H., Blakely E.A., Tobias C.A., Chang P.Y. and Lommel L. (1988). Sequential exposures of mammalian cells to low– and high–LET radiations. II. As a function of cell–cycle stages. Radiat. Res. 115, 54 – 69.

Ono K., Wandle E., Tsutsui K., Sasai K. and Abe M. (1989). The correlation between cell survival curve and dose response curve of micronucleus (MN) frequency. Strahlenther. Onkol. 165, 824 – 827.

Ono K., Nagata Y., Akuta K., Abe M., Ando K. and Koike S. (1990). Frequency of micronuclei in hepatocytes following X and fast neutron irradiations – An analysis by a linear–quadratic model. Radiat. Res. 123, 345 – 347.

Palcic B., Brosing J.W. and Skarsgard L.D. (1982). Survival measurements at low doses: oxygen enhancement ratio. Br. J. Cancer 46, 980 – 984.

Palcic B. (1984). In vivo and in vitro mechanisms of radiation sensitization, drugs synthesis and screening: can we learn it all from high dose data ?. Int. J. of Radiat. Oncol. Biol. Phys. 10, 1185 – 1193.

Peacock J.H., Cassoni A.M., McMillan T.J. and Steel G. (1988). Radiosensitive human cell lines may not be recovery deficient. Int. J. Radiat. Biol. 54, 945 – 953.

Pejuan A. (1980). The dosimetry of 3 MeV and 14 Mev neutrons with the ferrous sulphate solution. Manuskript. Gesellscaft Für Strahlen und Umweltforschung MBH Munchen.

Pejuan A. and Kühn H. (1981). Properties of a modified Fricke solution for radiation dosimetry. Proc. 4th Symp. on Neutron Dosimetry, Radiat. Prot. vol II (Munich–Neuherberg: Commission of European Communities), 455 – 464.

Pejuan A. and Kühn H. (1981). The G–value of the ferrous sulfate dosemeter for 3 and 14 MeV neutrons. Phys. Med. Biol. 26, 163 – 169.

Pike M.C. and Alper T. (1964). A method for determining dose–modification factors. Brit. J. Radiol. 37, 458 – 462.

Pincu M., Bass D. and Norman A. (1984). An improved micronuclear assay in lymphocytes Mutation Res. 139, 61 – 65.

Raju M.R. and Jett J.H. (1974). RBE and OER variations of mixtures of plutonium alpha particles and X–rays for damage to human kidney cells (T–1). Radiat. Res. 60, 473 – 481.

Raju M.R., Amols H.I., Bain E., Carpenter S.G., Cox R.A. and Robertson J.B. A heavy particle comparartive study. Brit. J. Radiol. 51, 712 – 719.

Ramalho A., Sunjevaric I. and Natarajan A.T. (1988). Use of the frequencies of micronuclei as quantitative indicators of X–ray induced chromosomal aberrations in human lymphocytes: Comparison of two methods. Mutat. Res. 207, 141 – 146.

Rasey J.S., Carpenter R.E., Nelson N.J. et al (1977). Cure of EMT–6 tumors by x rays or neutrons: effect of mixed–fractionation schemes. Radiology 132, 207 – 212.

Redpath J.L. (1980). Mechanisms in combination therapy: isobologram analysis and sequence. Int. J. Radiat. Biol. 38, 355 – 356.

Revell S.H. (1983). Relationships between chromosome damage and cell death. In Radiation Induced Chromosome Damage in Man, eds. T.Ishihara and M.S. Sasaki (New York, R. Liss) p 215.

Rialton R., Porter D, Lawson R.C. and Hannan W.J. (1974). The oxygen enhancement ratio and relative biological effectiveness for combined irradiations of Chinese hamster cells by neutrons and b–rays. Int. J. Radiat. Biol. 25, 121 – 127.

Rialton R., Lawson R.C. and Porter D. (1975). Interaction of b–ray and neutron effects on the proliferative capacity of Chinese hamster cells. Int. J. Radiat. Biol. 27, 75 – 82.

Rossi H.H. (1968). Microscopic energy distribution in irradiated matter. In Radiation Dosimetry. Vol. I. Eds. F.H. Attix, W. C. Roesch and E. Tochilin. Academic Press New York.

Rothman K.J. (1974). Synergy and antagonism in cause–effect relationships. American J. Epidemiolgy 99, 385 – 388.

Sachs L. (1982). Applied Statistics. A Handbook of Techniques. Springer–Verlag, New York.

Sakai K., Suzuki S., Nakamura N. and Okada S. (1987). Induction and subsequent repair of DNA damage by fast neutrons in cultured mammalian cells. Radiat. Res. 110, 311 – 320.

Savage J.R.K. (1976). Classification and relationship of induced chromosomal structural changes. J. Med. Genet. 13, 103 – 122.

Savage J.R.K. (1970). Sites of radiation induced chromosome exchanges. Curr. Top. in Radiat. Res. 6, 129 – 194.

Scalliet P. (1991). The trouble with neutrons. Eur, J. Cancer 27, 225 – 230.

Schimmerling W. and Curtis S.B. (1989). Biomedical and space–related research with heavy ions at the BEVALAC. Radiat. Res. 119, 193 – 204.

Scott B.R. (1983). Theoretical models for estimation dose–effect relationships after combined exposure to cytotoxicants. Bull. of Mathematical Biology 45, 323 – 345.

Scott B.R. (1984). Methodologies for predicting the expected combined stochastic radiobiological effects of different ionizing radiations and some applications. Radiat. Res. 98, 182 – 197.

Sinclair W.K. (1966). The shape of radiation survival curves of mammalian cells cultured in vitro. In Biophysical Aspects of Radiation Quality. Report 58. Vienna, International Atomic Energy Agency. p 21.

Slabbert J.P., Binns P.J., Jones H.L. and Hough J.H. (1989). A quality assessment of the effects of a hydrogenous filter on a p(66)Be(40) neutron beam. Brit. J. Radiol. 62, 989 – 994.

Smathers J.B. and Victor O. (1977). Composition of A–150 tissue equivalent plastic Med. Phys. 4, 74 – 77.

Sokal R.R. and Rohlf. (1969). Biometry. The principles and practice of statistics in biological research. W.H. Freeman, San Francisco. p 527.

Stap J. and Aten J.A. (1990). Comparison of radiation sensitivity for three cell lines as measured by the cloning assay and the micro–nucleus test. Strahlenther. Onkol. 166, 761 – 763.

Steel G.G. and Peckham M.J. (1979). Exploitable mechanisms in combined radiotherapy–chemotherapy: The concept of additivity. Int. J. of Radiat. Oncol. Biol. Phys. 5, 85 – 91.

Steel G.G. and Peacock J.H. (1989). Why are some human tumors more radiosensitive than others ?. Radiother. and Oncol. 15, 63 – 72.

Steel G.G. (1991). Cellular sensitivity to low dose–rate irradiation focuses the problem of tumour radioresistance. Radiother. Oncol. 20, 71 – 83.

Stephens T.C., Eady J.J., Peacock J.H. and Steel G.G. (1987). Split–dose and low dose–rate recovery in four experimental tumour systems. Int. J. Radiat. Biol. 52, 157 – 170.

Streffer C. and Müller W.U. (1987). Dose–effect relationships and general mechanisms of combined exposures. Int. J. Radiat. Biol. 51, 961 – 969.

Suit H.D., Goiten M., Tepper J., Koehler A.M., Schmidt M.A. and Schneider R. (1975). Exploratory study of proton radiation therapy using large field techniques and fractionated dose schedules. Cancer 35, 1646 – 1657.

Suzuki S. (1993). Survival of Chinese hamster V79 cells after irradiation with a mixture of neutrons and ^{60}Co γ–rays: Experiment and theoretical analysis of mixed irradiation. Radiat. Res. 133, 327 – 333.

Takatsuji T. and Sasaki M.S. (1984). Dose–effect relationship of chromosome aberrations induced by 23 MeV alpha particles in human lymphocytes. Int. J. Radiat. Biol. 45, 237 – 243.

Taylor Y.C. and Brown M. (1987). Radiosensitization in multifraction schedules. Radiat. Res. 112, 124 – 133.

Tenforde T.S., Montoya V.J., Afzal S.M.J., Parr S.S. and Curtis S.B. (1989). Response of rat rhabdomyosarcoma tumors to split doses of mixed high– and low–LET radiation. Int. J. of Radiat. Oncol. Biol. Phys. 16, 1529 – 1536.

Thames H.D. (1985). An 'incomplete–repair' model for survival after fractionated and continuous irradiation. Int. J. Radiat. Biol. 47, 319 – 339.

Thames H.D., Bentzen S.M., Turesson I., Overgaard M. and van den Bogaert W. (1990). Time–dose factors in radiotherapy: a review of the human data. Radiother. Oncol. 19, 219 – 235.

Thierens H., Vral A., and de Ridder L. (1991). Biological dosimetry using the micronucleus assay for lymphocytes: Interindividual differences in dose response. Health Physics 61, 623 – 630.

Tobias C.A., Blakely E.A., Ngo F.Q.H. and Yang T.C.H. (1980). The repair–misrepair model of cell survival. In. Radiation Biology in Cancer Research (Eds. R.E Meyn and H.R. Withers). Raven Press New York. p 195.

Tobias C.A., Blakely E.A., Alpen E.L., Castro J.R., Ainsworth E.J., Curtis S.B., Ngo F.Q.H., Rodriguez A., Roots R.J., Tenforde T. and Yang C.H. (1982). Molecular and cellular radiobiology of heavy ions. Int. J. of Radiat. Oncol. Biol. Phys. 8, 2109 – 2120.

Tsai C.M., Gazdar A.F., Venzon D.J., Steinberg S.M., Dedrick R.L., Mulshine J.L. and Kramer B.S. (1989). Lack of in vitro synergy between etoposide and cis–diammine–dichloroplatinum(II). Cancer Res. 49, 2390 – 2397.

Tubiana M., Dutreix J. and Wambersie A. (1990). Introduction to Radiobiology. Taylor & Francis, London.

Tyrrell R.M. (1978). Radiation synergism and antagonism. Photobiol. Rev. 3, 35 – 113.

UNSCEAR (1982). Ionizing Radiation: Sources and Biological Effects. (United Nations Publications, New York).

Upadhyay S.N., Reddy A.R., Gupta M.M. and Nagaratnam A. (1982). A tissue–equivalent modified FBX dosimeter system. Int. J. Appl. Radiat. Isot. 33, 47 – 49.

Urano M. and Koike S. (1980). Comparison of the effects of neutron and/or photon irradiaton on spontaneous squamous–cell carcinoma in mice. Radiology 134, 219 – 225.

Valeriote F. and Lin H. (1975). Synergistic interaction of anticancer agents: a cellular perspective. Cancer Chemotherapy reports 5, 895 – 900.

Van Dam J.,Billiet G., Wambersie A., Bridier A., Dutreix A. and Bouhnik C. (1980). RBE of d(50)–Be Neutrons and of 650–MeV Helium Ions at different depths for growth reduction in Vicia faba. Radiat. Res. 81, 31 – 47.

Van Dam J. and Wambersie A. (1981). OER and RBE variation between p(75)–Be and d(50)–Be neutron beams. Brit. J. Radiol. 54, 921 – 922.

Van Dam J., Billiet G., Zoetelief J., Broerse J.J. and Wambersie A. (1983). OER and RBE of high energy neutron beams for Growth inhibition in Vicia faba. Acta Radiologica Oncology. 22, 493 – 496.

Volkmer B. and Virsik–Peuckert R.P. (1990). Kinetics of chromosome lesion repair in synchronized quiescent and proliferating CHO cells. Int. J. Radiat. Biol. 58, 1009 – 1023.

Vral A., Thierens H. and de Ridder L. (1992). Study of dose–rate and split–dose effects on the in vitro micronucleus yield in human lymphocytes. Int. J. Radiat. Biol. 61, 777 – 784.

Wakabayashi H., Suzuki S. and Ito A. (1983). Measurement of relative biological effectiveness (RBE) for the radiation beam from neutron source reactor YAYOI. J. Radiat. Res. 24, 305 – 316.

Wambersie A., Barendsen G.W. and Breteau N. (1984). Overview and prospects of the application of fast neutrons in cancer therapy. J. Eur. Radiother. 5, 248 – 264.

Wandl E.O., Ono K., Kain R., Herbsthofer T., Heinert G. and H barth K. (1989). Linear correlation between surviving fraction and the micronucleus frequency. Int. J. Radiat. Biol. 56, 771 – 775.

Ward J.F., (1985). Biochemistry of DNA lesions. Radiat. Res. 104, S103 – S111.

Watts M.E., Hodgkiss R.J., Jones N.R. and Fowler J.F. (1986). Radiosensitization of Chinese hamster cells by oxygen and misonidazole at low X–ray doses. Int. J. Radiat. Biol. 50, 1009 – 1021.

Whitherspoon J.P. and Corney A.K. (1970). Differential and combined effects of beta, gamma and fast neutron irradiation of Soybean seedlings. Radiat. Bot. 10, 429 – 435.

Winzel E., van der Merwe E.J., Groenewald W., Pistorius S., Slabbert J.P., Robinson L. and Böhm H.M.L. (1987). The relatice biological effectiveness of 100 kV X–rays determined by the V–79 cell colony assay. S. Afr. Med. J. 71, 693 – 695.

Wolff S., Atwood K.C., Randolph M.L. and Luippold H.E. (1958). Factors limiting the number of radiation–induced chromosome exchanges. I. Distance: Evidence from non–interaction of X–ray– and neutron–induced breaks. J. Biophysic. and Biochem. Cytol. 4, 365 – 372.

Zaider M. and Rossi H.H. (1980). The synergistic effects of different radiations. Radiat. Res. 83, 732 – 739.

Zaider M. and Brenner D.J. (1984). Comments on "V79 survival following simultaneous or sequential irradiation by 15–MeV neutrons and ^{60}Co photons" by Higgins et al. [Radiat. Res. 95, 45–56 (1983)]. Radiat. Res. 99, 438 – 441. Zaider M. (1990). Concepts for describing the interaction of two agents. Radiat. Res. 123, 257 – 262.

Zaider M. (1991). The interaction of two agents revisited: response to M.C. Berenbaum. Radiat. Res. 126, 266 – 268.

Zoetelief J. and J.J. Broerse (1990). Dosimetry for radiation accidents: present status and prospects for biological dosemeters. Int. J. Radiat. Biol. 57, 737 – 750.

Zywiets F., Menzel H.G., Van Beuningen D. and Schmidt R. (1982). A biological and microdosimetric intercomparison of 14 MeV d–T neutrons and 6 MeV cyclotron neutrons. Int. J. Radiat. Biol. 42, 223 – 228.